Self-Healing Process Based on Spontaneous Copolymerisation of Electron Rich and Electron Poor Monomers

HOU, SHENGHUI

Self-Healing Process Based on Spontaneous Copolymerisation of Electron Rich and Electron Poor Monomers

A thesis submitted for the degree of

Doctor of Philosophy

by

Shenghui Hou

Department of Chemistry

Durham University

2016

Abstract

This project involves on developing highly efficient self-healing polymer systems based on spontaneous copolymerisation.

Several different self-healing systems, examples of micro-encapsulation processes, basic concepts of free radical polymerisation and copolymerisation, mechanism and examples of spontaneous copolymerisation, and fracture mechanics of polymeric materials were reviewed.

The linear spontaneous copolymerisation of electron donor and acceptor monomers was investigated. Linear copolymers were synthesised by the spontaneous copolymerisation of electron donor monomers (4-methoxy styrene and styrene) and acceptor monomers (maleic anhydride and N-methylmaleimide) in bulk at ambient temperature and at 50 °C. The reaction of 4-methoxy styrene with ethoxymethylene malononitrile was carried out at 50 °C and produced homopolymer of 4-methoxystyrene. The resulting linear polymers were found to be soluble in tetrahydrofuran and acetone and fully characterised by 1D and 2D NMR spectroscopy, SEC, and FTIR.

Cross-linked spontaneous copolymerisation of electron donor and acceptor monomers were synthesised. By adding divinylbenzene to 4-methoxy styrene, styrene, N-methylmaleimide, and maleic anhydride, cross-linked materials were obtained. Those materials, as expected, were completely insoluble in normal organic solvent. The cross-linked polymers were characterised by sol-gel technique and FTIR.

The micro-capsules were obtained by using urea-formaldehyde micro-encapsulation process. The liquid healing agents (4-methoxy styrene, styrene, divinylbenzene, and their mixtures) were encapsulated using a process involving polymerisation of urea-formaldehyde in oil-water emulsion. The average diameter of the micro-capsule was controlled by adjusting the agitation rate. Micro-capsules with diameter were selected using seivesfor self-healing specimen preparation.

The fracture toughness of epoxy matrix was investigated. Fracture toughness of pure epoxy matrix specimen was tested by compact tension geometry. The influence of micro-capsules and solid healing agents on the fracture toughness of epoxy matrix was investigated. The micro-capsules (5-20 wt. %) in the epoxy resin did not change the fracture toughness of

matrix. However, solid healing agents MA and MeMal reduced the fracture toughness of epoxy resin as the amount of MA and MeMal added to the matrix. To keep the fracture toughness of specimen closed to that of pure epoxy resin, 10% solid healing was decided to add into the matrix for self-healing preparation. And the fracture toughness of the specimen did not change by adding EtOCN into the epoxy resin matrix.

The self-healing performance was assessed by fracture toughness recovery. The self-healing efficiency of those system designed in this project was first evaluated by injecting the liquid healing agents into the crack of the specimen containing solid healing agents. Then, the autonomous self-healing specimen was prepared by adding the micro-capsules and solid healing agents in the epoxy resin matrix. The specimens were subjected to fracture testing to establish healing efficiency. The self-healing system based on obtained good healing efficiency.

Declaration

This project was carried out in the IRC Chemistry laboratories of the Durham University between October 2012 and January 2016. This work has not been submitted for any other degree and is the original work of the author, excepted where acknowledged by reference.

Statement of copyright

Acknowledgements

Firstly, I would like to express my gratitude to Dr. Ezat Khosravi and Prof. Robert H. Grubbs (California Institute of Technology, USA), for supervising the project and their guidance throughout, especially Dr. Ezat Khosravi, the great care and continuous help in all ways. I would like to acknowledge Dr. Peter Hine from University of Leeds for supporting my mechanical tests, answering every question I had, and teaching me with the data calculation of the tests. And I appreciate the help of all the technical and analytical staff in the department who have provided me with sufficient support for analysis and characterisation. Particular thanks should be given to Ms. H.J. Riggs for assistance with SEM. I would like to express my gratitude to everyone in Khosravi research group. I would like to express my thanks to my parents for their great care and continuous support from day one. Last but not least, I would also like to thank my wife Dr. Yanan Song for her consistent encouragement and support.

Contents

Chapter 2 Linear Spontaneous Copolymerisation

Chapter 3 Cross-Linked Spontaneous Copolymerisation

Chapter 4 Micro-Encapsulation

Chapter 5 Fracture Toughness Test of Epoxy Matrix

Chapter 6 Assessment of Self-Healing Performance

Chapter 7 Conclusions and Future Work

List of abbreviations

AN	Acrylonitrile
DA	Diels-Alder
DEPT	Distortionless enhancement by polarisation transfer
DETA	Diethylenetriamine
DBTL	Di-n-butyltin dilaurate
DCM	Dichloromethane
DCPD	Dicyclopentadiene
DMa	Dimethyl maleate
DMDNT	Dimethyldineodecanoate tin
DVB	Divinylbenzene
EDA	Electron donor-acceptor
EMMA	Ethylene-co-methacrylic acid
EPON	Epoxy monomer
EPR	Electron paramagnetic resonance
EtOCN	Ethoxymethylene malononitrile
FTIR	Fourier transform infrared spectroscopy
HOPDMS	Hydroxyl end-functionalised polydimethylsiloxane
HMBC	heteronuclear multiple-bond correlation spectroscopy
HSQC	heteronuclear single-quantum correlation spectroscopy
Poly(DCPD)	Polydicyclopentadiene
IPDI	Isophorone diisocyanate
MA	Maleic anhydride
MeMal	N-methylmaleimide
4MeOSt	4-Methoxystyrene
MF	Melamine-formaldehyde
NCAP	Nematic curvilinear aligned phase
NMR	Nuclear magnetic resonance spectroscopy
NVCZ	N-vinylcarbazole
RDA	Retro-Diels-Alder
RDP	Rack Drive Panel
ROMP	Ring-opening metathesis polymerisation

SEC	Size exclusion chromatography
SEM	Scanning electron microscope
St	Styrene
TCNE	Tetracyanoethylene
TCNQ	Tetracyanoquinodimethane
TDCB	Tapered Double Cantilever Beam
THF	Tetrahydrofuran
PDES	Polydiethoxysiloxane
PDMS	Polydimethylsiloxane
PMEA	Poly(methoxy ethylacrylate)
PMMA	Poly(methyl methacrylate)
PU	Polyurethane
UF	Urea-formaldehyde
4VC	4-Vinylcarbazole
2VP	2-Vinylpyridine

Chapter 1

Introduction

1.1 Classification of self-healing polymer materials

With the development of technology, varieties of new smart materials are widely involved in all ways of life. These smart materials have designed properties that can be significantly changed by specific conditions, such as stress, temperature, pH, and even damage of the material. Self-healing materials are one class of smart materials that have the ability to repair damage.[1]

Initiation of cracks and other types of damage on microscopic level has been shown to change thermal, electrical, and acoustical properties, and eventually lead to whole scale failure of the material.[2] Usually, cracks that are difficult to detect are very hard to be repaired by hand. A material that can intrinsically correct damage or crack caused by normal usage could lower production costs of a number of different industrial processes through longer lifetime, reduction of inefficiency over time caused by degradation, as well as preventing costs incurred by material failure. Damage, degradation, and failure are natural consequences of material applications. Engineering research has been focused traditionally on either the design of new materials with increased robustness or the development of nondestructive evaluation methods for material inspection. Self-healing materials exhibit the ability to repair themselves and to recover functionality using the resources inherently available to them. Self-healing materials offer a new route toward safer, longer-lasting products and components.

The self-healing mechanism comes from biological systems, which have the ability to heal after being wounded after suffering injury.[3] In the biological system, the inflammatory response will stop bleeding. Similarly, in the synthetic system, the actuation will cause triggering. The biological system will have cell proliferation while the synthetic system will have transport.

Depending on the repair process being autonomic or externally assisted (e.g., by heating), these self-healing materials are categorised into two classes: autonomic and non-autonomic self-healing materials.[4] Autonomic self-healing materials respond without external intervention to environmental stimuli, and the chemical healing agents is automatically released and facilitates the healing in response to damage.[5] On the other hand non-autonomic self-healing materials need external intervention. Based on the healing agents employed, self-healing polymer materials also can be classified two categories: extrinsic and

intrinsic.[6]

Extrinsic healing systems rely on an external healing agent in the form of capsules or vascular networks.[7-9] In extrinsic self-healing, the design of the autonomic materials is based upon the healing agent and a catalyst to be embedded in the matrix. The two designs frequently used to prepare such materials include the micro-encapsulation and micro-vascular network. In both approaches, the self-healing process is initiated by the damage.[10] Each approach differs by the mechanism used to keep apart the healing functionality until triggered by damage. The type of sequestration dictates the damage volume that can be healed, the repeatability of healing, and the recovery rate for each approach.

Intrinsic self-healing polymer materials, known as re-mendable polymer, generally are based on either non-covalent chemistries or reversible reactions.[11] The non-covalent chemistry approach uses ionomeric coupling or hydrogen bonding.[12, 13] While reversible reactions use Diels-Alder reaction, radical exchange, dynamic urea bond, and trans-esterification.[14, 15] The re-formation of chemical bonds in intrinsic materials is triggered by a number of external stimuli including pH change, light, temperature, or mechanical pressure. Diels-Alder reactions are most frequently used to create self-healing polymers containing reversible bond formation. Autonomic self-healing without external intervention is not available in these materials for the time being.

1.2 Micro-capsule based self-healing polymer system

Micro-capsule based self-healing materials store the healing agent in micro-capsules. When the capsules are ruptured by damage, the self-healing mechanism is triggered through the release and reaction of the healing agent in the region of damage. After release, the local healing agent is depleted, leading to only a singular local healing event.[16]

Self-healing materials have been developed for some commonly used synthetic polymers and elastomers using a variety of capsule-based systems. Each system contains a healing agent in a micro-capsule until damage triggers its release.

1.2.1 System based on dicyclopentadiene with Grubbs' catalyst

Polydicyclopentadiene (polyDCPD) is a highly cross-linked polymer of high toughness formed by a ring-opening metathesis polymerisation (ROMP), scheme 1.1. Grubbs' catalyst

shows high metathesis activity with the dicyclopentadiene (DCPD) monomer coupled with good chemical stability.[17-19]

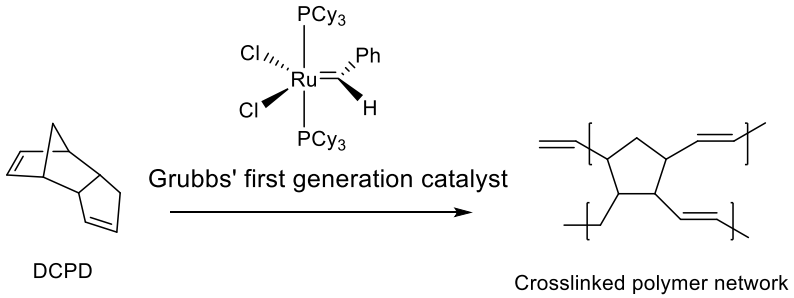

Scheme 1.1: ROMP of DCPD with Grubbs' catalyst

The most thoroughly studied system for mechanically induced healing using the micro-encapsulation method containing DCPD is the liquid healing agent.[20] Also included in the system is a Ruthenium catalyst that will initiate the ROMP of DCPD, which is responsible for the healing of the damaged materials.

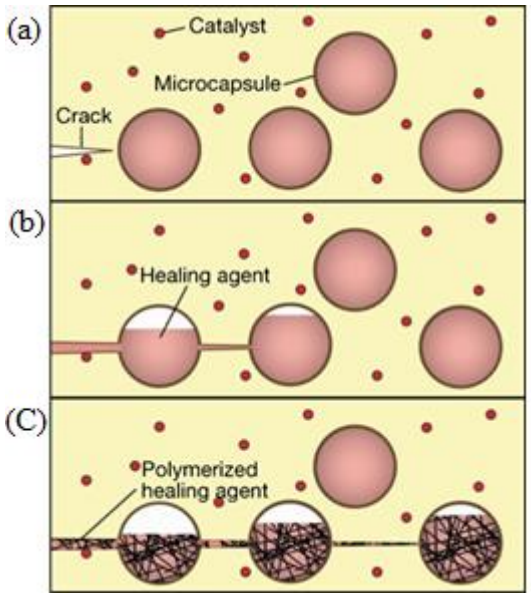

Figure 1.1: The capsule-catalyst self-healing process. Where (a) is the crack occurred, (b) is the rupture of micro-capsules by crack, and (c) is the healing of the rack by polymerisation of healing agents. Reprinted from Nature, 409:794–97, White *et al*, copyright (2001), with permission from Macmillan Publishers Ltd.

The first practical demonstration of self-healing materials was performed in 2001 by White *et al.*[21] Self-healing capabilities were achieved by embedding encapsulated healing agents

into polymer matrix containing dispersed catalysts. In this design, the healing agent is an encapsulated dicyclopentadiene (DCPD) by urea-formaldehyde (UF), and the initiator is a dispersed Grubbs' first generation catalyst in the epoxy resin matrix.

When the matrix damaged, cracks are formed, figure 1.1a. The micro-capsules are ruptured and the healing agents are released into the cracks, figure 1.1b. The polymerisation triggered when the healing agents meet the catalyst, which is dispersed in the matrix, figure 1.1c. The polymerised healing agent will heal the cracks.

Majchrazk *et al.* reported an autonomous self-healing process at ambient temperature based on the ROMP of mono- and di-functional norbornene dicarboximides, figure 1.2. It was found that the specimens containing healing agent of high viscosity comprising of just a mixture of mono- and di-functional norbornene dicarboximide monomers required clamping to initiate healing. However, the spcimen containing healing agent of low viscosity comprising a mixture of these two monomers and 25% of ethylidene norbornene, as a reactive diluent monomer, healed unclamped giving healing efficiency of 33% and this was developed between 11 and 24 h.[22]

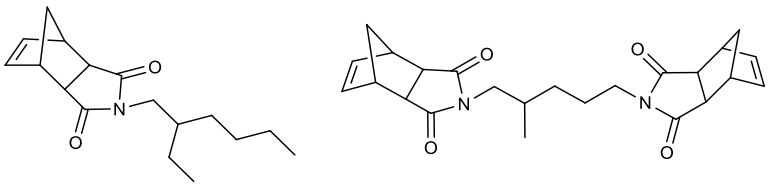

Figure 1.2: Structure of mono- (1) and di-functional (2) norbornene dicarboximides

In 2002, Brown *et al.* reported an autonomic self-healing system using a UF encapsulated DCPD healing agent and Grubbs' catalyst with high healing efficiencies.[23] The use of tapered double-cantilever beam (TDCB) fracture geometry provided an accurate method to measure the fracture behavior and healing efficiency of self-healing polymer composites and to compare with appropriate controls. Virgin fracture properties of the polymer composite were improved by the inclusion of micro-capsules and catalyst particles. The size and concentration of the catalyst were shown to have a significant impact on the virgin properties of the composite and the ability to catalyse the healing agent. The highest healing efficiency was obtained with 180–355 μm catalyst particles. Catalyst concentrations of greater than 2.5 wt% provided diminishing gains in healed fracture toughness. A significant loss of virgin

fracture toughness was observed for a catalyst concentration of about 3%. The addition of micro-capsules, up to 15 wt%, served to increase the virgin toughness. Capsule size had a direct influence on the volume of DCPD monomer released into the crack plane but, over the range of capsule sizes investigated, healing efficiency was not restricted by lack of healing agent. Maximum healing efficiency was obtained within 10 h of the fracture event. By adjusting the concentrations of catalyst and micro-capsules, the healing efficiency of the system was increased to over 90 %, figure 1.3.

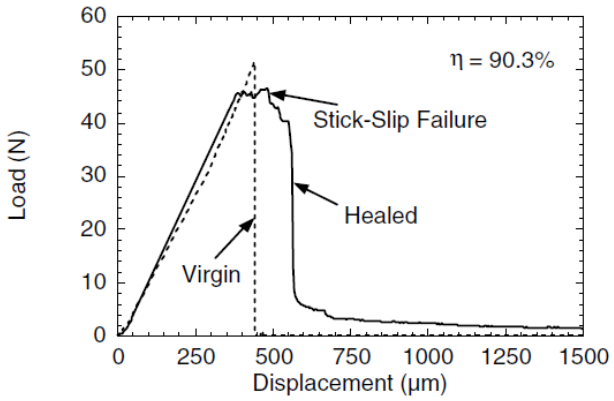

Figure 1.3: Load-displacement curve for an in-situ sample with 2.5 wt% Grubbs and 5 wt% micro-capsules. Reprinted from Exp. Mech., 42(4):372–9, Brown *et al*, copyright (2002), with permission from Springer.

DCPD-Grubbs' self-healing system provides good healing performances, so it has been widely used in many materials, such as bulk matrices of epoxy[24-27], epoxy vinyl ester[28, 29], and thermoplastic-elastomeric block copolymers[30].

1.2.2 System based on PDMS multi-capsule

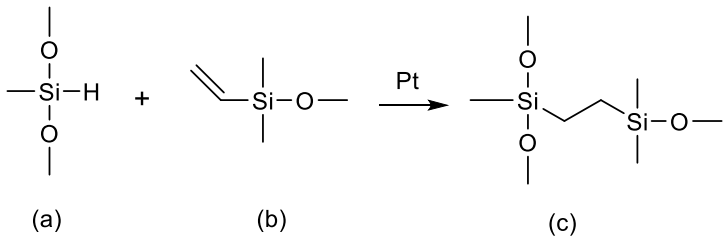

Scheme 1.2: Platinum-catalyzed hydrosilylation of vinyl terminated PDMS where (a) is the initiator material, (b) is the vinyl functionalised resin, and (c) is the resulting cross-linked network.

Keller *et al.* demonstrated multi-capsule self-healing, at ambient temperature, of a silicone elastomeric matrix (polydimethylsiloxane (PDMS)) based on hydrosilylation in the presence of platinum catalyst, scheme 1.2. The system involved two types of UF micro-capsules, one containing vinyl functionalised PDMS resin (scheme 1.2b) containing a Pt catalyst and the other containing a liquid initiator material (hydrosiloxane copolymer, scheme 1.2a). Tear testing demonstrated the capability of the self-healing elastomer to routinely recover at least 70% of the original tear properties.[31]

PDMS multi-capsule system has been extended to perform corrosion inhibition. Cho *et al.* incorporated PDMS resin capsules and dimethyldineodecanoate tin (DMDNT) catalyst capsules in an epoxy coating.[32] The healing performance was assessed by salt-immersion corrosion tests, figure 1.4.

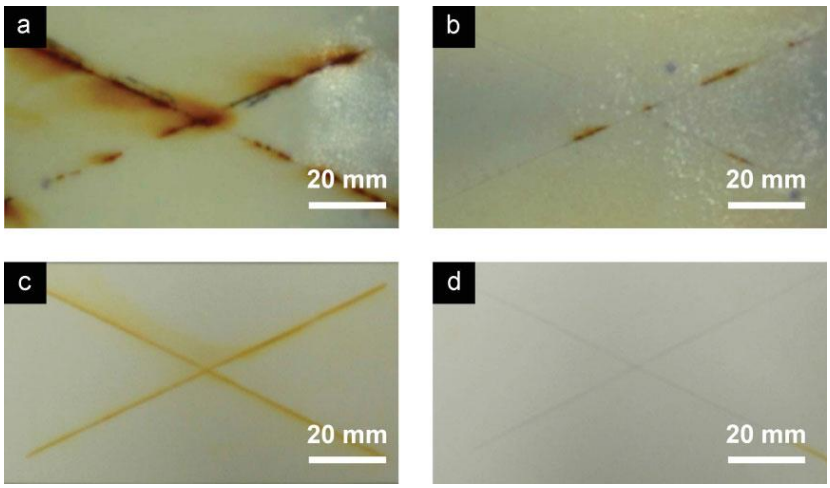

Figure 1.4: Salt-immersion corrosion testing of control and of room-temperature self-healing epoxy coatings. All images were obtained after healing at 20 °C for 24 h and 120 h immersion in salt water. Reprinted from Adv. Mater., 21(6):645–9, Cho et al, copyright (2009), with permission from Wiley Materials.

In the report, a control sample consisting of the epoxy-amine matrix coated on a primed substrate was scribed and left in salt water, figure 1.4a. The self-healing coating prepared as sample (a), with the addition of PDMS healing-agent capsules and TKAS-catalyst capsules, was shown in figure 1.4b after salt-immersion corrosion tests. Two-layer containing adhesion promoter (control sample) was tested and shown in figure 1.4c. And self-healing coating prepared as sample (c), with the addition of PDMS healing-agent capsules and TKAS-catalyst capsules, was shown in figure 1.4d after the tests. Corrosion-test results after

scribing and healing for 24 h at room temperature show the efficacy of the room-temperature activity for both these systems This healing chemistry is attractive because it is air- and water- stable, and remains active even after exposure to elevated temperatures (up to 150 °C), enabling its use in systems requiring a thermal cure. While the mechanical properties of the resultant cross-linked siloxane are not exceptional, in a coating system the mechanical strength of the healed matrix is of secondary importance, compared to chemical stability, two areas where siloxanes show exceptional performance.

1.2.3 System based on epoxy-amine latent functionality

In the latent functionality self-healing systems, the matrix contains residual reactive functionality and the healing agent is encapsulated. When the crack opens the micro-capsules, the healing agent will be released and meet the reactive function group in the matrix initiating the polymerisation.[33-34]

Zako and Takano developed a separate system with latent functionality by incorporating thermally polymerisable or meltable epoxy particles into epoxy composite.[35] Small amount of epoxy particle-type adhesive is embedded in a glass/ epoxy composite laminate. When the matrix damaged, the embedded particles in the matrix was melted by heat and flow into the crack. The melted epoxy adhesive was cross-linked by the amine group in the matrix and hence healed the crack. And the embedded particles are found to not change the stiffness of the glass/epoxy composite laminate. This healing system was developed by many researchers by embedding epoxy monomer via micro-capsules.

In 2008, Caruso *et al.* demonstrated an example of a latent self-healing system based on the solvent-promoted and resin-solvent self-healing system.[36] The residual amine functionality in an epoxy matrix was used to initiate polymerisation of the delivered healing agent. An autonomic system yielding complete recovery of fracture toughness after crack propagation was achieved by embedding micro-capsules containing a mixture of epoxy monomer (EPON 828) and solvent (chlorobenzene) into an epoxy matrix. However, the concentrate of epoxy monomer in chlorobenzene was not stated. This autonomic self-healing system is reported to show 100% of the materials' original fracture toughness recovery.

1.2.4 System based on phase separation

In 2006, Cho *et al.* demonstrated the concept by phase-separating hydroxyl end-functionalised polydimethylsiloxane (HOPDMS) and polydiethoxysiloxane (PDES) in a matrix of epoxy vinyl ester to restore mechanical integrity.[37] The catalyst, di-n-butyltin dilaurate (DBTL), was contained within PU micro-capsules embedded in a vinyl ester matrix and was released when the capsules were broken by mechanical damage. This system possessed a number of advantages such as the stability of healing chemistry in wet environments and at elevated temperature (>100 °C) and comparatively low cost. Comparing with the original fracture toughness of vinyl ester matrix, a healing efficiency as high as 46 % was achieved.

1.3 Micro-vascular based self-healing materials

Micro-vascular self-healing materials store the healing agent in a network in the form of capillaries or hollow channels, which may be interconnected until damage triggers self-healing. For vascular systems, additional connectivity adds numerous performance advantages. Any location in the network has multiple connection points, leading to increased reliability with regard to channel blockages and a larger accessible reservoir for the healing agents. Multiple connections between channels also allow for easier refilling of the network after depletion.[38]

As opposed to capsule-based systems, for vascular materials the healing agents are introduced after the network has been integrated into the matrix. Thus, some properties that determine the choice of healing agents are surface wettability, chemical reactivity, and viscosity. High viscosities and/or unfavorable wetting properties prevent efficient filling of the network, whereas chemical incompatibility endangers long-term stability of the system. These properties also affect vascular network design, especially the channel diameter, because viscosity and wettability affect the release and transport of the healing agents.

The mechanical properties of a matrix with an embedded network are affected by the network wall stiffness, the bonding between the matrix and the network, the network volume fraction, and channel distribution and uniformity. The triggering mechanisms are validated and the healing performance characterised in a manner similar to capsule-based systems. Importantly, for vascular healing systems, access to a large reservoir of healing agents and the ability to replenish the network enable repeated healing of multiple damage events.

Building upon the hollow glass fiber and micro-capsule healing systems, and striving to create the ultimate biomimetic material, new research has focused on the fabrication of microvascular self-healing composite materials. One of the main complaints about both the glass fiber and micro-capsule systems is their inability to heal the same location in the material more than once; often, a second fracture event will occur along the plane of the initial crack. By providing a material with a semi-continuous flow of healing agent, multiple healing cycles can be achieved.

Scientists and engineers are constantly looking to nature for inspiration on how to create more effective and efficient systems; this is no different in the case of intelligent materials. Both animals and plants feature fluid flow networks integrated into load-bearing materials and therefore serve as a useful source of inspiration for probable failure modes and reliability strategies since it can be assumed that these have evolved to ensure system success.[39] Certain plants have canals in them that contain latex and/or resin which are used in defense mechanisms; upon rupture, secretions from the canals become sticky and serve to protect the plant from pathogens.[40] This type of self-sensing and self-repairing system is a great source of inspiration for engineers. By studying the various vascular systems in plants and noting the different mechanics and corresponding effectiveness, scientists can design better materials that accomplish the same functions.

In 2007, Toohey *et al.* published one of the first example of composite materials containing micro-vascular self-healing system. [41] This system used the liquid DCPD as the healing agent and solid Grubbs' catalyst to initiate polymerisation. The specimen was an epoxy coating deposited on a substrate that contains a three-dimensional (3D) micro-vascular network, figure 1.5.

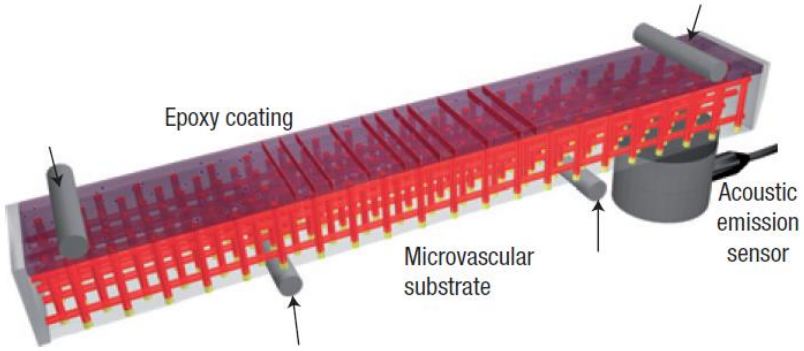

Figure 1.5: Schematic diagram of the self-healing structure composed of a microvascular substrate and a brittle epoxy coating containing embedded catalyst in a four-point bending configuration monitored with an acoustic-emission sensor. Reprinted from Nature Material, 6:581–5, Toohey et al, copyright (2007), with permission from Macmillan Publishers Ltd.

The catalyst was incorporated into epoxy coating that was applied to the top surface of the micro-vascular substrate; the micro-channels were filled with DCPD and then sealed. This network of micro-channels can be replenished with adding more DCPD healing agent, allowing for multiple healing events to occur at the same location within the material. This system achieved a peak healing efficiency of 70% with 10 wt% catalyst in the top coating, and was able to demonstrate healing for up to seven cycles. It was reported that the amount of catalyst in the top epoxy layer did not affect the average healing efficiency per cycle but rather dictated how many cycles of testing and that healing could be performed successfully.

Williams *et al.* published their version of a micro-vascular containing mechanically stimulated healable material in the form of a sandwich structure composite consisting of high performing skin materials, such as glass or carbon fiber composites, separated by a lightweight core to obtain a material with very high specific flexural stiffness. [42]

A vascular network incorporated into a sandwich structure is reported to address the larger damage volume, as well as allowing for multiple healing events to occur. Samples were fabricated with channels containing healing agents (epoxy resin and hardener in separated channels), which had a small effect on the mechanical properties of the composite. Rupture of the vessels released the healing agent, filling the void that formed as a result of impact damage on the sample leading to healing. It is reported that self-healing was successful, but the healing efficiency was not stated.

1.4 Intrinsic self-healing materials

The intrinsic healing system, also known as re-mendable polymers, is a class of non-autonomic self-healing process. These polymers achieve repair though inherent reversibility of bonding of the matrix polymer, such as reversible reactions, ionomeric coupling, hydrogen bonding, or molecular diffusion.[43]

1.4.1 Reversible system

Reversible systems are broadly defined as polymeric systems that can revert to either their monomeric, oligomeric, or non-cross-linked states. For the polymer to be stable under normal working conditions, the reverting process would normally require an external stimulus for it to occur. For mending purposes, ideally the material would revert to its constituents after cracking, but could be repaired by applying the conditions that were used to polymerise it.

Self-healing materials based on reversible reactions include components that can be reversibly transformed from the monomeric state to the cross-linked polymeric state through the addition of external energy. Generally, a damaged polymer is subjected to heat or light irradiation, triggering enhanced mobility in the damage region, bond reformation, and polymer re-mending.

The most widely used reaction scheme for re-mendable self-healing materials is based on the Diels-Alder (DA) and retro-Diels-Alder (RDA) reactions. Chen *et al.* demonstrated a thermally activated self-healing system based on the DA reaction of synthesised furan-maleimide polymers.[44]

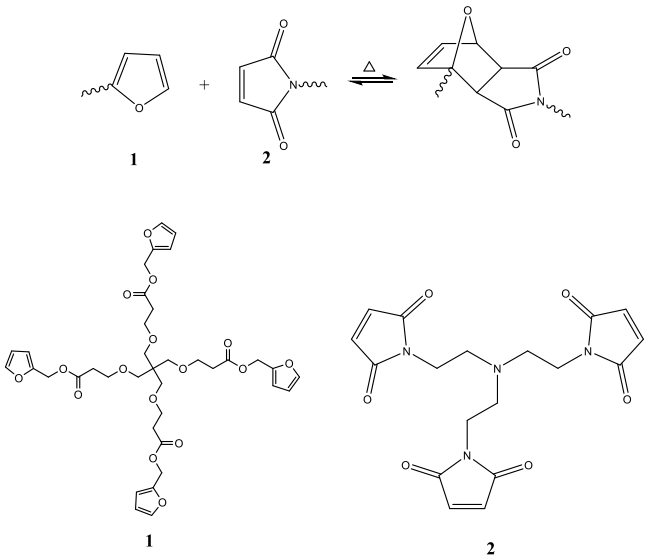

Scheme 1.3: The DA reaction of synthesised furan monomer (1) and maleimide monomer (2)

A thermally reversible DA cycloaddition of a multi-diene (furan monomer 1) and multidienophile (maleimide monomer 2) was used to prepare a polymeric material (scheme 1.3). A highly cross-linked polymer specimen was formed via the DA reaction of furan and maleimide moieties, and thermal reversibility was accomplished by the retro-DA reaction. The average mending efficiency of about 50% and 41% was achieved at 150°C and at 120°C, respectively.

This healing system was developed by Plaisted *et al.* and demonstrated increased healing efficiency up to 78% at 115 °C using furan-maleimide polymer.[45] The furan monomer (1) was the same as that used by Chen *et al.* and maleimide monomer (3) was shown in figure 1.6.

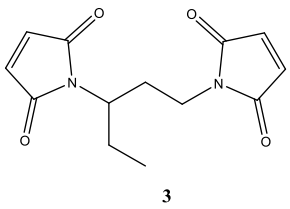

Figure 1.6: The maleimide monomer (3)

Park *et al.* used the DA reaction to incorporate healing functionality in polymer derived from dicyclopentadiene monomers (figure 1.7) in a matrix containing a carbon fiber.[46] The design is reported to display much faster healing rate by heating. The healing performance was examined by SEM. Crack healing was observed at a relatively low temperature range of 70–

108 °C, and was complete within minutes at these temperatures. However, the value for healing efficiency was not reported.

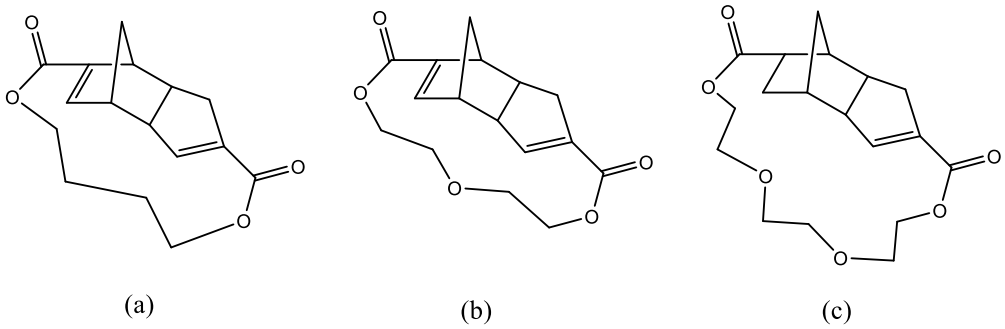

Figure 1.7: The monomer (a, b, and c) synthesised by Park *et al.*

1.4.2 Ionomeric system

Ionomeric copolymers are a class of materials with ionic segments that can form clusters that act as reversible cross-links. These clusters can be activated by external triggers such as temperature or UV irradiation. Because the formation of the clusters is reversible, multiple local healing events are possible.

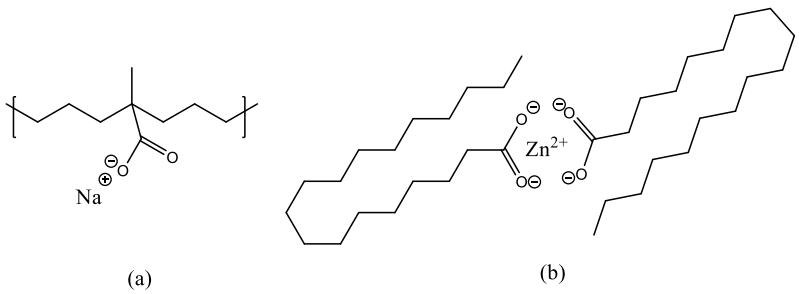

Figure 1.8: Neutralised random ionomer co-polymer used by Varley *et al.*

The ionomeric self-healing system using poly(ethylene-co-methacrylic acid) (EMMA) copolymers with ionic segments was first reported by Kalista *et al.* in 2007.[47] And it was investigated further by Varley *et al.*[48] The polymer used was a partially neutralised EMMA random ionomer co-polymer (figure 1.8). It contains 5.4 mol.% of methacrylic acid groups, 30% of them have been neutralised with sodium. EMMA films were able to heal upon damage. This occurred through a heat-generating frictional process. The healing behavior was observed according to elastomeric and viscous response.

1.4.3 Supramolecular system

Supramolecular polymer materials can be designed to form self-healing system via reversible hydrogen bonding. Cordier *et al.* designed and synthesised macromolecules that associate to form cross-links via hydrogen bonding (figure 1.9).[49]

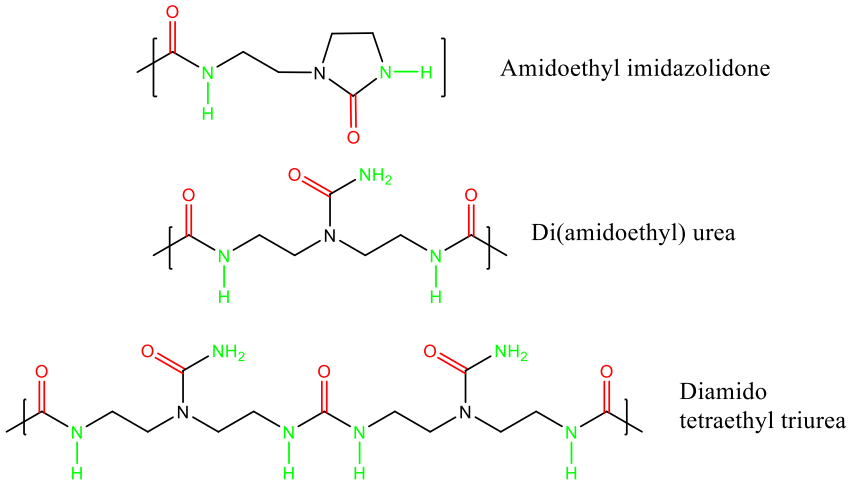

Figure 1.9: Macromolecules containing reversible hydrogen bonding

The system showed recoverable extensibility up to several hundred per cent and little creep under load. These systems, when broken or cut, can be repaired by bringing together fractured surfaces to self-heal at ambient temperature. Repaired samples recuperate their enormous extensibility. The process of breaking and healing is reported to be repeatable.

1.4.4 Molecular diffusion system

Self-healing polymer via molecular inter-diffusion has been the subject of extensive research in the 1980s. The polymers investigated cover amorphous, semi-crystalline, block copolymers, and fiber-reinforced composites. It has been discovered that when two pieces of the same polymer are brought into contact at a temperature above its glass transition temperature (T_g), the interface gradually disappears and the mechanical strength at the polymer – polymer interface increases. This behavior was used to heal the crack in the material.[50]

Jud and Kausch studied the effect of molecular weight and degree of copolymerisation on the crack healing behavior of poly(methyl methacrylate) (PMMA) and PMMA – poly(methoxy ethylacrylate) (PMEA) copolymers.[51] The self-healing ability of the copolymers was tested

by clamping and heating these samples in which the fractured surfaces (of single-edge notched and compact tension specimens) were brought together and held for set periods of time. Various experimental parameters were investigated, which included the time between fracturing and joining of the fractured surfaces, the healing time, the healing temperature and the clamping pressure. It appeared that a temperature of 5 °C higher than the T_g and a healing time of over 1 min were required to produce healing greater than that could be attributed to simple surface adhesion. An increase of the time between fracture initiation and self-healing of the fractured surfaces was found to significantly inhibit healing, dropping optimum property recovery from 120% to 80%. Visual healing of the fracture surfaces was found to occur before a significant recovery in strength was achieved, with the interdiffusion of numerous chain segments (rather than entire chains) being reported as the most likely healing mechanism.

1.5 Micro-encapsulation

Micro-encapsulation is a technique by which solid, liquid or gaseous active ingredients are packaged within a second material for the purpose of shielding the active ingredient from the surrounding environment. Thus the active ingredient is designated as the core material whereas the surrounding material forms the shell.[52] This technique has been employed in a diverse range of fields from chemicals and pharmaceuticals to cosmetics and printing. For this reason, widespread interest has developed in micro-encapsulation technology.

In the 1950s, Green and Schleicher produced first micro-encapsulation process, in which dyes was packaged by complex coacervation of gelatin and gum arabic, for the manufacture of carbonless copying paper.[53]

In the 1960s, micro-encapsulation of cholesteric liquid crystal by complex coacervation of gelatin and acacia was reported to produce a thermosensitive display material. Fergason *et al.* developed nematic curvilinear aligned phase (NCAP), a liquid crystal display system by micro-encapsulation of nematic liquid crystal. Encapsulation technology has provided the enlargement of display areas and wider viewing angles.[54]

Since the mid of 1970s, micro-encapsulation has become increasingly popular in pharmaceutical industry as well as for many other products and processes in daily use. A very important application for this technology is used for self-healing composites.

The micro-capsules in self-healing systems not only store the healing agent, but provide a mechanical trigger for the self-healing process when damage occurs in the host material. For self-healing materials, the most common encapsulation techniques are produced in-situ polymerisation.[55]

In-situ and interfacial encapsulations proceed by reaction of urea-formaldehyde (UF), melamine-formaldehyde (MF), or polyurethane (PU) formation of a polymer shell wall at the interface of droplets in oil-water emulsion.

1.5.1 Urea-formaldehyde

In 2003, Brown *et al.* investigated that UF micro-capsules containing dicyclopentadiene were prepared by in-situ polymerisation in an oil-water emulsion that meet requirements for self-healing epoxy.[56] Micro-capsules of 10–1000 μm in diameter were produced by appropriate selection of agitation rate in the range of 200–2000 rpm. A linear relation was reported between log (mean diameter) and log(agitation rate). Surface morphology and shell wall thickness were investigated by optical and electron microscopy. Micro-capsules were composed of a smooth 160–220nm inner membrane and a rough, porous outer surface of agglomerated UF nanoparticles. Surface morphology was reported to be influenced by pH of the reacting emulsion and interfacial surface area at the core–water interface. High yields (80–90%) of a free flowing powder of spherical micro-capsules were produced with a fill content of 83–92 wt% as determined by CHN analysis.

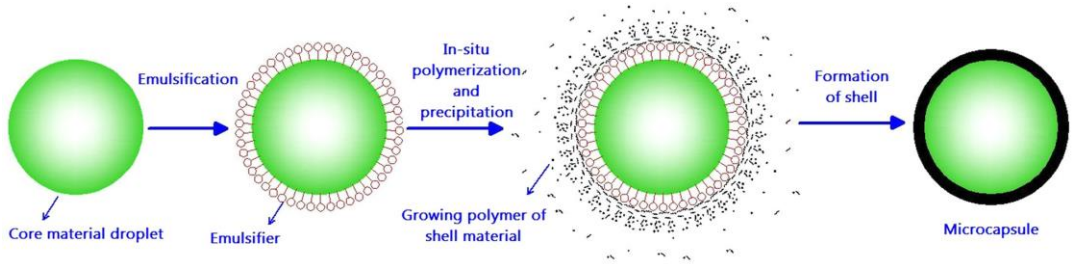

Figure 1.10: Process of micro-encapsulation by in-situ polymerisation of UF. Reprinted from J. Microencapsul, 20(6):719–30, Brown et al, copyright (2003), with permission from Taylor & Francis

The process of micro-encapsulation by in-situ polymerisation was shown in figure 1.10. The monomers to be encapsulated form as droplets in urea emulsion. During in-situ polymerisation, oil emulsions in water are first produced under vigorous agitation or

sonication of a biphasic liquid. The core chemical acts as the dispersed phase. The monomers and initiators used for constructing the capsule wall are dissolved in either the dispersed or the continuous phase. After addition of formaldehyde, the polymer synthesised by urea and formaldehyde is insoluble in the emulsion, therefore, polymerisation often takes place on the surface of the core material droplets or the resulting polymer accumulates onto the droplets surface, thus generating micro-capsules with the desired core material. For in-situ micro-encapsulation, the thickness and size of the micro-capsules is controllable. Average micro-capsule diameter is controlled by agitation rate. As the agitation rate is increased, a finer emulsion is obtained and the average micro-capsule diameter decreases. Micro-capsules with average diameter in the range of 10–1000 μm are obtained by adjusting the agitation rate between 200–2000 rpm.[56]

1.5.2 Melamine-formaldehyde

In 2002, Lee *et al.* reported Micro-capsules containing fragrant oil (Foral oil) synthesised via the in-situ polymerisation method using melamine-formaldehyde (MF) as a wall material.[57] The encapsulation efficiency and other physical properties were analysed with varying mole ratio of melamine with formaldehyde and pH of emulsion medium. The pH of the reaction medium was varied from 5.0 to 6.0 and the F/M molar ratio, 2.3 ~ 5.5. Micro-capsules containing fragrant oil were synthesised successfully and their particle sizes ranged from 12 ± 5 mm. Encapsulation efficiency of fragrant oil varied from 67 ± 8%.

1.5.3 Polyurethane

In 2008, Yang *et al*. demonstrated that Micro-capsules containing reactive diisocyanate for use in self-healing polymers are successfully fabricated via interfacial polymerisation of polyurethane (PU). Isocyanates are potential catalyst-free healing agents for use in humid or wet environments. The preparation of PU prepolymer and micro-encapsulation of isophorone diisocyanate (IPDI) healing agent were presented. Smooth spherical micro-capsules of 40-400 μm in diameter are produced by controlling agitation rate (500-1500 rpm). The PU shell wall thickness varies linearly with capsule diameter, such that the capsules wall thickness to diameter ratio was constant (~0.05). High yields (~70%) of a free-flowing powder of IPDI/PU capsules were produced with a liquid core content of 70 wt % as determined by TGA analysis. The micro-capsules were stable with only ~10 wt % loss of IPDI was detected after 6 months storage under ambient conditions. Direct mechanical compression

testing of micro-capsules revealed a brittle fracture mode and normalised shell wall strength that varied with capsule diameter.[58]

1.6 Polymerisation

The background knowledge of polymerisation is reviewed, the concepts of free radical polymerisation and copolymerisation were written according to the textbook of polymer. [59, 60]

1.6.1 Polymerisation reactions

Polymerisation could be divided into two general groups, according to their mechanisms: step-growth polymerisation and chain-growth polymerisation. This subdivision makes a distinction between polymers prepared by the stepwise reaction of monomers and those formed by chain reactions.

A step-growth polymerisation can be described as a process that at the beginning involves one or more monomers having at least two reactive sites, i.e. functional groups. Two monomers can react together to give a dimer, a monomer may add to a trimer, or two dimers combine to form a tetramer and so on to form the polymer chains. The monomer is consumed at the beginning of the reaction and step growth polymerisation does not need an initiator to start the reaction. The monomers can react with or without elimination: the former is the case of polycondensation reactions; the latter is the case of polyaddition reactions. It is possible to synthesise with this type of polymerisation polymers like polyester, polyamide, polyurethane, polysiloxane, polycarbonates, polyurea and polysulfides. The reactions involved are reactions to the carbonyl group or nucleophilic substitutions.

In the polymerisations that occur via a chain reaction, the monomers are usually converted into polymers by reaction of the double bond of substituted alkene monomers with a free radical or ionic initiator. The product, then, unlike that obtained from step-growth polymerisation, has the same chemical composition of the starting monomer, i.e., each unit in the chain is a complete monomer and not a residue as in the most step-growth reactions.

1.6.2 Free radical polymerisation

In general when the polymerisation mechanism proceeds by the reaction of radicals, the reaction is called Free Radical Polymerisation. The chain grows by addition of one monomer unit at a time and the active radical species are always at the chain end. The complete

polymerisation proceeds in three distinct stages: initiation, propagation and termination, scheme 1.4.

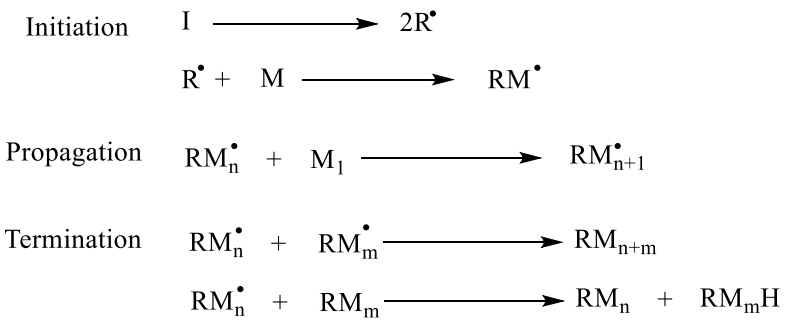

Scheme 1.4: Reaction steps in free radical polymerisation: initiation, propagation, and termination

The radical precise mechanism and rate of each step are dependent on a number of factors including temperature, solvent and the chemistry of each component. The polymerisation process continues until either the monomer is entirely consumed or all the growing free radical chains are terminated without the prospect for the further initiation and propagation of new polymer chains.

The radical can be formed in several radical producing reactions. Free radicals can be produced by thermal decomposition of organic peroxides (-O-O-), such as benzoyl peroxide (scheme 1.5a), and azo compounds (-N=N-), such as Azobisisobutyronitrile (AIBN), scheme 1.5b.

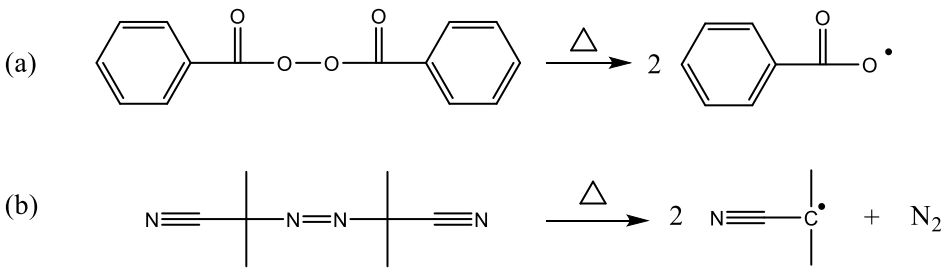

Scheme 1.5: Thermal decomposition of benzoyl peroxide (a) and AIBN (b)

Photolysis can also produce free radical. This can be applied to azo compounds, metal iodides and metal alkyls, for example, AIBN that is also decomposed by radiation.

The free radical can also be formed by redox reactions. An example is the reaction between

the ferrous ions and hydrogen peroxide in solution that produces hydroxyl radicals, but it is also possible to use alkyl hydroperoxides instead of hydrogen peroxide, scheme 1.6.

$$H_2O_2 + Fe^{2+} \longrightarrow Fe^{3+} + OH^- + OH^\bullet$$

Scheme 1.6: the reaction between the ferrous ions and hydrogen peroxide in solution

The radical reacts rapidly with a large number of unsaturated monomers containing double bond. It is possible to have two types of reaction (I and II, scheme 1.7) with the double bond due to the unsymmetrical nature of the double bond but type I is the favoured because of stabilisation due to the resonance effect.

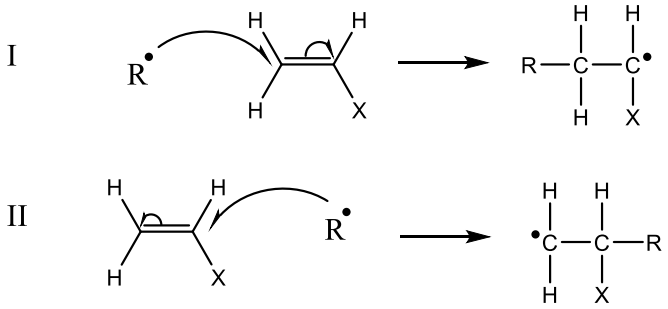

Scheme 1.7 Mechanism of a radical attack to a double bond.

In the propagation step, the new radical species reacts with another monomer forming the polymer chain. The chain propagation proceeds rapidly by addition of a monomer unit to the chain carrier. The active centre is displaced after every addition to the end of the growing chain. The average life time of the growing chain is short, in the order of second or less.

Termination occurs when the active radical at the chain end is deactivated, ending the growth of the polymer chain. In theory, the chain could continue to propagate until all the monomer in the system has been consumed, but free radicals are very reactive and so they can react with other radicals to form inactive covalent bonds. Termination of chains can take place in several ways: reaction between two active chain ends combination; reaction of an active chain end with an initiator radical; transfer of the active center to another molecule such as a solvent, initiator or monomer (chain transfer); and interaction with impurities or inhibitors.

Free radical polymerisation leads to high molar-mass polymers as soon as the reaction starts, the monomer concentration decreases steadily throughout the reaction, only the active centre can react with the monomer and add units to the chain, and furthermore long reaction times increase the polymer yield, but not the molar mass of the polymer. It is important to mention

that this type of polymerisation is difficult to control because of the numerous, fast, irreversible, termination and chain transfer reactions that occur. It results in a product with a broad molecular weight distribution. Therefore, free radical polymerisation is not a good method for producing well-defined polymers or block copolymers. To obtain a better control on the polymers produced whilst maintaining the versatility of free radical polymerisation, a range of "controlled/living radical polymerisation" mechanisms have been developed.

1.6.3 Copolymerisation

(a) AABBAAAABBBBABABABBABABABBBAB

(b) ABABABABABABABABABABABABABAB

(a) AAAAAAAAAAAAAAABBBBBBBBBBBBB

Figure 1.11: Structural representation of a variety of copolymer architectures wherein A and B represent monomers (a) random copolymer, (b) alternating copolymer, (c) block copolymer.

The polymerisation reaction involving just one monomer is termed as homopolymerisation. When a polymerisation is conducted in the presence of more than one monomer, the process is known as copolymerisation. The relative distribution of co-monomers defines the architecture of the resulting copolymer. There are five common copolymer architectures namely: random (statistical), alternating, block, and graft copolymers, figure 1.11.

The final copolymer architecture is determined by two principle factors: the relative concentration of the co-monomers (feed ratio), and the reactivity ratio of the two co-monomers. If two monomers are polymerised radically there are four possible propagation reactions (a-d, scheme 1.8).

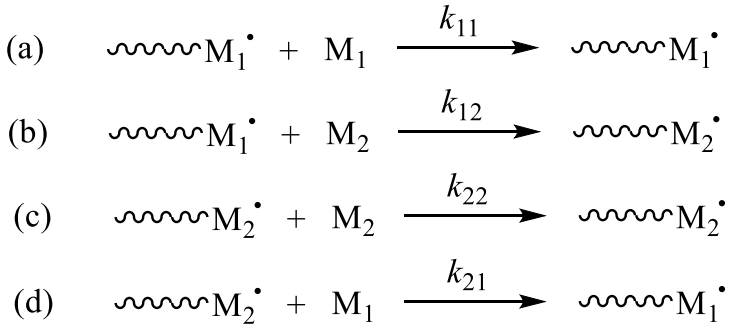

Scheme 1.8: Possible propagation steps for the co-copolymerisation of monomers M1 and

M2. (a, c) represent homopolymerisation steps whereas (b,d) represent copolymerisation steps.

Each step has an associated rate constant (k) which provides a direct measure of how favourable each reaction is. Therefore, the propensity of the monomers to react with either themselves or a co-monomer can be measured by the ratio of the rate constant of each reaction.

$$r_1 = \frac{k_{11}}{k_{12}} \qquad \text{Eq. 1.1}$$

$$r_2 = \frac{k_{22}}{k_{21}} \qquad \text{Eq. 1.2}$$

Equations 1.1 and 1.2 are defined as the relative reactivity ratios where r_1 and r_2 are measures of the reactivity of monomers M_1 and M_2, respectively. Therefore, the relative reactivity ratios can be used to predict the final copolymer architecture. When $r_1 \approx r_2 \approx 1$ the monomers would exhibit no preference for self-propagation or cross-propagation, and a truly random copolymer would result (figure 1.12a). When $r_1 = r_2 = 0$, the monomer would exhibit no tendency to self-propagation and a truly alternating co-polymer would result (figure 1.12b). A third possibility is that when $r_1 = r_2 > 1$ indicating preference to self-propagation and therefore tendency to form black copolymers (figure 1.12c).

The factors which affect the relative reaction rates include: resonance, steric and polar effects both in the monomers and the radical species. It has been observed that alternating copolymers tend to be composed of monomers with opposite polarity, for example stilbene (strongly nucelophilic alkene) and maleic anhydride (strongly electrophilic alkene), neither of these monomers is easily homopolymerised but will copolymerise with each other to form a perfectly alternating copolymer.[61]

1.6.4 Spontaneous (co-)polymerisation

Upon mixing of the electron-rich and electron-poor olefins, cycloadditions or spontaneous (co-)polymerisation would be expected to occur, without added initiator. The reactions involving electron-rich and electron-poor compounds show visually transient colours ascribed to charge-transfer complexes and have become known as ‘charge-transfer’ polymerisations.[62] ‘Charge transfer’ is a weak interaction of electron-rich with electron-poor molecules, which is detectable by UV or NMR spectroscopy.[63]

In 1983, Hall *et al.* proposed the fundamentals of the bond forming initiation theory to explain the spontaneous initiation of the spontaneous copolymerisations. The intermediates occur in the reactions was defined as tetramethylenes.[64] These tetramethylenes form by "charge transfer" between the olefins at their α-positions and can be either diradical or zwitterionic depending on the terminal β-substituents.[65,66]

The outcome of 'charge-transfer' polymerisations has been systematized.[67] A correlation of polymerisation behavior with the value of the electron donor-acceptor (EDA) complex equilibrium constant had been reported.[68] With very weak donor and acceptor olefins, spontaneous polymerisation is reported to be difficult to take place. As the donor and acceptor strength of the olefins increases, the formation of diradicals and hence spontaneous initiation rates for radical copolymerisation increases (1 in scheme 1.9). Even stronger donor and acceptor olefins, increases the formation of zwitterions and hence ionic homopolymerisation either cationic or anionic (2 and 3 in scheme 1.9).[69] Cycloaddtion to form cyclobutanes often accompany the polymers formed by spontaneous (co-)polymerisation.[70]

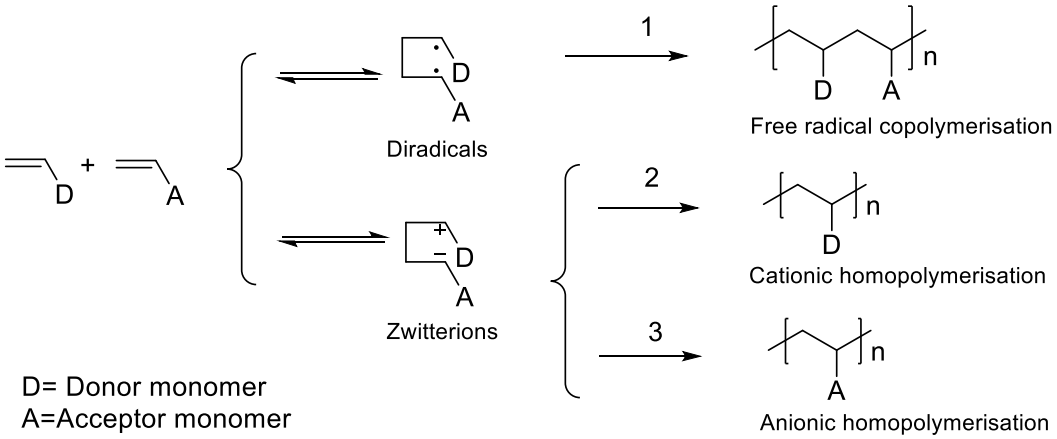

Scheme 1.9: The bond-forming initiation theory to the spontaneous reactions

Although spontaneous homopolymerisations are rare, spontaneous free radical copolymerisations of monomers with different polarities are often encountered. The observed spontaneous polymerisations varied from spontaneous free radical copolymerisations to ionic homopolymerisations. Several suggestions as to the origin of the initiating radicals of the spontaneous polymerisations have been made, ranging from charge-transfer complexes to electron transfer to bond forming initiation involving diradicals.

1.6.4.1 Diradicals

In 1987, Hall *et al.* reported the 1: l alternating copolymerisation of p-methoxystyrene with dimethyl cyanofumarate carried out spontaneously in acetonitrile or 1,2-dichloroethane at 28 °C (scheme 1.10).[71] The equilibrium constant for EDA complex formation was determined by nuclear magnetic resonance (NMR) spectroscopy. Propagation at the diradical is attested by the increase of molecular weight with conversion. The tetramethylene diradical can be trapped. A mixture of p-methoxystyrene and dimethyl cyanofumarate yielded diradical tetramethylene and a perfectly alternating copolymer in concentrated solutions or a cycloadduct dihydropyran in high dilution. However, there was no clear explanation given for this behaviour.

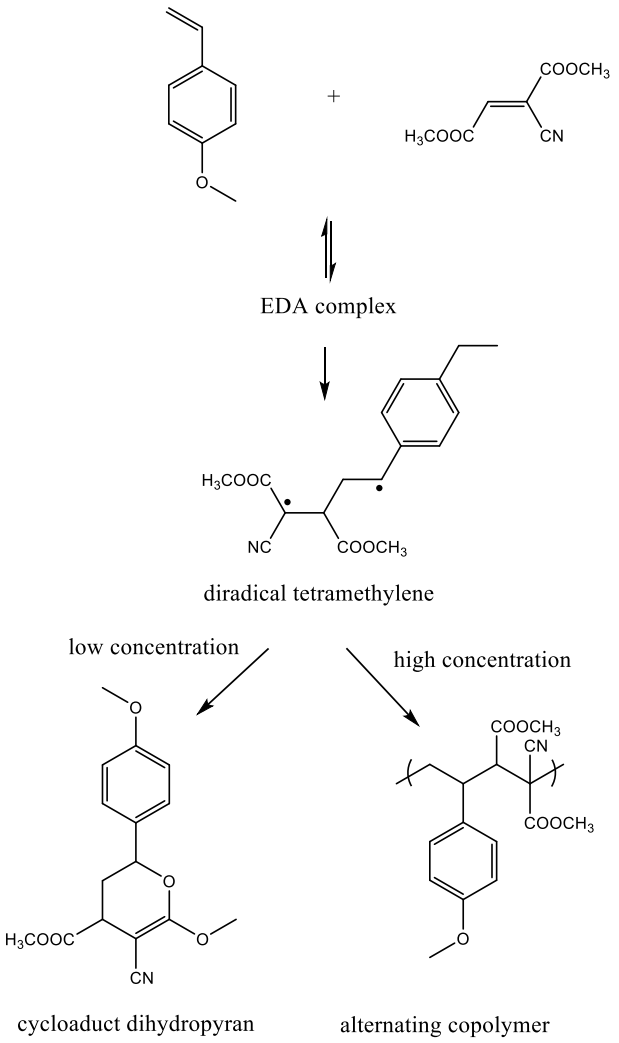

Scheme 1.10: The spontaneous alternating copolymerisation of p-methoxystyrene with dimethyl cyanofumarate

In 1990, Hall *et al.* reported that the spontaneous copolymerisations of electrophilic p-quinodimethanes with electron-rich olefins forming alternating copolymers.[72] They reported that diradicals initiate free-radical alternating copolymerisation between the two participants: tetracyanoquinodimethane (TCNQ) and styrene, scheme 1.11.

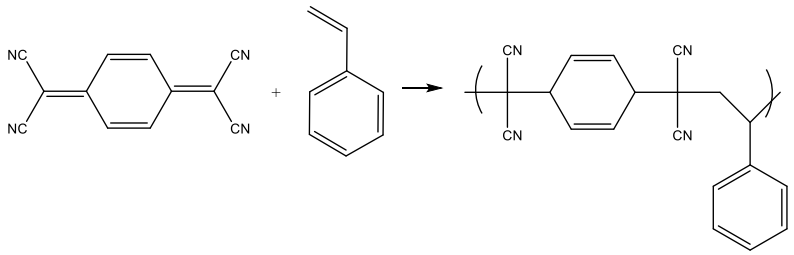

Scheme 1.11 Spontaneous alternating copolymerisation of TCNQ and styrene

In 2000, Hall *et al.* have used EPR spectroscopy and product isolation to investigate the initiation of spontaneous copolymerisations of donor and acceptor monomers.[70] The results established the presence of tetramethylene diradicals as the only experimentally supported intermediates in the initiation for the spontaneous copolymerisations. The observed alternation is currently explained by considering the polarity of radicals and monomers: an electron-rich carbon radical will preferentially combine with an electron-poor monomer to give an electron-poor radical, while the latter will preferentially combine with an electron-rich monomer to form an electron-rich radical.[73]

1.6.4.2 Zwitterions

In 1986, Gotoh *et al*. demonstrated the spontaneous, thermal reaction of electron-rich olefins with electron-poor olefins leading to a rich diversity of both small organic molecules and polymers.[74] The reactions (scheme 1.12) of N-vinylcarbazole (NVCZ) (1) with electrophilic tetrasubstituted ethylenes (2) were studied in detail as an example. The formation of EDA complex resulted in zwitterions (3) to give poly(vinylcarbazole) via cationic polymerisation. The report concluded that spontaneous polymerisation is usually accompany with cycloaddition. Also the product given by cycloaddition of zwitterions was identified (5-7).

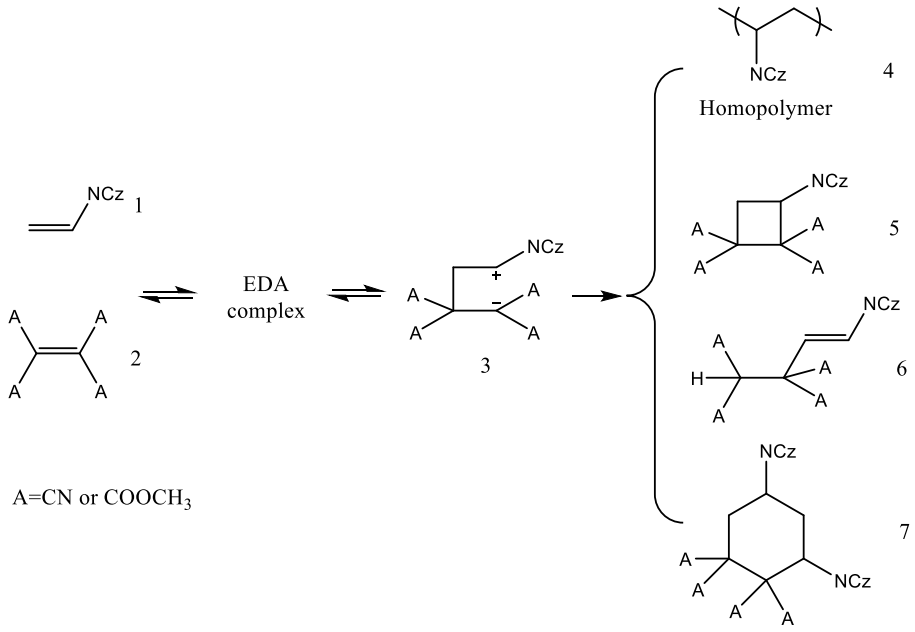

Scheme 1.12: The spontaneous reaction of electron-rich olefins with electron-poor olefins demonstrated

In 1987, Abdelkader *et al.* investigated the spontaneous copolymerisation of electron-rich vinyl monomers with electrophilic olefins.[75] They reported that tetramethylene zwitterion could initiate cationic polymerisation of electron-rich vinyl monomers, which is caused by incorporating a leaving group into the β-position of the electrophilic olefins (figure 1.12). In this study N-Ethyl-3-vinylcarbazole (l) and N-vinylcarbazole (2) were selected as electron-donor and methyl β,β-dicyanoacrylate (3), tetracyanoethylene (4), and β,β-dicyanovinyl chloride (5) as electron-acceptors. The investigation shows that only electrophilic olefin 5 restulted in cationic polymerisation of electron-rich olefins 1 and 2 due to presence of strong Cl leaving group.

1, D=NEt3Cz
2, D=NCz

3, A_1=$COOCH_3$; A_2=H
4, A_1=A_2=CN
5, A_1=Cl; A_2=H

Figure 1.12: The electron-rich vinyl monomers (1-2) and electrophilic olefins (3-5)

In 1990, Hall *et al.* reported that the spontaneous copolymerisations of electrophilic TCNQ

with electron-rich olefins (vinyl ether) which formed homo-poly(vinyl ether).[76] They reported that zwitterionic intermediates initiated the cationic homopolymerisation of the electron-rich olefin, scheme 1.13.

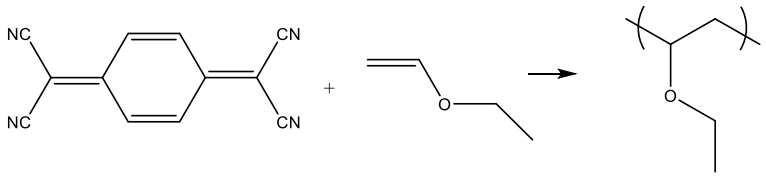

Scheme 1.13 Homopolymerisation of vinyl ethers in the presence of TCNQ

1.7 Fracture mechanics of polymeric materials

Although thermal, chemical and other environmental factors can cause damage in polymers, impact and cyclic fatigue associated failures are receiving the most attention for structural applications of polymeric materials.[77] Both of these failure mechanisms proceed via crack propagation, with a monotonic load experienced during impact type incidents and cyclic loads experienced during fatigue. Crack propagation[78-80] and the mechanics[81,82] associated with these failures in polymeric materials have been modeled and researched extensively.

For a crack to propagate, the energy released during cracking must be equal to, or larger than the energy required generating new surfaces on the material.[83] Although new models for crack propagation are still being developed[84,85], most crack propagation modeling is based on a parameter called the (K_I).[86,87] During crack opening type failure growth, K_I is related to crack depth, material/crack geometry and the applied stresses. As the applied stress and crack geometry change during monotonic or cyclic loading, a critical stress intensity factor (K_{IC}) is reached and then crack growth occurs. During an impact damage incident (consisting of a monotonic load) the extent of crack propagation is related to the maximum stress intensity factor (K_{IMax}) experienced. During fatigue-type damage crack propagation is related to both K_{IMax} and the change in K_I during cycling (ΔK).[88] In order to heal cracked polymers, the fractured surfaces need to be resealed or alternatively crack growth must be impaired.

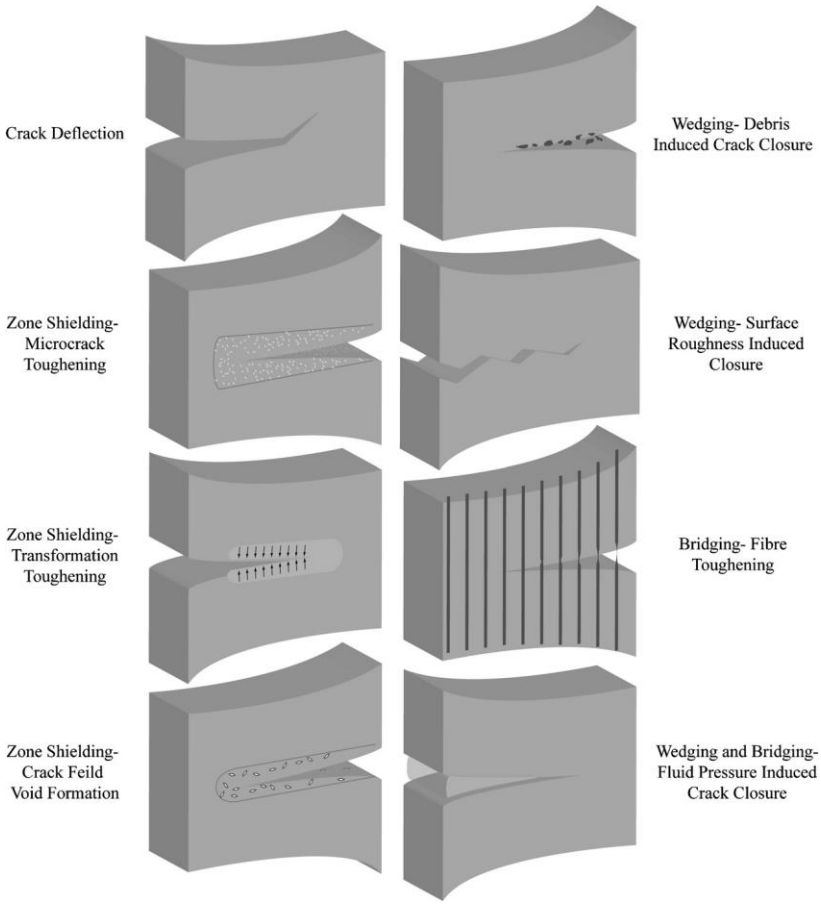

Figure 1.13: Extrinsic mechanisms of crack growth retardation. Reprinted from Int. J. Fract., 100:55–83, Ritchie et al, copyright (1999), with permission from Springer.

A number of methods to retard crack growth are demonstrated in figure 1.13.[89] Basically, crack growth retardation occurs when energy is dissipated within the loaded material without extending an existing crack. Intrinsic crack growth retardation can be achieved through selection of appropriate monomer and curing agent system[90,91], varying the ratio of curing components[92–94], or use of additives or modifiers.[95–97] These intrinsic approaches to crack growth retardation provide alternative avenues for stress relief within the original structure, and they are generally used to improve the intrinsic properties of the virgin materials rather than to heal-damaged components.

Extrinsic crack growth retardation mechanisms are used as the primary method of repairing damage in both the traditional and the self-healing techniques. This generally involves dissipation of energy away from the propagating crack tip via a mechanical change behind the crack tip. Additives can act as intrinsic toughness and as extrinsic toughness when they are stretched or compressed in the void behind the crack tip.[98] A more common extrinsic

toughening mechanism is that of patching, where a cracked surface is covered or filled with a rigid material. Patching can provide bridging- and wedging-type mechanical support for the damaged material, retarding crack propagation and restoring structural integrity to the polymer composite.

1.8 The aim of the project

A self-healing process based on the formation linear or cross-linked polymer from the spontaneous reaction of electron-rich olefins (donor) with electron-poor olefins (accepter) without the use of a catalyst or initiator will be explored.

Initially, the reactions between the liquid electron donor monomers (4-methoxystyrene, styrene, 2-vinylpyridine, and divinylbenzene) and the solid acceptor monomers (maleic anhydride, N-methylmaleimide, ethoxymethylene malononitrile, maleic acid, tetracyanoethylene, acrylonitrile, and dimethyl maleate) will be tested in the sample vials at ambient temperature or at 50 °C to evaluate their reaction profile. The electron donor and acceptor monomers producing linear or cross-linked polymer, will be used for designing the self-healing system. The product of these reactions will be tested for their solubility in organic solvents. The linear polymer product will be characterised by ^{1}H and ^{13}C NMR, size exclusion chromatography (SEC), and FTIR. The cross-linked polymer will be characterised by sol-gel technique and FTIR.

The next stage will involve encapsulation of liquid monomers. The liquid healing agents, electron-rich monomers, will be encapsulated in a process involving in-situ polymerisation of urea-formaldehyde in oil-water emulsion. The obtained micro-capsules will be characterised by scanning electron microscopy (SEM). The sieves will be used to select unique size (100-250 μm) of those micro-capsules for self-healing investigations.

The third stage will be preparation of specimens for the evaluation of fracture toughness. The epoxy matrix of the self-healing specimen will be bisphenol-A based epoxide cured by diethylenetriamine. The fracture toughness of background specimen (pure epoxy resin specimen, specimen only containing solid healing agents, or specimen only containing micro-capsules) will be investigated by compact tension geometry.

The last stage will be the self-healing performance assessment. The self-healing performance will be assessed by fracture toughness recovery of specimen containing solid healing agents and micro-capsules containing liquid healing agents. The self-healing potential of the system designed in this project will be first evaluated for their healing efficiency by injecting the liquid healing agents into the induced crack of the specimen containing only solid healing agents. Then, the autonomous self-healing will be performed on specimen containing micro-capsules and solid healing agents in the epoxy resin matrix.

Reference

1. Zwaag, S. (2007) (ed.) *Self-Healing Materials,* Springer.
2. Zang, M. Q. (2008) 'Self-Healing in Polymers and Polymer Composites. Concepts, Realisation and Outlook: A Review', *Polymer Letters*, 2(4):238–50.
3. Blaiszik, B. J., *et al.* (2010) 'Self-Healing Polymers and Composites', *Annu. Rev. Mater. Res.*, 40:179-211.
4. Williams, K. A., Dreyer, D. R., and Bielawski, C. W. (2008) 'The Underlying Chemistry of Self-Healing Materials', *MRS Bull*, 33:759-65.
5. Rule, J. D. *et al.* (2005) 'Wax-Protected Catalyst Microspheres for Efficient Self-Healing Materials', *Adv. Mater.,* 17:205.
6. Bergman, S. D., Wudl, F. (2008) 'Mendable Polymers', *J Mater Chem*, 18:41-62.
7. White, S. R., *et al.* (2001) 'Autonomic Healing of Polymer Composites', *Nature*, 409(6822):794–97.
8. Billiet, S., *et al.* (2013) 'Chemistry of Crosslinking Processes for Self-Healing Polymers', *Macromol Rapid Commun*, 34:290-309.
9. Olugebefola, S. C., *et al.* (2014) 'Structural Reinforcement of Microvascular Networks Using Electrostatic Layer-by-Layer Assembly with Halloysite Nanotubes', *Soft Matter*, 10:544-8.
10. Hansen, C. J., *et al.* (2009) 'Self-healing Materials with Interpenetrating Microvascular Networks', *Adv Mater*, 21:4143-7.
11. Bai, Y., Chen, Y., Wang, Q. and Wang, T. (2014) 'Poly(vinyl butyral) Based Polymer Networks with Dual-Responsive Shape Memory and Self-Healing Properties', *J Mater Chem A,* 2:9169-77.
12. Burnworth, M., *et al.* (2011) 'Optically Healable Supramolecular Polymers', *Nature,* 472:334-7.
13. Coulibaly, S., *et al.* (2014) 'Reinforcement of Optically Healable Supramolecular Polymers with Cellulose Nanocrystals', *Macromolecules*, 47:152-160.
14. Chen, X., *et al*. (2002) 'A Thermally Remendable Cross-Linked Polymeric Material', *Science*, 295:1698-1702.
15. Adzima, B. J., Kloxin, C. J., and Bowman, C. N. (2010) 'Externally Triggered Healing of a Thermoreversible Covalent Network via Self-Limited Hysteresis Heating', *Adv Mater*, 22:2784-7.

16. Blaiszik, B. J., *et al.* (2010) 'Self-Healing Polymers and Composites', *Annu. Rev. Mater. Res.*, 40:179-211.
17. Grubbs, R. H., and Tumas, W. (1989) 'Polymer Synthesis and Organotransition Metal Chemistry', *Science*, 243:907-915.
18. Rule, J. D., and Moore, J. S. (2002) 'ROMP Reactivity of Endo- and Exo-Dicyclopentadiene', *Macromolecules*, 35: 7878-82.
19. Wilson, G. O., *et al.* (2008) 'Autonomic Healing of Epoxy Vinyl Esters via Ring Opening Metathesis Polymerisation', *Adv. Funct. Mater.,* 18(1):44–52.
20. Jung, D., *et al.* (1997) 'Self-healing composites using embedded micro-spheres', *Composite and Functionally Graded Materials*, 80:265–75.
21. White, S. R., *et al.* (2001) 'Autonomic Healing of Polymer Composites', *Nature*, 409(6822):794–97.
22. Majchrzak, M., Hine, P., and Khosravi, E. (2012) 'An Autonomous Self-Healing System Based on ROMP of Norbornene Dicarboximide Monomers', *Polymer*, 53: 5251-5257.
23. Brown, E. N., Sottos, N. R., and White, S. R. (2002) 'Fracture Testing of A Self-Healing Polymer Composite', *Exp. Mech,* 42(4):372–9.
24. Brown, E. N., White, S. R., and Sottos, N. R. (2005) 'Retardation and Repair of Fatigue Cracks in A Micro-capsule Toughened Epoxy Composite. II. In-situ Self-Healing', *Compos. Sci. Technol.,* 65(15–16):2474–80.
25. Brown, E. N., White, S. R., and Sottos, N. R. (2004) 'Micro-capsule Induced Toughening in A Self-Healing Polymer Composite', *J. Mater. Sci.,* 39(5):1703–10.
26. Rule, J. D., Sottos, N. R., and White, S. R. (2007) 'Effect of Micro-capsule Size on the Performance of Self-Healing Polymers', *Polymer*, 48(12):3520–9.
27. Kirkby, E. L., *et al.* (2008) 'Embedded Shape-Memory Alloy Wires for Improved Performance of Self-Healing Polymers', *Adv. Funct. Mater.,* 18(15):2253–60.
28. Jones, A. S., *et al.* (2007) 'Life Extension of Self-Healing Polymers with Rapidly Growing Fatigue Cracks', *J. R. Soc. Interface*, 4(13):395–403.
29. Kirkby E.L., *et al.* (2009) 'Performance of Self-Healing Epoxy with Microencapsulated Healing Agent and Shape Memory Alloy Wires', *Polymer*, 50(23):5533–8.
30. Chipara, M. D., Chipara M., Shansky, E. and Zaleski, J.M. (2009) 'Self-Healing of High Elasticity Block Copolymers', *Polym. Adv. Technol.,* 20(4):427–31.
31. Keller, M. W., White, S. R., and Sottos, N. R. (2007) 'A Self-Healing Poly(dimethyl siloxane) elastomer', *Adv. Funct. Mater.,* 17(14):2399–404.

32. Cho, S. H., White, S. R., and Braun, P. V. (2009) 'Self-Healing Polymer Coatings', *Adv. Mater.,* 21(6):645–9.
33. Beiermann, B. A., Keller, M. W., and Sottos, N. R. (2009) 'Self-Healing Flexible Laminates for Resealing of Puncture Damage', *Smart Mater. Struct.,* 18(8):085001.
34. Yuan, Y. C., *et al.* (2008) 'Self-Healing Polymeric Materials Using Epoxy/Mercaptan as the Healant', *Macromolecules*, 41(14):5197–202.
35. Zako, M., and Takano, N. (1999) 'Intelligent Material Systems Using Epoxy Particles to Repair Microcracks and Delamination Damage in GFRP', *J. Intell. Mater. Syst. Struct.,* 10(10):836–41.
36. Caruso, M. M., *et al.* (2007) 'Full recovery of fracture toughness using a nontoxic solvent-based self-healing system', *Adv. Funct. Mater.*, 18(13):1898–904.
37. Cho, S. H., *et al.* (2006) 'Polydimethylsiloxane-Based Self-healing Materials', *Adv. Mater*, 18(8):997–1000.
38. Huang, J., *et al.* (2009) 'Rapid Fabrication of Bio-Inspired 3D Microfluidic Vascular Networks', *Adv. Mater*, 21(35):3567–71.
39. Williams, H. R., *et al.* (2008) 'Biomimetic Reliability Strategies for Self-Healing Vascular Networks in Engineering Materials', *J Roy Soc Interface*, 5:735–47.
40. Farrell, B. D., Dussourd, D. E., and Mitter, C. (1991) 'Escalation of Plant Defense: Do Latex and Resin Canals Spur Plant Diversification?', *Am Naturalist*, 138:881–900.
41. Toohey, K. S., *et al.* (2007) 'Self-Healing Materials with Microvascular Networks', *Nat Mater*, 6:581–5
42. Williams, H. R., Trask, R. S., and Bond, I. P. (2007) 'Self-Healing Composite Sandwich Structures', *Smart Mater Struct*, 16:1198–207.
43. Hayes, S. A., *et al.* (2007) 'A self-healing thermosetting composite material', *Composites A* 38(4):1116–20
44. Chen, X. X., *et al.* (2002) 'Athermally Remendable Cross-Linked Polymeric Material', *Science*, 295(5560):1698–702.
45. Plaisted, T. A., and Nemat-Nasser, S. (2007) 'Quantitative Evaluation of Fracture, Healing and Rehealing of a Reversibly Cross-Linked Polymer', *Acta Mater*, 55(17):5684–96.
46. Park, J. S., *et al.* (2008) 'Towards Development of A Self-Healing Composite Using a Mendable Polymer and Resistive Heating', *J. Compos. Mater.,* 42(26):2869–81.

47. Kalista, S. J., Ward, T. C., and Oyetunji, Z. (2007) 'Self-Healing of Poly(ethylene-comethacrylic acid) Copolymers Following Projectile Puncture', *Mech. Adv. Mater. Struct*., 14(5):391–7
48. Varley, R. J., van der Zwaag, S. (2008) 'Towards an Understanding of Thermally Activated Self-Healing of an Ionomer System During Ballistic Penetration', *Acta Mater,* 56(19):5737–50.
49. Cordier, P., *et al.* (2008) 'Self-Healing and Thermoreversible Rubber From Supramolecular Assembly' *Nature,* 451(7181):977 – 80.
50. Wu, D., Meure, S., and Solomon, D. (2008) 'Self-Healing Polymeric Materials: A Review of Recent Developments', *Progress in Polymer Science,* 33(5): 479-522.
51. Jud, K. and Kausch, H. H. (1979) 'Load Transfer Through Chain Molecules after Interpenetration at Interfaces', *Polym Bull*, 1:697–707.
52. Dubey, R., Shami, T. C., and Rao, K. U. (2009) 'Micro-encapsulation Technology and Applications', *Defence Science Journal*, 59(1):82-95.
53. Green, B. K. and Schleicher, L. (1957) 'Oil Containing Microscopiccapsules and Method of Making Them', *US Patent* 2800457
54. Fergason, J. L. (1985) 'Polymer Encapsulated Nematic Liquid Crystals for Display and Light Control Applications', *SID Int. Symp. Digest*, 16:68-70.
55. Ghosh, S. K. (2006) (ed.) *Functional Coatings,* WILEY-VCH GmbH & Co. KGaA, Weinheim.
56. Brown, E. N., *et al.* (2003) 'In-situ Poly(urea-formaldehyde) Micro-encapsulation of Dicyclopentadiene', *J. Microencapsul.,* 20(6):719–30.
57. Lee, H. Y., Lee, S. J., Cheong, I. W. and Kim, J. H. (2002) 'Micro-encapsulation of Fragrant Oil via in-situ Polymerisation: Effects of pH and Melamine-Formaldehyde Molar Ratio', *J. Micro-encapsulation*, 19(5):559-69
58. Jung, D., *et al.* (1997) 'Self-healing composites using embedded micro-spheres', *Composite and Functionally Graded Materials*, 80:265–75.
59. Cowie J. M. G. and Arrighi V. (2008) *Polymers: Chemistry and Physics of Modern Materials*, CRC Press
60. Billmeyer, F. W. (1984) *Textbook of Polymer science 3rd Edition*, Wiley-Intersicence
61. Evenson, S. A.; Fail, C. A.; Badyal, J. P. S. Journal of Physical Chemistry Part B 1998, 102, 3500.

62. Iwatsuki, S. and Yamashita, Y. (1971) 'Radical alternating copolymerisations' *Prog. Polym. Sci. Jpn.* 2(1):167.
63. Kim, T., Sarker, H., and Bauld, N. L. (1995) 'On the Long-Standing Question of an ET or Polar Mechanism for the Cycloaddition of Tetracyanoethylene with Electron Rich Alkenes', *J. Chem Soc., Perkin Trans. 2*, 3:577-80.
64. Hall, H. K. (1983) 'Bond-Forming Initiation in Spontaneous Addition and Polymerisation Reactions of Alkenes', *Chem., Int. Ed. Engl.,* 22(6):440-55.
65. Hoffmann, R. and Woodward, R. B. (1965) 'Selection Rules for Concerted Cycloaddition Reactions', *J. Am. Chem. Soc.* 87(9):2046-8.
66. Huisgen, R. (1977) 'Can tetramethylene intermediates be intercepted?', *Acc. Chem. Res.* 10(6):199-206.
67. Gotoh, T., Padias, A. B., and Hall, H. K. Jr., (1986) 'Zwitterionic Tetramethylenes as the Common Intermediates in the Cycloaddition and Polymerisation Reactions of N-Vinylcarbazole with Electrophilic Tetrasubstituted Ethylenes: A New Explanation for Charge-Transfer Initiation', *J. Am. Chem. Soc.*, 108:4920-31.
68. Hall, H. K., and Padias, A. B., (1990) 'Zwitterion and Diradical Tetramethylenes as Initiators of "Charge-Transfer" Polymerisations', *Acc. Chem. Res.,* 23:3-9.
69. Hall, H. K. and Padias, A. B. (1997) 'Bond Forming Initiation of "Charge-Transfer" Polymerisations and the Accompanying Cycloadditions', *Acc. Chem. Res.* 30:322-29
70. Mistuad, Y., *et al.* (2004) 'Spontaneous Polymerisation Mechanism of Electron-Accepting Substituted Quinodimethane with Vinyl Ether and Cyclic Ketene Acetal', *Wiley InterScience*, DOI: 10.1002/pola.20235
71. Hall, H. K., Padias, A. B., Pandya, A., and Tanaka, H. (1987) 'A tetramethylene diradical as the initiating species in the spontaneous charge-transfer copolymerisation of p-methoxystyrene with dimethyl cyanofumarate', *Macromolecules*, 20(2):247-54
72. Lee, C. and Hall, H. K. (1989) 'Photocopolymerisations of electron-rich olefins with electron-poor olefins by irradiation of their EDA complexes', *Macromolecules*, 22(1):21-5
73. Renaud, P. and Sibi, M. P. (2001) (ed.) *Radicals in Organic Synthesis*, Wiley-VCH Verlag GmbH.
74. Gotoh, T., Padias, A. B., and Hall, H. K. Jr., (1986) 'Zwitterionic Tetramethylenes as the Common Intermediates in the Cycloaddition and Polymerisation Reactions of N-Vinylcarbazole with Electrophilic Tetrasubstituted Ethylenes: A New Explanation for Charge-Transfer Initiation', *J. Am. Chem. Soc.*, 108:4920-31.

75. Abdelkader, M., Padias, A. B., and Hall, H. K. (1987) 'Cationic polymerisation of nitrogen-containing electron-rich vinyl monomers by electrophilic olefins and their cyclobutane cycloadducts', *Macromolecules*, 20(5):944-8
76. Hall, H. K. *et al.* (1990) 'p-Phenylenetetramethylene diradical and zwitterion intermediates in the spontaneous copolymerisations of electrophilic p-quinodimethanes with electron-rich olefins', *Macromolecules*, 23(4):913-7
77. Baker, A. A, Jones, R., and Callinan, R. J. (1985) 'Damage Tolerance of Graphite Epoxy Composites', *Compos Struct*, 4:15–44.
78. Fischer, M., Martin, D., and Pasquier, M. (1995) 'Fatigue-Crack Growth in Cross-Linked Polymers', *Macromol Symp*, 93:325–36.
79. Kawaguchi, T. and Pearson, R. A. (2004) 'The Moisture Effect on the Fatigue Crack Growth of Glass Particle and Fiber Reinforced Epoxies with Strong and Weak Bonding Conditions Part 1: Macroscopic Fatigue Crack Propagation Behavior', *Compos Sci Technol*, 64:1981–9.
80. Kawaguchi, T. and Pearson, R. A. (2004) 'The Moisture Effect on the Fatigue Crack Growth of Glass Particle and Fiber Reinforced Epoxies with Strong and Weak Bonding Conditions Part 2: A Microscopic Study on Toughening Mechanism', *Compos Sci Technol*, 64:1991–2007.
81. Morgan, R. J. and O'Neal, J. E. (1977) 'Microscopic Failure Processes and Their Relation to Structure of Amine-Cured Bis-Phenola- Diglycidyl Ether Epoxies', *J Mater Sci*, 12:1966–80.
82. Richardson, M. O. W. and Wisheart, M. J. (1996) 'Review of Low-Velocity Impact Properties of Composite Materials', *Compos Part A—Appl Sci Manuf*, 27:1123–31.
83. Kinloch, A. J. (1985) 'Mechanics and Mechanisms of Fracture of Thermosetting Epoxy Polymers', *Adv Polym Sci*, 72: 45–67.
84. Maiti, S. and Geubelle, P. H. (2005) 'A Cohesive Model for Fatigue Failure of Polymers', *Eng Fract Mech*, 72:691–708.
85. Maiti, S and Geubelle, P. H. (2006) 'Cohesive Modeling of Fatigue Crack Retardation in Polymers: Crack Closure Effect', *Eng Fract Mech*, 73:22–41.
86. Ritchie, R. O. (1999) 'Mechanisms of Fatigue-Crack Propagation in Ductile and Brittle Solids', *Int J Fract*, 100:55–83.
87. Sauer, J. A. and Richardson, G. C. (1980) 'Fatigue of Polymers', *Int J Fract*, 16:499–532.

88. Vasudeven, A. K., Sadananda, K., and Louat, N. (1994) 'A Review of Crack Closure, Fatigue-Crack Threshold and Related Phenomena', *Mater Sci Eng Part A—Struct Mater Prop Microstruct Process*, 188:1–22.
89. Ritchie, R. O. (1988) 'Mechanisms of Fatigue Crack-Propagation in Metals, Ceramics and Composites—Role of Crack Tip Shielding', *Mater Sci Eng Part A—Struct Mater Prop Microstruct Process*, 103:15–28.
90. Espuche, E., *et al.* (1995) 'Influence of Cross-Link Density and Chain Flexibility on Mechanical-Properties of Model Epoxy Networks', *Macromol Symp*, 93:107–15.
91. Pham, H. Q, and Marks, M. J. (1991) 'Epoxy Resins' in Kirk, R. E., *et al.* (ed.) *Encyclopaedia of Chemical Technology*, New York: Wiley, 347–471.
92. Kim, S. L., *et al.* (1978) 'Tensile, Impact and Fatigue Behaviour of an amine-cured epoxy-resin', *Polym Eng Sci*, 18: 1093–100.
93. Shin, S. and Jang, J. (1997) 'The Effect of Amine/Epoxy Ratio on the Fracture Toughness of Tetrafunctional Epoxy Resin', *Polym Bull*, 39:353–9.
94. Wingard, C. D, and Beatty, C. L. (1990) 'Cross-Linking of an Epoxy with a Mixed Amine as a Function of Stoichiometry, 2: Final Properties via Dynamic Mechanical Spectroscopy', *J Appl Polym Sci*, 41:2539–54.
95. Kim, N. H. and Kim, H. S. (2005) 'Micro-Void Toughening of Thermosets and Its Mechanism', *J Appl Polym Sci*, 98:1290–5.
96. Kinloch, A. J. and Taylor, A. C. (2006) 'The Mechanical Properties and Fracture Behaviour of Epoxy-Inorganic Micro- and Nanocomposites', *J Mater Sci*, 41:3271–97.
97. Unnikrishnan, K. P. and Thachil, E. T. (2006) 'Toughening of Epoxy Resins', *Des Monomers Polym*, 9:129–52.
98. Coleman, J. N., *et al.* (2006) 'Small but Strong: A Review of the Mechanical Properties of Carbon Nanotube–Polymer Composites', *Carbon*, 44:1624–52.

Chapter 2

Linear Spontaneous Copolymerisation

2.1 Introduction

The spontaneous (co-)polymerisation of electron-rich and electron-poor olefins was investigated to produce linear polymers.

Four electron donor monomers (1-4, figure 2.1): 4-methoxystyrene (4MeOSt) (1), styrene (St) (2), 2-vinylpyridine (2VP) (3), and 4-vinylcarbazole (4VC) (4) were chosen. Also, six electron acceptor monomers (5-11, figure 2.1): maleic anhydride (MA) (5), N-methylmaleimide (MeMal) (6), ethoxymethylene malononitrile (EtOCN) (7), maleic acid (8), tetracyanoethylene (TCNE) (9), acrylonitrile (AN) (10), and dimethyl maleate (DMa) (11) were selected for investigation of spontaneous (co-)polymerisation reactions with electron donor monomers named above, in bulk.

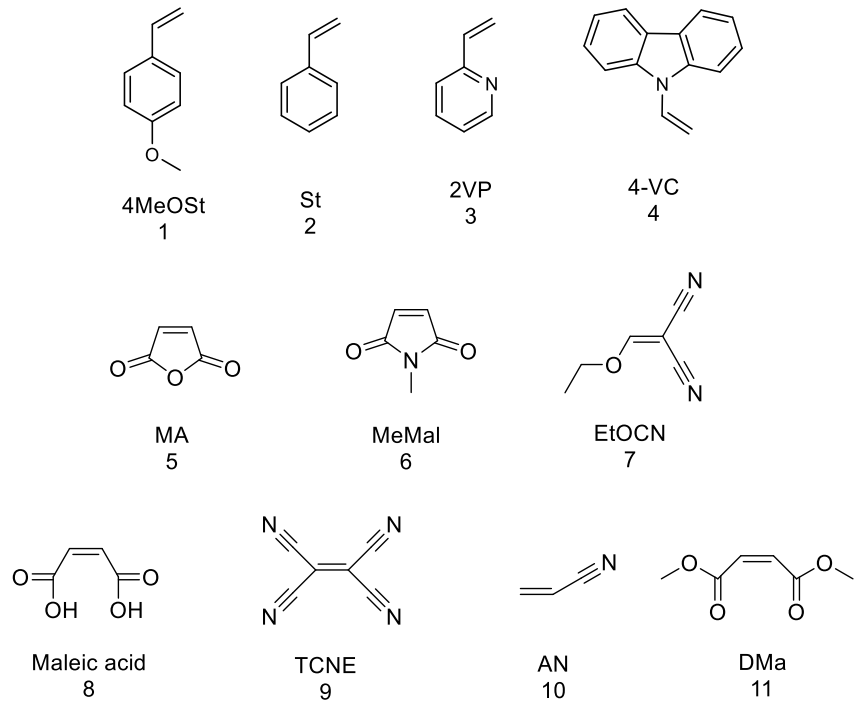

Figure 2.1: Electron-donor (1-4) and electron-acceptor monomers (5-11)

The reactions between the electron donor and acceptor monomers, which could produce linear polymer product, were carried out for further characterisation. The electron donor monomers (liquid monomers): 4MeOSt and St were selected and electron acceptor monomers (solid monomers): MA, MeMal, and EtOCN were chosen. Due to 4-VC is solid electron donor monomer, it is difficult to be applied in self-healing process design. And there is no solid product formed by 2VP with any electron-poor monomers, maleic acid, TCNE, AN, or DMa with any electron-rich monomers, hence those monomers will not be further

investigated.

2.2 Materials

Maleic anhydride (MA) (≥99.0%), 4-methoxystyrene (4MeOSt) (97%), styrene (St) (≥99.0%), ethoxymethylene malononitrile (EtOCN) (98%), and N-methylmaleimide (MeMal) (97%) were purchased from Aldrich and used as supplied. Dichloromethane (DCM) (analytical grade, Fisher Scientific), toluene (Analytical Grade, Fisher Scientific), acetone (analytical grade, Fisher Scientific), tetrahydrofuran (THF) (anhydrous, ≥99.9%), chloroform (analytical reagent grade, 99.5%), were used as supplied.

2.3 Instrumentation

NMR spectra were either recorded on a Bruker Avance 400 spectrometer at 400.0 MHz (^{1}H) and 100.6 MHz (^{13}C); or a Varian Inova 500 spectrometer at 499.8 MHz (^{1}H, HSQC) and 125.7 MHz (^{13}C, HMBC). All chemical shifts were referenced to the residual of the deuterated solvent.

Molecular weight analysis was carried out by size exclusion chromatography (SEC) on a Viscotek TDA 302 with refractive index detector. Two 300 mm PLgel 5 μm mixed C columns (with a linear range of molecular weight from 200 to 2 000 000 g/mol) were used. THF was used as the eluent with a flow rate of 1.0 mL/min at 30 °C.

FTIR spectra were recorded on Perkin Elmer 1600 series FTIR spectrometer fitted with a golden gate. The samples were used as solids or liquid. The IR spectra were collected from 4000 to 400 cm^{-1}, with 10 scans per spectrum and 4.00 cm^{-1} resolution. The IR spectra was analysed using Infrared spectroscopy correlation table.[1]

2.4 Experimental

2.4.1 Reaction of maleic anhydride with 4-methoxystyrene

MA (0.98 g, 10 mmol) and 4MeOSt (1.37 g, 10 mmol) were mixed in a sample vial at ambient temperature, upon which the mixture became yellow. The mixture was heated to 50 °C upon which MA dissolved completely in 4MeOSt and the mixture became viscous after 2 h. The mixture was kept at 50 °C for 48 h. THF (5 mL) was added to dissolve the yellow solid and the mixture precipitated in methanol (50 mL). The solid product was filtered and dried in a vacuum oven, giving 1.26 g white solid, 53 % yield.

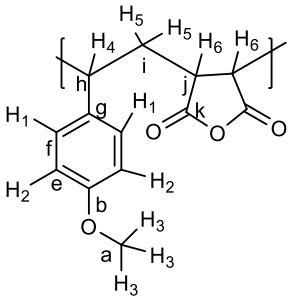

^{1}H NMR, (d_6-acetone, 500 MHz, δ(ppm)): 6.66 (4H, H_1 and H_2), 3.74 (3H, H_3), 3.26 (2H, H_6), 1.88 (1H, H_4), 1.55 (2H, H_5). **^{13}C NMR**, (d_6-acetone, 126MHz, δ(ppm)): 172.7 (k), 158.8 (b), 137.6 (g), 129.4 (e), 114.1 (f), 54.6 (a), 51.7 (j), 43.0 (i), 39.8 (h). **SEC**, M_n = 85845 Da with dispersity (Đ) of 3.11. **FTIR**, (cm^{-1}): 1779 (C=O), 1610 (aromatic C=C), 1511 (aromatic C=C), 1247 (C-O), 830 (aromatic C-H).

Table 2.1: Reaction of 4MeOSt and MA (LP01-07)

Reaction	4MeOSt (g, mmol)	MA (g, mmol)	4MeOSt : MA	Temperature (˚C)	Yield (%)
LP01	1.37, 10	0.98, 10	1:1	50	53
LP02	2.74, 20	0.98, 10	2:1	50	44
LP03	2.74, 20	0.49, 5	4:1	50	29
LP04	5.48, 40	0.49, 5	8:1	50	17
LP05	1.37, 10	0.10, 1	10:1	50	12
LP06	2.74, 20	0.10, 1	20:1	50	<1
LP07	1.37, 10	0.98, 10	1:1	RT	36

LP01-06 were prepared with different ratio of starting materials and kept for 48 h at 50 °C (table 2.1). After the same recovery process as LP01, LP02-06 were obtained with 53%, 44%, 29%, 17%, 12%, and 1 % yields, respectively. LP07 was repeated with the same amount of starting materials as LP01 at ambient temperature and kept for 48 h. Similar recovery procedure gave 0.85 g white solid, 36 % yield.

2.4.2 Reaction of N-methylmaleimide with 4-methoyxtryrene

MeMal (1.11 g, 10 mmol) and 4MeOSt (1.37 g, 10 mmol) were mixed in a sample vial at ambient temperature, upon which the clear liquid became yellow. The mixture was heated to 50 °C, however, MeMal did not dissolved completely in 4MeOSt upon heating. The MeMal dissolved and the mixture became viscous after 24 h. The mixture was kept at 50 °C for further 48 h. THF (5 mL) was added to dissolve the mixture and the mixture precipitated in methanol (50 mL). The white solid was filtered and dried in a vacuum oven, giving 1.81g, 46% yield.

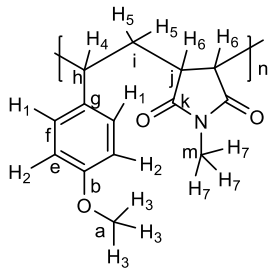

^{1}H NMR, ($CDCl_3$, 500 MHz, δ(ppm)): 6.65 (4H, H_1 and H_2), 3.75 (3H, H_3), 2.73 (3H, H_7), 2.47 (1H, H_4), 2.20 (2H, H_5), 1.95 (2H, H_6). **^{13}C NMR**, ($CDCl_3$, 126MHz, δ(ppm)): 178.3 (k), 159.2 (b), 129.9 (e), 129.8 (g), 114.2 (f), 55.3 (a), 51.7 (h), 42.0 (j), 35.1 (i), 24.8 (m). **SEC**, M_n = 60467 Da with PDI=4.70. **FTIR**, (cm^{-1}) 1696 (C=O), 1610 (aromatic C=C), 1512 (aromatic C=C), 1250 (C-O), 1032 (C-N), 831 (aromatic C-H).

Table 2.2: Reaction of 4MeOSt and MeMal (LP08-13)

Reaction	4MeOSt (g, mmol)	MeMal (g, mmol)	4MeOSt : MeMal	Temperature (˚C)	Yield (%)
LP08	1.37, 10	1.11, 10	1:1	50	46
LP09	2.74, 20	1.11, 10	2:1	50	41
LP10	2.74, 20	0.56, 5	4:1	50	10
LP11	5.48, 40	0.56, 5	8:1	50	0
LP12	1.37, 10	0.11, 1	10:1	50	0
LP13	1.37, 10	1.11, 10	1:1	RT	31

LP08-12 were prepared with different ratio of starting materials and kept for 48 h at 50 °C (table 2.2). After the same recovery process as LP08, LP09 and 10 were obtained with 41 and 10 % yields, respectively, and LP11 and 12 did not produce any solid. LP13 was prepared with the same amount of starting materials as LP08 at ambient temperature and kept for 48 h. Similar recovery procedure gave 0.77 g white solid, 31 % yield.

2.4.3 Reaction of ethoxymethylene malononitrile with 4-methoxystyrene

EtOCN (1.22 g, 10 mmol) and 4MeOSt (1.37 g, 10 mmol) were mixed in a sample vial at ambient temperature, upon which became brown. The mixture was heated to 50 °C and became viscous after 24 h and was kept for another 24 h. THF (5 mL) was added to dissolve the mixture and then precipitated in methanol (50 mL). The white solid was filtered and dried in a vacuum oven, giving 1.01 g, 38 % yield.

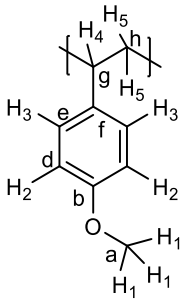

^{1}H NMR, (DMSO-d_6, 500 MHz, δ(ppm)): 6.61 (4H, H_2 and H_3), 3.65 (3H, H_1), 1.74 (1H, H_4), 1.37 (2H, H_5). **^{13}C NMR**, (DMSO-d_6, 126MHz, δ(ppm)): 157.6 (b), 137.9 (f), 128.5 (d), 113.7 (e), 55.3 (a), 44.3 (h), 39.0 (g). **SEC**, M_n = 22911 Da with dispersity (Đ) of 1.63. **FTIR**, (cm^{-1}): 1609 (aromatic C=C), 1509 (aromatic C=C), 1242 (C-O), 826 (aromatic C-H).

Table 2.3: Reaction of 4MeOSt and EtOCN (LP14-21)

Reaction	4MeOSt (g, mmol)	EtOCN (g, mmol)	4MeOSt : EtOCN	Temperature (˚C)	Yield (%)
LP14	1.37, 10	1.22, 10	1:1	50	75
LP15	2.74, 20	1.22, 10	2:1	50	69
LP16	2.74, 20	0.61, 5	4:1	50	72
LP17	5.48, 40	0.61, 5	8:1	50	1
LP18	1.37, 10	0.12, 1	10:1	50	1
LP19	1.37, 10	1.22, 10	1:1	RT	0
LP20	1.37, 10	1.22, 10	1:1	30	0
LP21	1.37, 10	1.22, 10	1:1	40	54

LP15-18 were prepared with different ratio of starting materials and kept for 48 h at 50 °C (table 2.3). After the same recovery process as LP14, LP15-18 were obtained with 46%, 61%, 9%, and 2 % yield, respectively. LP19, LP20, and LP21 were prepared with the same amount of starting materials as LP14 at ambient temperature, 30 and 40 °C, respectively. They were kept for 7 days. LP19 and 20 did not form any solid product; however, LP21 gave 29% yield after 7 days.

2.4.4 Reaction of maleic anhydride with styrene

St (1.04 g, 10 mmol) and MA (0.98 g, 10 mmol) were mixed in a sample vial at ambient temperature, upon which the mixture became white. The mixture was kept at 50 °C for 5 days. THF (5 mL) was added to dissolve the mixture and was precipitated in methanol (50 mL). The white solid product was filtered and dried in a vacuum oven, giving 0.61 g, 21 % yield. The reaction was repeated with the same amount starting materials and kept at 50 °C

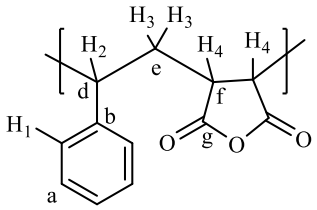

^{1}H NMR, (d_6-acetone, 500 MHz, δ(ppm)): 7.23 (5H, H_1), 3.27 (1H, H_2), 2.30 (2H, H_3), 1.61 (2H, H_4). **^{13}C NMR**, (d_6-acetone, 126MHz, δ(ppm)): 173.5 (g), 146.7 (b), 128.6 (a), 52.3 (d), 42.7 (f), 35.1 (e). **SEC**, M_n = 14407 Da with dispersity (Đ) of 1.63. **FTIR**, (cm^{-1}): 1776 (C=O), 1454-1496 (aromatic C=C), 1225 (C-O), 922 (aromatic C-H).

Table 2.4: Reaction of St and MA (LP22-27)

Reaction	St (g, mmol)	MA (g, mmol)	St : MA	Temperature (˚C)	Yield (%)
LP22	1.04, 10	0.98, 10	1:1	50	29
LP23	2.08, 20	0.98, 10	2:1	50	18
LP24	2.08, 20	0.49, 5	4:1	50	14
LP25	4.16, 40	0.49, 5	8:1	50	0
LP26	1.04, 10	0.10, 1	10:1	50	0
LP27	1.04, 10	0.98, 10	1:1	RT	0

LP22-26 were prepared with different ratio of starting materials and kept for 7 days at 50 °C (table 2.4). After the same recovery process as LP22, LP23-26 were obtained with 38%, 33%, 18%, 0, and 0 yields, respectively. LP27 was repeated with the same amount of starting materials as LP22 at ambient temperature and kept for 7 days. The mixture was left for 7 days. Similar recovery procedure gave none solid, 0 % yield.

2.5 Results and discussion

2.5.1 Maleic anhydride with 4-methoxystyrene

The spontaneous copolymerisation of 4MeOSt and MA was carried out at 50 °C and at ambient temperature (scheme 2.1) and a yellow solid was produced, which was found to be soluble in acetone and THF. The polymer product obtained at 50 °C (LP01) was characterised by ^{1}H and ^{13}C NMR spectroscopy.

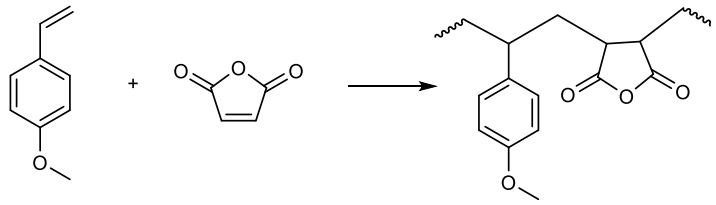

Scheme 2.1: Spontaneous copolymerisation reaction of 4MeOSt and MA

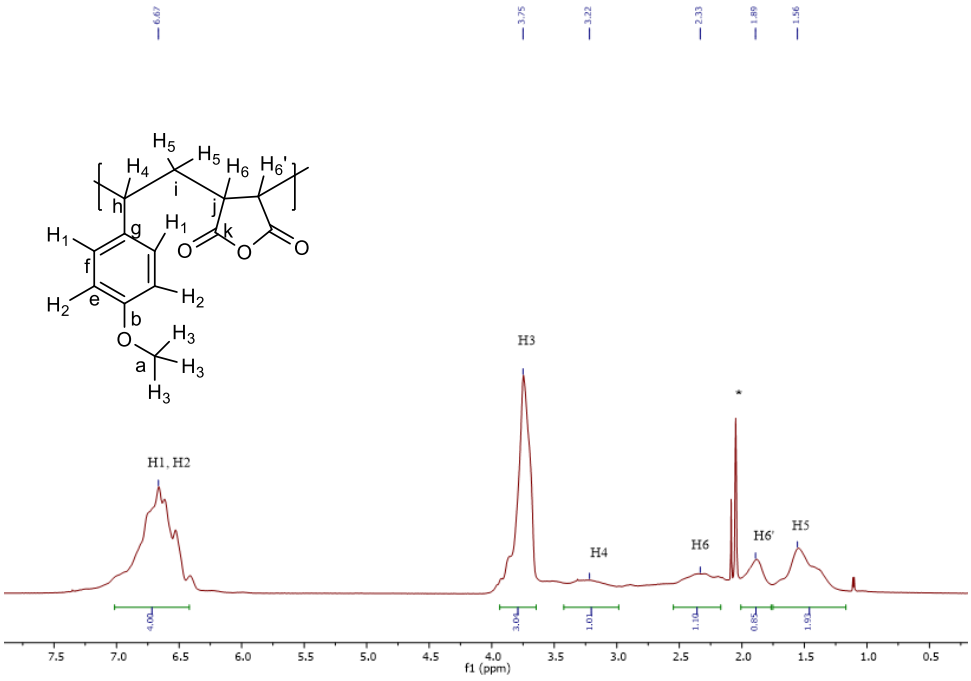

Figure 2.2: ^{1}H NMR spectrum of poly(4MeOSt-*alt*-MA)

The ^{1}H NMR spectrum of the product is shown in figure 2.2, which clearly shows resonances due to the protons of both reacted MA and 4MeOSt. The broad multiplet resonance at 6.63 ppm due to the 4 protons of the aromatic ring (H_1 and H_2); the broad singlet resonance at 3.74 ppm due to the 3 protons of the methyl group (H_3) can be observed. The resonance at 3.22 ppm corresponds to the methine proton of the backbone chain, H_4. The resonance at 2.33 ppm and 1.89 ppm corresponds to the methine protons of the backbone

chain of the maleic anhydride, H_6 and H_6'. The resonance at 1.56 ppm corresponds to methylene protons of the backbone chain, H_5. The ratio between protons H_3 and H_6 (including H_6') was calculated to be 3:2, as expected, confirming that the repeat units of 4MeOSt and MA are in a ratio of 1:1.

The ^{13}C NMR spectrum of the product is shown in figure 2.3. The resonances observed were chracterised in conjunction with 2D NMR including heteronuclear single-quantum correlation spectroscopy (HSQC) and heteronuclear multiple-bond correlation spectroscopy (HMBC).

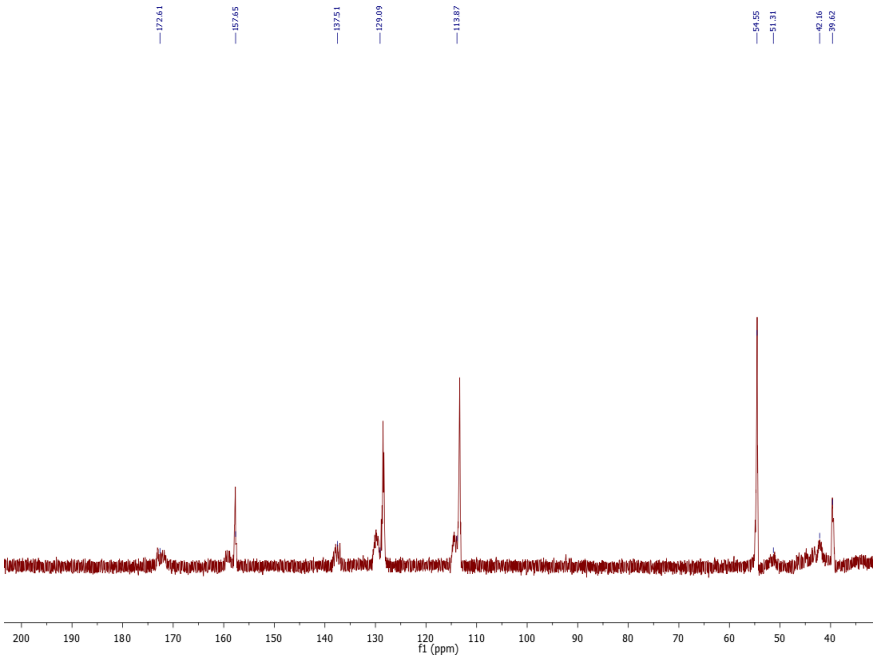

Figure 2.3: ^{13}C NMR spectrum of poly(4MeOSt-*alt*-MA)

The proposed structure for poly(4MeOSt-*alt*-MA) indicates the following couplings: 1) the aromatic ring (H_1, H_2) with carbons **f** and **e**; 2) protons of the methyl group (H_3) with carbon **a**; 3) proton H_4 with carbon **h**; 4) proton H_5 with carbon **i**; and 5) proton H_6 with carbon **j**. Using ^{1}H-^{13}C HSQC map (figure 2.4), the protons bonded to a carbon atom through a single bond can be easily assigned. In the carbon spectrum, the resonances at 128 ppm and 113 ppm are due to carbons **f** and **e**, respectively, and the resonance at 55 ppm is due to carbon **a**. Usually, one peak is observed at the frequency of each proton-carbon resonance, although occasionally two are seen and this is indicative of a diastereotopic CH_2 group, which was displayed as different phase colours in the 2D map. The resonance at 42 ppm is due to carbon **i**, which is coupling with the CH_2 of H_5. The resonances at 52 ppm and 39 ppm are due to carbons **j** and **h**, respectively. The resonances at 138 ppm, 158 ppm, and 173 ppm are

not coupling with protons, therefore identification of the carbon resonances are achieved *via* ^{1}H-^{13}C HMBC spectroscopy.

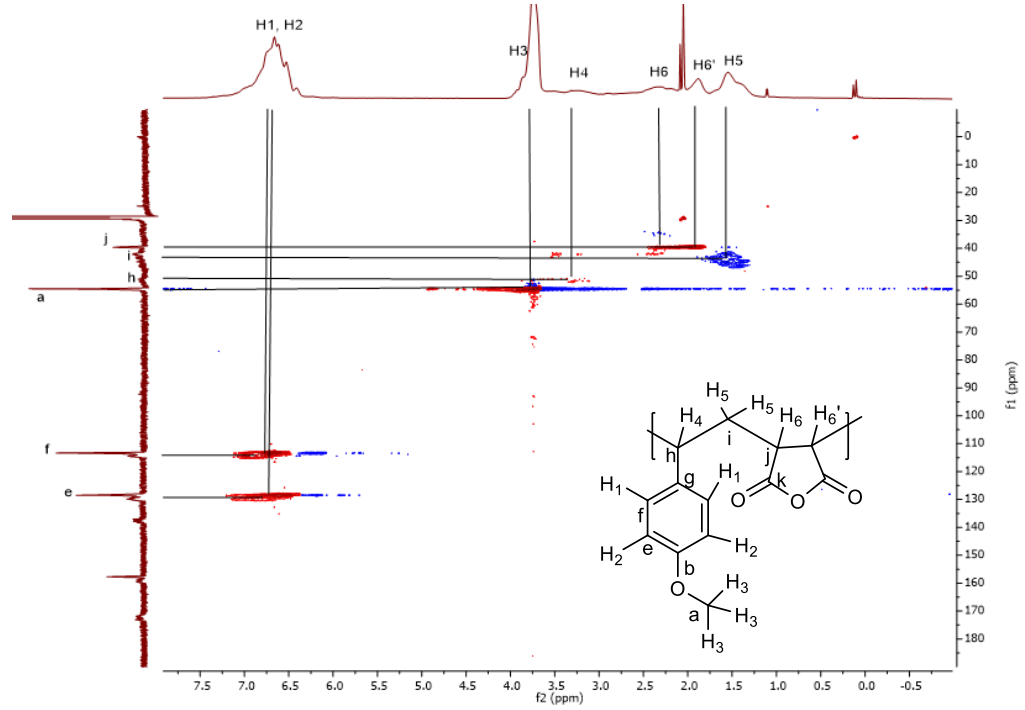

Figure 2.4: ^{1}H-^{13}C HSQC of poly(4MeOSt-*alt*-MA)

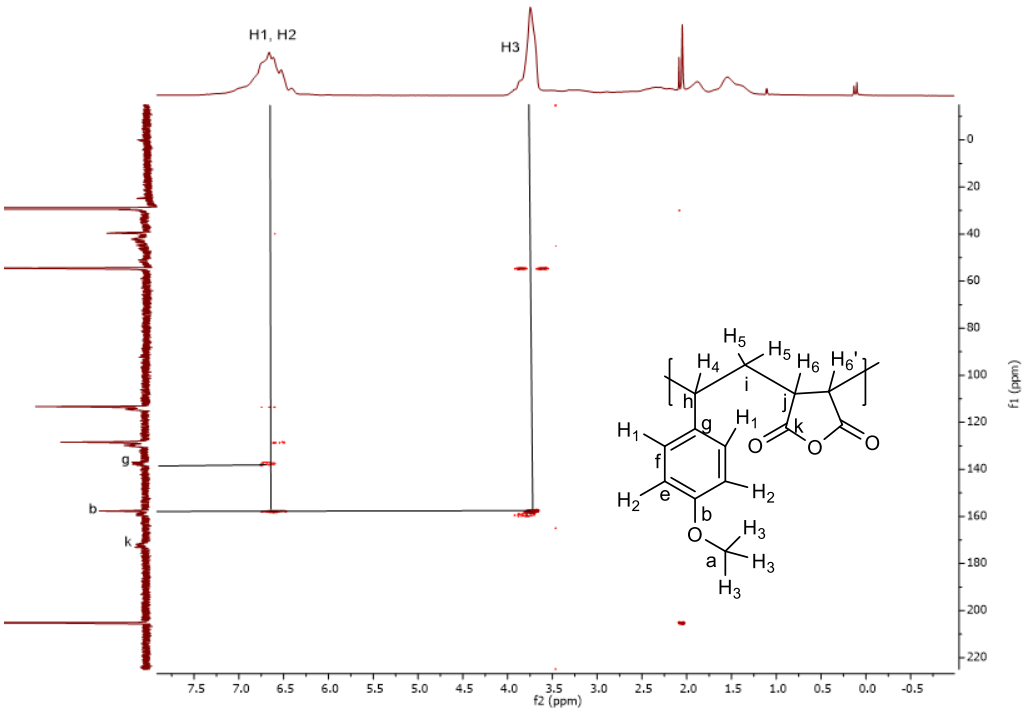

Figure 2.5: ^{1}H-^{13}C HMBC of poly(4MeOSt-*alt*-MA)

The proposed structure for poly(4MeOSt-*alt*-MA) indicates that protons H_1 and H_2 should exhibit coupling to carbons **b** and **g**; proton H_3 to carbon **b**. In the ^{1}H-^{13}C HMBC map (figure 2.5), the resonance at 138 ppm is confirmed due to carbon **g** (multiple coupling with H_1 and H_2), and the resonance at 158 ppm is confirmed due to carbon **b** (multiple coupling with H_1, H_2, and H_3). The final ^{13}C NMR resonances resonance at 173 ppm is due to the carbon **k**. Carbon **k** is expected to couple with H_6, however, the coupling is very weak caused by the conformational freedom of polymer chain in solution.

The presence of 4MeOPh and succinic anhydride repeated units in the product was further confirmed by the IR spectroscopy, figure 2.6. The figure clearly shows the presence of a peak at 1779 cm^{-1} due to C=O stretch (figure 2.6c), similar to that seen for MA, figure 2.6b. The figure 2.5c also shows peaks at 1037 and 1247 cm^{-1} due to C-O stretch (MeO), and 1511 and 1612 cm^{-1} due to aromatic C=C, similar to that seen for 4MeOSt, figure 2.6a.

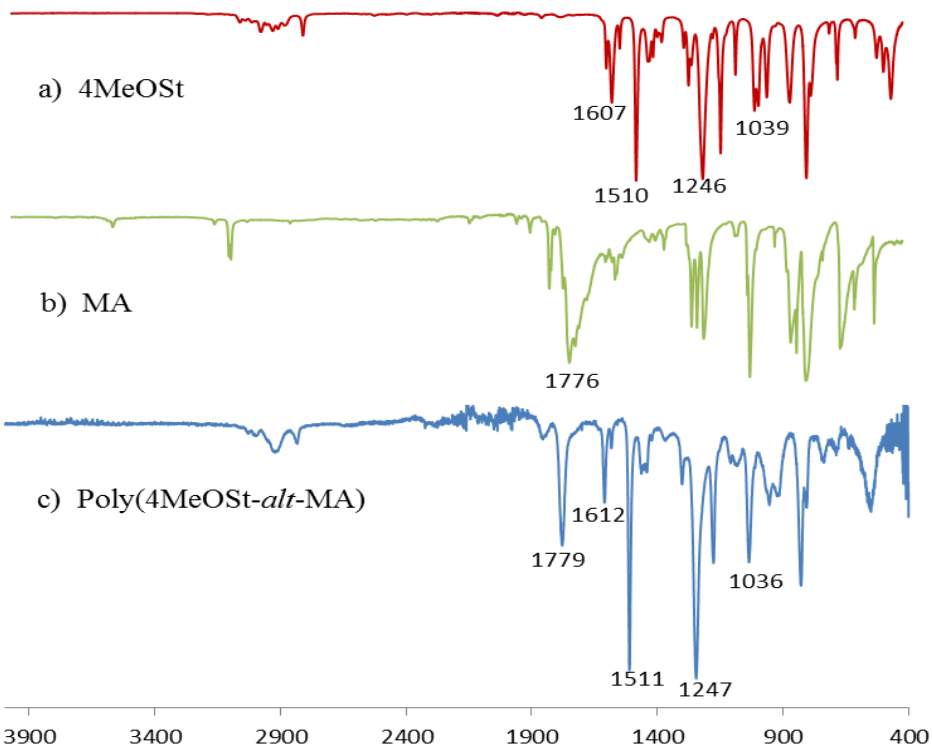

Figure 2.6: the IR spectrum of a) 4MeOSt; b) MA; c) poly(4MeOSt-*alt*-MA)

The polymerisation reaction involves 4MeOSt (an electron donor) and MA (an electron acceptor). 4MeOSt is a conjugated system and electrons at the oxygen atom of OMe group participate in the delocalisation of electron in the phenol ring making vinyl group electron-rich, scheme 2.2.

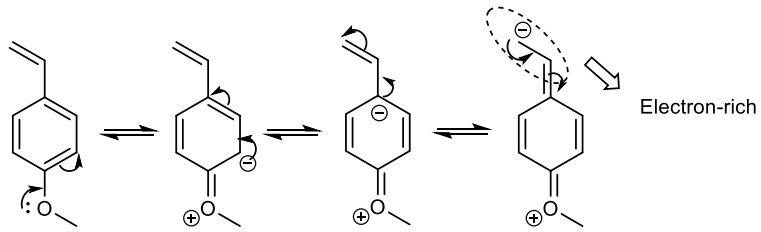

Scheme 2.2: the conjugated system of 4MeOSt

In MA, the presence of two electron withdrawing carbonyl groups decreases the electron density at the double bond and hence electron deficient, scheme 2.3

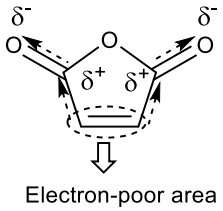

Scheme 2.3: the electron-poor olefin in MA

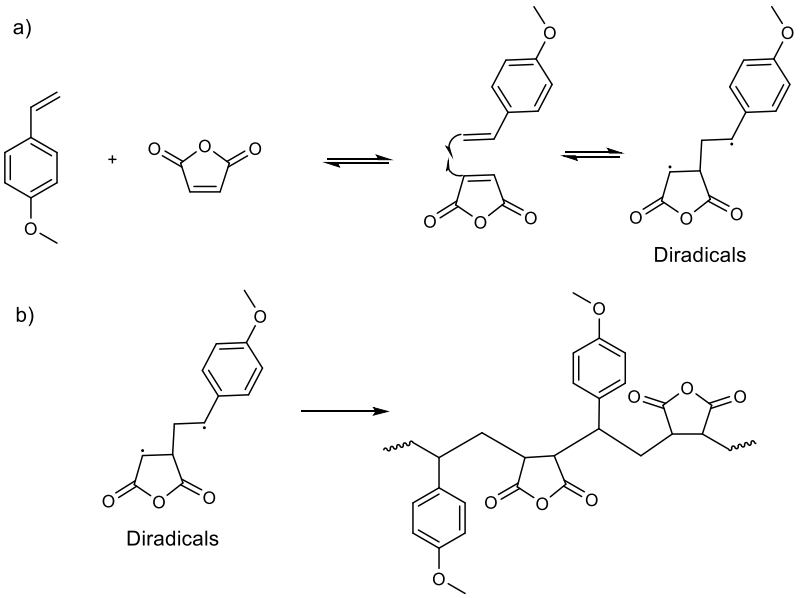

Scheme 2.4: Proposed mechanism: a) formation of diradicals; b) formation of spontaneous co-polymer.

The spontaneous (co-)polymerisation is expected to occur by electron transfer from donor (4MeOSt) to the acceptor (MA). The diradicals then initiate the copolymerisation. Several suggestions as to the origin of the initiating radicals for the spontaneous (co-)polymerisations have been made, ranging from charge-transfer complexes to electron transfer, to bond forming initiation involving diradicals (scheme 2.4a).[2] Diradicals between donor and

acceptor have already been trapped and characterised by electron paramagnetic resonance (EPR) spectroscopy.[2] Therefore, 4MeOSt and MA form diradicals at the initiation step leading to the formation of linear co-polymer, scheme 2.4b.

In order to investigate the reaction rate, six reactions of LP01, LP02, LP03, and LP05 using the molar ratio of 4MeOSt: MA of 1:1, 2:1, 4:1, and 10:1 were prepared in respective vials and placed in an oven set at 50 °C. A vial was taken out and analysed for the reaction yield after 2, 4, 6, 12, 24, and 48 h, and the results are showed in figure 2.7.

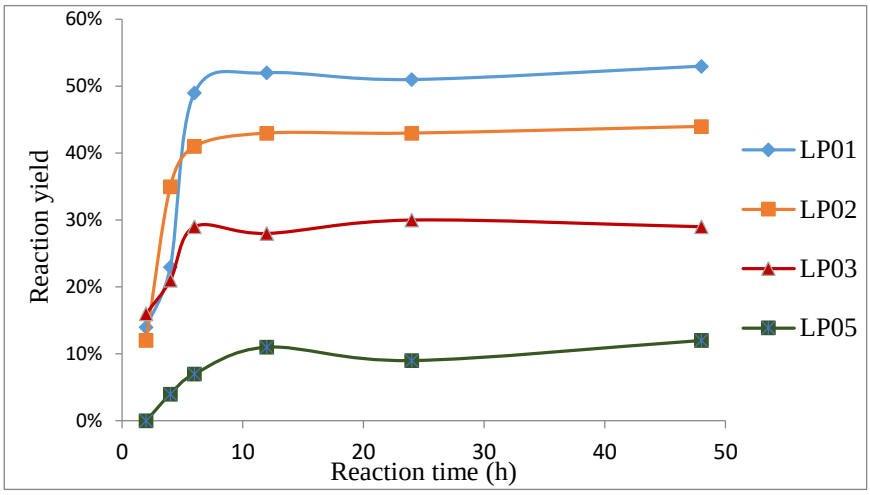

Figure 2.7: The reaction yield of MA and 4MeOSt at 50°C.

Table 2.5: the reaction of MA and 4MeOSt in different ratio

Reaction	MA (mol %)	MA : 4MeOSt	Yield (after 48 h)
LP01	50	1 : 1	53%
LP02	33	1 : 2	44%
LP03	20	1 : 4	29%
LP04	11	1:8	17%
LP05	9	1 : 10	12%
LP06	5	1 : 20	<1%

The table 2.5 and figure 2.7 show that the yield of the reaction after 48 h was decreasing with the increasing amount of MA. Initially, the reaction yield was increased up to 12 h, after which it reached a plateau at 50% yield. The reaction was undertaken in bulk giving solid product which is believed to be responsible for stopping the progress of the reaction and hence reaching a plateau. The yield of the reaction also decreased as the amount of 4MeOSt increased and the maximum yield obtained when the ratio of MA: 4MeOSt is 1:1. This is expected as equimolar of both monomers is essential to form a spontaneous co-polymer.

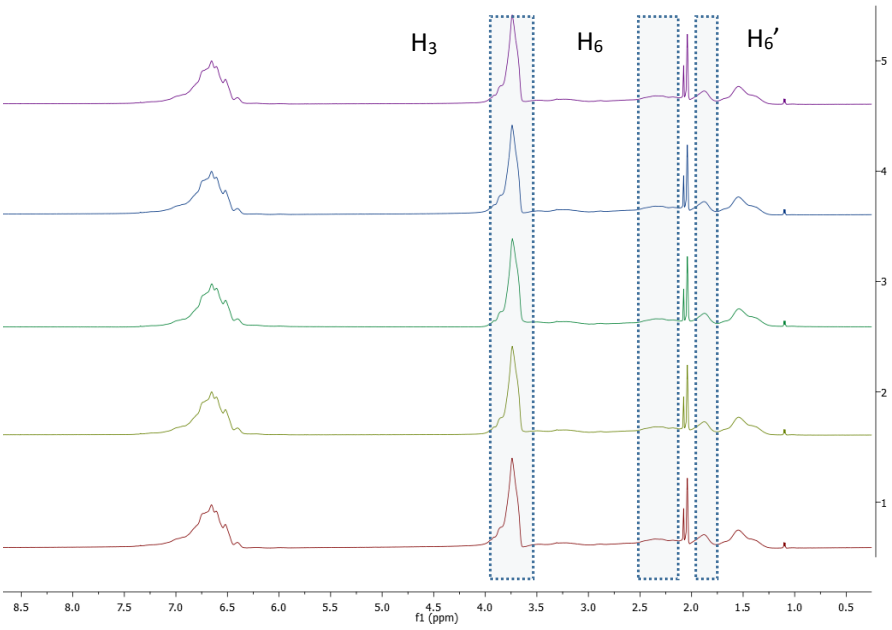

Figure 2.8: The ^{1}H NMR spectra of LP01-05

The ^{1}H NMR spectra of LP01-05 are shown in figure 2.8. The ratio of integration of resonances at 3.26 ppm and 2.27 ppm corresponding H_6 and H_6' (succinic anhydride) to resonance at 3.74 ppm corresponding H_3 (4MeOSt) give a ratio of 3:1.91, 3:1.74, 3:1.82, 3:1.84, 3:1.93 for LP01, LP02, LP03, LP04, LP05, respectively (table 2.6). The ratio is very close, within the experimental error, to the expected ratio of the protons of CH_3 of 4MeOSt to methine protons of MA repeat units is 3:2. This confirmed that the polymer product is an alternating co-polymer with the repeat units of both 4MeOSt and MA in the ratio of 1:1.

Table 2.6: of integration of the H_3 and H_6

	H_3	H_6 and H_6'
LP01	3	1.91
LP02	3	1.74
LP03	3	1.82
LP04	3	1.84
LP05	3	1.93

2.5.2 N-Methylmaleimide with 4-methoxystyrene

The spontaneous copolymerisation of 4MeOSt and MeMal was carried out at 50 °C and at ambient temperature (scheme 2.5) and a yellow solid was produced which was found to be soluble in acetone and THF. The polymer product obtained was characterised by ^{1}H and ^{13}C NMR spectroscopy.

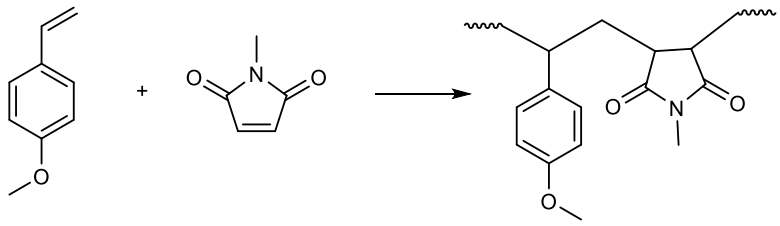

Scheme 2.5: Spontaneous copolymerisation reaction of 4MeOSt and MeMal

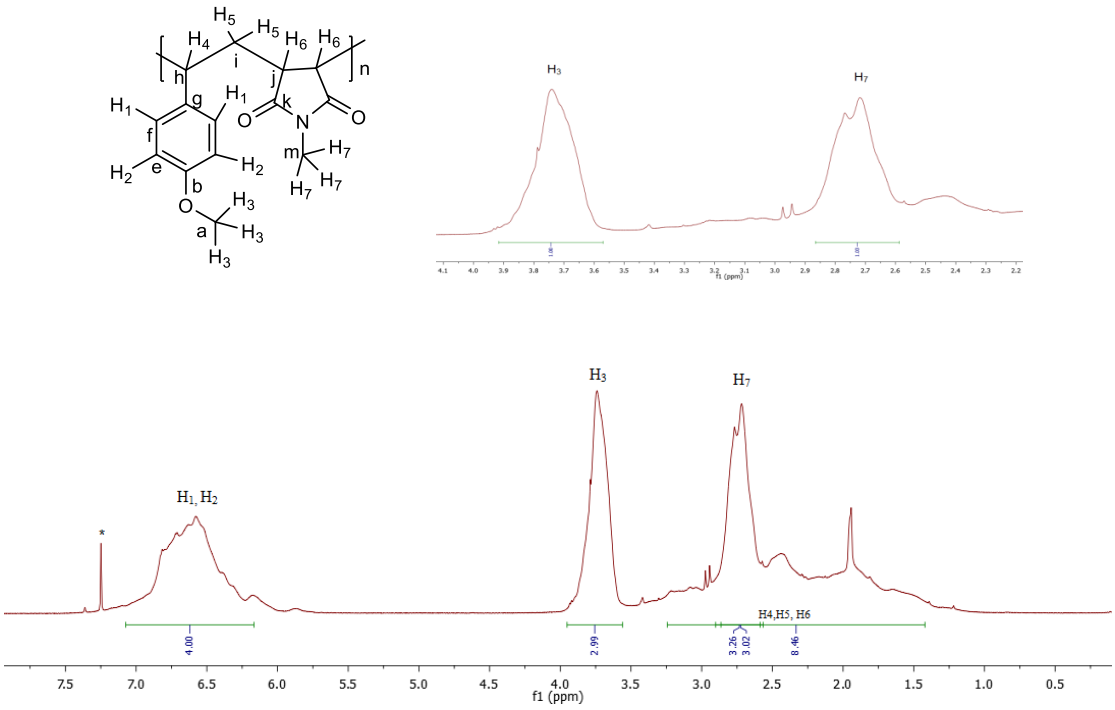

Figure 2.9: ^{1}H NMR spectrum of poly(MeMal-*alt*-4MeOSt)

The ^{1}H NMR spectrum of the polymer product is shown in figure 2.9, which clearly shows resonances due to the protons of both repeat units of 4MeOSt and MeMal. The resonance at 2.72 ppm due to 3 protons of the methyl group (H_7) (–NCH_3); the resonance at 3.74 ppm due to the methyl group (H_3) (–OCH_3); the resonance at 6.63 ppm due to 4 protons of the aromatic ring (H_1 and H_2); and the resonance between 1.27-3.45 ppm due to backbone protons of the polymer (H_4, H_5, and H_6) can be observed. The expected ratio between proton of H_3 and H_7 is 1:1 and the integration ratio of peaks at 3.75 and 2.71 ppm was found to be 1:1, indicating the ratio of 4MeOSt with MeMal is 1:1.

The ^{13}C NMR spectrum of the product is shown in figure 2.10. The resonances were chracterised in conjunction with 2D NMR (HSQC and HMBC NMR) spectroscopy.

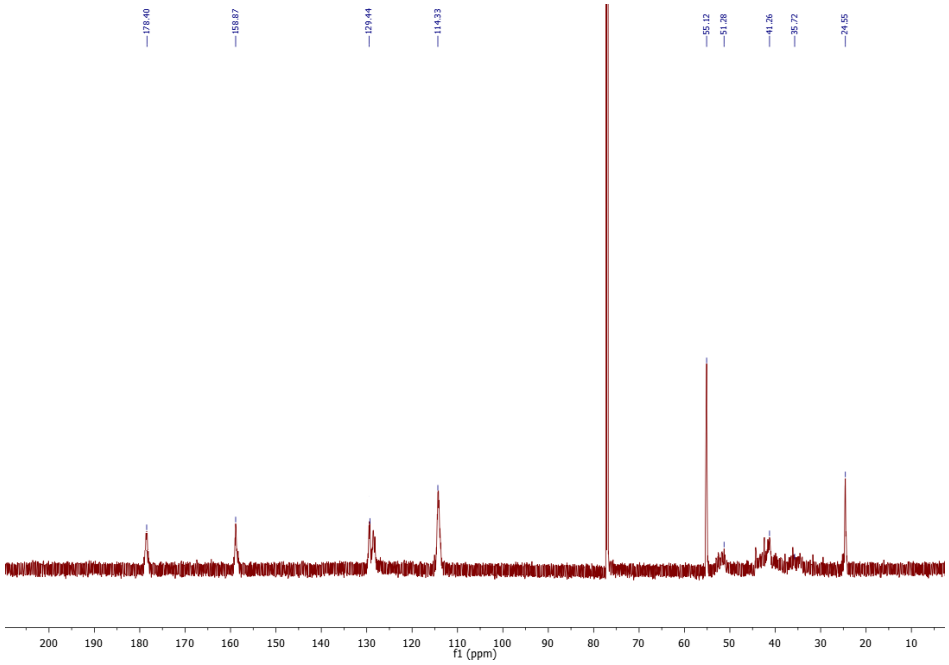

Figure 2.10: ^{13}C NMR spectrum of poly(MeMal-*alt*-4MeOSt)

The proposed structure of poly(MeMal-*alt*-4MeOSt) indicates the following couplings: 1) the aromatic ring (H_1, H_2) with carbons **f** and **e**; 2) protons of the methyl group (H_3) with carbon **a**; 3) proton H_4 with carbon **h**; 4) proton H_5 with carbon **i**; 5) proton H_6 with carbon **j**; and 6) proton H_7 with carbon **m**. Using ^{1}H-^{13}C HSQC map (figure 2.11), the protons bonded to a carbon atom through a single bond can be easily assigned. In the carbon spectrum, the resonances at 129 ppm and 114 ppm are due to carbons **f** and **e**, respectively, and the resonance at 25 ppm and 55 ppm is due to carbon **m** and **a**, respectively. Usually, one peak is observed at the frequency of each proton-carbon resonance, although occasionally two are seen and this is indicative of CH_2 group, which was displayed as different phase colours in the 2D map. Therefore, the resonance at 35 ppm is due to carbon **i**, which is coupling with the CH_2 of H_5. The resonances due to the backbone of the polymer are very broad, therefore, it is very difficult to identify H_4, H_6, and H_6'. The resonances at 158 ppm and 178 ppm are not coupling with protons, therefore identification of the carbon resonances are achieved *via* ^{1}H-^{13}C HMBC spectroscopy.

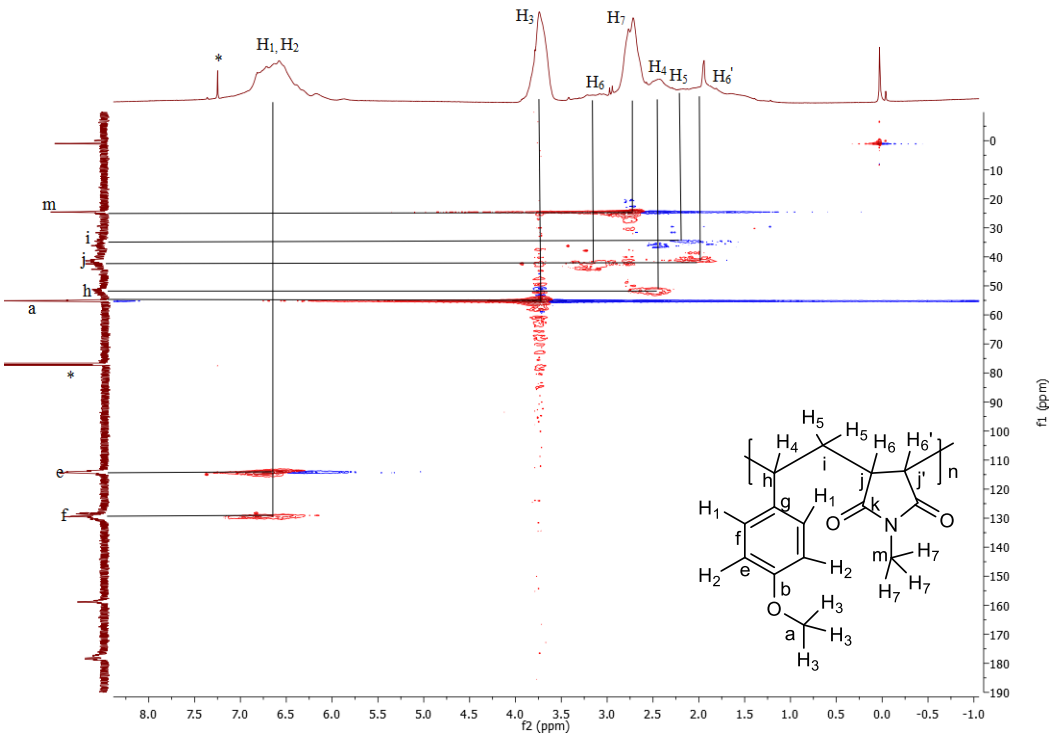

Figure 2.11: ^{1}H-^{13}C HSQC of poly(MeMal-*alt*-4MeOSt)

The proposed structure of poly(MeMal-*alt*-4MeOSt) indicates the following multiple couplings: 1) protons H_1 and H_2 with carbons **b** and **g**; 2) proton H_3 with carbon **b**; and 3) proton H_7 with carbon **k**. Using the ^{1}H-^{13}C HMBC map (figure 2.12a), the resonance at 158 ppm is confirmed due to carbon **b** (multiple coupling with H_1, H_2, and H_3) and the resonance at 178 ppm is confirmed due to carbon **k** (multiple coupling with H_7). There is no resonance due to carbon **g** observed in the ^{13}C NMR spectrum. However, the resonance at 138 ppm, which is already confirmed due to carbon **f**, exhibit multiple coupling to a proton of the polymer backbone (H_4). However, carbon **g** should exhibit multiple coupling to H_4 as the proposed structure of poly(4MeOSt-co-MA) shows. Also in the zoom-in 2D map (figure 2.12b), this conjunction area (carbon **f** or **g** with aromatic protons) is much bigger than others. So the resonance due to carbon **g** may stack with carbon **f**.

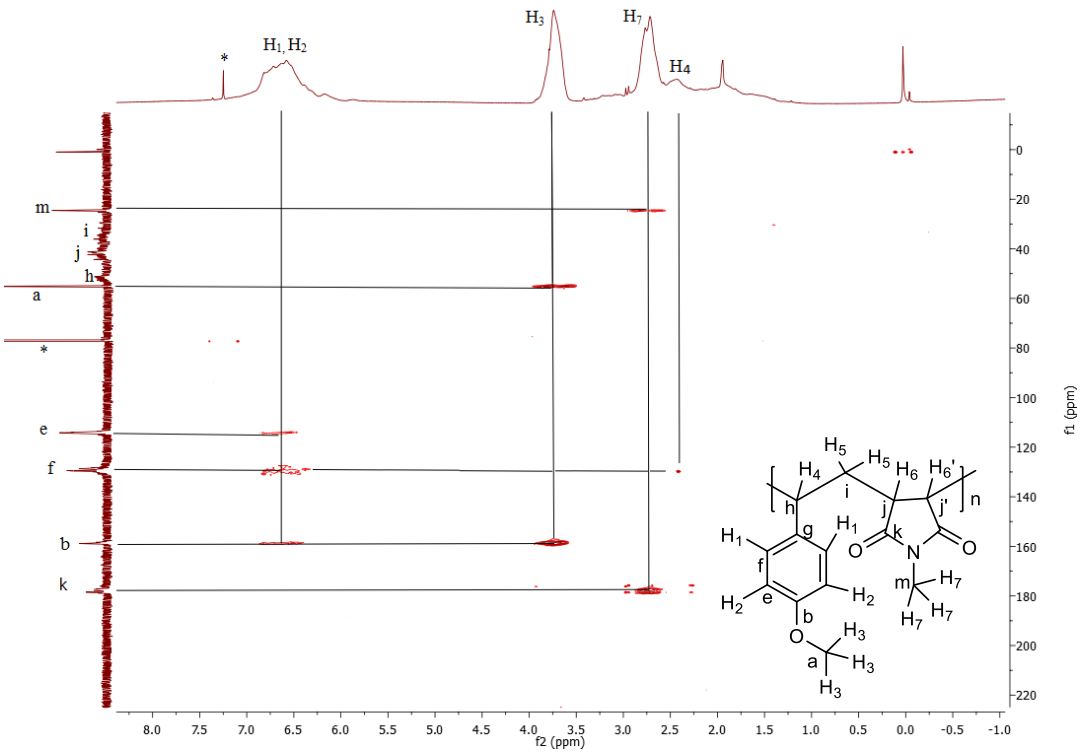

(a)

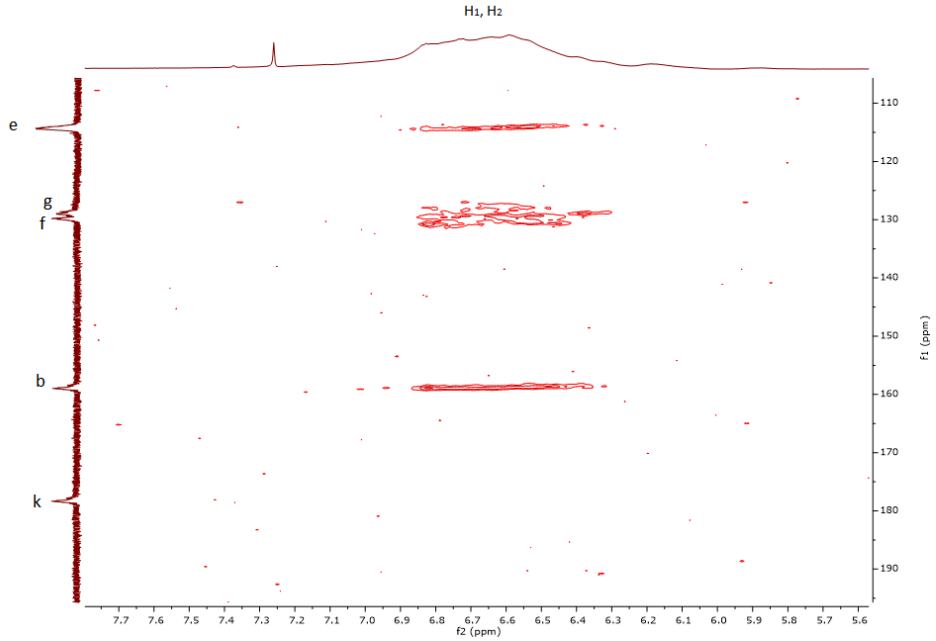

(b)

Figure 2.12: (a) ^{1}H-^{13}C HMBC of poly(MeMal-*alt*-4MeOSt); (b) the details of coupling area for protons H_1 and H_2 with carbon **e**, **g**, **f**, **b**, and **k**

The IR spectrum (figure 2.13) clearly shows the presence of peaks at 1512 cm^{-1} and 1250

cm^{-1} corresponding to aromatic C=C and C-O of 4MeOSt, respectively. It also shows peaks at 1696 cm^{-1} and 1032 cm^{-1} due to C=O and C-N of MeMal, respectively.

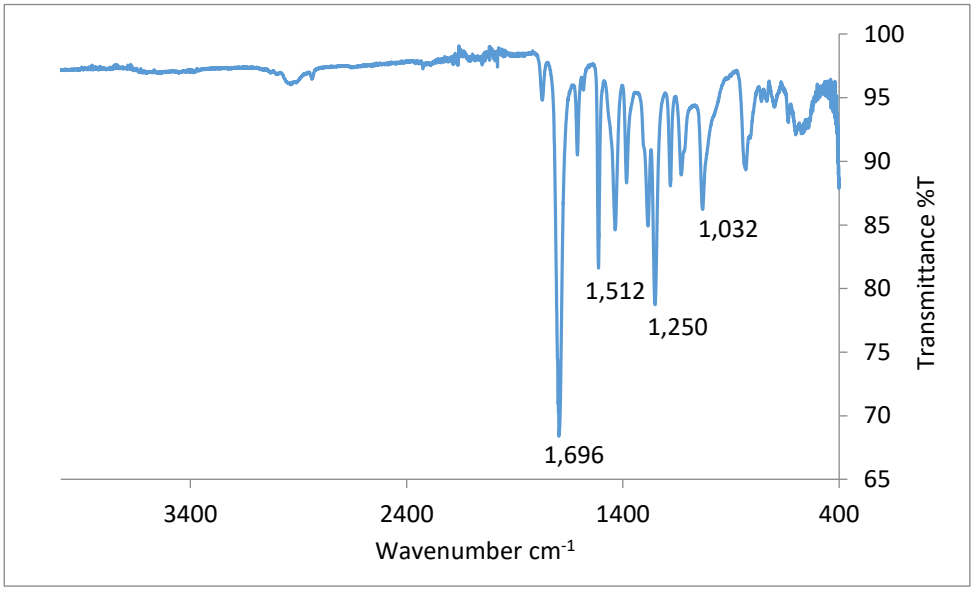

Figure 2.13: The IR spectrum of poly(MeMal-*alt*-4MeOSt)

This reaction involves 4MeOSt (an electron donor) and MeMal (an electron acceptor) monomers. The electron donating of 4MeOSt was described in section 2.4.1. The MeMal is electron deficient, but not as strong as MA due to the presence of nitrogen atom. The electron deficiency is caused by two carbonyl groups drawing electron density away from C=C (scheme 2.6).

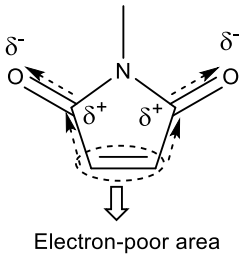

Scheme 2.6: The electron deficiency of MeMal

The proposed mechanism for the polymerisation of 4MeOSt and MeMal is shown in scheme 2.7. This involves electron transfer from donor (4MeOSt) to acceptor (MeMal) to form diradicals, scheme 2.6a. The diradicals then initiate the copolymerisation, scheme 2.6b.

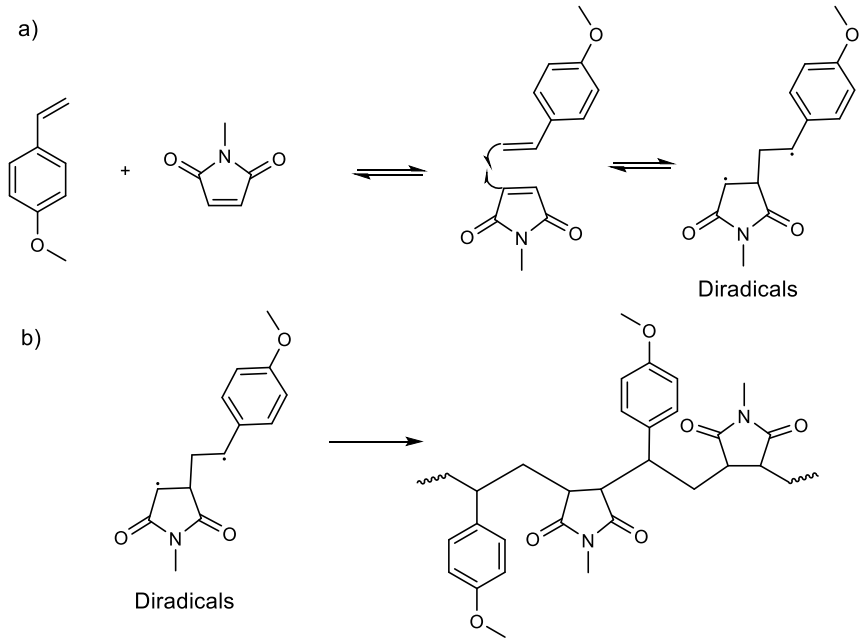

Scheme 2.7: Proposed formation of a) 4MeOSt-MeMal diradicals; b) co-polymer

Reaction LP07-11 using ratio of MeMal: 4MeOSt of 1:1, 1:2, 1:4, 1:8, and 1:10 were prepared in respective vials and placed in an oven at 50 °C. A vial was taken out and analysed the reaction yield after 12, 24, 36, 48, 60, and 72 h, in order to investigate the reaction rate, and the results are shown in figure 2.14.

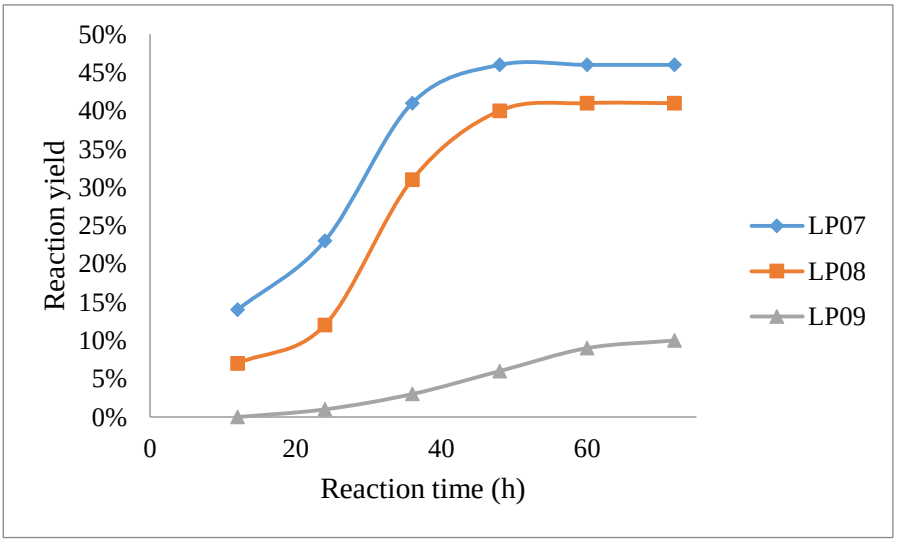

Figure 2.14: The reaction yield of MeMal and 4MeOSt

Initially, the reaction yield was increased up to 48 h, after which it reached a plateau. The reaction was undertaken in bulk during which solid product was formed which is believed to be possible for stopping the progress of the reaction and hence reaching a plateau. The yield

of the reaction also decreased as the amount of 4MeOSt increased and the maximum yield obtained when the ratio of MA: 4MeOSt is 1:1. This is expected as equimolar of both monomers is essential to form a spontaneous co-polymer.

Table 2.7: the reaction of 4MeOSt and MeMal in different ratio

Reaction	MeMal (mol %)	MeMal : 4MeOSt	Yield (after 48 h)
LP07	50	1 : 1	46%
LP08	33	1 : 2	41%
LP09	20	1 : 4	10%
LP10	11	1 : 8	0
LP11	9	1 : 10	0

The table 2.7 shows that the yield of the reaction was decreasing with the increased amount of MeMal. As more 4MeOSt was added, the yield of the reaction decreased. LP10 and 11 did not form any solid. This indicates that a molar ratio for MeMal: 4MeOSt of 1:1 is essential for the formation of diradicals and hence poly(4MeOSt-*alt*-MeMal).

2.5.3 Ethoxymethylene malononitrile with 4-methoxystyrene

The spontaneous copolymerisation of 4MeOSt and EtOCN was carried out at 50°C (scheme 2.8) using a molar ratio of 1:1 and produced a light brown solid, which was found to be soluble in acetone and THF. The reaction did not produce any solid at ambient temperature. The product was dissolved in THF and then precipitated in methanol giving a light yellow solid which was characterised by ^{1}H and ^{13}C NMR spectroscopy.

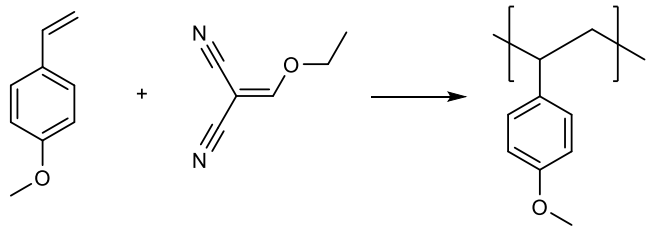

Scheme 2.8: Proposed reaction of 4MeOSt and EtOCN

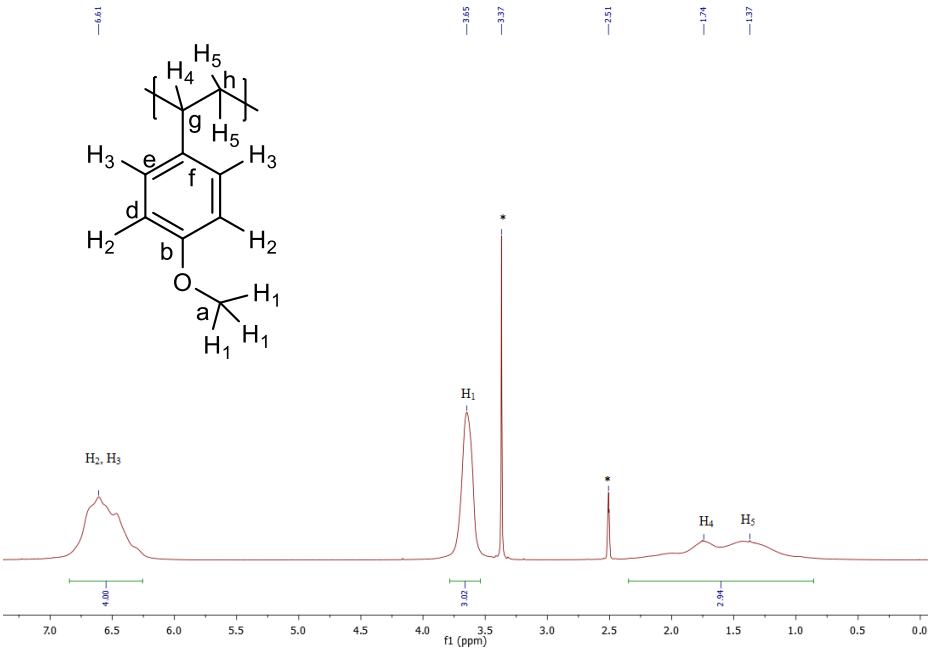

Figure 2.15: ^{1}H NMR spectrum of the product

The ^{1}H NMR spectrum of the product is shown in figure 2.15 which clearly shows resonances only due to the protons of 4MeOSt and there is no resonance due to the protons of EtOCN. The resonance at 6.61 ppm due to 4 protons of the aromatic ring (H_1 and H_2); the resonance at 3.65 ppm was due to 3 protons of the methyl group (H_3); and the resonance between 0.80-2.25 ppm due to backbone protons of the polymer (H_4 and H_5) are observed. The integration shows the ratio of H_1 : (H2+H3) : (H4+H5) is 3:4:3.

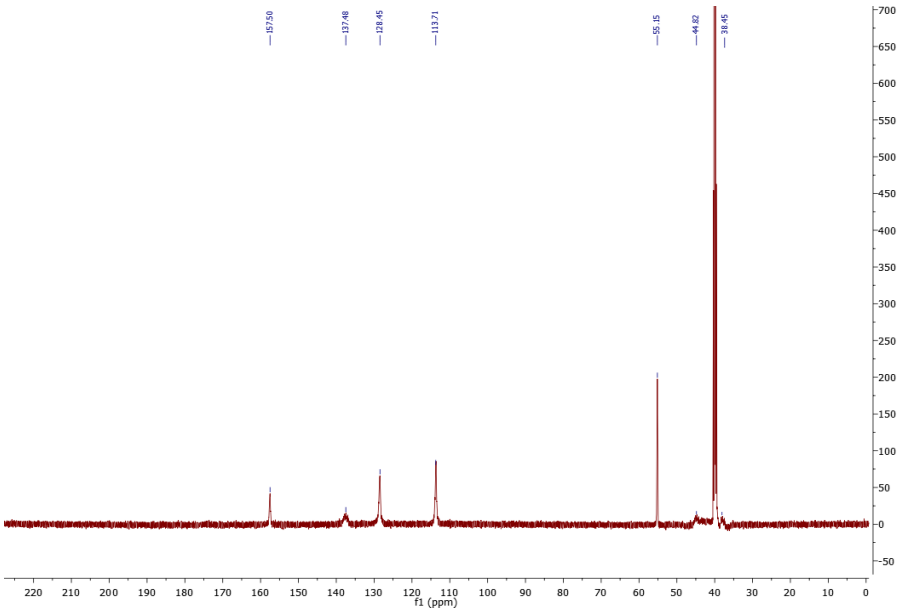

Figure 2.16: ^{13}C NMR spectrum of the product

The presence of MeOPh repeat unit in the product was further confirmed by ^{13}C NMR, figure 2.16. ^{13}C NMR resonances observed were characterised in conjunction with 2D NMR (HSQC and HMBC NMR) spectroscopy.

The proposed structure of poly(4MeOSt) indicates the following couplings: 1) the aromatic ring (H_2, H_3) with carbon **d** and **e**; 2) protons of the methyl group (H_1) with carbon **a**; 3) proton H_4 with carbon **g**; and 4) protons H_5 with carbon **h**. Using ^{1}H-^{13}C HSQC map (figure 2.17), the protons bonded to a carbon atom through a single bond can be easily assigned. In the carbon spectrum, the resonances at 129 ppm and 114 ppm are due to carbon **d** and **e,** respectively; the resonance at 55 ppm is due to carbon **a;** the resonance at 38 ppm is due to backbone of the polymer carbon **g**. The CH_2 group was displayed as different phase colours (blue) in the 2D map. Therefore, the resonance at 44 ppm is due to carbon **h**, which is coupling with the CH_2 of H_5. The resonances at 138 ppm and 158 ppm are not coupling with protons, therefore identification of the carbon resonances are achieved *via* ^{1}H-^{13}C HMBC spectroscopy.

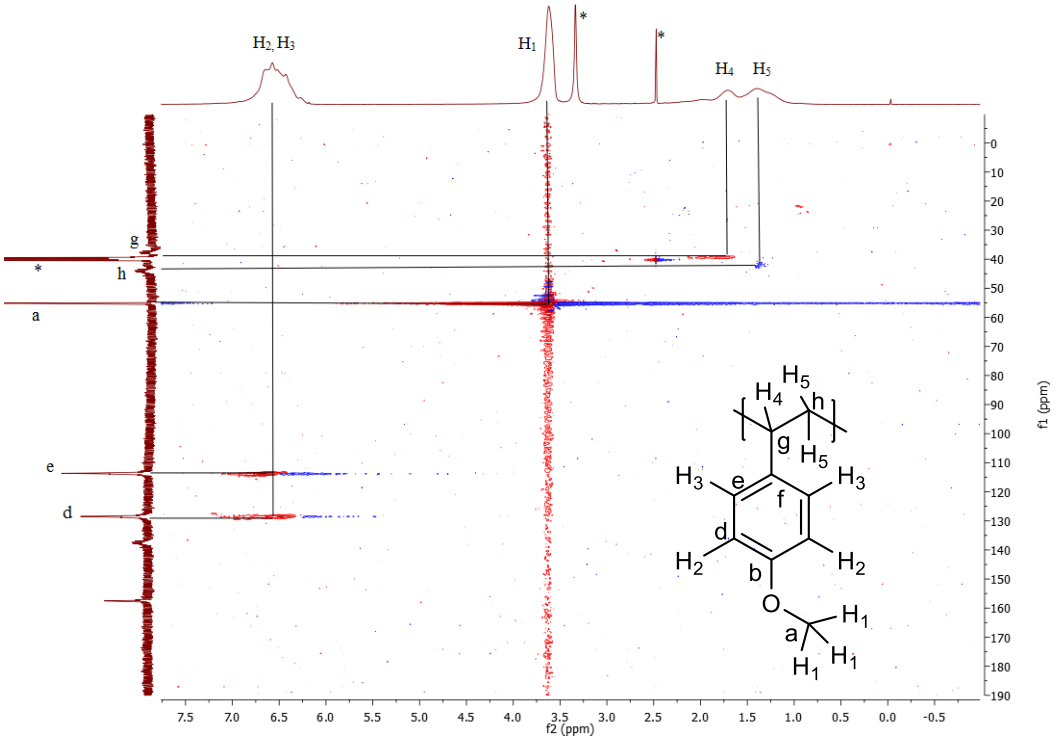

Figure 2.17: ^{1}H-^{13}C HSQC of the product

The proposed structure of poly(4MeOSt) indicates protons H_2 and H_3 exhibit multiple coupling to carbons **b** and **f**; proton H_1 couples to carbon **b**. Therefore, in the ^{1}H-^{13}C HMBC

map (figure 2.18), the resonance at 158 ppm is due to carbon **b** (multiple coupling with H_2, H_3 and H_1). The resonance at 138 ppm is due to carbon **f** (multiple coupling with H_2 and H_3).

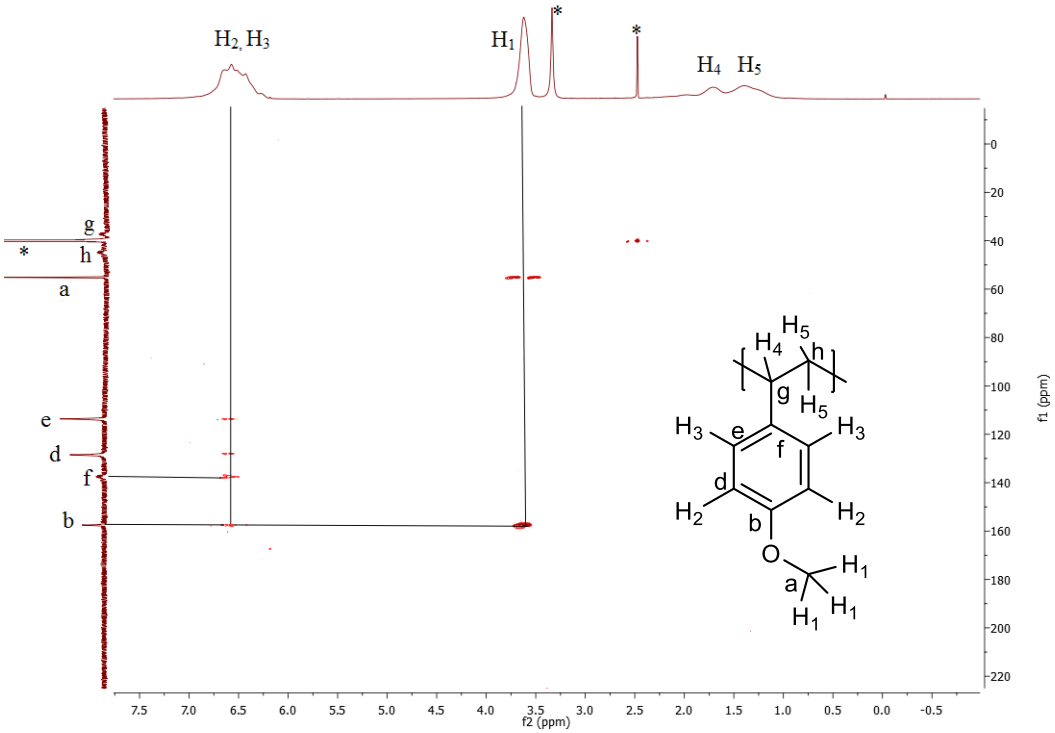

Figure 2.18: ^{1}H-^{13}C HMBC of the product

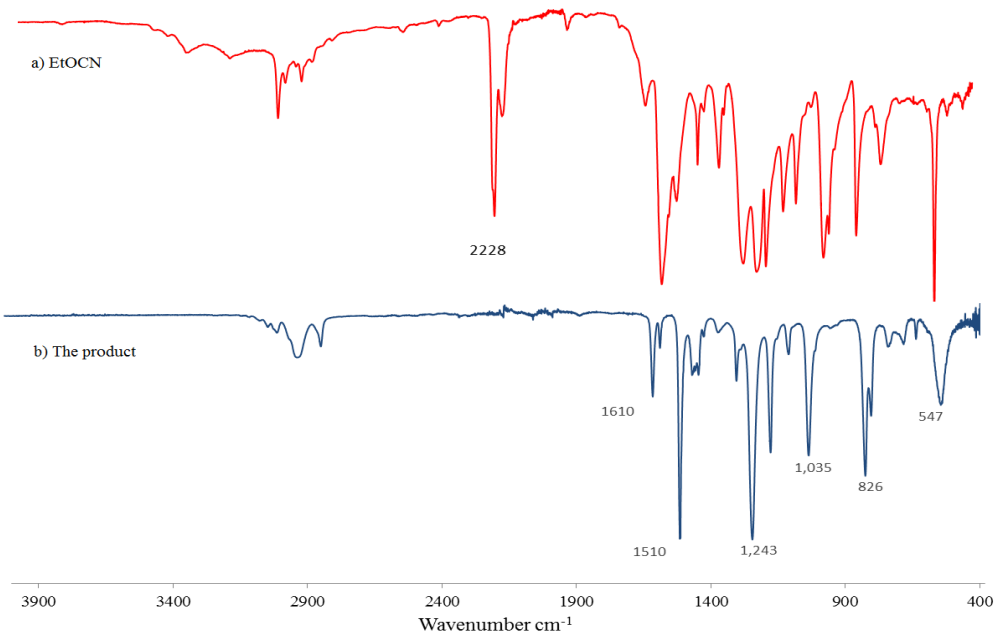

Figure 2.19: The IR spectrum of EtOCN (a) and the product (b)

The presence of MeOPh in the product was further confirmed by the IR spectroscopy. The

peaks at 1035 and 1243 cm^{-1} due to C-O stretch (MeO), and 1510 and 1610 cm^{-1} due to aromatic C=C were observed. The IR spectrum of EtOCN (figure 2.19a) shows the CN group come at 2228 cm^{-1} which not observed in the IR spectroscopy of the product, figure 2.19b. The result confirmed that the product is homopoly(4MeOSt).

This reaction involves 4MeOSt as an electron donor monomer and EtOCN as an electron acceptor. The conjugated system of 4MeOSt was introduced in previously section. The electron deficiency of EtOCN is caused by the conjugated nitrile group. In EtOCN, the presence of two electron withdrawing nitrile groups decreases the electron density at the double bond and hence electron deficient, figure 2.20.

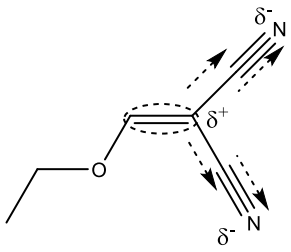

Figure 2.20: The conjugated system in EtOCN

As the ^{13}C NMR spectrum and FTIR spectroscopy both showed the presence of 4MeOSt repeat units, the reaction is believed to be homopolymerisation of 4MeOSt forming poly(4MeOSt) initiated by EtOCN. As it is explained in chapter 1 (section 1.6.4), spontaneous copolymerisation between electron-rich and electron-poor olefins could form zwitterions resulting in either cationic or anionic homopolymerisation. Therefore, it is concluded that the poly(4MeOSt) is formed via cationic polymerisation and the mechanism is shown in scheme 2.9. The reaction of 4MeOSt with EtOCN form zwitterions, scheme 2.9a. This is followed by the polymerisation of 4MeOSt, scheme 2.9b.

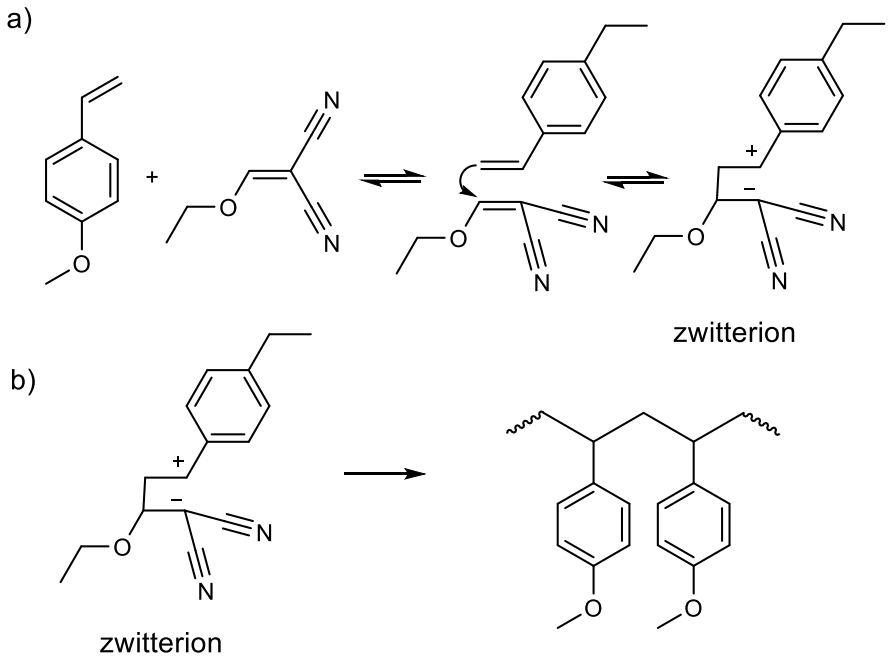

Scheme 2.9: The mechanism of the formation of a) 4MeOSt-EtOCN zwitterions; b) poly (4MeOSt) via cationic polymerisation

It is believed that most likely the mechanism of polymerisation of 4MeOSt is cationic, as the carbocation is stabilised by the phenyl ring. However, the reaction at ambient temperature did not produce any solid polymer. Therefore, the reaction was further investigated at 50 °C with different ratios of 4MeOSt and EtOCN and reaction time, was shown in figure 2.21.

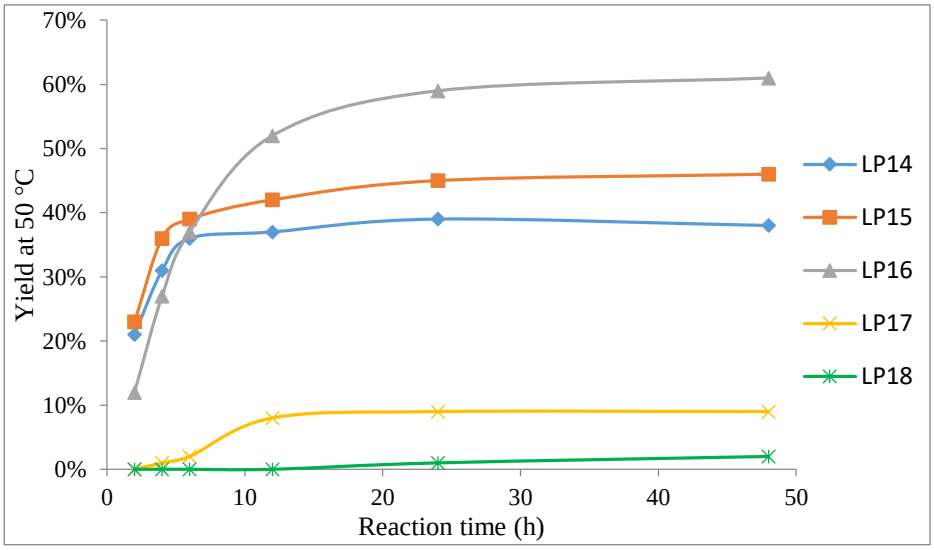

Figure 2.21: The reaction yield of 4MeOSt with EtOCN

The ratio of 4MeOSt: EtOCN for LP14 was 1:1, LP15 was 2:1, LP16 was 4:1, LP17 was 8:1,

and LP18 was 10:1. The result shows that the final yield for LP14-16 is increased as the amount of 4MeOSt is increased from 1:1 to 4:1 (with respect to EtOCN). However, LP17 and 18 gave low yields as the amount of 4MeOSt is increased to 8:1 and 10:1 (with respect to EtOCN). A reasonable explanation is that sufficient amount of EtOCN is required to form enough zwitterions to initiate the homopolymerisation of 4MeOSt.

Interestingly, as it is shown in the table 2.8 and figure 2.22, the yield, M_n, and Đ remain constant, within the experimental error, for LP14-16 despite more 4MeOSt monomer being present. The reason for this behavior is not clear but one possible explanation is that, in bulk polymerisation, the polymer chain growth to the same length, due to steric hindrance.

Table 2.8: The molecular weight and yield for LP14-16

Reaction	4MeOSt : EtOCN	Mn (Da)	Đ	Yield (%)
LP14	1:1	22911	1.63	75
LP15	2:1	24381	1.61	69
LP16	4:1	23732	1.64	72

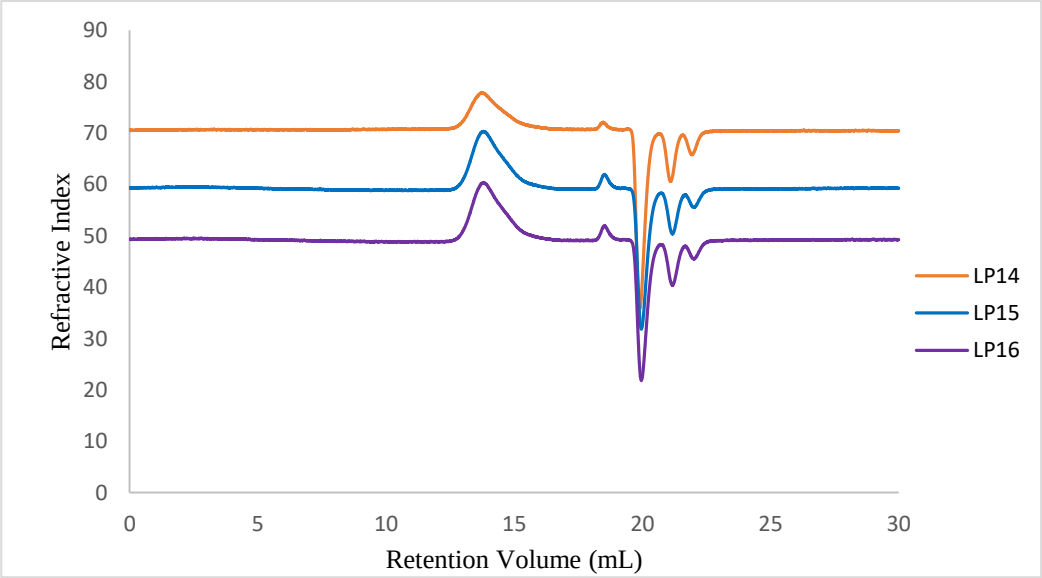

Figure 2.22: Stacks of SEC chromatograms for LP14-16

2.5.4 Maleic anhydride with styrene

The spontaneous copolymerisation of St and MA (scheme 2.10) was carried out at 50 °C and a yellow solid was produced, which was found to be soluble in acetone and THF. The

reaction did not produce any solid at ambient temperature. The polymer product obtained was characterised by ^{1}H and ^{13}C NMR spectroscopy.

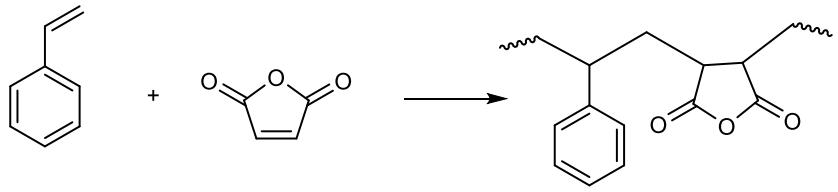

Scheme 2.10: the reaction of St and MA

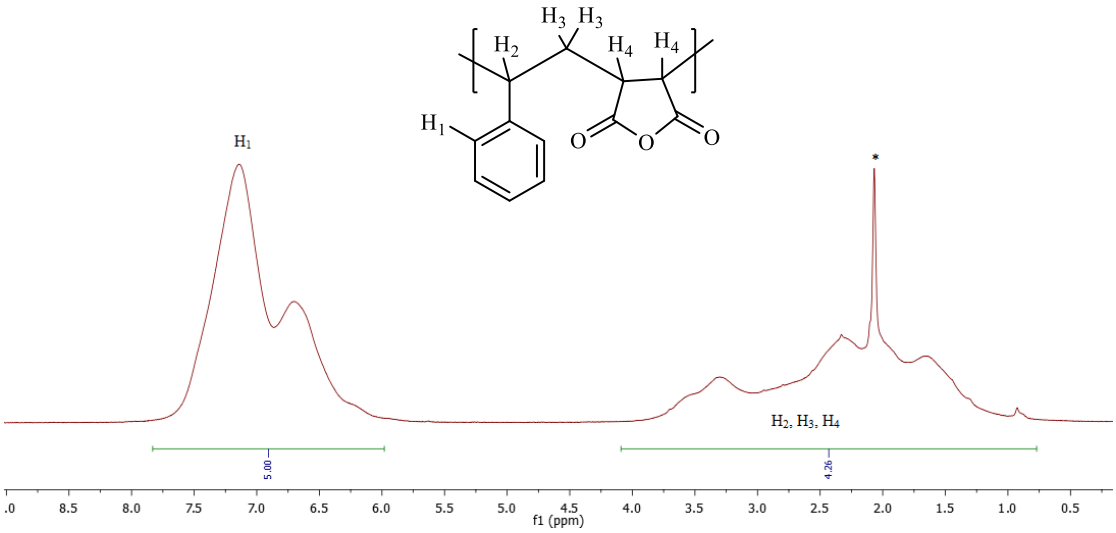

Figure 2.23: ^{1}H NMR spectrum of poly(MA-*alt*-St)

The ^{1}H NMR spectrum of the product is shown in figure 2.23, which clearly shows resonances due to the protons of both MA and St repeat units. The broad multiplet resonance at 7.11 ppm due to 5 protons of the aromatic ring (H_1); and the resonance between 0.77 - 4.06 ppm due to backbone protons of the polymer (H_2, H_3, and H_4) are observed. The integration ratio between protons H_1 and backbone protons was calculated to be 1:1, as expected for poly(MA-*alt*-St).

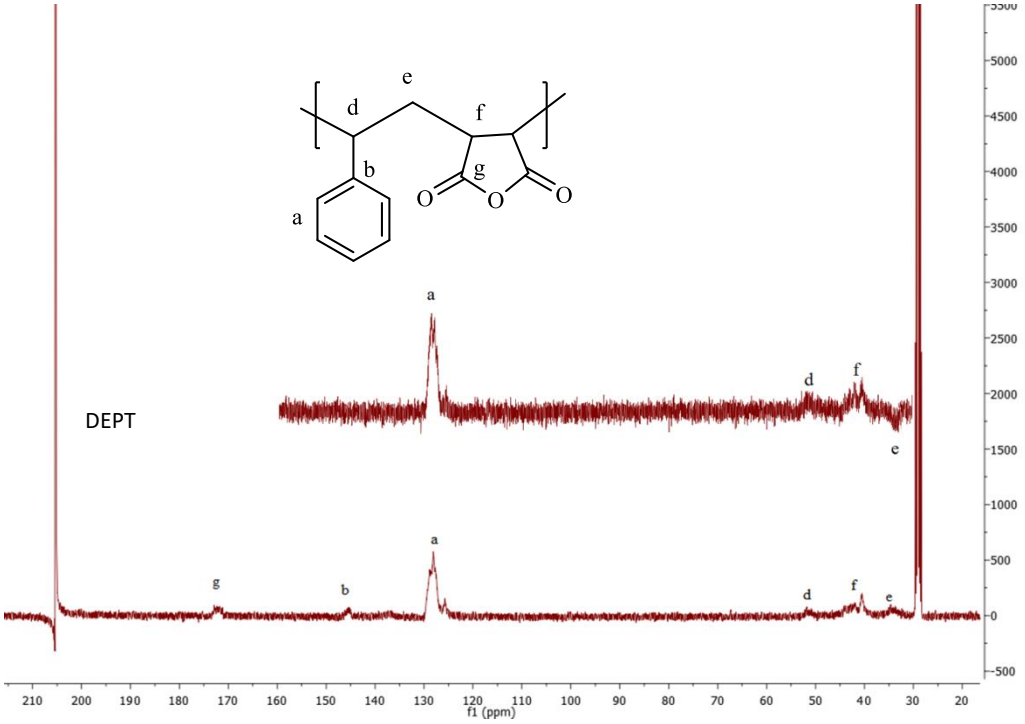

Figure 2.24: ^{13}C and DEPT NMR spectra of poly(MA-*alt*-St)

Distortionless enhancement by polarisation transfer (DEPT) was used to identify the ^{13}C NMR resonances, figure 2.24. Non-proton-bearing carbons are not seen in DEPT spectra because the technique relies on polarisation transfer, in this case, the transfer of proton magnetisation onto the directly bound carbon. Particularly, DEPT in most cases is sufficient to distinguish between methine (CH), methyl (CH_3), and methylene (CH_2) groups, normally. CH and CH_3 will stay up and CH_2 will transfer down to the base line. The resonance at 146 ppm and 173 ppm are not observed in DEPT, meaning they are due to non-proton-bearing carbons. As the proposed structure shows that carbon **b** and **g** are non-proton-bearing carbons. The resonance at 173 ppm is due to carbon **g** and the resonance at 146 ppm is due to carbon **b**. The resonance at 34 ppm in DEPT was displayed below the base line due to CH_2 group (carbon **e**). The resonance at 128 ppm is due to carbon **a**. The resonance at 40 ppm and 52 ppm is due to carbon **f** and **d**, respectively.

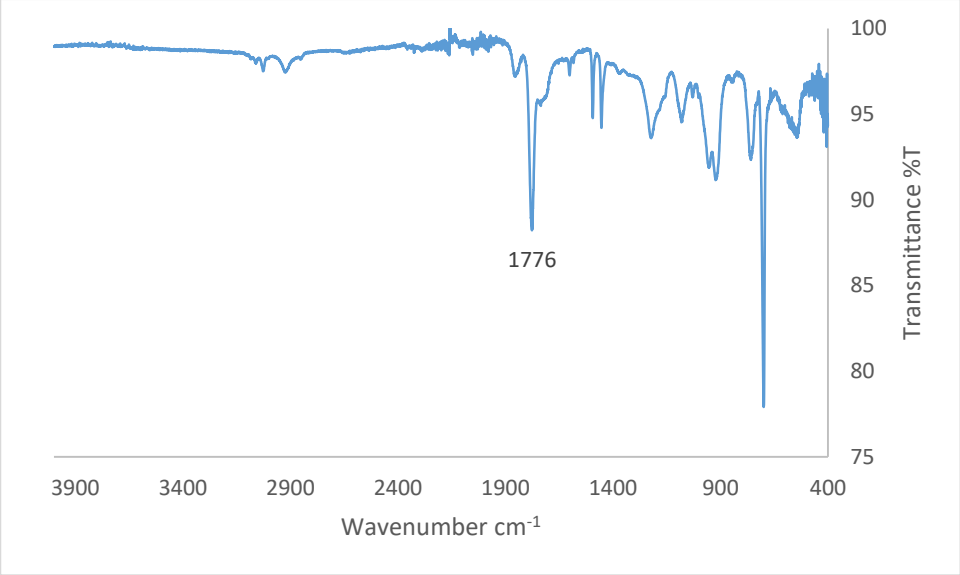

Figure 2.25: the IR spectroscopy of poly(MA-*alt*-St)

The presence of succinic anhydride repeat unit in the product was further confirmed by the IR spectroscopy of poly(MA-*alt*-St), figure 2.25. The peak at 1776 cm^{-1} due to C=O from succinic anhydride. Therefore, the ^{13}C NMR and IR confirm the product to be poly(MA-*alt*-St).

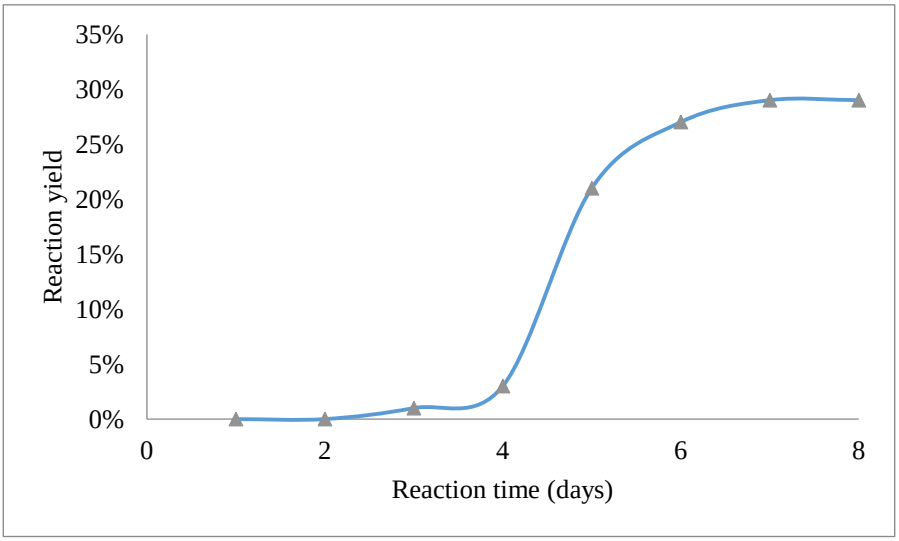

Figure 2.26: The reaction yield of LP22

Reaction LP22 using ratio of MA: St of 1:1 were prepared in respective vials and placed in an oven at 50 °C. A vial was taken out and analysed the reaction yield after 12, 24, 36, 48, 60, and 72 h, in order to investigate the reaction rate, and the results are shown in figure 2.26. Initially, the reaction yield was increased up to 48 h, after which it reached a plateau. The

reaction was undertaken in bulk during which solid product was formed which is believed to be possible for stopping the progress of the reaction and hence reaching a plateau.

Reaction LP22-26 using ratio of MA: St of 1:1, 1:2, 1:4, 1:8, and 1:10 were prepared in respective vials at 50 °C. The table 2.9 shows that the yield of the reaction was decreasing with the increased amount of MA. As more St was added, the yield of the reaction decreased. LP25 and 26 did not form any solid. This indicates that a molar ratio for MA: St of 1:1 is essential for the formation of diradicals and hence poly(St-*alt*-MA).

Table 2.9: the reaction of 4MeOSt and MeMal in different ratio

Reaction	St : MA	Temperature (˚C)	Yield (%)
LP22	1:1	50	29
LP23	2:1	50	18
LP24	4:1	50	14
LP25	8:1	50	0
LP26	10:1	50	0
LP27	1:1	RT	0

2.6 Conclusion

The spontaneous copolymerisations of electron-rich monomers (4MeOSt and St) with electron-poor monomers (MA, MeMal, and EtOCN) were investigated and the resulting linear polymer products were characterised.

The spontaneous copolymerisation of 4MeOSt with MA and 4MeOSt with MeMal were carried out at 50 °C and at ambient temperature and yellow solid was produced, which was found to be soluble in acetone and THF. The products were characterised by 1D NMR (^{1}H and ^{13}C), 2D NMR (^{1}H-^{13}C HSQC and HMBC), SEC, and FTIR. The results confirmed that the polymer products are alternating copolymers. The test followed by different reaction times showed that the cpolymerisations of 4MeOSt with MA in bulk reached a plateau at 50% yield after 12 h and that 4MeOSt with MeMal in bulk reached a plateau at 46% yield after 48 h. The reactions were undertaken in bulk giving solid product which is believed to be responsible for stopping the progress of the reaction and hence reaching a plateau.

The spontaneous copolymerisation of 4MeOSt with EtOCN was carried out at 50 °C and a red-brown solid was produced, which was found to be soluble in acetone and THF. The product was characterised by 1D NMR (^{1}H and ^{13}C), 2D NMR (^{1}H-^{13}C HSQC and HMBC), SEC, and FTIR. The reaction was found to produce poly(4MeOSt) with a yield of 75% after 12 h, believed to be result of homopolymerisation of 4MeOSt initiated by EtOCN. As it is explained in chapter 1 (section 1.6.4), spontaneous copolymerisation between electron-rich and electron-poor olefins could also form zwitterions resulting in either cationic or anionic homopolymerisation. Therefore, it is concluded that the poly(4MeOSt) is formed in the presence of EtOCN via cationic polymerisation. However, the reaction of 4MeOSt with EtOCN did not produce any solid at ambient temperature.

The spontaneous copolymerisation of St with MA was carried out at 50 °C and a yellow solid was produced, which was found to be soluble in acetone and THF. The product was fully characterised. The results confirmed that the polymer product of St with MA is an alternating co-polymer. The tests followed by different reaction times shows that the copolymerisation of St with MA reached a plateau at 30% yield after 60 h. The reaction was undertaken in bulk giving solid product which is believed to be responsible for stopping the progress of the reaction and hence reaching a plateau. However, the reaction of St with MA did not produce any solid at ambient temperature.

Reference

1. Kazuo Nakamoto (16 January 2009). *Infrared and Raman Spectra of Inorganic and Coordination Compounds, Applications in Coordination, Organometallic, and Bioinorganic Chemistry*. John Wiley & Sons. pp. 9. ISBN 978-0-470-40587-1.
2. Hall H. K., Padias A.B., (1990) 'Zwitterion and Diradical Tetramethylenes as Initiators of "Charge-Transfer" Polymerisations', *Acc. Chem. Res.,* 23, 3-9.
3. Eberson L., Persson O., Hall H.K., Padias A.B. (2000) 'Spin Trapping of Radicals from the Reactions between Donor and Acceptor Olefins. Further Evidence for the Tetramethylene Diradical Intermediate as the Initiator of Spontaneous Copolymerisation' *Macromolecules*, 22, 2021-2029.

Chapter 3

Cross-Linked Spontaneous Copolymerisation

3.1 Introduction

The spontaneous (co-)polymerisation of electron-rich and electron-poor olefins was investigated to produce cross-linked polymers (thermoset materials) using di-functional monomers divinylbenzene (DVB). DVB consists of a benzene ring bonded to two vinyl groups. It is related to styrene by the addition of a second vinyl group. Therefore, DVB is used as a cross-linking agent.

Thermoset materials are an important class of materials with excellent thermal and mechanical properties. They have been used in a wide range of applications particularly as coatings, adhesives, and encapsulants.[1] Thermoset materials are stronger than thermoplastic materials due to their three-dimensional network of bonds. The polymer chains lose some of their ability to move as individual one when they are linked together by cross-links. The cross-link brings the polymer toughness, good adhesive and high stable temperature. Low cross-link densities increase the viscosities of polymer melts; intermediate cross-link densities transform gummy polymers into materials that possess elastomeric properties and potentially high strengths; very high cross-link densities can make materials become very rigid or glassy, for example, phenol-formaldehyde materials.[2]

3.2 Materials

Maleic anhydride (MA), 4-methoxystyrene (4MeOSt), divinylbenzene (DVB), styrene, were purchased from Aldrich and used as supplied. Dichloromethane (DCM) (analytical grade, Fisher Scientific), toluene (Analytical Grade, Fisher Scientific), acetone (analytical grade, Fisher Scientific), tetrahydrofuran (THF) (anhydrous, ≥99.9%), chloroform (analytical reagent grade, 99.5%, fisher scientific), were used as supplied.

3.3 Instrumentation

FTIR spectra were recorded on Perkin Elmer 1600 series FTIR spectrometer fitted with a golden gate. The samples were used as solids or liquid. The IR spectra were collected from 4000 to 400 cm^{-1}, with 10 scans per spectrum and 4.00 cm^{-1} resolution. The IR spectra was analysed using Infrared spectroscopy correlation table.[3]

3.4 Experimental

3.4.1 Gel content test

The cross-linked polymer product was weighed as W_1 (1±0.1g) and placed into a clean and dry flask containing a stirring bar and fitted with a condenser. THF (20 mL) was added and the flask was placed into an oil bath. The mixture was refluxed for 5 h. A filter paper was folded and placed into a clean sample vial and was put into an oven set at 100°C and dried for 2 h. The sample vial was sealed by a cap after taken out from the oven, cooled to ambient temperature and was weighed as W_2. The reaction mixture was filtered through a glass funnel fitted with the pre-weighed filter paper. The solid was wrapped by the filter paper and placed in the sample vial. The sample vial was placed into the oven set at 100°C for 4 h. The sample vial was sealed by the same cap after taken out from the oven, cooled to ambient temperature and was weighed as W_3.

The gel content was calculated by: $\frac{W_3-W_2}{W_1} X100\%$.

3.4.2 Reaction of maleic anhydride with divinylbenzene

DVB (0.81 g, 5 mmol) and MA (0.98 g, 10 mmol) were mixed in a sample vial at ambient temperature, upon which the mixture became light yellow. The mixture was kept at 50 °C for 7 days, resulting light yellow solid. The solid product was ground into powder and was subjected to sol-gel analysis, giving 0.75 g, 32 % yield.

FTIR, (cm^{-1}): 1768 (C=O), 1455 (aromatic C=C), 1178-1230 (C-O), 953 (aromatic C-H).

Table 3.1: Reaction of DVB and MA (CP01-05)

Reaction	DVB (g, mmol)	MA (g, mmol)	DVB : MA	Temperature (˚C)	Yield* (%)
CP01	0.81, 5	0.98, 10	1:2	50	32
CP02	1.62, 10	0.98, 10	1:1	50	32
CP03	3.24, 20	0.98, 10	2:1	50	28
CP04	3.24, 20	0.49, 5	4:1	50	10
CP05	0.81, 5	0.98, 10	1:2	RT	29

*Yield is quoted after sol-gel analysis.

CP01-04 were prepared with different ratio of starting materials and kept for 7 days at 50 °C (table 3.1). After the same recovery process as CP01, CP02-04 obtained with 32%, 28% and 10% yields, respectively. CP05 was repeated with the same amount of starting materials as

CP01 at ambient temperature and kept for 7 days. Similar recovery procedure gave 0.52 g white solid, 29 % yield.

3.4.3 Reaction of maleic anhydride, 4-methoxystyrene with divinylbenzene

MA (1.18 g, 12 mmol), 4MeOSt (1.10 g, 8 mmol), and DVB (0.30 g, 2 mmol) using the ratio of DVB: 4MeOSt: MA of 1:4:6 were mixed in a sample vial at ambient temperature, upon which the mixture became yellow. The mixture was heated to 50 °C and kept for 7 days, resulting yellow solid. The solid product was ground into powder and was subjected to sol-gel analysis, giving 1.62 g, 53 % yield.

FTIR, (cm^{-1}): 1775 (C=O), 1440-1609 (aromatic C=C), 1175-1240 (C-O), 826 (aromatic C-H).

CP06-08 were prepared with different ratio of starting materials and kept for 7 days at 50 °C (table 3.2). CP07 and CP08 gave 52% and 27% yields, respectively, following the same recovery process as CP06. CP09 was repeated with the same amount of starting materials as CP06 at ambient temperature and kept for 7 days. Similar recovery procedure gave 1.17 g white solid, 41 % yield.

Table 3.2: Reaction of DVB, 4MeOSt and MA (CP06-09)

Reaction	DVB (g, mmol)	4MeOSt (g, mmol)	MA (g, mmol)	DVB : 4MeOSt : MA	Temperature (˚C)	Yield* (%)
CP06	0.30, 2	0.55, 4	0.78, 8	1:2:4	50	53
CP07	0.30, 2	1.10, 8	1.18, 12	1:4:6	50	52
CP08	0.30, 2	1.64, 12	2.19, 16	1:6:8	50	27
CP09	0.30, 2	0.55, 4	0.78, 8	1:2:4	RT	41

*Yield is quoted after sol-gel analysis.

3.4.4 Reaction of maleic anhydride, styrene with divinylbenzene

MA (1.18 g, 12 mmol), St (0.85 g, 8 mmol), and DVB (0.30 g, 2 mmol) were mixed in a sample vial at ambient temperature, upon which the mixture became yellow. The mixture was heated to 50 °C and kept for 7 days, resulting light yellow solid. The solid product was ground into powder and was subjected to sol-gel analysis, giving 1.19 g, 57 % yield.

FTIR, (cm^{-1}): 1773 (C=O), 1457 (aromatic C=C), 1220 (C-O), 700-912 (aromatic C-H).

CP10-12 were prepared with different ratio of starting materials and kept for 7 days at 50 °C (table 3.3). CP11 and CP12 obtained with 55% and 23% yield, respectively, following the same recovery process as CP10. CP13 was repeated at ambient temperature and left for 7 days, however, no solid was produced.

Table 3.3: Reaction of DVB, St and MA (CP10-13)

Reaction	DVB (g, mmol)	St (g, mmol)	MA (g, mmol)	DVB : St : MA	Temperature (˚C)	Yield* (%)
CP10	0.30, 2	0.43, 4	0.78, 8	1:2:4	50	57
CP11	0.30, 2	0.85, 8	1.18, 12	1:4:6	50	55
CP12	0.30, 2	1.27, 12	1.57, 16	1:6:8	50	23
CP13	0.30, 2	0.43, 4	0.78, 8	1:2:4	RT	0

*Yield is quoted after sol-gel analysis.

3.4.5 Reaction of N-methylmaleimide with divinylbenzene

MeMal (1.10 g, 10 mmol) and DVB (0.81 g, 5 mmol) were mixed in a sample vial at ambient temperature, upon which the mixture became yellow. The mixture was heated up to 50 °C and kept for 7 days, resulting light yellow solid. The solid product was ground into powder and was subjected to sol-gel analysis, giving 0.66 g, 40 % yield.

FTIR, (cm^{-1}): 1700 (C=O), 1281-1430 (aromatic C=C), 1127 (C-N), 953 (aromatic C-H).

CP15-16 were prepared with different ratio of starting materials and kept for 7 days at 50 °C (table 3.4). CP15-16 obtained with 41 and 25% yield, respectively, after the same recovery process as CP14. And CP17 was repeated with the same amount of starting materials as CP14 at ambient temperature and kept for 7 days. Similar recovery procedure gave 0.47 g white solid, 26 % yield.

Table 3.4: Reaction of DVB and MeMal (CP14-17)

Reaction	DVB (g, mmol)	MeMal (g, mmol)	DVB : MeMal	Temperature (˚C)	Yield* (%)
CP14	0.81, 5	1.10, 10	1:2	50	40
CP15	1.62, 10	1.10, 10	1:1	50	41
CP16	3.24, 20	1.10, 10	2:1	50	25
CP17	0.81, 5	1.10, 10	1:2	RT	26

*Yield is quoted after sol-gel analysis.

3.4.6 Reaction of N-methylmaleimide, 4-methoxystyrene with divinylbenzene

DVB (0.3 g, 2 mmol), 4MeOSt (1.10 g, 8 mmol), and MeMal (1.33 g, 12 mmol) were mixed in a sample vial at ambient temperature, upon which the mixture became yellow. The mixture was heated up to 50 °C and kept for 48 h, resulting yellow solid. The solid product was ground into powder and was subjected to sol-gel analysis, giving 1.22 g, 56 % yield.

FTIR, (cm^{-1}) 1685 (C=O), 1382-1432 (aromatic C=C), 1281 (C-O), 1061-1127 (C-N), 703-757 (aromatic C-H).

CP18-20 were prepared with different ratio of starting materials and kept for 7 days at 50 °C (table 3.5). After the same recovery process as CP18, CP19-20 obtained with 56 and 42% yield, respectively. Furthermore, CP21 was repeated with the same amount of starting materials as CP18 at ambient temperature and left for 7 days. Similar recovery procedure gave 0.53 g white solid, 23 % yield.

Table 3.5: Reaction of DVB, MeOSt and MeMal (CP18-21)

Reaction	DVB (g, mmol)	4MeOSt (g, mmol)	MeMal (g, mmol)	DVB : 4MeOSt : MeMal	Temperature (˚C)	Yield* (%)
CP18	0.30, 2	0.55, 4	0.89, 8	1:2:4	50	56
CP19	0.30, 2	1.10, 8	1.33, 12	1:4:6	50	44
CP20	0.30, 2	1.64, 12	1.78, 16	1:6:8	50	42
CP21	0.30, 2	0.55, 4	0.89, 8	1:2:4	RT	23

*Yield is quoted after sol-gel analysis.

3.5 Results and discussion

3.5.1 Maleic anhydride with divinylbenzene

The spontaneous copolymerisation of DVB and MA was carried out at 50 °C and at ambient temperature and a yellow solid was produced, which was found to be insoluble in organic solvents. The cross-linked polymer product obtained at 50 °C was characterised by FTIR, figure 3.1. The presence of C=O at 1768 cm^{-1} corresponding to MA repeat unit is observed.

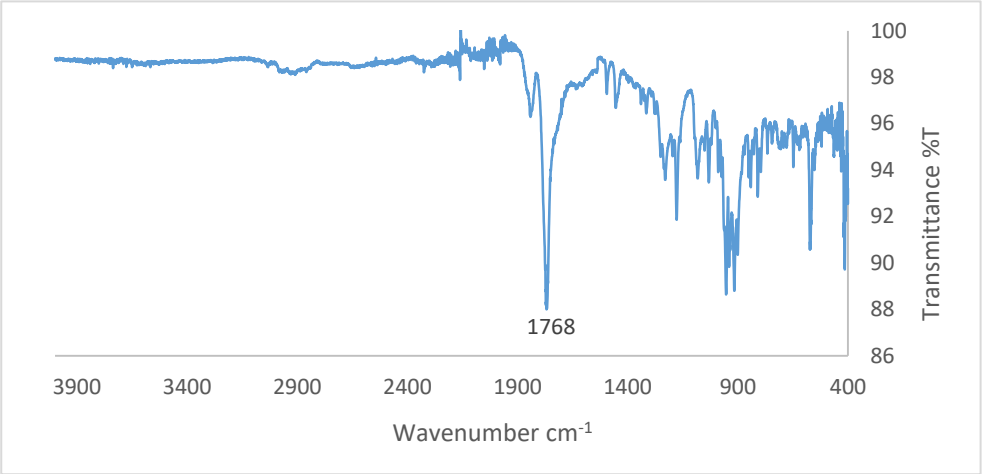

Figure 3.1: the IR spectroscopy of poly(DVB-*alt*-MA)

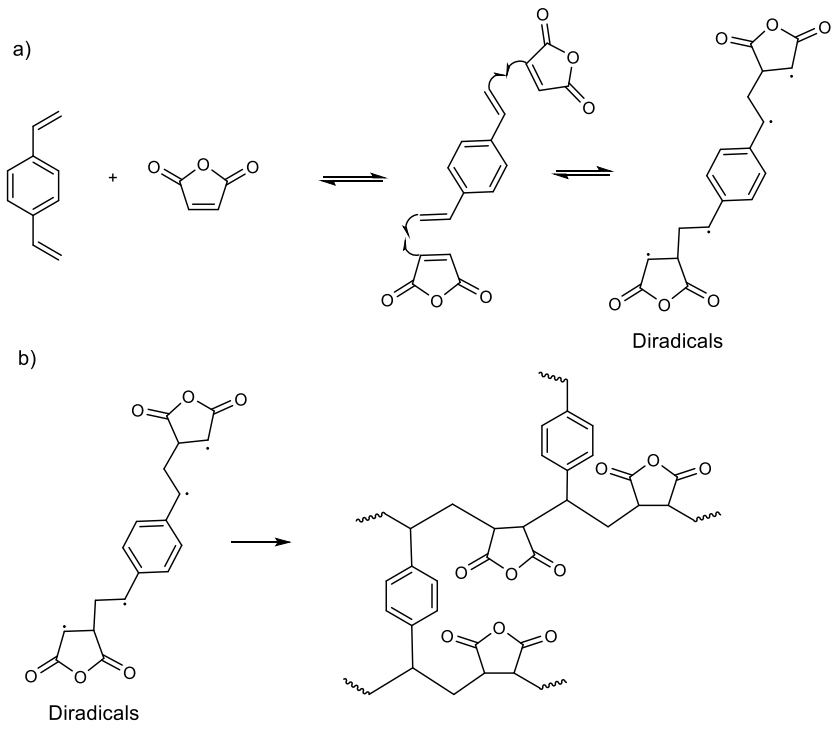

Scheme 3.1: The mechanism of a) formation of diradicals; b) cross-linked polymer

The polymerisation reaction involves DVB (an electron donor) and MA (an electron acceptor) monomers. As it is explained in chapter 1 (section 1.6.4), the spontaneous (co-)polymerisation is believed to occur by electron transfer from donor (DVB) to acceptor (MA) forming diradicals, scheme 3.1a. The diradicals then initiate the copolymerisation (scheme 3.1b) to give cross-linked materials.

The reaction of DVB and MA in a molar ratio of 1:2 (CP01) at 50 °C was followed by gel content determination over a period of 7 days, figure 3.2. Initially, the gel content increased up to 5 days, after which it reached a plateau at 31% gel content. The reaction formed insoluble solid cross-linked material which is believed to be responsible for eventually stopping the progress of the reaction.

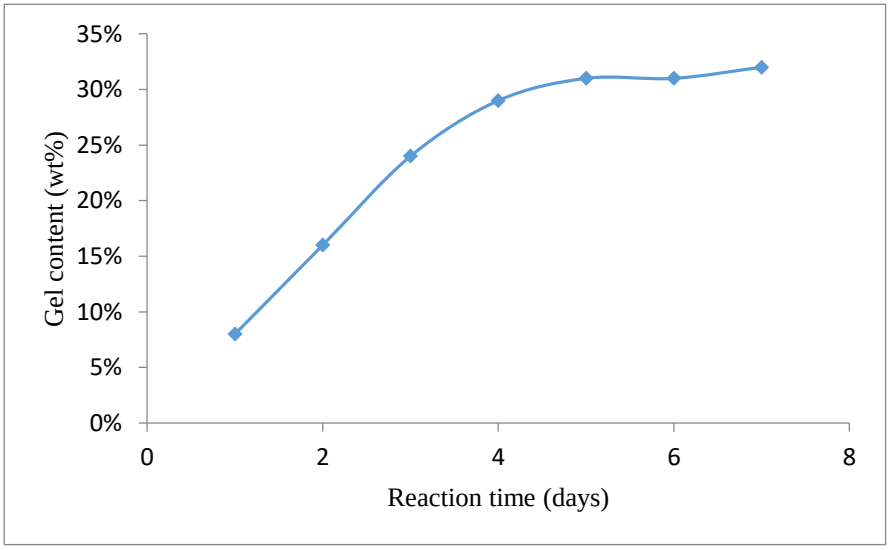

Figure 3.2: The gel content of reaction of DVB with MA

The reaction was repeated with different ratio of starting materials (CP01-04) and kept for 7 days at 50 °C (table 3.6). The gel contents of CP01-04 were found to be 32, 32, 28, and 10%, respectively. The gel content decreased as the amount of DVB increased. This is the expected as both monomers are necessary to form spontaneous co-polymer.

Table 3.6: Gel content of CP01-05

Reaction	DVB : MA	Temperature (˚C)	Gel content (%)
CP01	1:2	50	32
CP02	1:1	50	32
CP03	2:1	50	28
CP04	4:1	50	10

CP05	1:2	RT	29

The reaction of MA with DVB in a molar ratio of 2:1 (CP05) over 7 days produced 29% gel content at ambient temperature indicating that the cross-lined spontaneous copolymerisation of MA and DVB could be carried out without heating.

3.5.2 Maleic anhydride, 4-methoxystyrene, and divinylbenzene

The spontaneous copolymerisation of 4MeOSt, MA and DVB was carried out at 50 °C and at ambient temperature and a yellow solid was produced, which was found to be insoluble in organic solvents. The cross-linked polymer product obtained at 50 °C was characterised by FTIR, figure 3.3. The presence of C=O at 1779 cm^{-1} corresponding to MA repeat unit is observed. Furthermore, the figure 3.3 shows the presence of peaks at 1034 and 1242 cm^{-1} due to C-O stretch (MeO), and 1510 and 1608 cm^{-1} due to aromatic C=C.

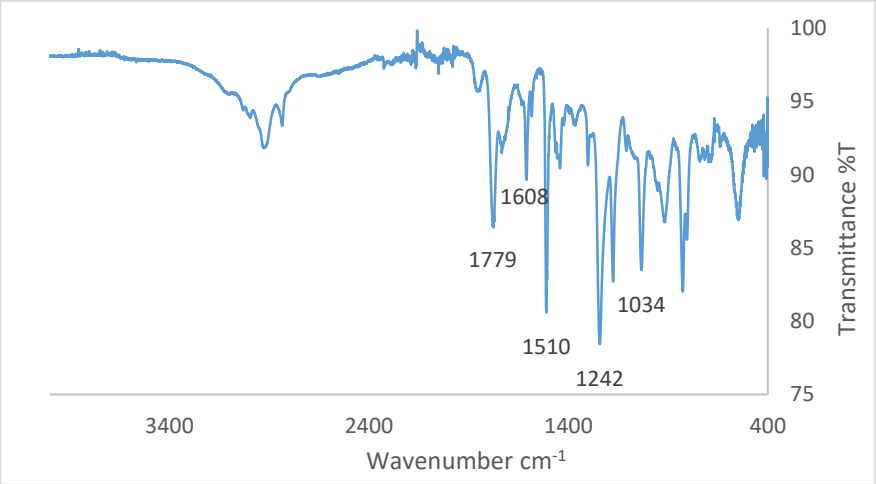

Figure 3.3: the IR spectrum of the product

The copolymerisation reaction involves DVB and 4MeOSt, both electron donor monomers and MA, an electron acceptor monomer. The spontaneous copolymerisation is postulated to occur by electron transfer from donor (DVB and 4MeOSt) to acceptor (MA) to form diradicals.

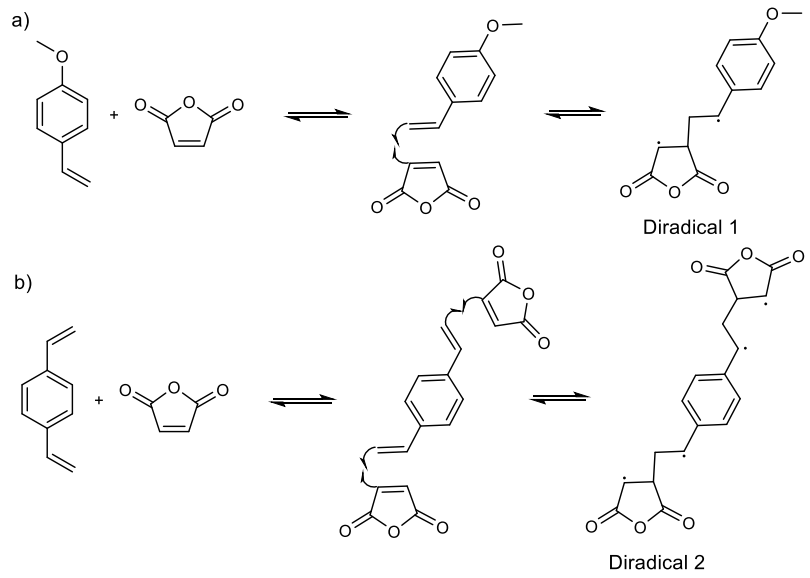

Scheme 3.2: The mechanism of formation of a) diradical 1 and b) diradical 2

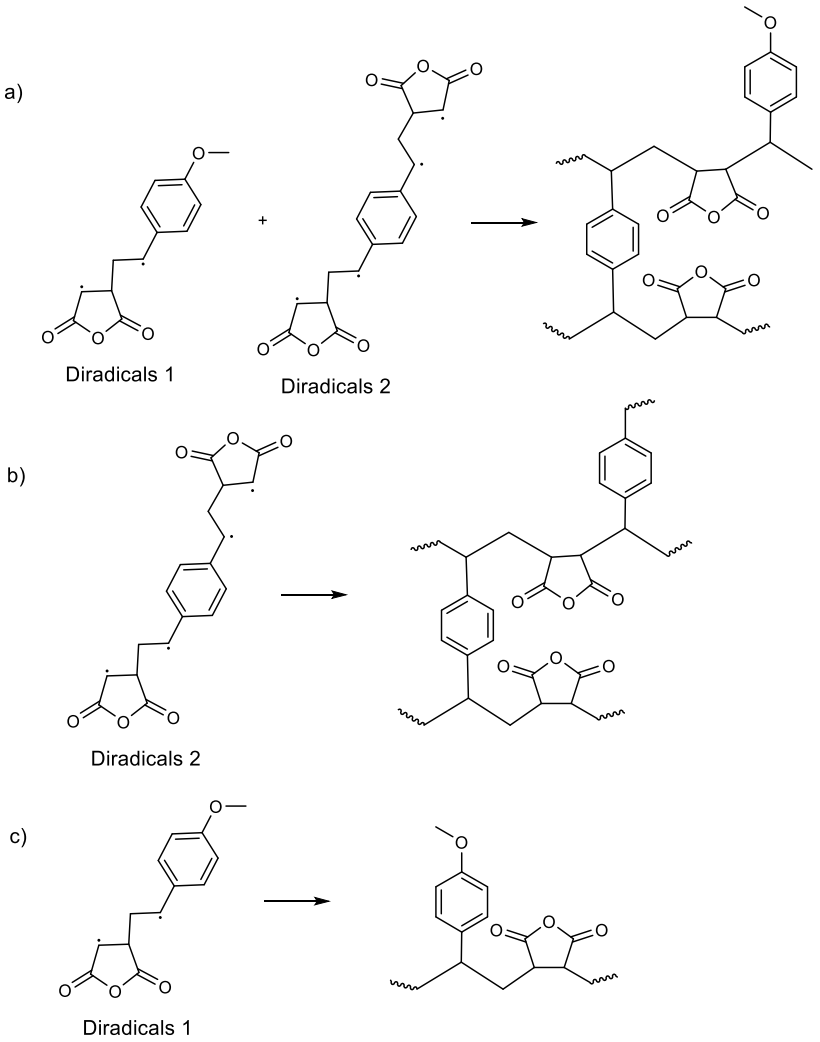

Scheme 3.3: The formation of a) poly(4MeOSt-*co*-MA-*co*-DVB); b) poly(DVB-*co*-MA); and c) poly(4MeOSt-*co*-MA)

The mechanism of the cross-linking reaction is complex. However, in this reaction diradicals 1 (scheme 3.2a) and 2 (scheme 3.2b) are expected to be formed. The two diradicals would then be expected to be involved in 3 possible reactions to give polymer products. The first is the result of the participation of both diradicals 1 and 2 in the polymerisation, scheme 3.3a. The second is the participation of diradical 2 in the polymerisation, scheme 3.3b. The third is the participation of diradical 1 in the polymerisation, scheme 3.3c.

The reaction CP06-08 (table 3.7 in the experimental section) at 50 °C was followed for the gel content over a period of 7 days (figure 3.4) using the ratio of 4MeOSt: DVB of 2:1, 4:1, and 6:1, respectively. The gel content is decreased as the amount of DVB is reduced. This is expected as DVB is the crosslinking agent and controls the degree of crosslinking and hence the gel content. The reaction of MA , 4MeOSt with DVB (CP09) over 7 days produced 41% gel content at ambient temperature indicating that the cross-lined spontaneous copolymerisation of those monomers could be carried out without heating.

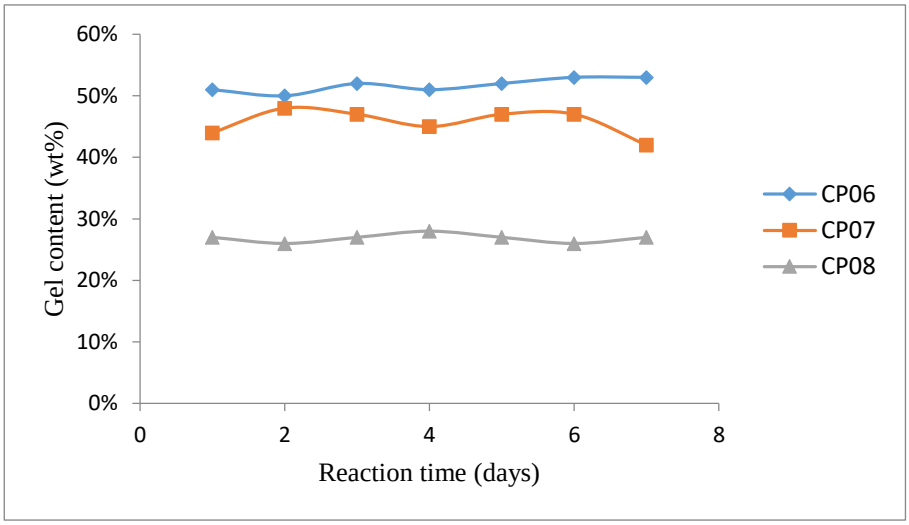

Figure 3.4: the gel content of copolymerisation of DVB, 4MeOSt with MA

3.5.3 Maleic anhydride, styrene, and divinylbenzene

The spontaneous copolymerisation of St, MA, and DVB was carried out at 50 °C and at ambient temperature and a yellow solid was produced, which was found to be insoluble in organic solvents. The cross-linked polymer product formed at 50 °C was characterised by FTIR (figure 3.5), showing the presence of C=O at 1769 cm^{-1} corresponding to MA repeat unit.

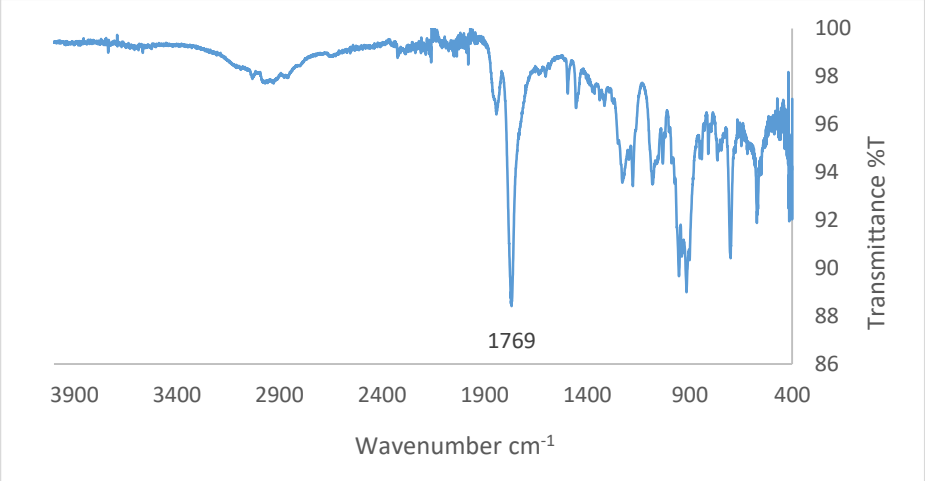

Figure 3.5: the IR spectroscopy of the product of St, MA, and DVB

The polymerisation reaction involves DVB and St, an electron donor monomer and MA, an electron acceptor monomer. The spontaneous (co-)polymerisation is postulated to occur by electron transfer from donor (DVB and St) to acceptor (MA) to form diradicals 1 (scheme 3.4a) and 2 (scheme 3.4b).

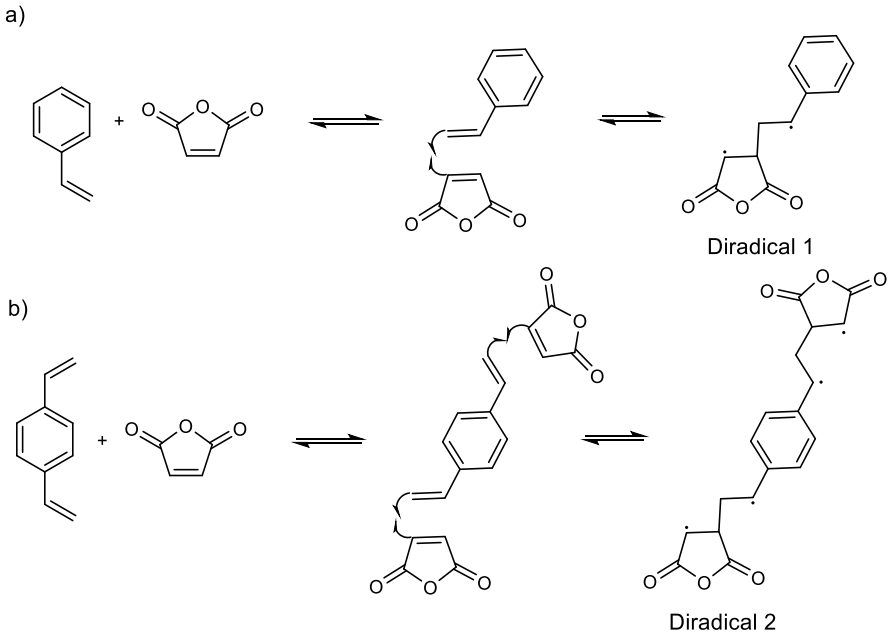

Scheme 3.4: The mechanism of formation of a) diradical 1 and b) diradical 2

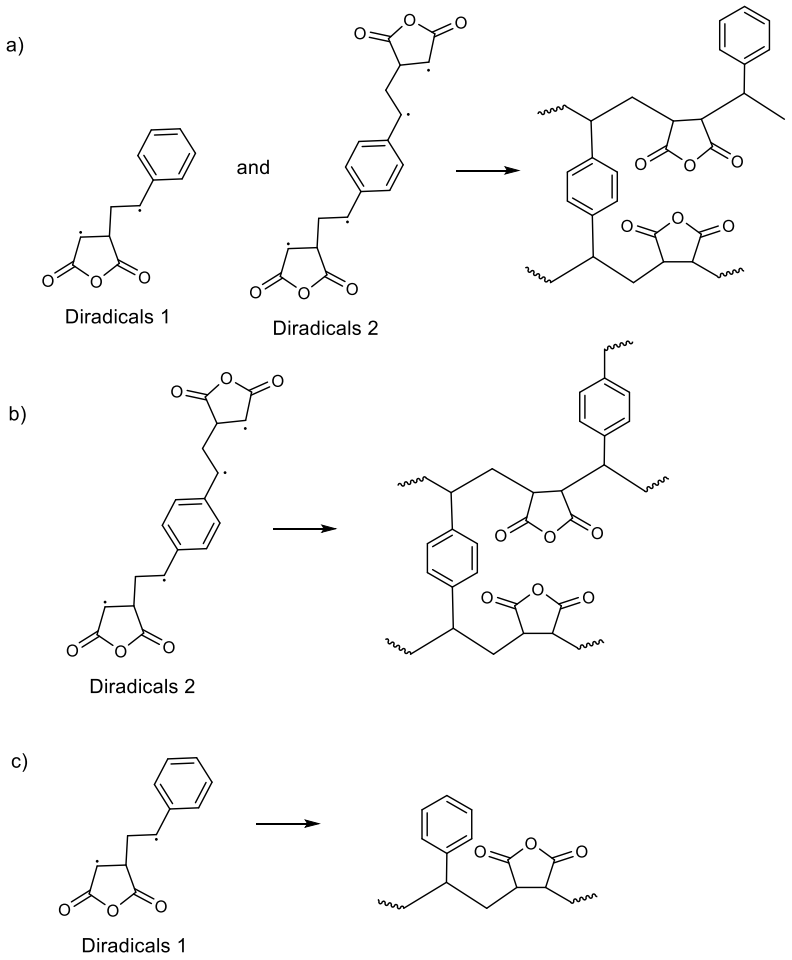

Scheme 3.5: The formation of a) poly(St-*co*-MA-*co*-DVB); b) poly(DVB-*co*-MA); and c) poly(St-*co*-MA)

Again, the mechanism of the cross-ling reaction is complex. The two diradicals would be expected to be involved in 3 possible reactions to give the polymer products. The first is the result of the participation of both diradicals 1 and 2 in the polymerisation, scheme 3.5a. The second is the participation of diradical 2 in the polymerisation, scheme 3.5b. The third is the participation of diradical 1 in the polymerisation, scheme 3.5c.

The reaction of St, MA and DVB at 50 °C was followed for the gel content over a period of 7 days using the molar ratio of DVB: St of 1:2, 1:4, and 1:6 (CP10-12), figure 3.6. Initially, the gel content increased up to 5 days, after which it reached a plateau at 56% gel content for CP10 & CP11 and 47% gel content for CP12. This is believed to be due to the formation of insoluble cross-linked material hindering and eventually stopping the progress of the reaction. The gel content is decreased as the amount of DVB is reduced. This is expected as DVB is a cross-linking agent and controls the degree of cross-linking and hence the gel content.

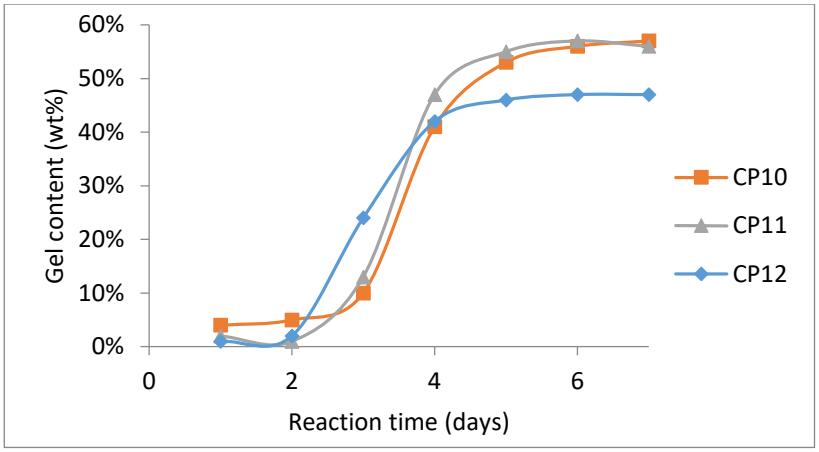

Figure 3.6: the gel content of DVB, St with MA

The reaction of MA, St with DVB (CP13) did not produce any solid at ambient temperature over 7 days indicating that the cross-lined spontaneous copolymerisation of those monomers is difficult to be carried out without heating due to the spontaneous copolymerisation of MA and St was difficult to carried out at ambient temperature (the results in Chapter 2).

3.5.4 N-Methylmaleimide with divinylbenzene

The spontaneous copolymerisation of MeMal and DVB was carried out at 50 °C and at ambient temperature and a yellow solid was produced, which was found to be insoluble in organic solvents.

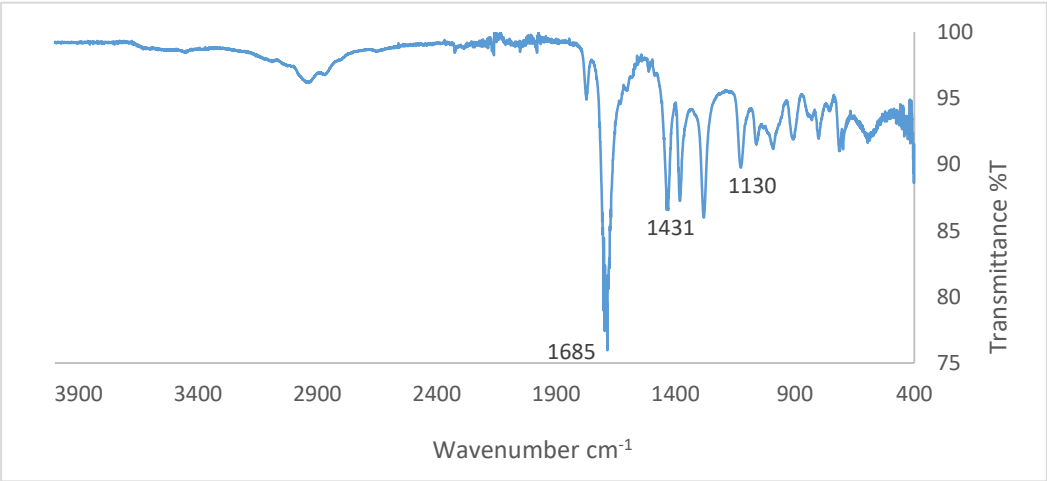

Figure 3.6: the IR spectrum of the product of DVB and MeMal

The cross-linked polymer product obtained at 50 °C was characterised by FTIR (figure 3.6) showing the presence of C=O at 1685 cm^{-1} and C-N at 1130 cm^{-1}corresponding to MeMal repeat unit. Furthermore, the presence of aromatic C=C at 1431 cm^{-1} corresponding to DVB

repeat unit is also observed.

The polymerisation reaction involves DVB, an electron donor monomer and MeMal, an electron acceptor monomer. The spontaneous (co-)polymerisation is postulated to occur by electron transfer from donor (DVB) to acceptor (MeMal) forming diradicals, scheme 3.6a. The diradicals then initiate the copolymerisation to form the product, scheme 3.6b.

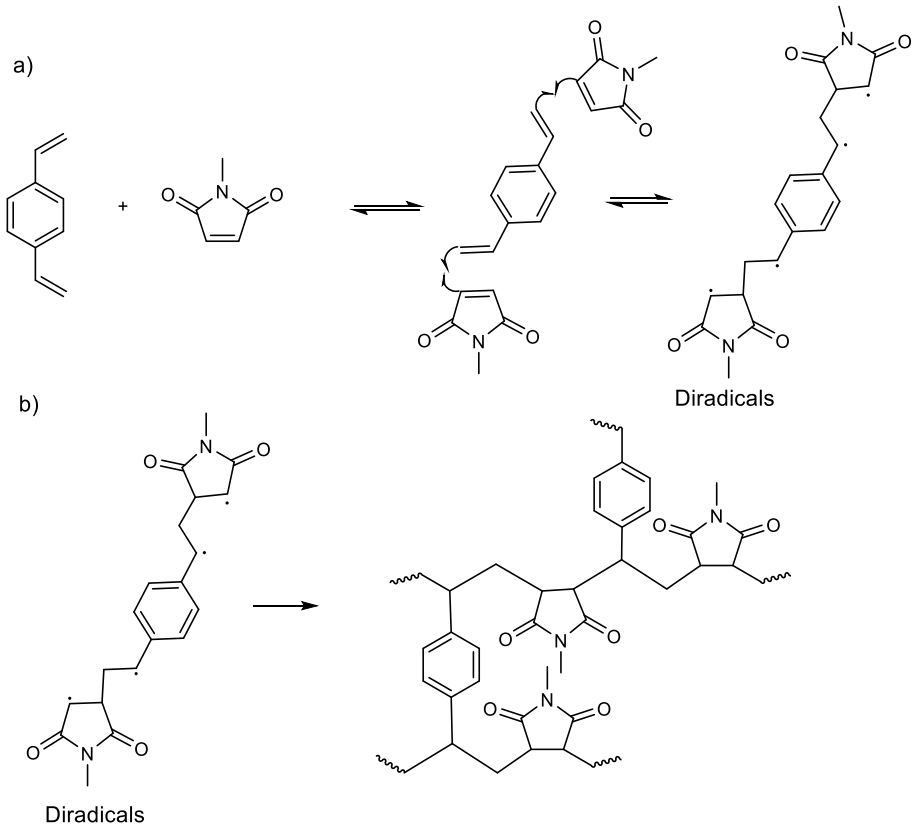

Scheme 3.6: The mechanism of a) formation of diradicals; b) cross-linked polymer

The reaction of DVB and MeMal in a molar ratio of 1:2 at 50 °C was followed for the gel content over a period of 7 days, figure 3.7. Initially, the gel content increased up to 5 days, after which it reached a plateau at 40% gel content. The reaction formed insoluble solid cross-linked material which is believed to be responsible for eventually stopping the progress of the reaction.

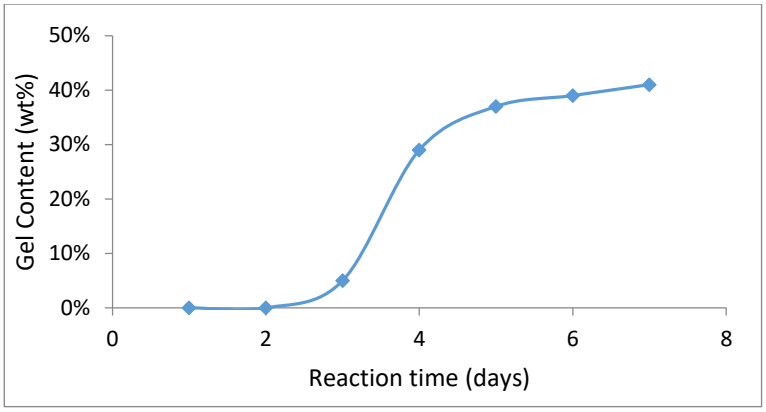

Figure 3.7: The gel content of reaction of DVB and MeMal

This reaction was prepared with ratios of DVB: MeMal of 1:2, 1:1, and 2:1 starting materials and kept for 7 days at 50 °C (CP14-16) (table 3.7). The gel content of CP14-16 was found to be 40%, 41%, and 25%, respectively. The gel content decreased as the amount of DVB increased. This is the expected as DVB is the crosslinking agent and more DVB result in more crosslinking and hence more gel content.

The reaction using malor ratio DVB: MeMal of 2:1 (CP17) left at ambient temperature for 7 days produced 26% gel content indicating that the cross-lined spontaneous copolymerisation of those monomers could be carried out without heating.

Table 3.7: The gel content of CP14-17

Reaction	DVB : MeMal	Temperature (˚C)	Gel content (%)
CP14	1:2	50	40
CP15	1:1	50	41
CP16	2:1	50	25
CP17	1:2	RT	26

3.5.5 N-Methylmaleimide, 4-methoxystyrene with divinylbenzene

The spontaneous copolymerisation of 4MeOSt, MeMal and DVB was carried out at 50 °C and at ambient temperature and a yellow solid was produced, which was found to be insoluble in organic solvents. The cross-linked polymer product was characterised by FTIR (figure 3.8) showing the presence of C=O at 1685 cm^{-1} and C-N at 1127 cm^{-1}corresponding to MeMal repeat unit. Furthermore, the presence of aromatic C=C at 1433 cm^{-1} corresponding to DVB and 4MeOSt repeat unit and the presence of aromatic C-O at 1282

cm^{-1} corresponding to 4MeOSt repeat unit is also observed.

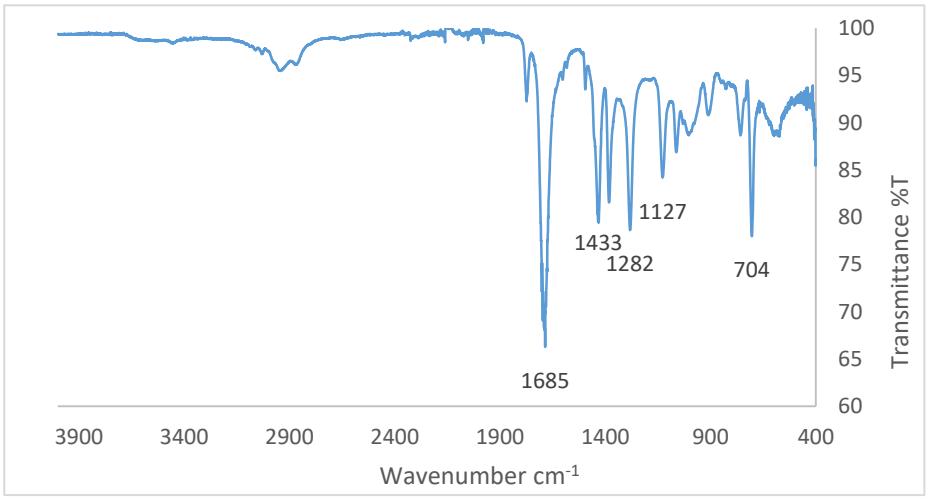

Figure 3.8: the IR spectrum of the product of DVB, 4MeOSt and MeMal

The copolymerisation reaction involves DVB and 4MeOSt, both electron donor monomers and MeMal, electron acceptor monomer. The spontaneous copolymerisation is postulated to occur by electron transfer from donor (DVB and 4MeOSt) to acceptor (MeMal) to form diradicals 1 (scheme 3.7a) and 2 (scheme 3.7b).

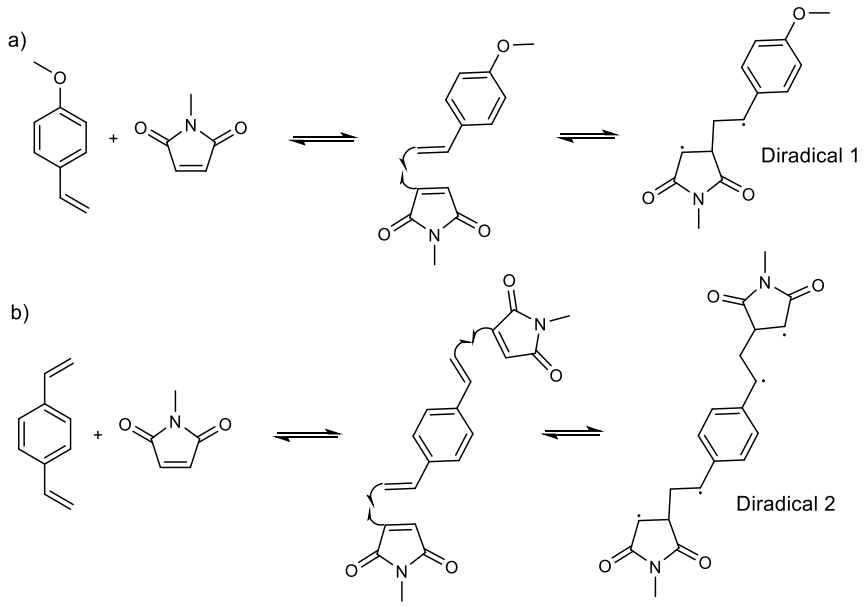

Scheme 3.7: The mechanism of formation of a) diradical 1 and b) diradical 2

As explained previously, the mechanism of the cross-linking reaction is complex. The two diradicals would be expected to be involved in 3 possible reactions to give the polymer products. The first is the result of the participation of both diradicals 1 and 2 in the

polymerisation, scheme 3.8a. The second is the participation of diradical 2 in the polymerisation, scheme 3.8b. The third is the participation of diradical 1 in the polymerisation, scheme 3.8c.

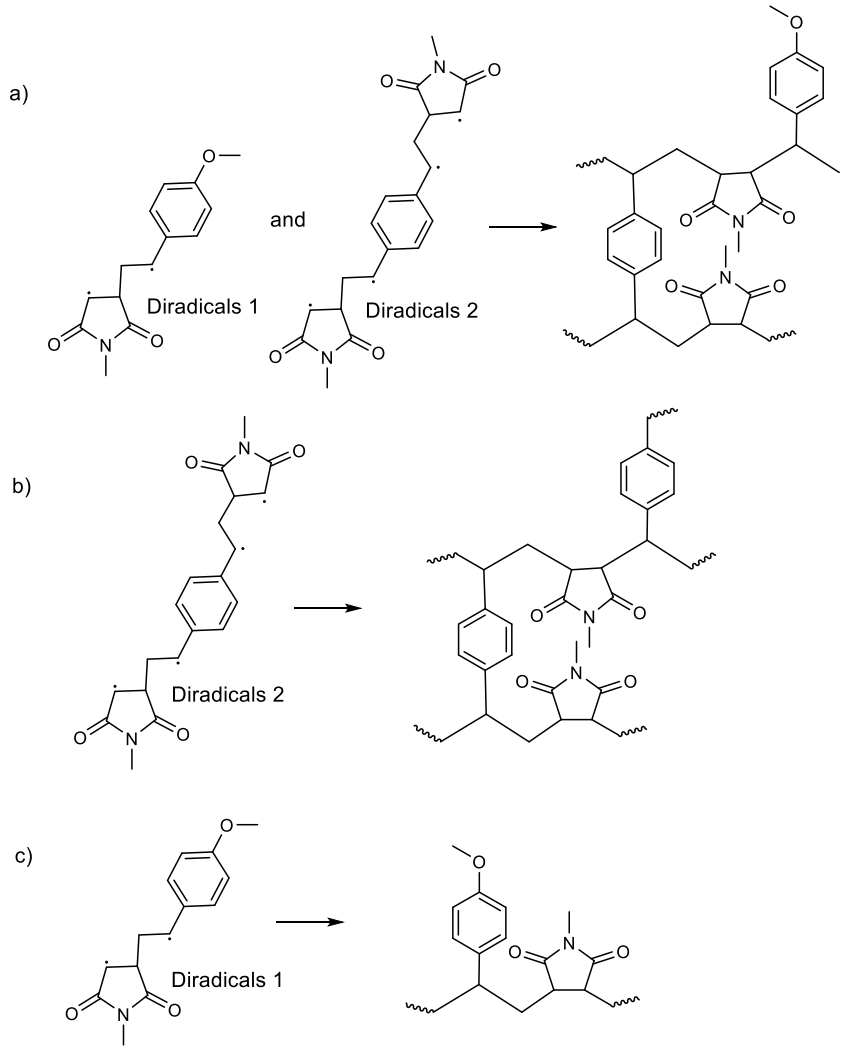

Scheme 3.8: The formation of a) poly(4MeOSt-*co*-MeMal-*co*-DVB); b) poly(DVB-*co*-MeMal); and c) poly(4MeOSt-*co*-MeMal)

The reaction CP18-20 carried out at 50 °C and was followed for the gel content over a period of 7 days (figure 3.9) using the ratio of 4MeOSt: DVB of 2:1, 4:1, and 6:1, respectively. The gel content is decreased as the amount of DVB is reduced. This is expected as DVB is crosslinking agent and control the degree of crosslinking and hence the gel content.

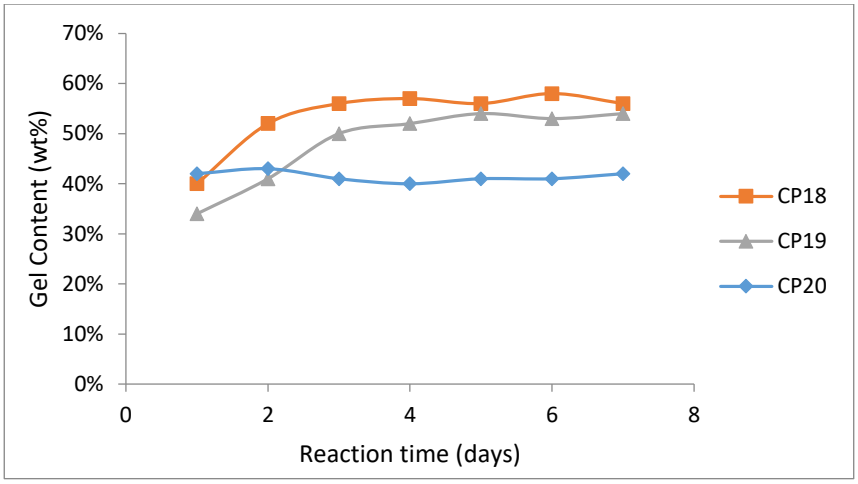

Figure 3.9: The gel content of reaction of DVB, 4MeOSt and MeMal

The reaction of MeMal, 4MeOStSt with DVB (CP21) produced 23% gel content at ambient temperature over 7 days indicating that the cross-lined spontaneous copolymerisation of those monomers could be carried out without heating.

3.6 Conclusion

The spontaneous copolymerisation of electron-rich monomers (4MeOSt, St, and DVB) with electron-poor monomers (MA and MeMal) was investigated at ambient temperature and at 50°C. The resulting insoluble cross-linked polymer products were characterised by FTIR. The results confirmed that the cross-linked polymer product contains the repeating units due to MA and MeMal monomers used in the reaction.

The copolymerisation of electron-rich monomers (4MeOSt, St, and DVB) with electron-poor monomers (MA and MeMal) was followed by gel content determination over a period of 7 days. Initially, the gel content increased for a few days, after which it reached a plateau around 33%-57% at 50 °C and 23%-41% at ambient temperature based on the monomers used. The reaction formed insoluble cross-linked material which is believed to be responsible for eventually stopping the progress of the reaction resulting in a plateau.

Reference

1. Malik, J.; Clarson, S.J.; *Int. J. Adhes. Adhes.*, 2002, **22**, 283-289
2. Chen, J.; Ober, C.K.; Poliks, M.D; *Polymer*, 2002, **43**, 131-139
3. Kazuo Nakamoto (16 January 2009). *Infrared and Raman Spectra of Inorganic and Coordination Compounds, Applications in Coordination, Organometallic, and Bioinorganic Chemistry*. John Wiley & Sons. pp. 9. ISBN 978-0-470-40587-1.
4. Hall H. K., Padias A.B., (1990) 'Zwitterion and Diradical Tetramethylenes as Initiators of "Charge-Transfer" Polymerisations', *Acc. Chem. Res.,* 23, 3-9.
5. Eberson L., Persson O., Hall H.K., Padias A.B. (2000) 'Spin Trapping of Radicals from the Reactions between Donor and Acceptor Olefins. Further Evidence for the Tetramethylene Diradical Intermediate as the Initiator of Spontaneous Copolymerisation' *Macromolecules*, 22, 2021-2029.

Chapter 4

Micro-Encapsulation

5.1 Introduction

Self-healing of polymers and composites containing micro-encapsulated healing agents offer tremendous potential for providing long-lived structural materials. The micro-capsules in self-healing polymers not only store the healing agent during quiescent states, but provide a mechanical trigger for the self-healing process when damage occurs in the host material and the capsules are ruptured. The key feature of self-healing materials is the highly engineered microencapsulated healing agent. The micro-capsules must possess sufficient strength to remain intact during processing of the host polymer, yet rupture when the polymer is damaged. High bond strength to the host polymer combined with a moderate strength of micro-capsule shell is required. To provide long shelf-life the capsules must be impervious to leakage and diffusion of the encapsulated (liquid) healing agent for considerable time. These combined characteristics are achieved with a system based on the in-situ polymerisation of urea-formaldehyde (UF) micro-capsules encapsulating healing agent. The addition of these micro-capsules to an epoxy matrix also provides a unique toughening mechanism for the composite system.

5.2 Materials

4-Methoxystyrene (4MeOSt) (technical grade, 80%), divinylbenzene (DVB) (technical grade, 80%), styrene (St) (analytical standard), poly (ethylene-*alt*-maleic anhydride) copolymer (EMA), urea (powder, Bio-reagent), ammonium chloride (≥99.5%), resorcinol (ReagentPlus®, 99%), sodium hydroxide (anhydrous, free-flowing, pellets, Redi-Dri™, ACS reagent, ≥97%), hydrochloric acid (36.5~38.0%), 1-octanol (analytical standard), and aqueous solution of formaldehyde (contains 10-15% methanol as stabiliser, 37 wt. % in H_2O) were purchased from Aldrich and used as supplied.

Dichloromethane (DCM) (analytical grade, Fisher Scientific), acetone (analytical grade, Fisher Scientific), and deionised water were used as supplied.

5.3 Instrumentation

SCILOGEX OS20-S LED digital overhead stirrer driving a three-bladed (50mm diameter); desktop-pH-meter FiveEasy™ Profi-Kit FE 20 ATC; and fine test sieves (Brass frame, pore size 250, 500 μm, and 1 mm).

NMR spectra were either recorded on a Bruker Avance 400 spectrometer at 400.0 MHz (^{1}H) and 100.6 MHz (^{13}C); or a Varian Inova 500 spectrometer at 499.8 MHz (^{1}H, COSY, HSQC) and 125.7 MHz (^{13}C). All chemical shifts were referenced to the residual proton of the deuterated solvent.

Scanning electron microscope (SEM) pictures were taken by Philips/FEI XL30 ESEM®; optical microscope linked to a digital image recording system。

5.4 Experimental

5.4.1 Preparation of aqueous solution of EMA copolymer

Aqueous solution of EMA co-polymer was prepared following the literature.[1]

EMA copolymer (2.5 g), sodium hydroxide (0.1 g, 0.1 wt. %) and deionised water (97.5 g) were mixed in a 250 mL round bottom flask with a manganic stir bar fitted with a reflux condenser. The flask was suspended in a temperature-controlled oil bath on a hotplate with external temperature probe. The mixture was heated up to 80 ºC and kept stirring for 12 h, after which became a transparent viscous solution.

5.4.2 Micro-encapsulation process

Micro-encapsulation process was carried out following the literature.[1]

Micro-capsules were prepared by in-situ polymerisation in an oil-water emulsion. The healing agents used in the micro-encapsulation experiments are shown in table 4.1. Deionised water (100 mL) and aqueous solution of EMA copolymer (2.5 wt. %, 25mL) were mixed in a 500 mL beaker at ambient temperature. The beaker was suspended in a temperature-controlled water bath on a hotplate with external temperature probe. The solution was agitated with a digital overhead stirrer driving a three-bladed, 50mm diameter low-shear mixing propeller placed just above the bottom of the beaker. Under agitation, urea (2.50 g, 0.04 mmol), ammonium chloride (0.25 g, 4.67 mmol) and resorcinol (0.25 g, 2.27 mmol) dissolved in the solution. The pH increased from ~2.60 to 3.50 by drop-wise addition of sodium hydroxide and hydrochloric acid. 1-octanol (1~2 drops) was added to eliminate surface bubbles.

Table 4.1: The amount of healing agents used in micro-encapsulation process

Experiment code	Healing agents	Amount (g)
MC01	4MeOSt	25
MC02	DVB	25
MC03	St	25
MC04	4MeOSt+DVB (4:1)	19+6
MC05	4MeOSt+DVB (2:1)	15+10
MC06	St+DVB (4:1)	18+7
MC07	St+DVB (2:1)	13+12

The required amount of healing agents was added to form an emulsion and allowed to stabilise for 10 min. Aqueous solution of formaldehyde (37 wt. %) (6.341 g, 0.076 mol) was

added to obtain a ratio of formaldehyde: urea of 1.9: 1. The beaker was covered with aluminium foil and heated slowly to 55 °C and left for 4 h under continuous agitation. Once cooled to ambient temperature, the suspension of micro-capsules was separated under vacuum using a coarse-fritted filter. The micro-capsules were rinsed with deionised water and dichloromethane (10: 1 in volume) and air dried for 48 h. The yield of fine micro-capsules was 76-88%.

5.4.3 Analysis of the size distribution and selection of micro-capsules

Micro-capsule size analysis was performed with SEM and image analysis software. Mean diameter and standard deviation were determined from data sets of at least 50 measurements.

All the micro-capsules after drying were sieved by fine test sieves. The pore size of 1 mm sieve was firstly used to remove large poly (urea-formaldehyde) particles. Then, the pore size of 250 μm and 500 μm sieves were used to collect the micro-capsules within size of 250-500 μm.

5.4.4 The content and shell thickness of micro-capsules

Micro-capsules (1 g) were placed into a mortar, and then were crushed by a pestle. Chloroform (10 mL) was added and the solution containing healing agent was filtered by coarse-fritted filter under reduced pressure. The solution was transferred into a round bottom flask, and then chloroform was removed by rotary evaporator under reduced pressure. The remains liquid in the flask was weigh and characterised by NMR. The solid powder was dried in a vacuum oven, after which were weighed and characterised by SEM to determine their thicknesses. The percentage of healing agent content for the micro-capsules were calculated and shown in table 4.2.

Table 4.2: The healing agent content of micro-capsules

Healing agent	Weight of micro-capsules (g)	Weight of the micro-capsules shall (g)	Healing agent content (%)
4MeOSt	1.00	0.29	71
DVB	1.00	0.27	73
St	1.00	0.25	75
4MeOSt with DVB	1.00	0.30	70
St with DVB	1.00	0.31	69

5.5 Results and discussion

5.5.1 Micro-encapsulation process

Micro-capsule diameter and surface morphology significantly influence capsule rupture behaviour and hence healing agent release in self-healing polymers. All the micro-capsules were analysed by SEM for the size distribution, surface quality, and shell thickness.

High quality urea-formaldehyde micro-capsules using for in self-healing process were prepaired. The core of these micro-capsules was liquid electron-rich monomers, 4MeOSt, DVB, St, and their mixtures. The micro-capsules were spherical and free flowing after drying (figure 4.1). The yields, defined by the ratio of the mass of micro-capsules to the total mass of 4MeOSt, DVB, St, urea, and formaldehyde, were 76–88%.

Figure 4.1: Micro-capsules containing different healing agents

The ratio of monomers (oil) and water was changed to see the effect of monomer concentration on the surface of micro-capsules.

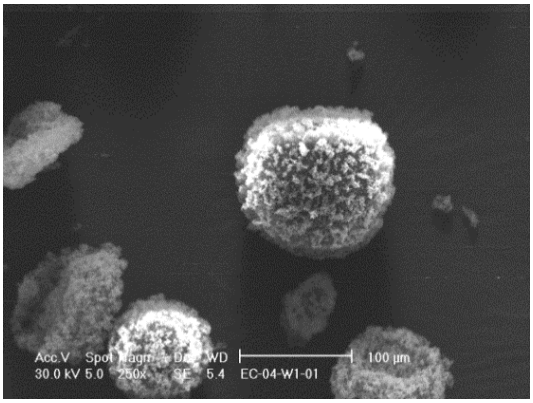

(a)

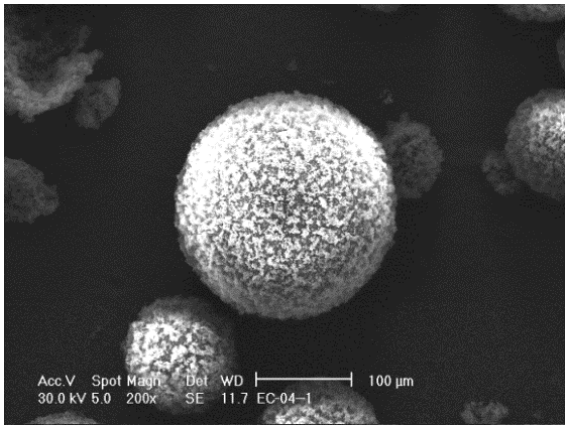

(b)

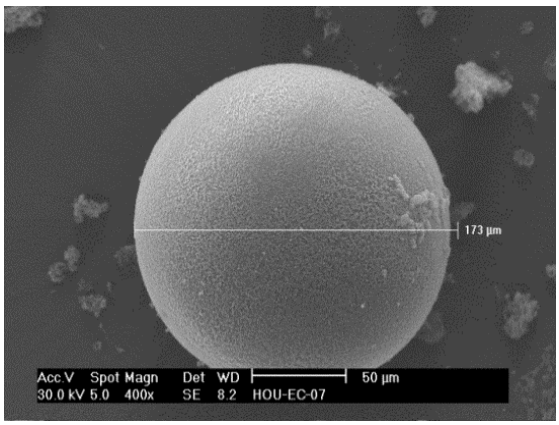

(c)

Figure 4.2: ESEM image of UF micro-capsules based the concentration (by vol%) of 4-methoxystyrene in oil-water emulsion: (a) 17%, (b) 20%, and (c) 23%.

Figure 4.2 shows micro-capsules made by using different concentration of oil (monomers) and water of 17% (a), 20% (b), and 23% (c), but with the same ratio of urea, ammonium chloride, resorcinol, and formaldehyde. As it can be seen, the surface of the micro-capsules was changed from very rough (a & b) to smoother (c) as the oil-water ratio increased.

The micro-capsules exhibited a rough surface could also be due to the presence of urea-formaldehyde. A smooth contact surface is essential to bond with the matrix materials. Moreover, if the surface of the micro-capsules is too rough, the tension force of matrix materials could crack open only small amount of micro-capsules. 4MeOSt micro-capsules were washed with deionised water and DCM to make the surface smooth and therefore to increase the surface quality.

Figure 4.3 shows micro-capsules prepared at different initial pH. At the pH of 2.5 micro-capsules were agglomerated (figure 4.3 a) whereas at pH of 3.5 they were free flowing and

well dispersed (figure 4.3 b). As the pH decreases, the viscosity is increased the affecting the droplet formation leading to agglomeration of micro-capsules, similar observation has previously been reported.[3]

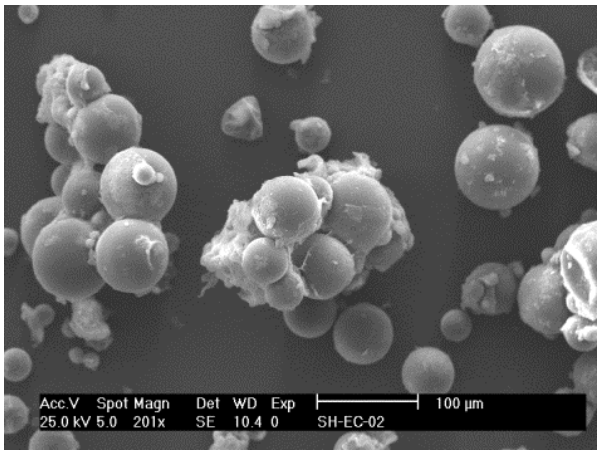

(a)

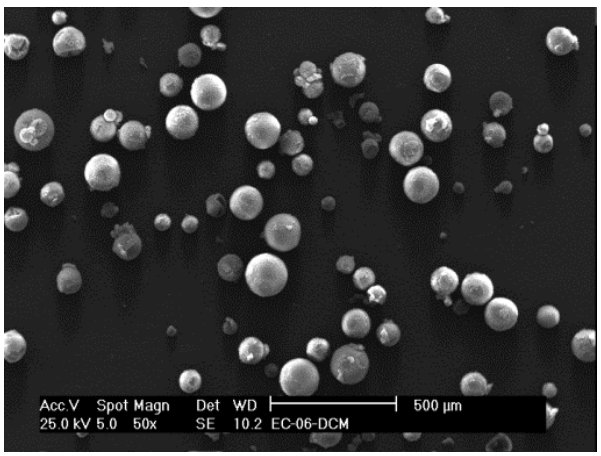

(b)

Figure 4.3: SEM image of UF micro-capsules containing 4MeOst prepared with the initial pH: (a) 2.5, and (b) 3.5

5.5.2 Micro-capsules size distributions

Average micro-capsule diameter is controlled by agitation rate, as shown in figure 4.4. As the agitation rate increased, a finer emulsion was obtained and the average micro-capsule diameter decreased. Micro-capsules with average diameter in the range of 10 – 1000 µm are obtained by adjusting agitation rate between 200 – 1500 rpm.

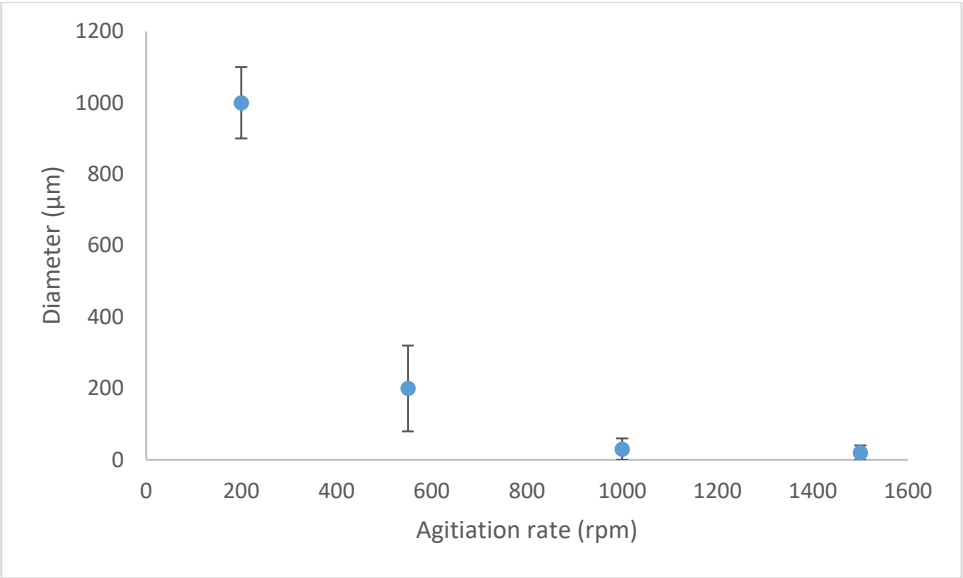

Figure 4.4: Mean micro-capsule diameter vs agitation rate.

Size analysis was performed by SEM on data sets of at least 50 measurements at each agitation rate. Error bars correspond to standard deviation of the data. The standard deviation was reduced as the agitation rate increased; however, the yield of fine micro-capsules was also reduced from 76-88% to 34-41%. Moreover, the amount of liquid content which is dependent as the size of the micro-capsules was reduced from 69-77% to 42-53%.

5.5.3 Micro-capsules

5.5.3.1 4-Meoxystyrene micro-capsules

The diameter of 4MeOSt micro-capsules prepared was found to be in the range of 50-500 μm at 550 rpm. These micro-capsules were subjected to sieving to collect those with the diameter of 100-200 μm, figure 4.5.

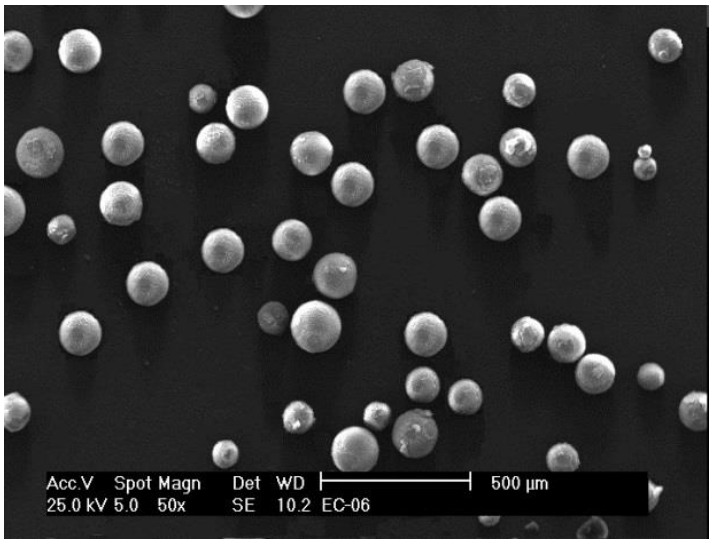

(a)

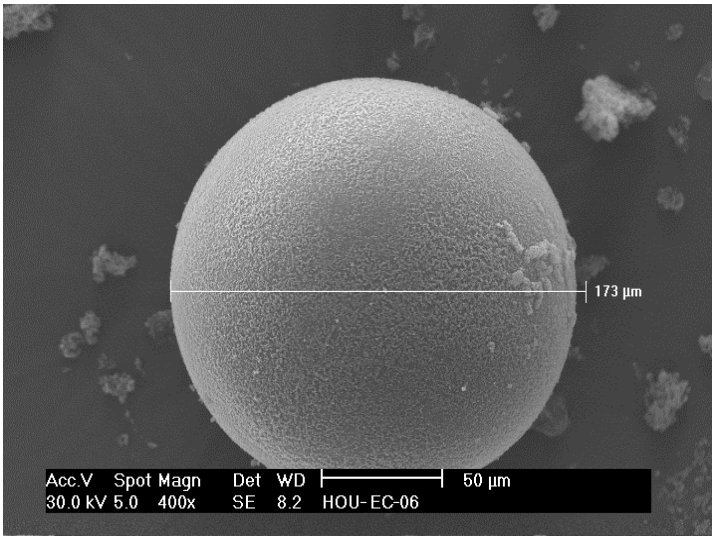

(b)

Figure 4.5: SEM image of the surface morphology of 4MeOSt micro-capsules, a) using magnification of 50×, b) using magnification of 400×

The liquid content of micro-capsules could be viewed by optical microscopy, figure 4.6. The light spot in the picture is the light refraction of liquid monomers indicating efficient encapsulation of liquid 4MeOSt healing agent.

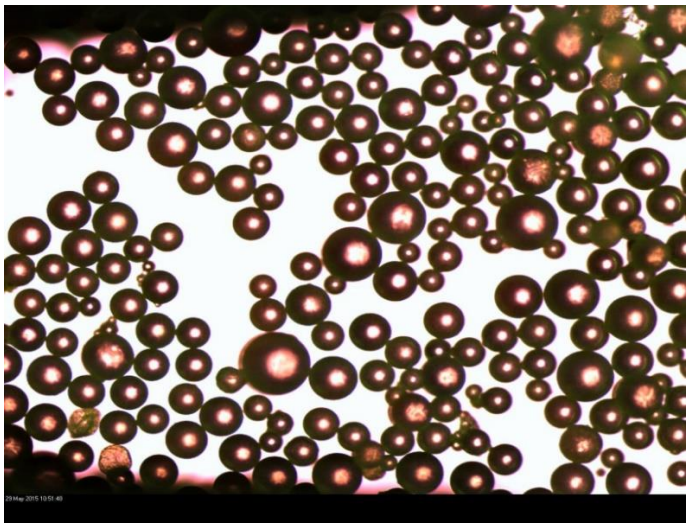

Figure 4.6: Optical microscopy (magnification of 20×) image of 4MeOSt micro-capsules

The shell wall thickness of 4MeOSt micro-capsules was also investigated by SEM, figure 4.7. The average thickness of 4MeOSt micro-capsules was found to be about 200 nm.

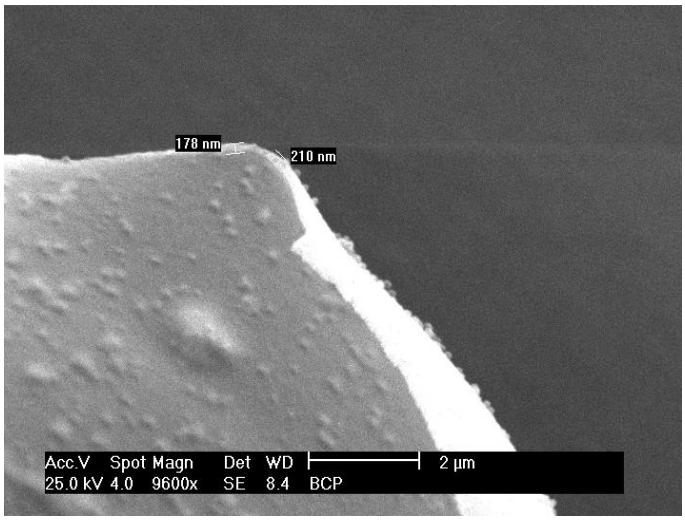

Figure 4.7: SEM image (magnification of 9600×) of the shell thickness of MeOSt micro-capsules

The healing agent contents of 4MeOSt micro-capsules were investigated. The ^{1}H NMR spectrum of the healing agents extracted from 4MeOSt micro-capsules is shown in figure 4.8. The spectrum shows the resonances at 7.49 ppm and 7.02 ppm due to the 4 protons of the

aromatic ring (H_1 and H_2); the resonance at 6.80 ppm due to the 1 proton of the –CH– group (H_3); the resonances at 5.81 ppm and 5.31 ppm due to the 2 protons of the $=CH_2$ group (H_4 and H_4'); and the resonance at 3.89 ppm due to the 3 protons of the methyl group (H_5). The result confirms that the extract was identical to that of the monomer (4MeOSt) used for micro-encapsulation.

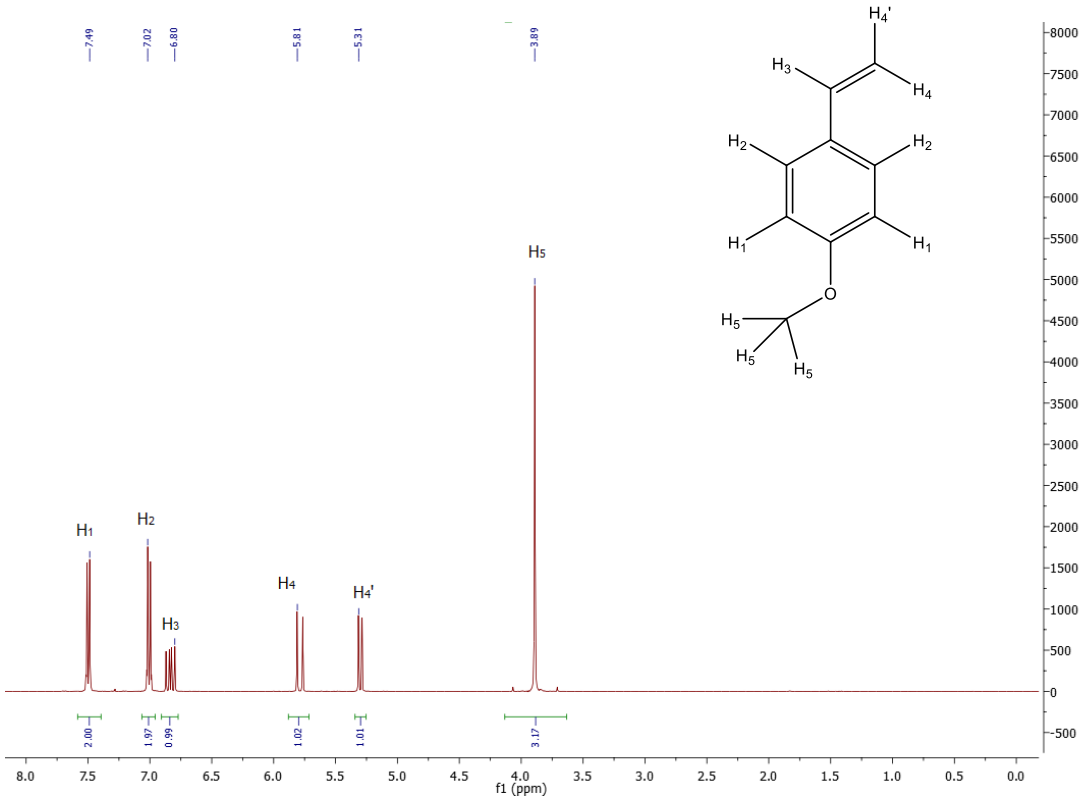

Figure 4.8: ^1H NMR spectrum of the healing agents extracted from 4MeOSt micro-capsules

5.5.3.2 Divinylbenzene micro-capsules

The diameter of DVB micro-capsules was found to be in the range of 50-500 μm at 550 rpm. DVB micro-capsules were subjected to sieving to collect diameter of 100-200 μm, figure 4.9.

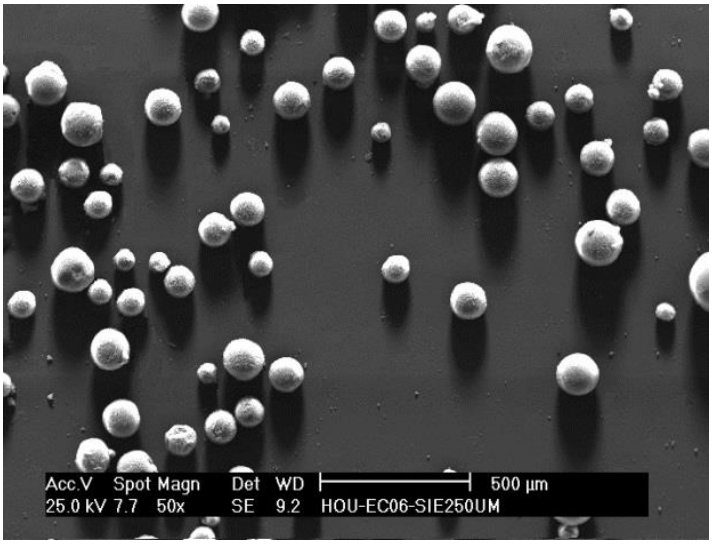

(a)

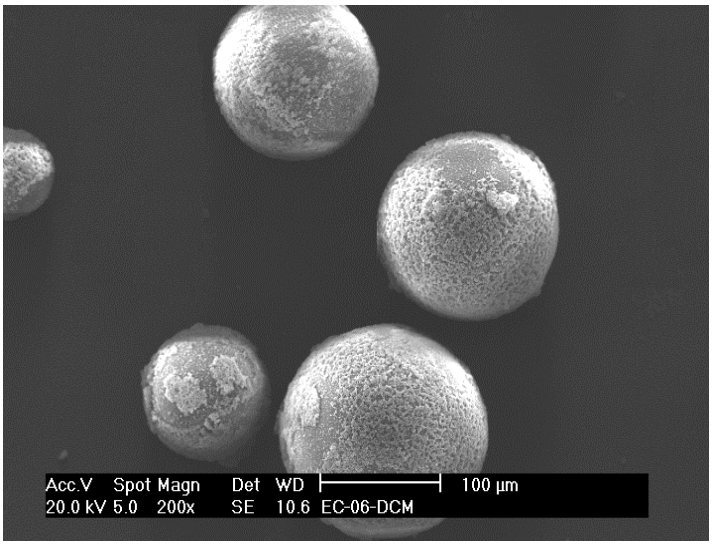

(b)

Figure 4.9: SEM image of the surface morphology of DVB micro-capsules, a) using magnification of 50×, b) using magnification of 200×

Optical microscopy showed that those DVB micro-capsules have liquid monomers, The liquid content of micro-capsules could be viewed by optical microscopy, figure 4.10. The light spot in the picture is the light refraction of liquid monomers indicating efficient encapsulation of liquid healing agents.

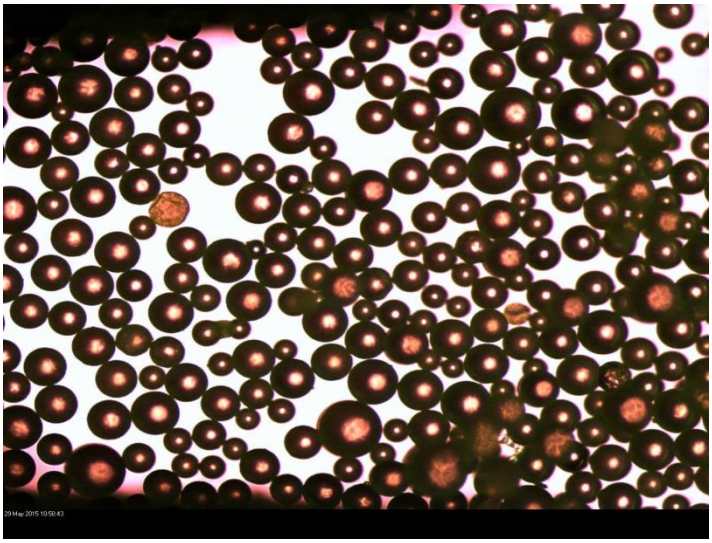

Figure 4.10: Optical microscopy (magnification of 20×) image of DVB micro-capsules

The shell wall thickness of DVB micro-capsules was also investigated by SEM. The average thickness was found to be 1.75-1.97 µm, figure 4.11.

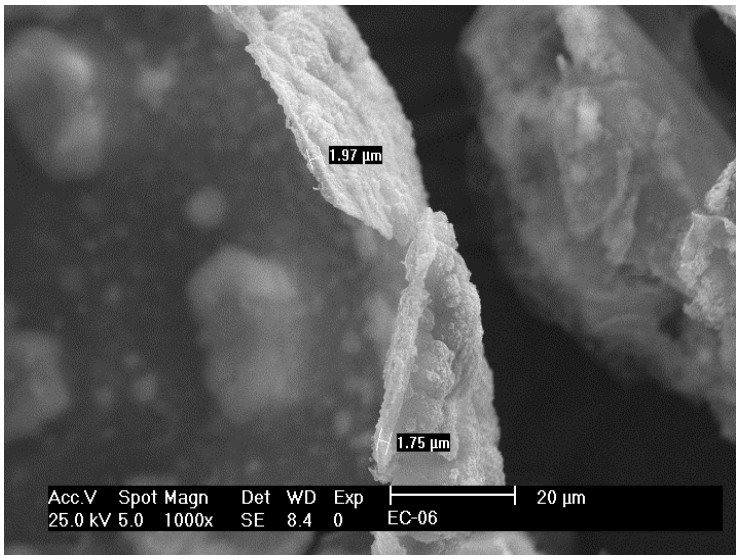

Figure 4.11: SEM image (magnification of 1000×) of the shell thickness of DVB micro-capsules

The healing agent contents of DVB micro-capsules were investigated. The ^{1}H NMR spectrum of the healing agents extracted from DVB micro-capsules is shown in figure 4.12. The spectrum shows the resonances at 7.60 ppm due to the 4 protons of the aromatic ring (H_1); the resonances at 6.80 ppm due to the 2 proton of the –CH– group (H_2); and the resonances at 6.06 ppm and 5.56 ppm due to the 4 protons of the $=CH_2$ group (H_3 and H_3').

The purity of DVB is 80% technical grade with 20% diethylbenzene, which is due to the resonances at 2.94 ppm and 1.57 ppm. The result confirms that the extract was identical to that of the monomer (DVB) used for micro-encapsulation.

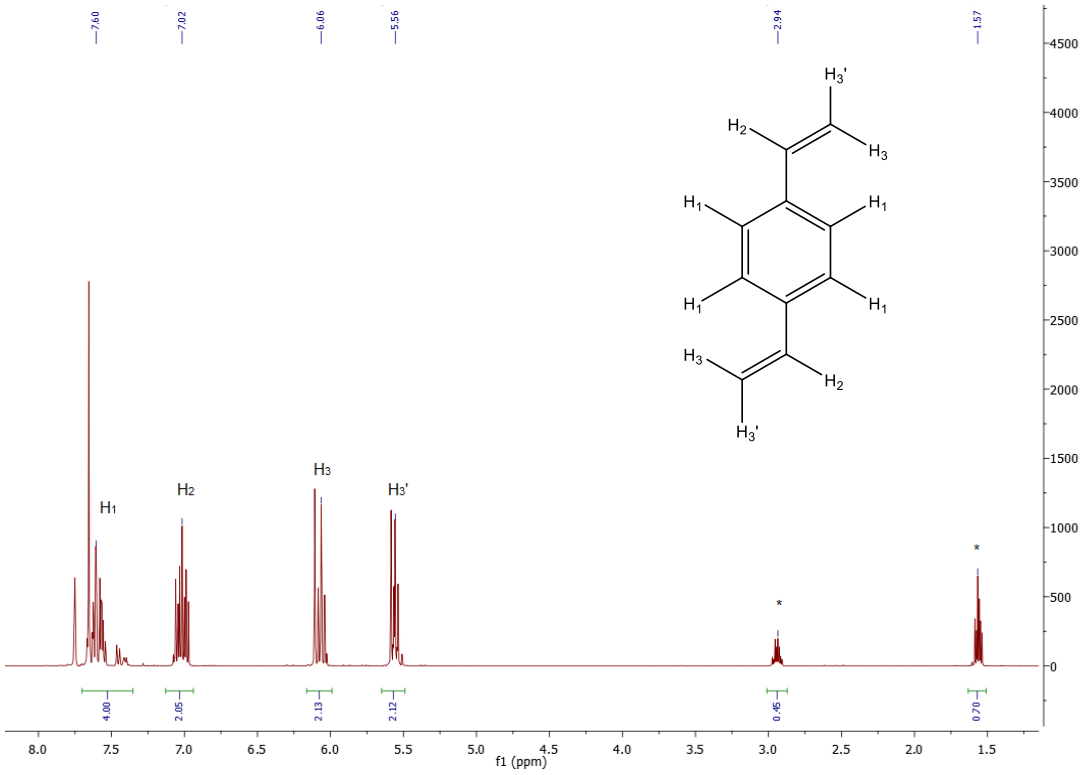

Figure 4.12: ^{1}H NMR spectrum of the healing agents extracted from DVB micro-capsules

5.5.3.3 Styrene micro-capsules

The diameter of St micro-capsules was found in the range of 50-500 μm for agitation rate at 550 rpm. Micro-capsules were subjected to sieving to collect diameter of 100-200 μm, figure 4.13.

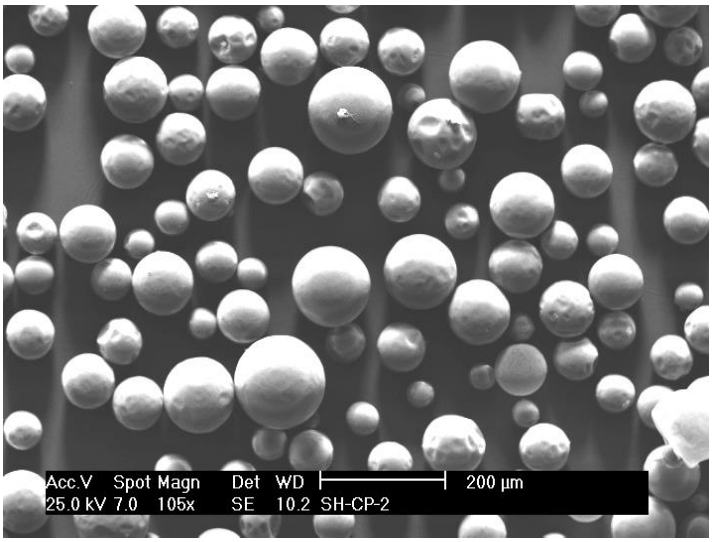

(a)

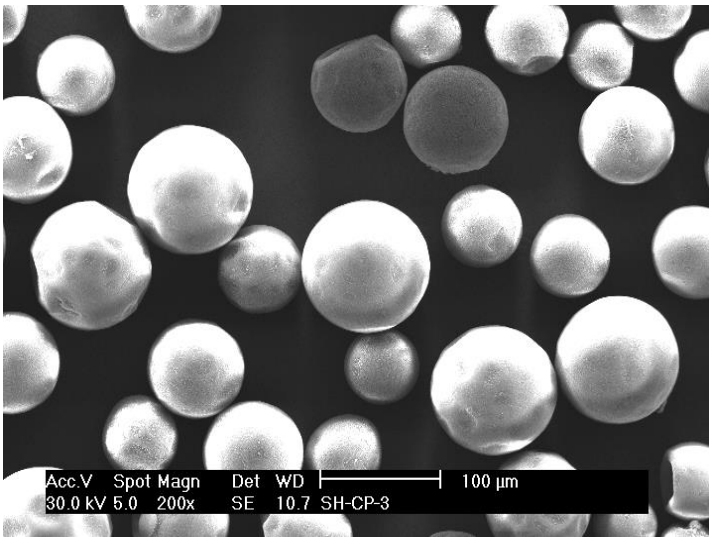

(b)

Figure 4.13: SEM image of the surface morphology of St micro-capsules, a) magnification of 105×, b) magnification of 200×

Optical microscopy showed that St micro-capsules have liquid monomers, figure 4.14. The light spot in the picture is the light refraction from liquid monomers.

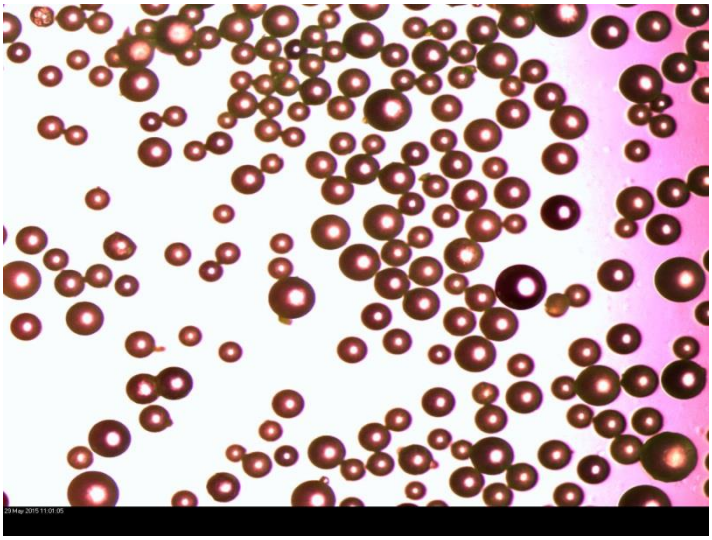

Figure 4.14: Optical microscopy (magnification of 20×) image of St micro-capsules

The shell wall thickness of St micro-capsules was also investigated by SEM. The average thickness was found to be 273~343 nm, figure 4.15.

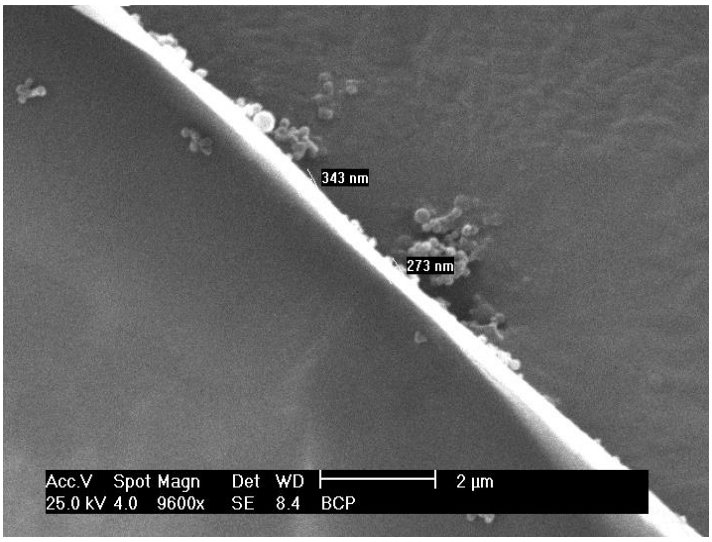

Figure 4.15: SEM image (magnification of 9600×) of the shell thickness of St micro-capsules

The healing agent contents of St micro-capsules were investigated. The ^{1}H NMR spectrum of the healing agents extracted from St micro-capsules is shown in figure 4.16. The spectrum shows the resonances at 7.45 ppm due to the 5 protons of the aromatic ring (H_1); the resonances at 6.85 ppm due to the 1 proton of the –CH– group (H_2); and the resonances at 5.91 ppm and 5.39 ppm due to the 2 protons of the $=CH_2$ group (H_3 and H_3'). The result confirms that the extract was identical to that of the monomer (St) used for micro-

encapsulation.

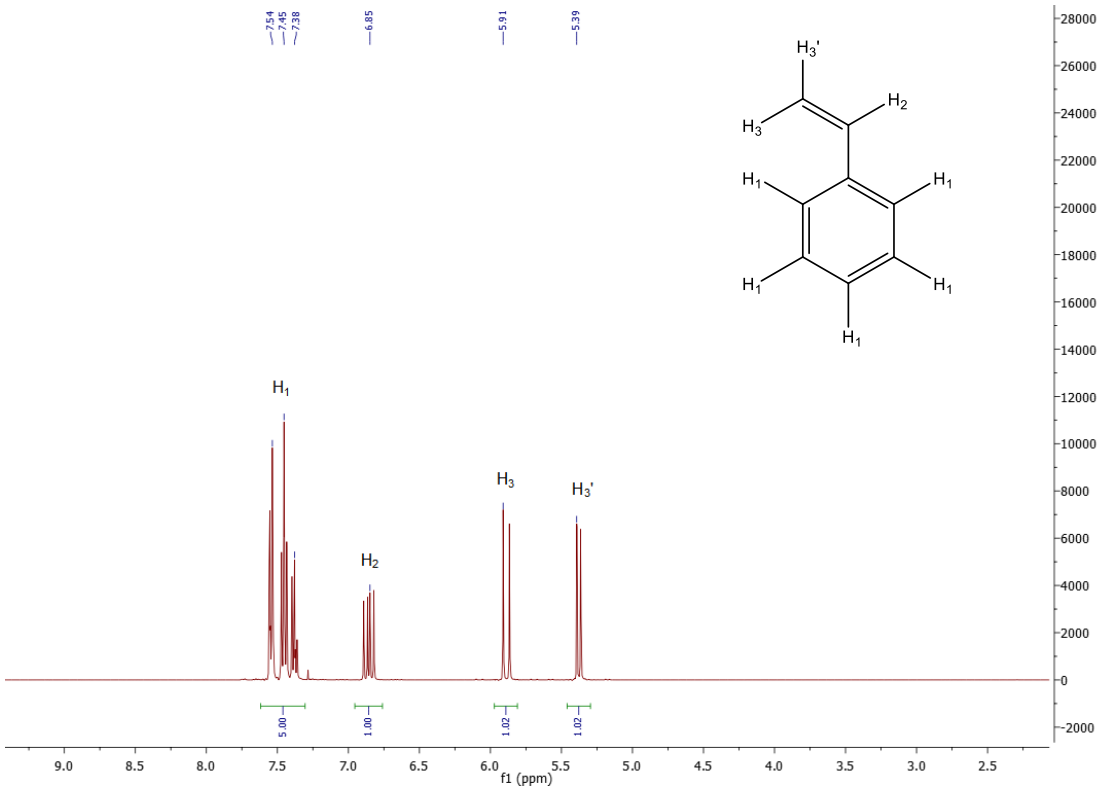

Figure 4.16: ^{1}H NMR spectrum of the healing agents extracted from St micro-capsules

5.5.3.4 4-Methoxystyrene-divinylbenzene micro-capsules

Micro-capsules with 4MeOSt and DVB content using the ratio of 4MeOSt with DVB of 4:1 were prepared. The micro-capsules diameter was found to be in the range of 50-500 μm for agitation rate at 550 rpm. These micro-capsules were subjected to sieving to collect the diameter of 100-200 μm, figure 4.17.

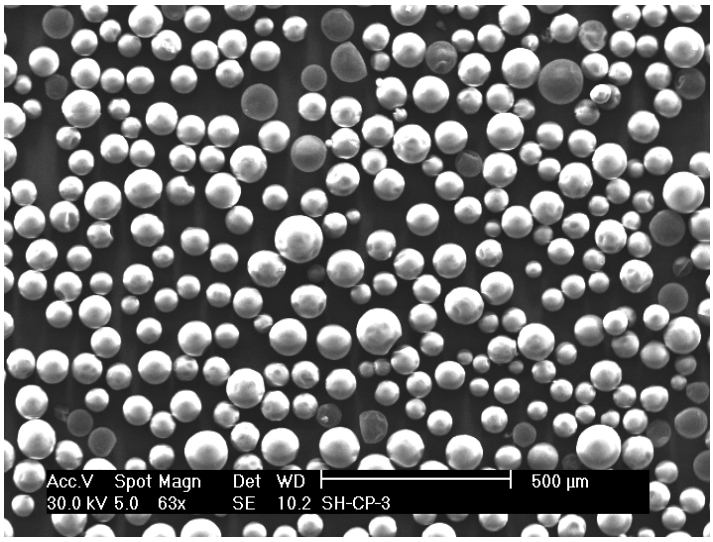

(a)

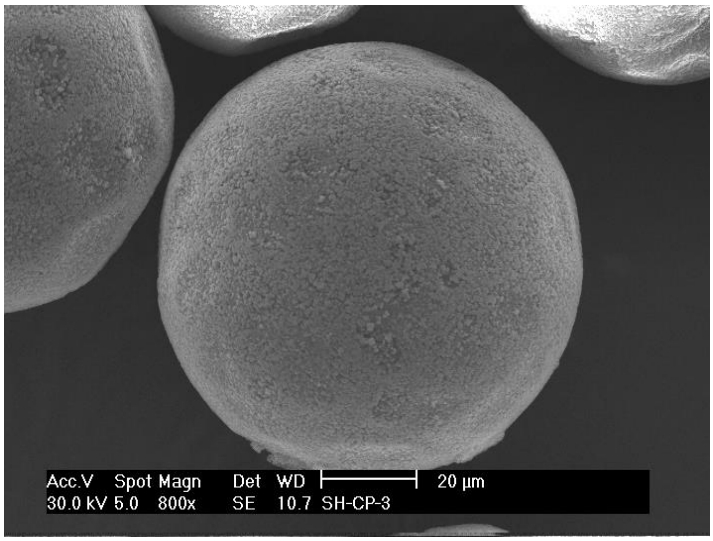

(b)

Figure 4.17: SEM image of the surface morphology of MeOSt-DVB micro-capsules, a) magnification of 63×, b) magnification of 800×

Optical microscopy showed that the 4MeOSt-DVB micro-capsules have liquid monomers,

figure 4.18. The light spot in the picture is the light refraction from liquid monomers.

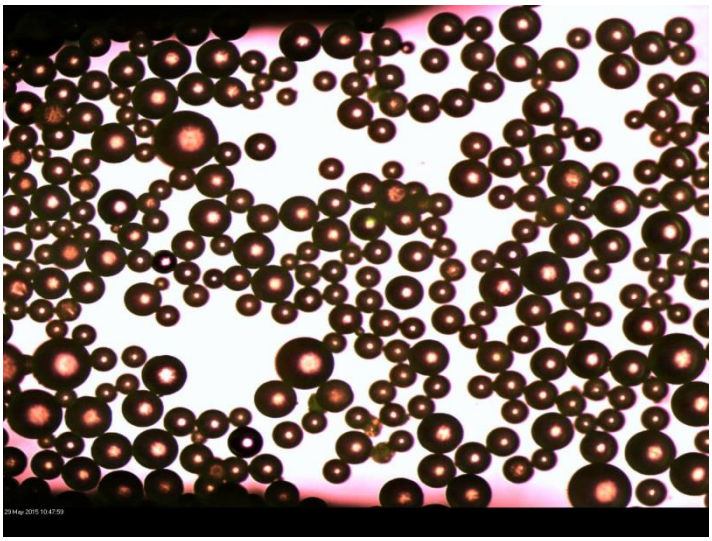

Figure 4.18: Optical microscopy image (magnification of 20×) of MeOSt-DVB micro-capsules

The shell wall thickness of MeOSt-DVB micro-capsules was also investigated by SEM, figure 4.19. The average thickness was found to be ~382 nm.

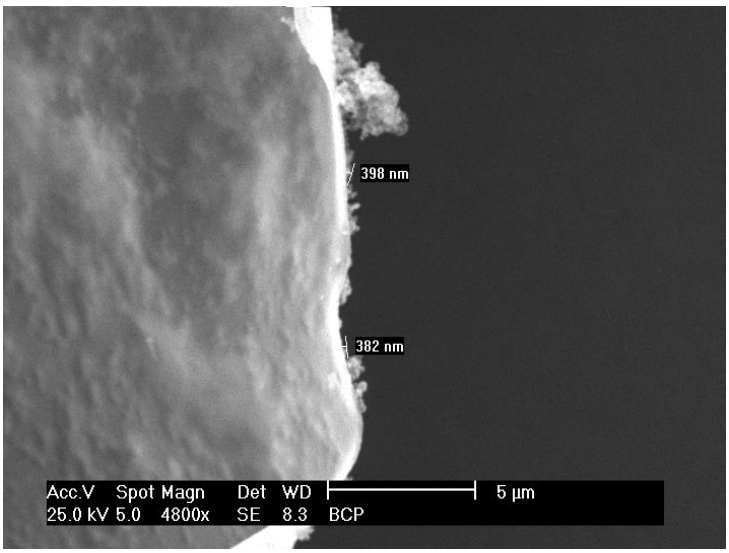

Figure 4.19: SEM image (magnification of 4800×) of the shell thickness of 4MeOSt-DVB micro-capsules

The healing agent contents of 4MeOSt and DVB micro-capsules were investigated. The ^{1}H NMR spectrum of the extract is shown in figure 4.20. The spectrum shows the resonances at 7.40 ppm due to the 4 protons of the aromatic ring (H_6) of DVB; the resonances at 6.93 ppm

due to the 4 proton of the aromatic ring (H_1, H_2) of 4MeOSt; the resonances at 6.80 ppm due to the 1 proton of the –CH– group (H_3) of 4MeOSt; the resonances at 6.70 ppm due to the 2 protons of the –CH– group (H_7) of DVB; the quartet resonances at 5.58 ppm and 5.27 ppm due to the 2 protons of the $=CH_2$ group (H_4 and H_4') of 4MeOSt; and the quartet resonances at 5.69 ppm and 5.13 ppm due to the 2 protons of the $=CH_2$ group (H_8 and H_8') of DVB. The result confirms that the extract was identical to that of the monomer (4MeOSt and DVB) used for micro-encapsulation.

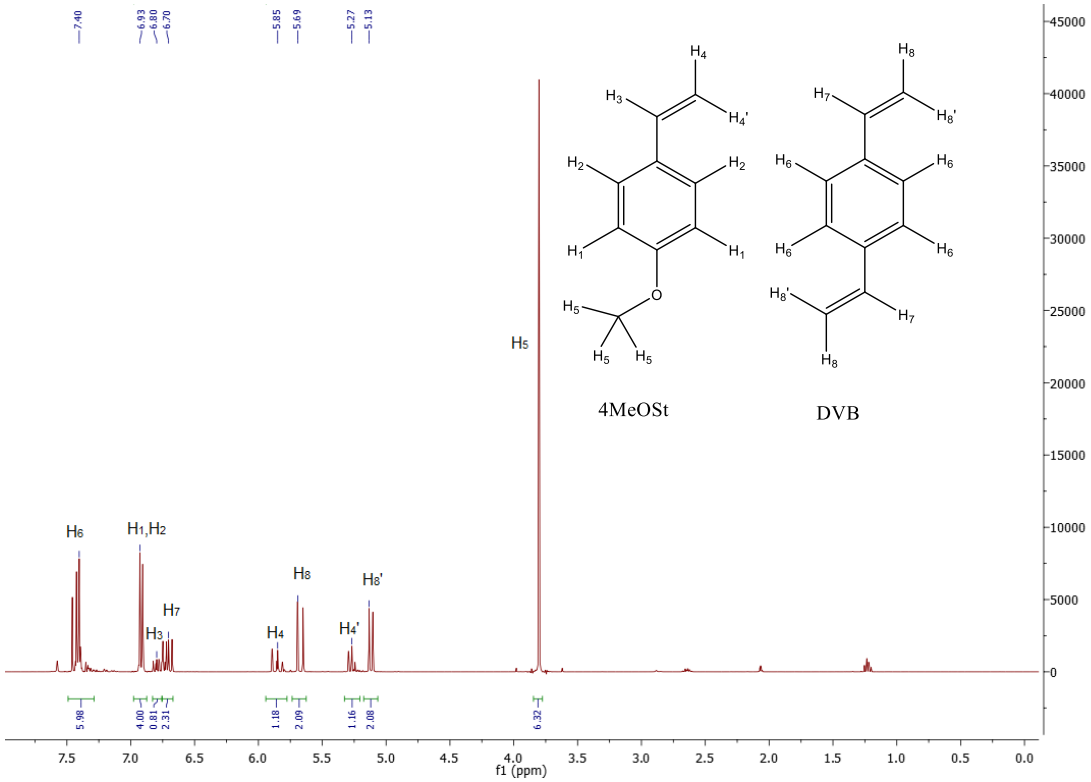

Figure 4.20: ^{1}H NMR spectrum of the healing agent extracted from 4MeOSt-DVB micro-capsules.

5.5.3.5 Styrene-divinylbenzene micro-capsules

Micro-capsules containing St and DVB with ratio of 4:1 were prepared. The diameter of the micro-capsules was found to be in the range of 50-500 μm for agitation rate of 550 rpm. These micro-capsules were subjected to sieving to collect diameter of 100-200 μm, figure 4.21.

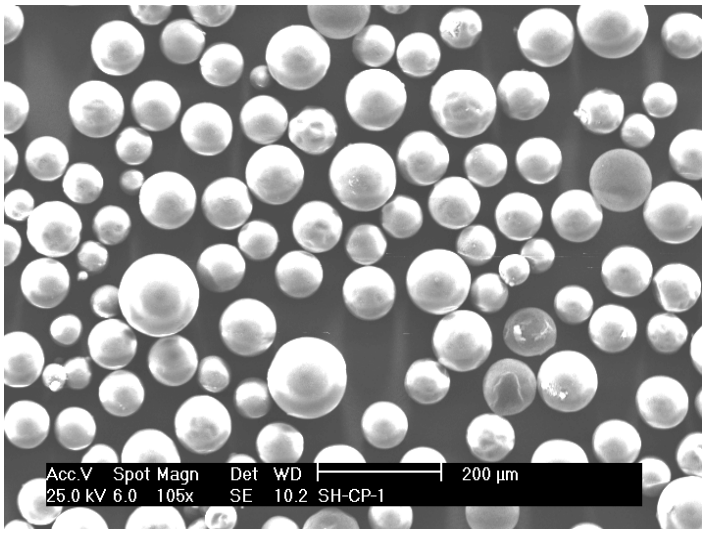

(a)

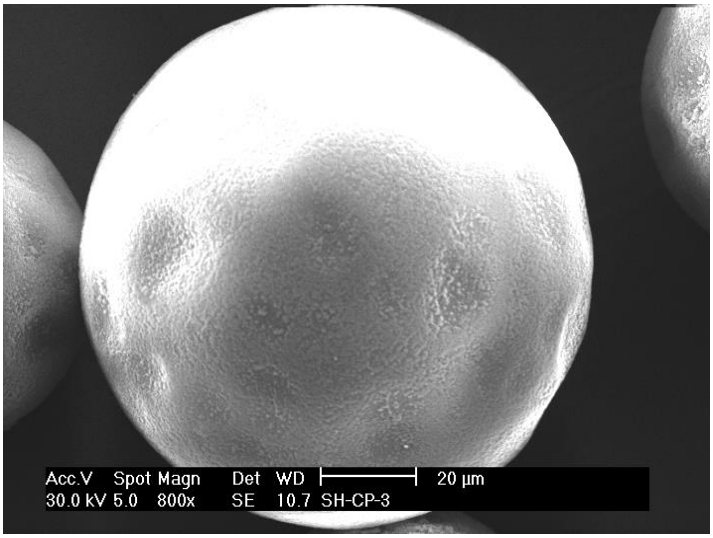

(b)

Figure 4.21: SEM image of the surface morphology of St-DVB micro-capsules, a) magnification of 105×, b) magnification of 800×

Optical microscopy could show that those St and DVB micro-capsules have liquid monomers, figure 4.22. The light spot in the picture is the light refraction from liquid monomers.

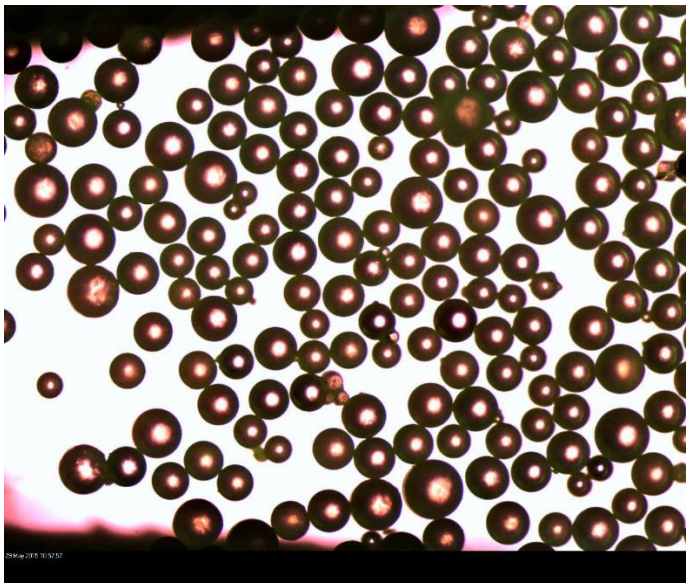

Figure 4.22: Optical microscopy image (magnification of 20×) of St-DVB micro-capsules

The shell wall thickness of the micro-capsules was also investigated by SEM, figure 4.23. The average thickness was found to be about 667 nm.

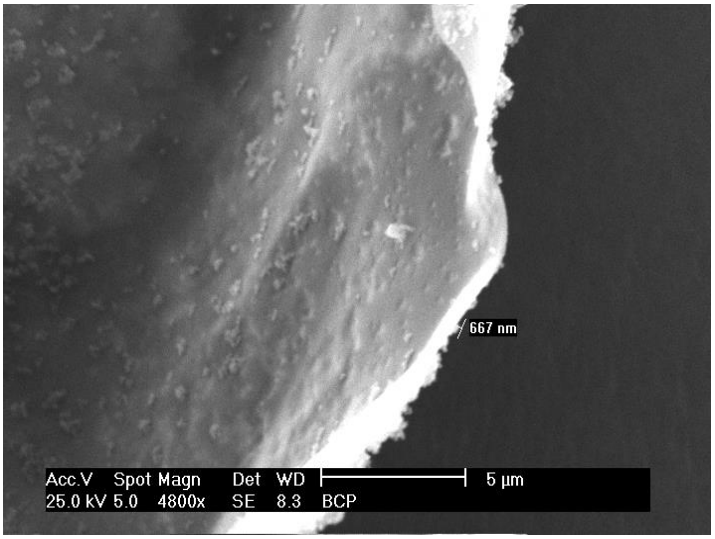

Figure 4.23: SEM image (magnification of 4800×) of the shell thickness of St-DVB micro-capsules

The healing agent contents of St and DVB micro-capsules were investigated. The ^{1}H NMR

spectrum of the extract is shown in figure 4.24. The resonances at 7.46 ppm due to the 4 protons of the aromatic ring (H_6) of DVB and 5 proton of the aromatic ring (H_1) of St; the resonances at 6.86 ppm due to the 1 proton of the –CH– group (H_2) of St and 2 protons of the –CH– group (H_5) of DVB; the quartet resonances at 5.92 ppm and 5.40 ppm due to the 2 protons of the $=CH_2$ group (H_3 and H_3') of St and the 2 protons of the $=CH_2$ group (H_4 and H_4') of DVB can be observed. The result confirms that the extract was identical to that of the monomer (St and DVB) used for micro-encapsulation.

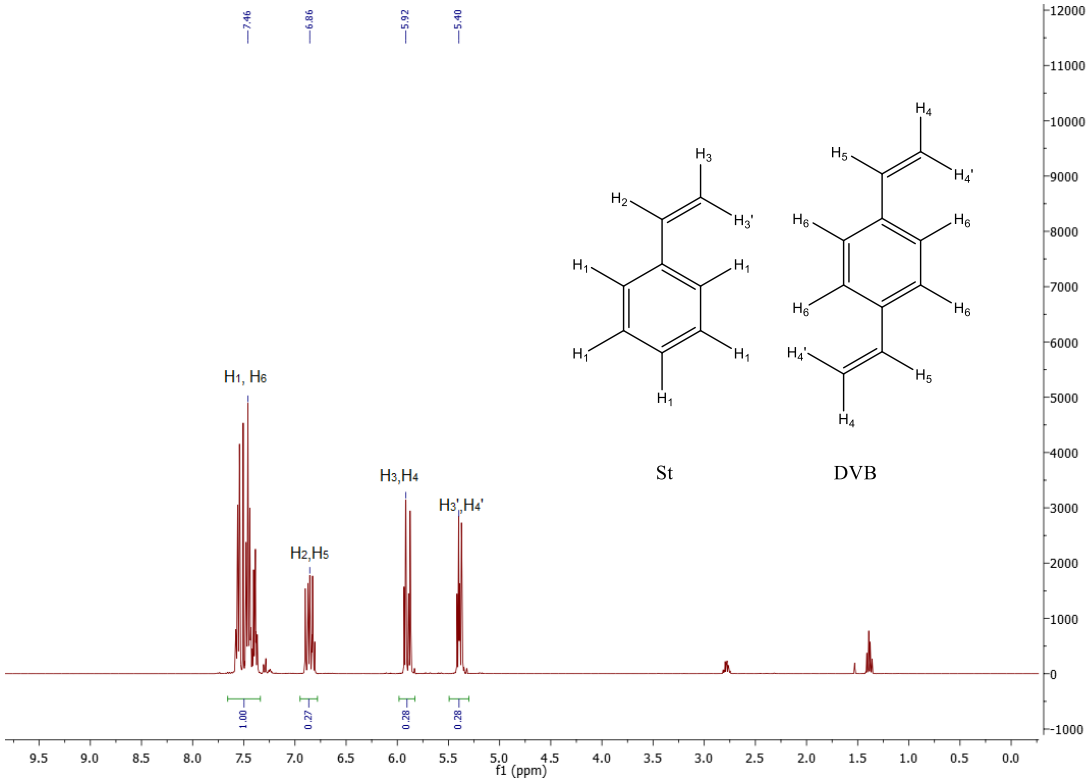

Figure 4.24: ^1H NMR spectrum of the healing agent extracted from St-DVB micro-capsules.

5.6 Conclusion

The micro-encapsulation of liquid healing agents (4MeOSt, DVB, St, and their mixtures) by in-situ polymerisation of urea-formaldehyde in an oil-water emulsion was carried out. The micro-capsules of high quality surface and good size distribution were produced and analysed by SEM. Micro-capsules with average diameter in the range of 50–500 μm were obtained at agitation of 550 rpm. These micro-capsules were subjected to sieving to collect those with diameter of 100-250 μm. During the micro-encapsulation process, UF nanoparticles formed and deposited on the micro-capsule surface producing a rough surface morphology. The deposition of UF nanoparticles was prevented by carrying out the reaction under constant pH (3.5) conditions and washing with DCM and deionised water. The liquid content was extracted and characterised by ^{1}H NMR. The fill content was measured by comparing the weight of filled micro-capsules with that of the dried broken shells and was found to be 70-80 wt. %.

Refercence

1. Brown E.N., Kessler M.R., Sottos N.R., White S.R. (2003) 'In-situ Poly(urea-formaldehyde) Micro-encapsulation of Dicyclopentadiene', *J. Microencapsul.,* 20(6):719–30.
2. Ghosh S.K. (2006) (ed.) *Functional Coatings,* WILEY-VCH GmbH & Co. KGaA, Weinheim.
3. DOBETTI, L. and PANTALEO, V., 2002, *Application of a hydrodynamic model to micro-encapsulation by coacervation*. Journal of Micro-encapsulation, 19, 139–151

Chapter 5

Fracture Toughness Test of Epoxy Matrix

5.1 Introduction

The design concept of self-healing system is to recover lost function due to damage in the matrix material. Damage in polymers and composites often involves some form of fracture. Complete filling of damage volume and reforming bonds across damage surfaces can restore fracture properties.[1]

The primary fracture loading conditions for self-healing specimens have been quasi-static fracture, fatigue, and impact. These loading conditions cause several types of fracture (figure 5.1), including Mode I crack opening, Mode II sliding, Mode III tearing, and mixed-mode.[2] In this project, the fracture crack separation mode was Mode I crack opening by compact tension. Mode I fracture allows for controlled crack growth along the centre line and a crack length independent fracture toughness that depends only on the applied load.[2] The healed crack length is difficult to measure in the matrix, however, the compact tension geometry of Mode I is more accurate evaluation of healing efficiency.

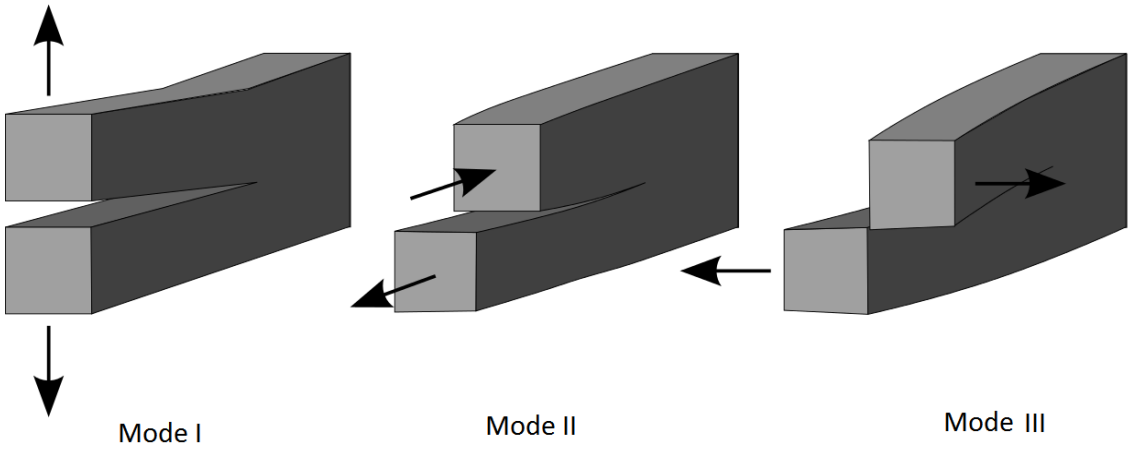

Figure 5.1: Fracture crack separation modes [2]

Fracture toughness is a property which describes the ability of a material containing a crack to resist fracture, and is one of the most important properties of any material for many design applications. Fracture toughness is a quantitative way of expressing a material's resistance to brittle fracture when a crack is present. If a material has high fracture toughness it will probably undergo ductile fracture. Brittle fracture is very characteristic of materials with low fracture toughness.[3] For polymer materials, the higher the density of cross-linking is, the more brittle the material is. Fracture toughness is determined from the stress intensity factor

K_{IC} at which a thin crack in the material begins to grow.

The curing of epoxy resin by DETA is expressed by the formula shown below. The reaction mechanism involving cyclic compounds such as epoxides is identified as ring-opening polymerisation. In cross-linking of an epoxy resin with an amine hardener, the epoxy group can react either with primary or secondary amine. Scheme 5.1 showed the reaction mechanism for a primary amine with an epoxy group yielding a hydroxyl secondary amine (step 1), which in turn is able to react with another epoxy to give a hydroxyl tertiary amine (step 3). As the reaction proceeds, further branching reactions lead to the formation of a three-dimensional network molecule (step 3).[4]

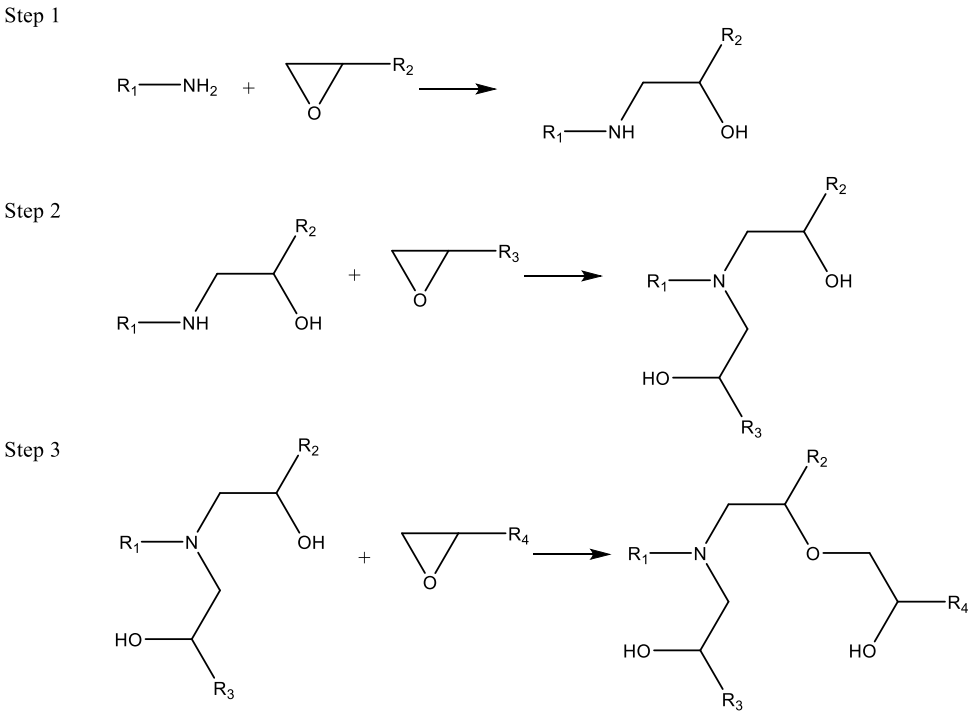

Scheme 5.1: Steps involved in the mechanism of epoxy-amine curing process

The hydroxyl amine groups are generated by epoxy-amine reactions act as catalysts. The activation of carbon atoms of the epoxy ring for nucleophilic attack by hydroxyl-containing amine molecules as shown in scheme 5.2, which was identified as a "termolecular transition state".[5] These secondary hydroxyl groups catalyse the reaction through the formation of a termolecular complex, which facilitates the nucleophilic attack of the amino groups. Therefore, as the reaction progresses the cross-linking reaction shows an accelerating rate. Tertiary amines are the general class of anionic catalysts used for cross-linking of epoxy resins.

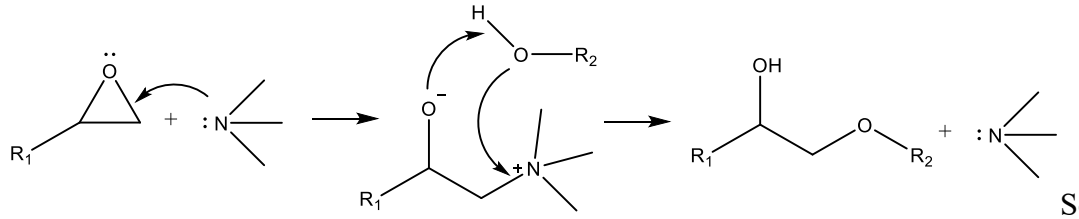

Scheme 5.2: Termolecular transition state of the epoxy-amine addition

At higher temperature or later stage of conversion, in spite of the main ring-opening reaction between epoxy and amine, slow side reactions such as homopolymerisation of epoxides and epoxy-hydroxyl reaction (etherification) take place at elevated temperatures as shown in scheme 5.3. [6, 7] But these reactions are not sequential rather it may occur simultaneously over a certain range of conversion. Progression of the epoxy-amine cross-linking also activates the homopolymerisation of epoxy resin by tertiary amine that is produced during the epoxy-amine reaction.

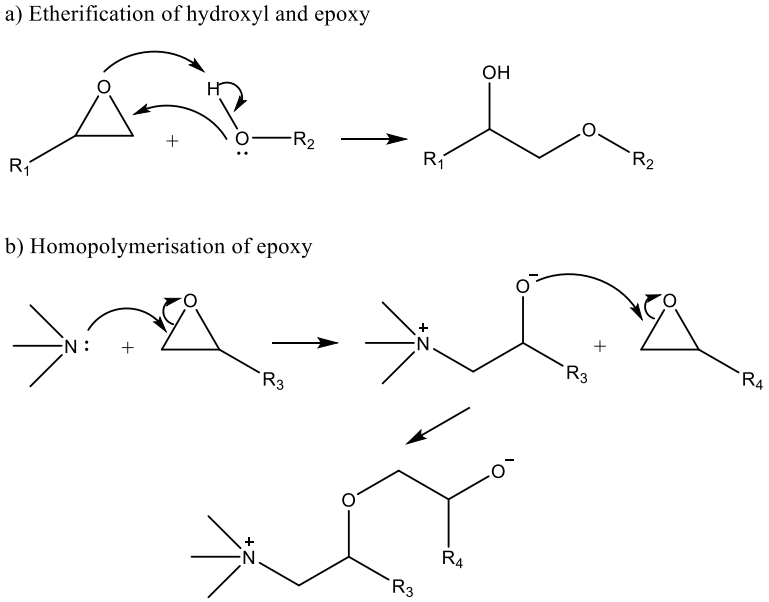

Scheme 5.3: Mechanism of etherification and homopolymerisation of epoxy-amine reaction

At the end of the curing process, the increase in the cross-link density or gelation constrains the mobility of chains and makes the reactive species more difficult to react and the curing process was completed.

5.2 Materials

Maleic anhydride (MA), 4-methoxystyrene (4MeOSt), divinylbenzene (DVB), styrene (St), ethoxymethylene malononitrile (EtOCN), N-methylmaleimide (MeMal), and

Diethylenetriamine (DETA) were purchased from Aldrich and used as supplied. Bisphenol-A based epoxide (EPON 828) resin was purchased from Hexion™ Specialty Chemicals.

5.3 Instrumentation

Fracture testing of the specimens was performed on a rack drive panel (RDP) servo-mechanical testing machine at a crosshead speed of 0.5 mm/ min, using compact tension geometry. The test process was carried out in University of Leeds. Rack-drive loads place special requirements on the servo control system. On one hand, rack-andpinion mechanisms have a relatively large amount of lost mechanical motion or backlash. On the other hand, the two drive systems are strongly linked through the rack. When the backlash is taken up, the average speed is the same for the two motors. This linkage prevents using fully independent, integrating velocity loops for the two drives.

5.4 Experimental

5.4.1 The preparation of blank specimens

DETA (10 wt%, 2 g) was added to bisphenol-A based epoxide resin (20 g), stirred and the final mixture was degassed. The mixture was then poured into a closed Teflon mould (60 mm × 50 mm × 5 mm) with silicon seals and cured at ambient temperature for 24 h. The specimen was further cured at 50 °C for 24 h, and cooled to ambient temperature to collect the blank epoxy resin specimen (EpoA1). EpoA2-5 specimens were prepared using the same process.

5.4.2 The preparation of specimen containing micro-capsules

The micro-capsules used for specimen EpoB1-5 were prepared by urea-formaldehyde micro-encapsulation of styrene. The preparation process was explained in chapter 4 micro-encapsulation.

DETA (10 wt. %, 2 g) was added to bisphenol-A based epoxide resin (20 g), stirred and the final mixture was degassed. The micro-capsules (5-20 wt. %) was added, stirred thoroughly to ensure uniform distribution and the mixture was degassed. The mixture was then poured into a closed Teflon mould (60 mm × 50 mm × 5 mm) with silicon seals and cured at ambient temperature for 24 h. The specimen was further cured at 50 °C for 24 h, and cooled to ambient temperature to collect the specimen. Concentration and quantity of micro-capsules used for the preparation of specimen (EpoB1-5) is shown in table 5.1.

Table 5.1: Concentration and quantity of micro-capsules

Specimen	Micro-capsules (wt%, g)
EpoB1	5, 1
EpoB2	7.5, 1.5
EpoB3	10, 2
EpoB4	15, 3
EpoB5	20, 4

5.4.3 The preparation of specimen containing solid healing agents

DETA (10 wt%, 2 g) was added to bisphenol-A based epoxide resin (20 g), stirred and the final mixture was degassed. The mixture was kept at ambient temperature for 4 h. Then, the finely powdered solid healing agents (5-20 wt. %) (MA, MeMal, or EtOCN) was added,

stirred slightly and the mixture was degassed again. The mixture was then poured into a closed Teflon mould (60 mm × 50 mm × 5 mm) with silicon seals and cured for 24 h at ambient temperature. The specimen was further cured at 50 °C for 24 h, and cooled to ambient temperature to collect the specimen. The concentration and quantity of solid healing agents (MA, MeMal, and EtOCN) used for the preparation of specimen (EpoC1-5, EpoD1-5, and EpoE1-5) is shown in table 5.2.

Table 5.2: Concentration and quantity of solid healing agents

Specimen	Solid healing agents	Amount(wt. %, g)
EpoC1	MA	5, 1
EpoC2	MA	10, 2
EpoC3	MA	15, 3
EpoC4	MA	20, 4
EpoD1	MeMal	5, 1
EpoD2	MeMal	10, 2
EpoD3	MeMal	15, 3
EpoD4	MeMal	20, 4
EpoE1	EtOCN	5, 1
EpoE2	EtOCN	10, 2
EpoE3	EtOCN	15, 3
EpoE4	EtOCN	20, 4

5.4.4 Fracture toughness test

Fracture tests were carried out at ambient temperature using the compact tension geometry (60 mm × 50 mm × 5 mm), figure 5.2.

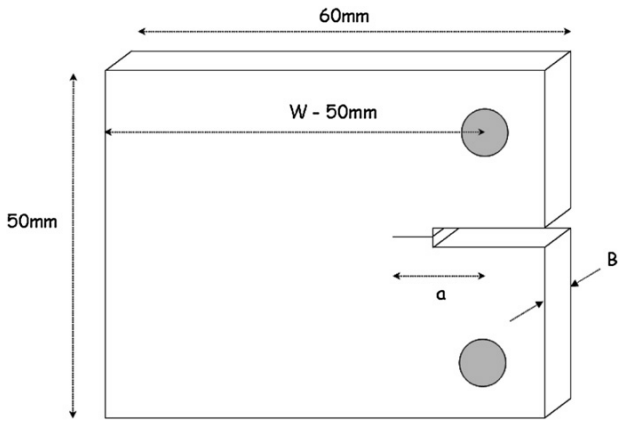

Figure 5.2: the geometry of the specimens for the compact tension. Where a is the crack length; B is the specimen thickness and W is loading width of the specimen.

The specimen shape is rectangular with loading holes placed 10 mm from the specimen

surfaces. A 20 mm long crack was first sawn into the specimen, followed by tapping the sharp pre-crack. Taking into account the unloaded area of 10 mm, the starter crack was therefore of the order of 15 mm.

The specimen was loaded until crack initiation occurred. The fracture behaviour was brittle in all cases, such that on initiation the crack travelled a distance across the specimen. The loading process was record by the force displacement curve. The fracture force (P) was obtained from the force-displacement curve. A value of the critical stress intensity factor, K_{IC}, was calculated for each fracture event from the equation 5.1.

$$K_{IC} = \frac{PY(\frac{a}{W})}{BW^{\frac{1}{2}}} \qquad \text{Eq. 5.1}$$

Where a is the crack length; P is the fracture load; B is the specimen thickness and W is the specimen width.

$$Y(\frac{a}{W}) = 29.6(\frac{a}{W})^{\frac{1}{2}} - 185.5(\frac{a}{W})^{\frac{3}{2}} - 655.7(\frac{a}{W})^{\frac{5}{2}} + 1017(\frac{a}{W})^{\frac{7}{2}} - 638.9(\frac{a}{W})^{\frac{9}{2}} \qquad \text{Eq.5.2}$$

Y(a/W) is a geometry factor which compensates for the fact that in the compact tension testing geometry, the compliance of the specimen depends on the crack length (a) to specimen width (W) ratio, equation 5.2. There are a number of different forms for this function, which are broadly equivalent, but are valid for different ranges of (a/W). For this study we have followed previous work and used the form shown by Kinloch and Young [8] from the original work of Brown and Srawley [9], which is valid for $0.2 < a/W < 0.7$.

5.5 Results and discussion

5.5.1 The preparation of epoxy resin specimens

Epoxy resins are thermosetting polymer resins where the resin molecule contains one or more epoxide groups. Epoxy resins are cured with the addition of a curing agent, which is commonly called a hardener. The most common type of curing agent is amine based. In this project, Bisphenol-A based epoxides resins (figure 5.3a) cured by diethylenetriamine (DETA) (figure 5.3b) were used as matrix materials for self-healing systems.

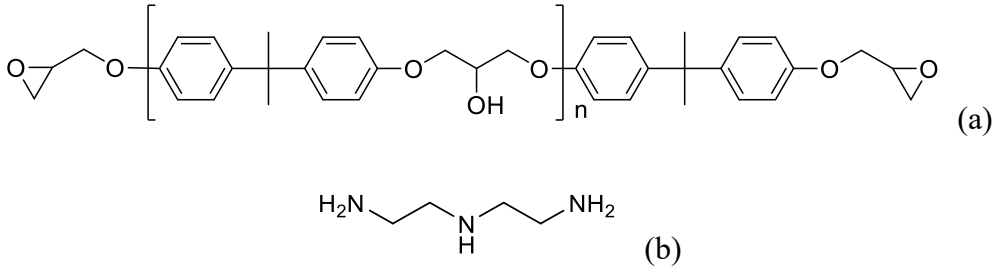

Figure 5.3: the structure of (a) Bisphenol-A based epoxide monomer and (b) the cross-linking agent diethylenetriamine (DETA)

5.5.2 Fracture toughness test of blank epoxy resin specimens

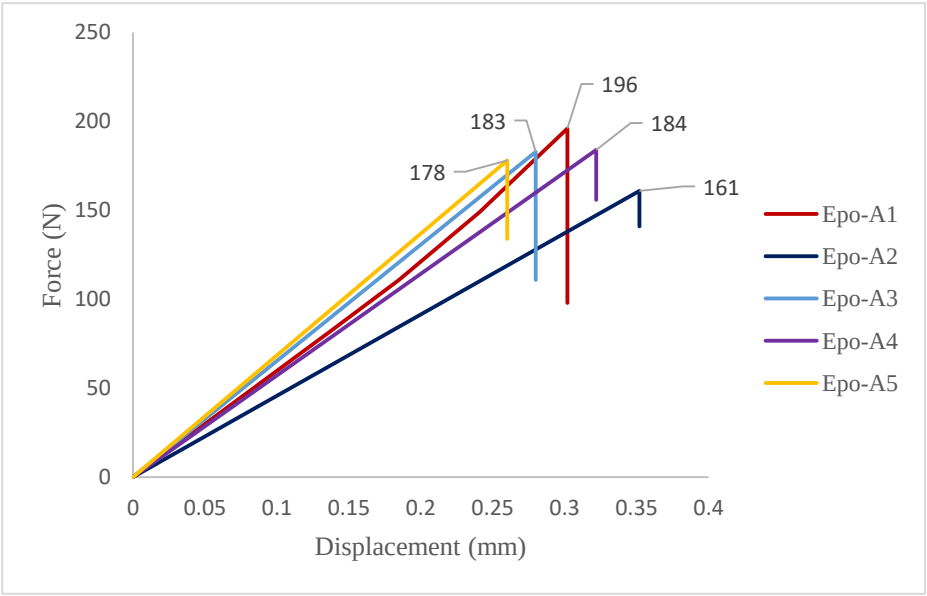

Figure 5.4: The force-displacement curve for the compact tension test of EpoA1-5.

The blank epoxy resin specimens (EpoA1-5) were cured by DETA (10 wt. %). The matrix specimens prepared in this ratio were with good toughness, which were not too soft or too

brittle. The fracture toughness of those blank specimens, which did not add any healing agents or micro-capsules, were tested by the compact tension geometry. The fracture toughness test were carried out at ambient temperature and the results were recorded by the force-displacement curve, figure 5.4.

The fracture force (P) is obtained in the force-displacement curve above. A value of the critical stress intensity factor, K_{IC}, is calculated for each fracture event and the results are shown in table 5.3. The fracture toughness of the blank epoxy resins is found to be K_{IC} = 0.801 ± 0.019 MPa·$m^{1/2}$.

Table 5.3: The fracture toughness of blank epoxy resin (EpoA1-5)

Test	a (mm)	B (mm)	Force (N)	Factor, Y	K_{IC} (MPa·$m^{1/2}$)
EpoA1	13.92	6.29	196	5.631	0.783
EpoA2	15.03	5.24	161	5.856	0.805
EpoA3	11.30	5.46	183	5.274	0.791
EpoA4	14.62	5.73	184	5.768	0.826
EpoA5	11.24	5.36	178	5.269	0.783

5.5.3 Fracture toughness of specimen containing micro-capsules

The epoxy resin specimens containing micro-capsules (EpoB1-5) were prepared to investigate influence of micro-capsules on the fracture toughness of the base materials. The liquid content of the micro-capsules would not affect the test. Therefore, the micro-capsules were prepared by UF micro-encapsulation of styrene.

The epoxy resin containing micro-capsules (5 wt. %) (EpoB1) were cured by DETA (10 wt. %). The 5 repeated testing were carried out at ambient temperature and the results were recorded by the force-displacement curve, figure 5.5.

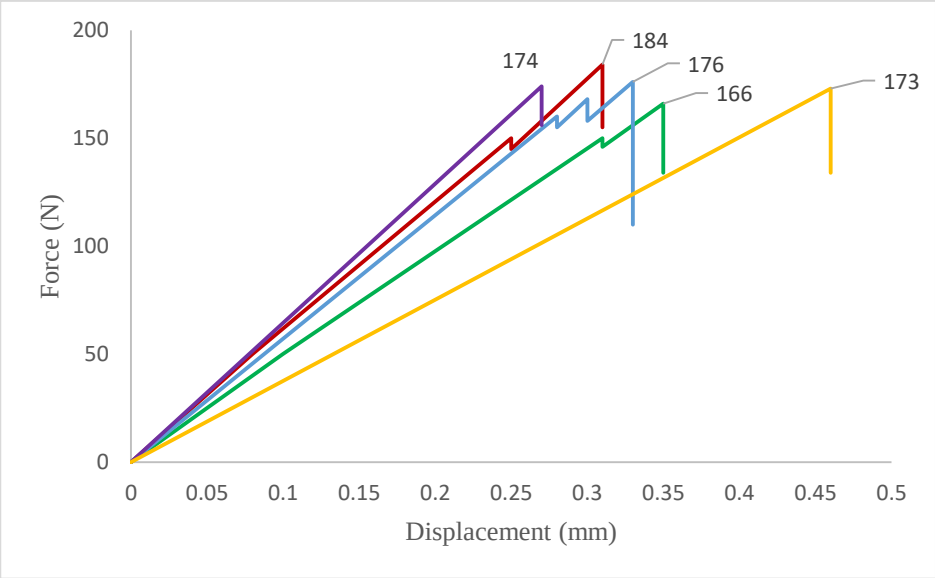

Figure 5.5: The force-displacement curve for the compact tension test of EpoB1

The fracture force (P) is obtained from the force-displacement curve above. A value of the critical stress intensity factor, K_{IC}, is calculated for each fracture event and the results are shown in table 5.4. The fracture toughness of EpoB1 is found to be K_{IC} = 0.765 ± 0.029 MPa·m$^{1/2}$.

Table 5.4: The fracture toughness of EpoB1

Test	A (mm)	B (mm)	Force (N)	Y	K_{IC} (MPa·m$^{1/2}$)
1	12.12	5.52	184	5.358	0.797
2	13.53	5.44	166	5.561	0.759
3	12.33	5.29	176	5.384	0.799
4	11.92	5.67	174	5.335	0.730
5	14.74	5.81	173	5.793	0.771

The epoxy resin containing micro-capsules (7.5 wt. %) (EpoB2) were cured by DETA (10 wt. %). The 5 repeated testing process were carried out at ambient temperature and the results were recorded by the force-displacement curve, figure 5.6.

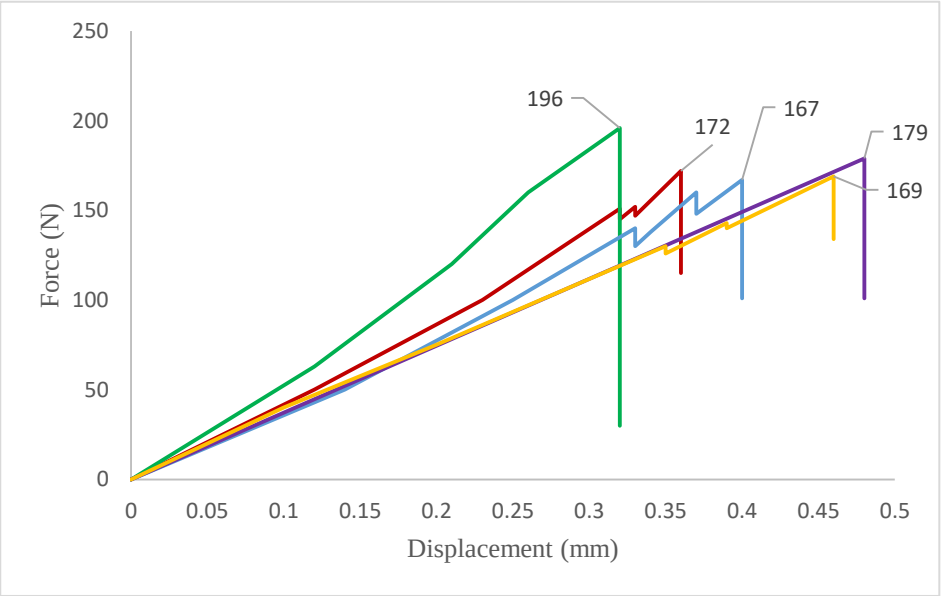

Figure 5.6: The force-displacement curve for the compact tension test of EpoB2

The fracture force (P) is obtained from the force-displacement curve above. A value of the critical stress intensity factor, K_{IC}, is calculated for each fracture event and the results are shown in table 5.5. The fracture toughness of EpoB2 is found to be K_{IC} = 0.768 ± 0.037 MPa·m$^{1/2}$.

Table 5.5: The fracture toughness of EpoB2

Test	A (mm)	B (mm)	Force (N)	Y	K_{IC} (MPa·m$^{1/2}$)
1	13.42	5.29	172	5.543	0.804
2	11.59	6.21	196	5.301	0.746
3	14.47	5.74	167	5.737	0.744
4	16.78	6.11	179	6.291	0.822
5	15.51	5.94	169	5.966	0.759

The epoxy resin containing micro-capsules (10 wt. %) (EpoB3) were cured by DETA (10 wt. %). The 5 repeated testing process were carried out at ambient temperature and the results were recorded by the force-displacement curve, figure 5.7.

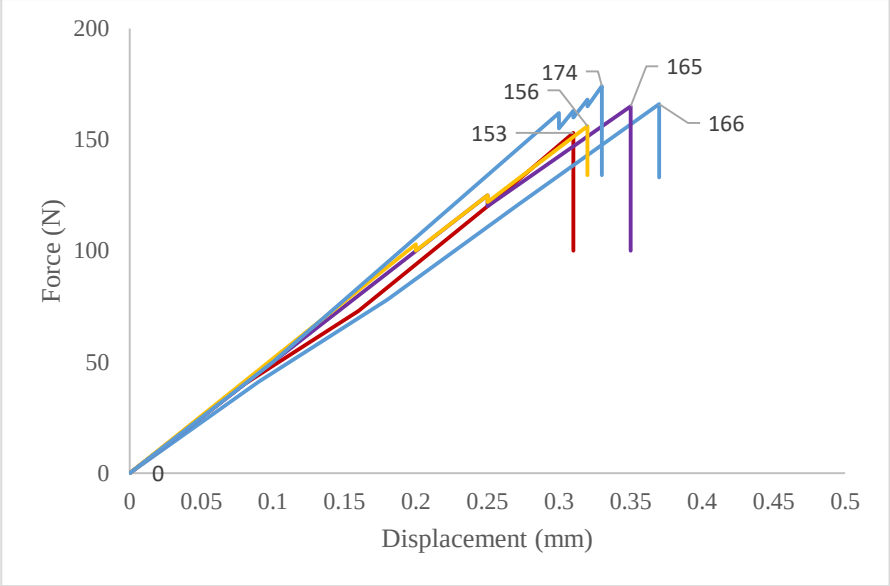

Figure 5.7: The force-displacement curve for the compact tension test of EpoB3

The fracture force (P) is obtained from the force-displacement curve above. A value of the critical stress intensity factor, K_{IC}, is calculated for each fracture event and the results are shown in table 5.6. The fracture toughness of EpoB3 is found to be K_{IC} = 0.777 ± 0.044 MPa·$m^{1/2}$.

Table 5.6: The fracture toughness of EpoB3

Test	A (mm)	B (mm)	Force (N)	Y	K_{IC} (MPa·$m^{1/2}$)
1	11.67	5.13	153	5.309	0.708
2	12.14	5.28	174	5.361	0.788
3	14.11	5.17	166	5.666	0.811
4	13.33	5.12	165	5.528	0.794
5	11.35	5.15	156	5.279	0.713

The epoxy resin containing micro-capsules (15 wt. %) (EpoB4) were cured by DETA (10 wt. %). The 5 repeated testing process were carried out at ambient temperature and the results were recorded by the force-displacement curve, figure 5.8.

The fracture force (P) is obtained from the force-displacement curve above. A value of the critical stress intensity factor, K_{IC}, is calculated for each fracture event and the results are shown in table 5.7. The fracture toughness of Epo-b4 is found to be K_{IC} = 0.752 ± 0.045 MPa·$m^{1/2}$.

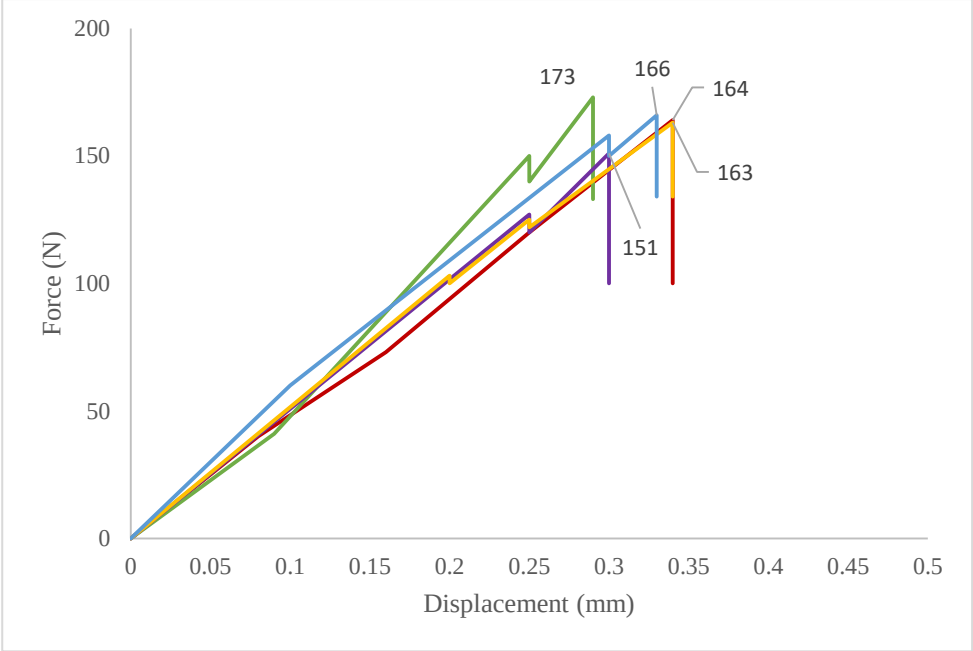

Figure 5.8: The force-displacement curve for the compact tension test of EpoB4

Table 5.7: The fracture toughness of EpoB4

Test	A (mm)	B (mm)	Force (N)	Y	K_{IC} (MPa·m$^{1/2}$)
1	12.53	5.22	164	5.410	0.758
2	12.74	5.27	166	5.438	0.764
3	11.27	5.14	173	5.272	0.791
4	11.49	5.19	151	5.292	0.686
5	12.36	5.12	163	5.388	0.765

The epoxy resin containing micro-capsules (20 wt. %) (EpoB5) were cured by DETA (10 wt. %). The 5 repeated testing process were carried out at ambient temperature and the results were recorded by the force-displacement curve, figure 5.9.

The fracture force (P) is obtained from the force-displacement curve above. A value of the critical stress intensity factor, K_{IC}, is calculated for each fracture event and the results are shown in table 5.8. The fracture toughness of Epo-b5 is found to be K_{IC} = 0.746 ± 0.048 MPa·m$^{1/2}$.

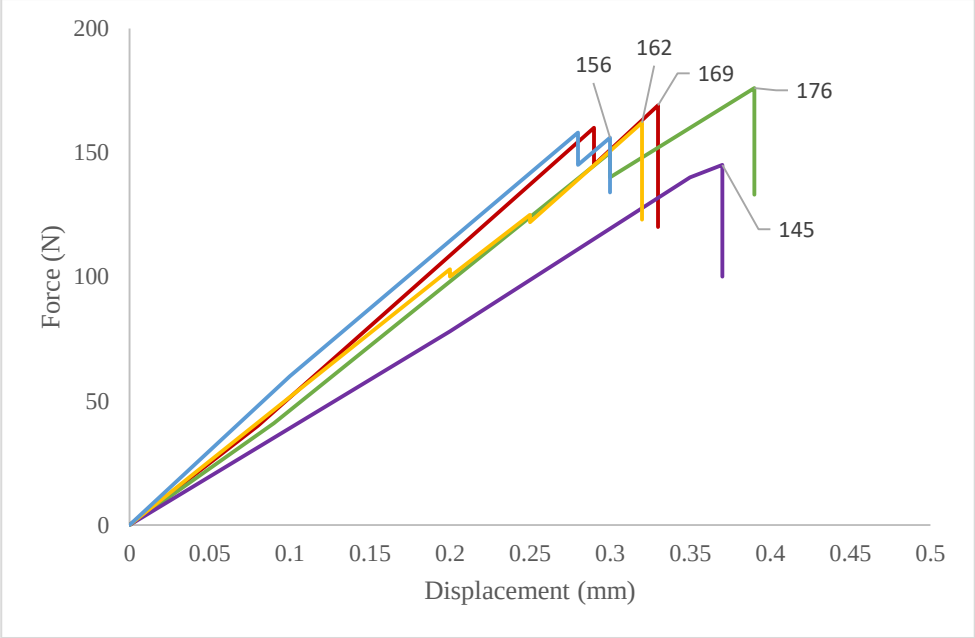

Figure 5.9: The force-displacement curve for the compact tension test of EpoB5

Table 5.8: The fracture toughness of EpoB5

Test	A (mm)	B (mm)	Force (N)	Y	K_{IC} (MPa·m$^{1/2}$)
1	12.36	5.26	169	5.388	0.772
2	11.51	5.11	156	5.293	0.723
3	14.58	5.63	176	5.759	0.803
4	13.99	5.26	145	5.643	0.693
5	12.79	5.14	162	5.446	0.765

The fracture toughness of epoxy resin containing 5-20% micro-capsules (EpoB1-5), comparing with pure epoxy resin specimens (0% micro-capsules) (EpoA) are shown in figure 5.10.

The fracture toughness of blank epoxy resin (EpoA) was 0.801 ± 0.019 MPa·m$^{1/2}$. The fracture toughness epoxy resin containing 5-20% micro-capsules (EpoB1-5) was found to be 0.764 ± 0.029, 0.768 ± 0.037, 0.777 ± 0.044, 0.752 ± 0.045, and 0.746 ± 0.048 MPa·m$^{1/2}$, respectively. The error bars representing standard deviation was between 0.027 and 0.047 MPa·m$^{1/2}$ (2.5% ~ 6.7%). The standard deviation of specimens containing micro-capsules is bigger than that of pure epoxy resin of 0.019 MPa·m$^{1/2}$. It was caused by the presence micro-capsules in the epoxy resin matrix. Perhaps the difference between the curves in figure 5.11 and 5.12, is that in figure 5.12 there is a bundle of micro-capsules directly in front

of the crack tip so that as it starts to propagate it is temporarily stopped. Once enough energy is stored then the crack travels through this region. One interesting aspect comparing figures 5.12 and 5.11 is that in 5.12 the crack travels much further on propagation (greater load drop) than figure 5.11. Of course, the difference in behaviour could also be due to the state of the original crack tip that is introduced.

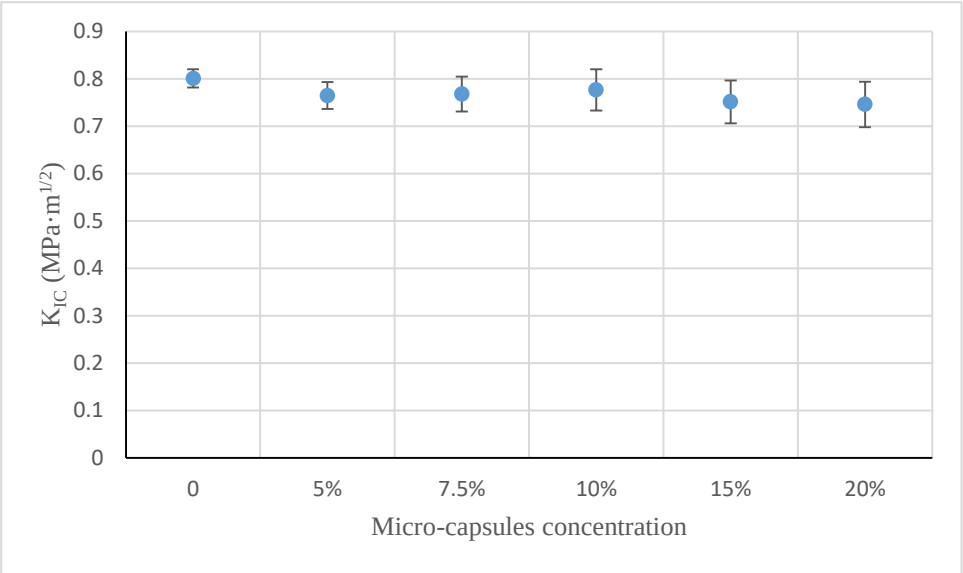

Figure 5.10: The fracture toughness of epoxy resin containing micro-capsules (5-20 %) compared with pure epoxy resin specimen (0)

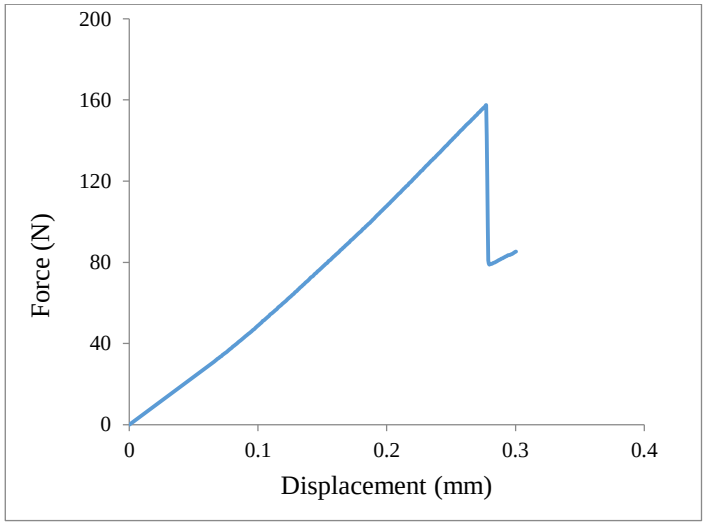

Figure 5.11: the force and displacement record of blank epoxy resin (EpoA) specimen

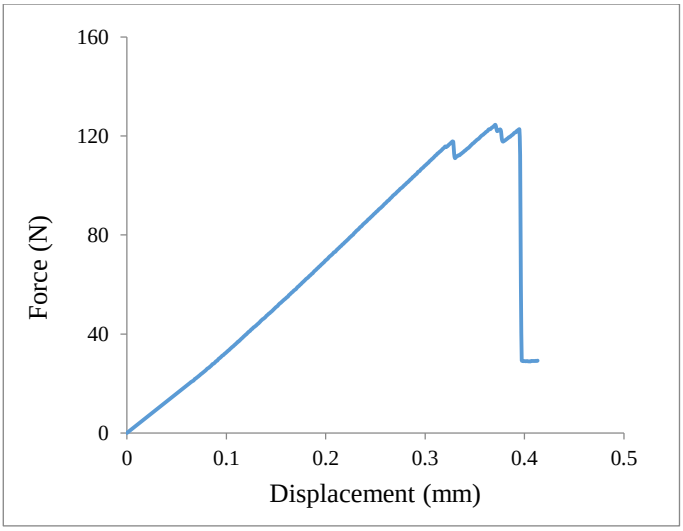

Figure 5.12: the force and displacement record of specimen containing micro-capsule

The specimens containing different concentration of micro-capsules (EpoB1-5) slightly increased the standard deviation, but no effect on the fracture toughness.

5.5.4 Fracture toughness of specimen containing solid healing agents

The solid healing agents used in this project were MA, MeMal, and EtOCN. In order to minimise or prevent the likelihood of any side reaction between the solid healing agents (MA and MeMal) and primary amine of DETA curing agent, the process of making specimen for self-healing assessment was modified. This involved mixing bisphenol-A based epoxide with DETA and leaving it at ambient temperature for 4 h before the addition of solid healing agents (MA and MeMal). This ensured the full consumption of primary amine and hence minimising or preventing any side reactions.

5.5.4.1 Epoxy resin containing maleic anhydride

The epoxy resin containing MA (5-20 wt. %) (EpoC1-4) were cured by DETA (10 wt. %). The 5 repeated testing process were carried out at ambient temperature and the results were recorded by the force-displacement curve.

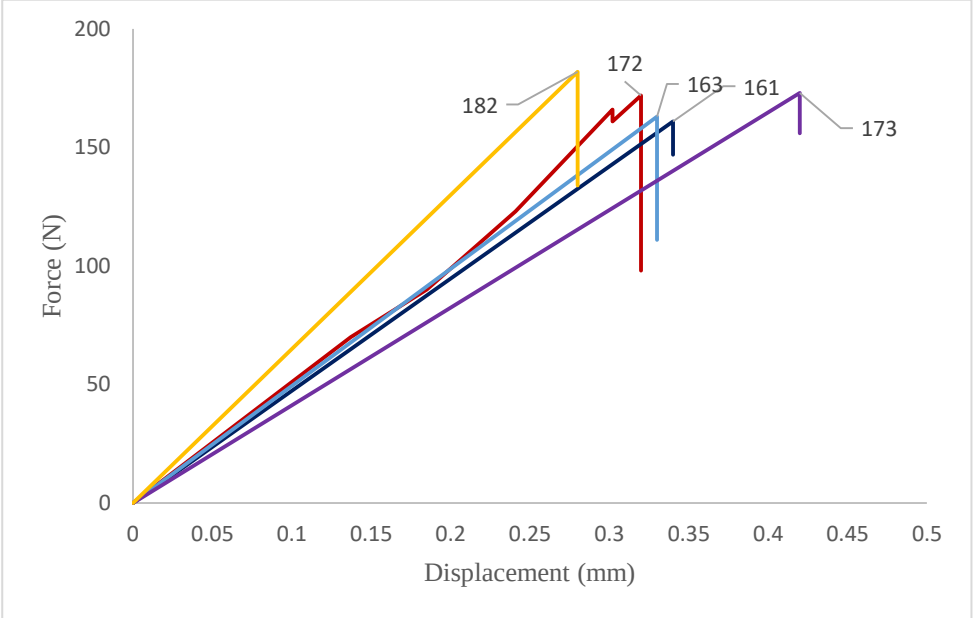

Figure 5.13: The force-displacement curve for the compact tension test of EpoC1

The force-displacement curve for the compact tension test of EpoC1 containing MA (5 wt. %) is shown in figure 5.13. The fracture force (P) is obtained in the force-displacement curve above. A value of the critical stress intensity factor, K_{IC}, is calculated for each fracture event and the results are shown in table 5.9. The fracture toughness of the EpoC1 is found to be $K_{IC} = 0.767 \pm 0.036$ MPa·m$^{1/2}$.

Table 5.9: The fracture toughness of EpoC1

Test	A (mm)	B (mm)	Force (N)	Y	K_{IC} (MPa·m$^{1/2}$)
1	12.28	5.57	172	5.378	0.740
2	13.73	5.24	161	5.596	0.767
3	13.21	5.47	163	5.509	0.732
4	15.39	5.63	173	5.938	0.816
5	11.14	5.66	182	5.261	0.754

The force-displacement curve for the compact tension test of EpoC2 containing MA (10 wt. %) is shown in figure 5.14.

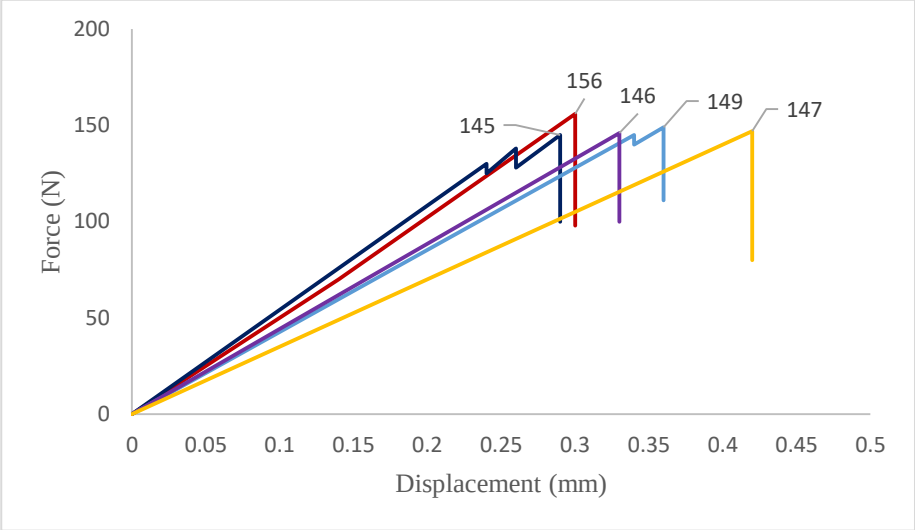

Figure 5.14: The force-displacement curve for the compact tension test of EpoC2

The fracture force (P) is obtained from the force-displacement curve above. A value of the critical stress intensity factor, K_{IC}, is calculated for each fracture event and the results are shown in table 5.10. The fracture toughness of the blank epoxy resins is found to be K_{IC} = 0.667 ± 0.043 MPa·m$^{1/2}$.

Table 5.10: The fracture toughness of EpoC2

Test	A (mm)	B (mm)	Force (N)	Y	K_{IC} (MPa·m$^{1/2}$)
1	11.47	5.12	156	5.290	0.718
2	11.29	5.34	145	5.274	0.638
3	13.11	5.64	149	5.493	0.647
4	12.38	5.39	146	5.390	0.651
5	15.57	5.37	147	5.980	0.730

The force-displacement curve for the compact tension test of EpoC3 containing MA (15

wt. %) is shown in figure 5.15.

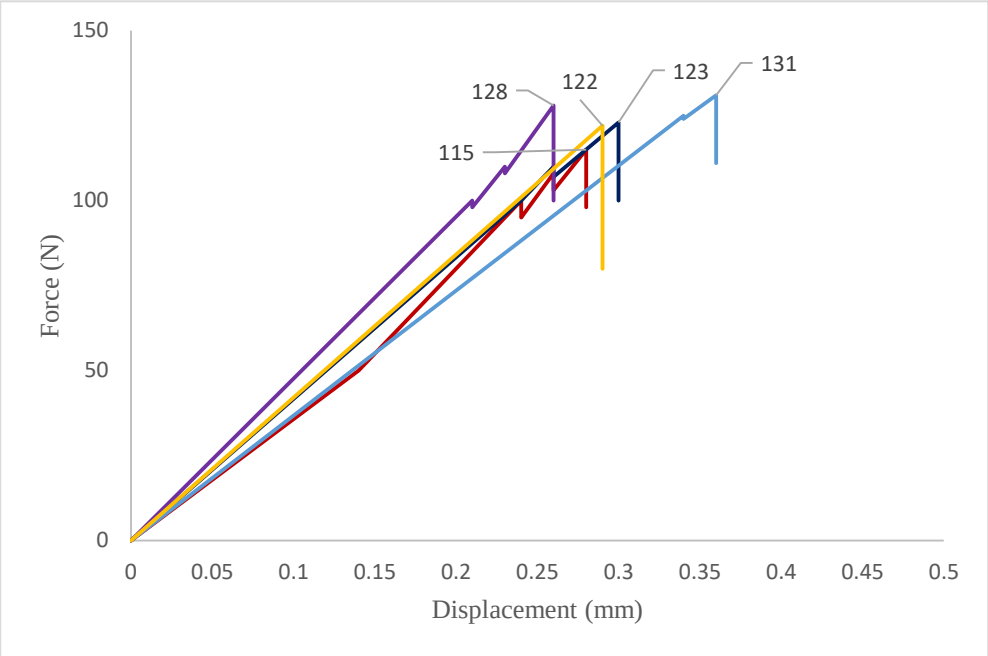

Figure 5.15: The force-displacement curve for the compact tension test of EpoC3

The fracture force (P) is obtained from the force-displacement curve above. A value of the critical stress intensity factor, K_{IC}, is calculated for each fracture event and the results are shown in table 5.11. The fracture toughness of the blank epoxy resins is found to be K_{IC} = 0.576 ± 0.037 MPa·m$^{1/2}$.

Table 5.11: The fracture toughness of EpoC3

Test	A (mm)	B (mm)	Force (N)	Y	K_{IC} (MPa·m$^{1/2}$)
1	12.49	5.31	115	5.404	0.521
2	13.27	5.33	123	5.518	0.570
3	14.21	5.28	131	5.685	0.628
4	11.57	5.35	128	5.299	0.567
5	12.73	5.49	122	5.437	0.540

The force-displacement curve for the compact tension test of EpoC4 containing MA (20 wt. %) is shown in figure 5.16.

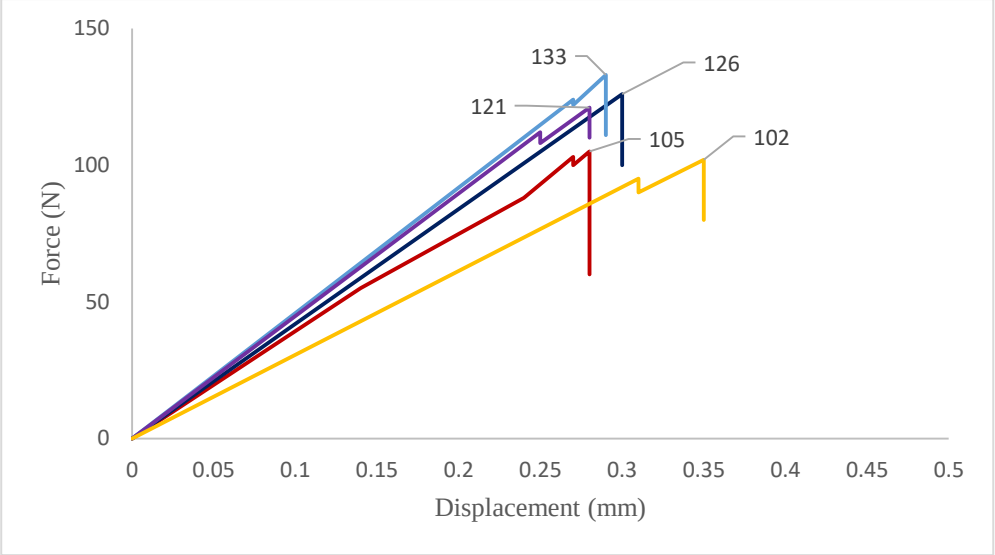

Figure 5.16: The force-displacement curve for the compact tension test of EpoC4

The fracture force (P) is obtained from the force-displacement curve above. A value of the critical stress intensity factor, K_{IC}, is calculated for each fracture event and the results are shown in table 5.12. The fracture toughness of the blank epoxy resins is found to be K_{IC} = 0.549 ± 0.046 MPa·$m^{1/2}$.

Table 5.12: The fracture toughness of EpoC4

Test	A (mm)	B (mm)	Force (N)	Y	K_{IC} (MPa·$m^{1/2}$)
1	11.88	5.64	105	5.331	0.442
2	12.46	5.36	126	5.400	0.568
3	11.27	5.33	133	5.272	0.588
4	12.15	5.17	121	5.362	0.559
5	13.51	5.26	102	5.558	0.482

The fracture toughness of epoxy resin containing different concentration of MA is compared and showed in figure 5.17. As the concentration of MA increased, the fracture toughness of the epoxy resin specimens was decreased. It has been reported that anhydrides is able to cross-link epoxy resin at 155 °C.[10] The preparation of the epoxy resin specimen for this project was carried out at 50 °C at which test carried out here showed no evidence for cross-linking bisphenol-A based epoxide with MA. The possibility of cross-linking of bisphenol-A based epoxide with MA is the presence of amine cannot be investigated. This is due to rapid cross-linking reaction between bisphenol-A and amine.

Also, there is a possibility of side reaction between MA and amine group of DETA curing

agent. This side reaction is likely to reduce the cross-link density and hence the fracture toughness. As it is mentioned in the section 5.4.4, the process of preparation of specimen containing MA was modified to minimise or prevent the side reaction. The decrease in the fracture toughness is possible due the presence of small amount of side reaction.

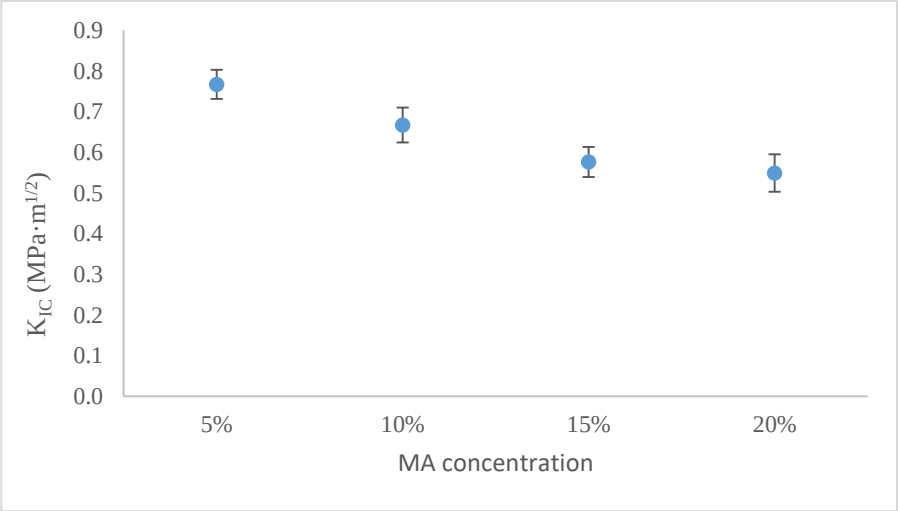

Figure 5.17: the fracture toughness of epoxy resin containing MA (EpoB1-5)

5.5.4.2 Epoxy resin containing N-methylmaleimide

The specimen containing MeMal (5-20 wt. %) (EpoD1-4) were cured by DETA (10 wt. %). The 5 repeated testing processes were carried out at ambient temperature and the results were recorded by the force-displacement curve. The force-displacement curve for the compact tension test of EpoD1 containing MeMal (5 wt. %) is shown in figure 5.18. The fracture force (P) is obtained from the force-displacement curve above. A value of the critical stress intensity factor, K_{IC}, is calculated for each fracture event and the results are shown in table 5.13. The fracture toughness of the blank epoxy resins is found to be K_{IC} = 0.766 ± 0.037 MPa·m$^{1/2}$.

Table 5.13: The fracture toughness of EpoD1

Test	A (mm)	B (mm)	Force (N)	Y	K_{IC} (MPa·m$^{1/2}$)
1	12.36	5.27	170	5.388	0.775
2	12.58	5.31	164	5.416	0.748
3	11.23	5.43	168	5.268	0.727
4	14.55	5.17	156	5.753	0.774
5	13.66	5.42	177	5.584	0.813

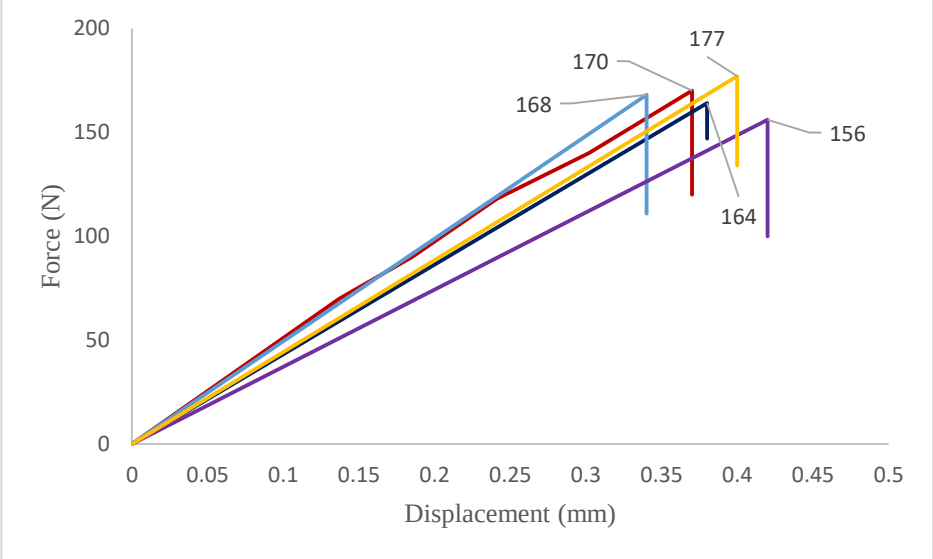

Figure 5.18: The force-displacement curve for the compact tension test of EpoD1

The force-displacement curve for the compact tension test of EpoD2 containing MeMal (10 wt. %) is shown in figure 5.19.

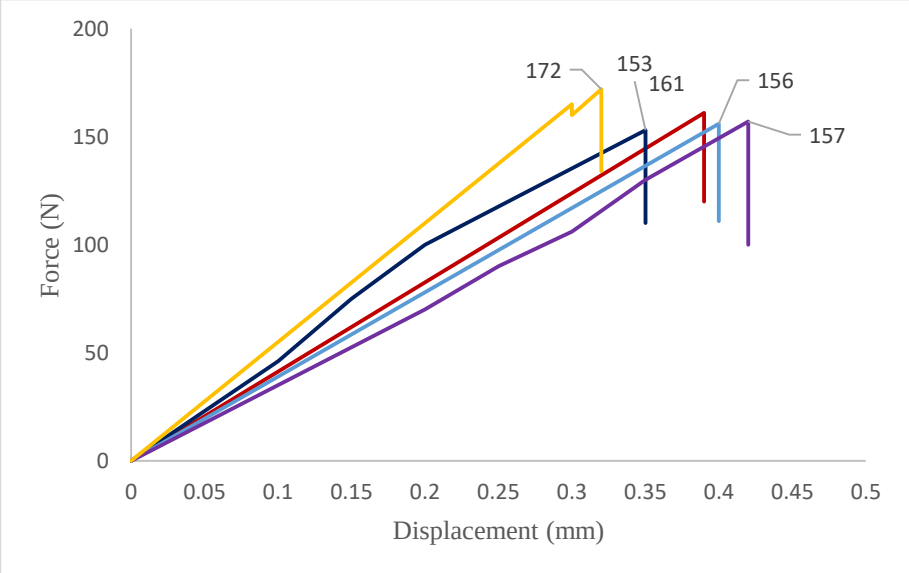

Figure 5.19: The force-displacement curve for the compact tension test of EpoD2

The fracture force (P) is obtained from the force-displacement curve above. A value of the critical stress intensity factor, K_{IC}, is calculated for each fracture event and the results are shown in table 5.14. The fracture toughness of the blank epoxy resins is found to be $K_{IC} = 0.715 \pm 0.057$ MPa·m$^{1/2}$.

Table 5.14: The fracture toughness of EpoD2

Test	A (mm)	B (mm)	Force (N)	Y	K_{IC} (MPa·m$^{1/2}$)
1	13.53	5.33	161	5.561	0.749
2	12.63	5.82	153	5.423	0.638
3	13.68	5.49	156	5.587	0.708
4	14.77	5.37	157	5.799	0.758
5	11.94	5.41	172	5.338	0.757

The force-displacement curve for the compact tension test of EpoD3 containing MeMal (15 wt. %) is shown in figure 5.20. The fracture force (P) is obtained from the force-displacement curve above. A value of the critical stress intensity factor, K_{IC}, is calculated for each fracture event and the results are shown in table 5.15. The fracture toughness of the blank epoxy resins is found to be $K_{IC} = 0.648 \pm 0.054$ MPa·m$^{1/2}$.

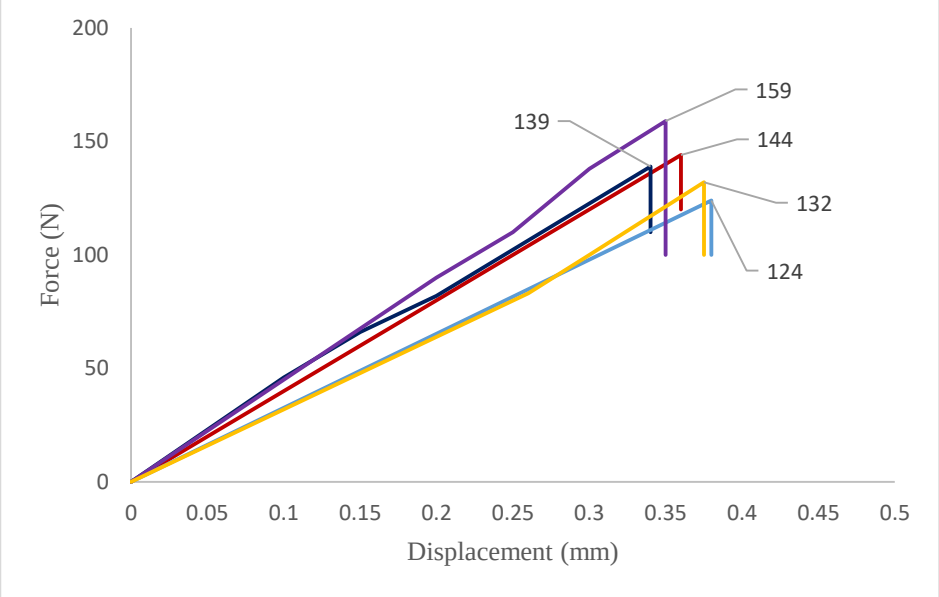

Figure 5.20: The force-displacement curve for the compact tension test of EpoD3

Table 5.15: The fracture toughness of EpoD3

Test	A (mm)	B (mm)	Force (N)	Y	K_{IC} (MPa·m$^{1/2}$)
1	12.75	5.13	144	5.440	0.683
2	11.34	5.15	139	5.278	0.635
3	13.52	5.11	124	5.560	0.601
4	11.92	5.21	159	5.335	0.726
5	13.46	5.17	132	5.550	0.631

The force-displacement curve for the compact tension test of EpoD4 containing MeMal (20 wt. %) is shown in figure 5.21. The fracture force (P) is obtained from the force-displacement curve above. A value of the critical stress intensity factor, K_{IC}, is calculated for each fracture event and the results are shown in table 5.16. The fracture toughness of the blank epoxy resins is found to be $K_{IC} = 0.602 \pm 0.042$ MPa·m$^{1/2}$.

Table 5.16: The fracture toughness of EpoD4

Test	A (mm)	B (mm)	Force (N)	Y	K_{IC} (MPa·m$^{1/2}$)
1	11.63	5.14	136	5.305	0.625
2	11.29	5.11	142	5.274	0.653
3	12.11	5.24	121	5.357	0.551
4	12.28	5.19	129	5.378	0.598
5	13.02	5.12	127	5.479	0.608

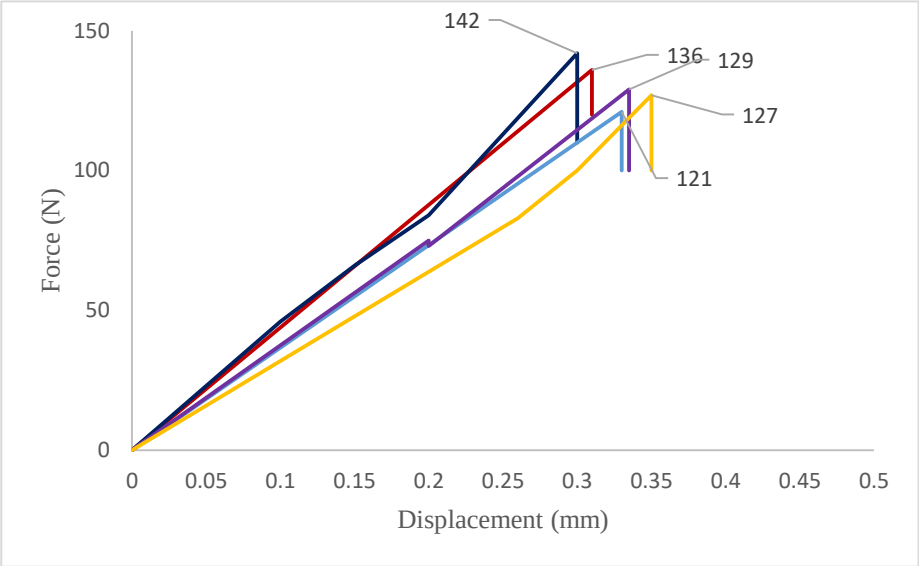

Figure 5.21: The force-displacement curve for the compact tension test of EpoD4

The fracture toughness of epoxy resin containing different concentration of MeMal is compared and showed in figure 5.22. As the concentration of MeMal increased, the fracture toughness of the epoxy resin specimens was decreased. There is a possibility of side reaction between MeMal and amine group of DETA curing agent. This side reaction is likely to reduce the cross-link density and hence the fracture toughness. As it is mentioned in the section 5.4.4, the process of preparation of specimen containing MeMal was modified to minimise or prevent the side reaction. The decrease in the fracture toughness is possible due the presence of small amount of side reaction.

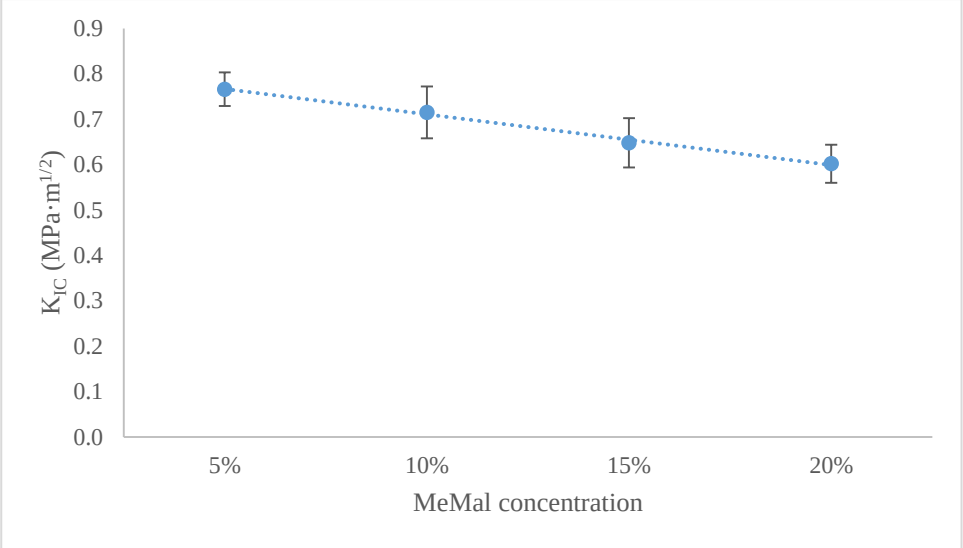

Figure 5.22: the fracture toughness of epoxy resin containing MeMal

5.5.4.3 Epoxy resin containing ethoxymethylene malononitrile

The epoxy resin containing EtOCN (5-20 wt. %) (EpoE1-4) were cured by DETA (10 wt. %). The 5 repeated testing process were carried out at ambient temperature and the results were recorded by the force-displacement curve.

The force-displacement curve for the compact tension test of EpoE1 containing EtOCN (5 wt. %) is shown in figure 5.23.

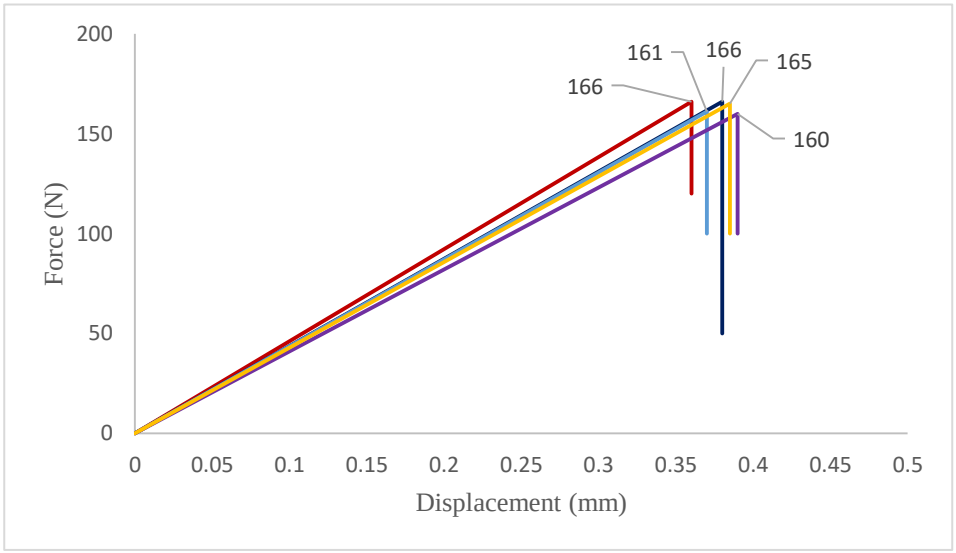

Figure 5.23: The force-displacement curve for the compact tension test of EpoE1

The fracture force (P) is obtained from the force-displacement curve above. A value of the critical stress intensity factor, K_{IC}, is calculated for each fracture event and the results are shown in table 5.17. The fracture toughness of the blank epoxy resins is found to be K_{IC} = 0.791 ± 0.014 MPa·m$^{1/2}$.

Table 5.17: The fracture toughness of EpoE1

Test	A (mm)	B (mm)	Force (N)	Y	K_{IC} (MPa·m$^{1/2}$)
1	12.56	5.03	166	5.414	0.799
2	13.77	5.11	166	5.603	0.812
3	13.23	5.05	161	5.512	0.783
4	14.01	5.16	160	5.647	0.783
5	13.78	5.25	165	5.605	0.785

The force-displacement curve for the compact tension test of EpoE2 containing EtOCN (10 wt. %) is shown in figure 5.24. The fracture force (P) is obtained from the force-displacement curve above. A value of the critical stress intensity factor, K_{IC}, is calculated for each fracture event and the results are shown in table 5.18. The fracture toughness of the blank epoxy resins is found to be K_{IC} = 0.792 ± 0.022 MPa·m$^{1/2}$.

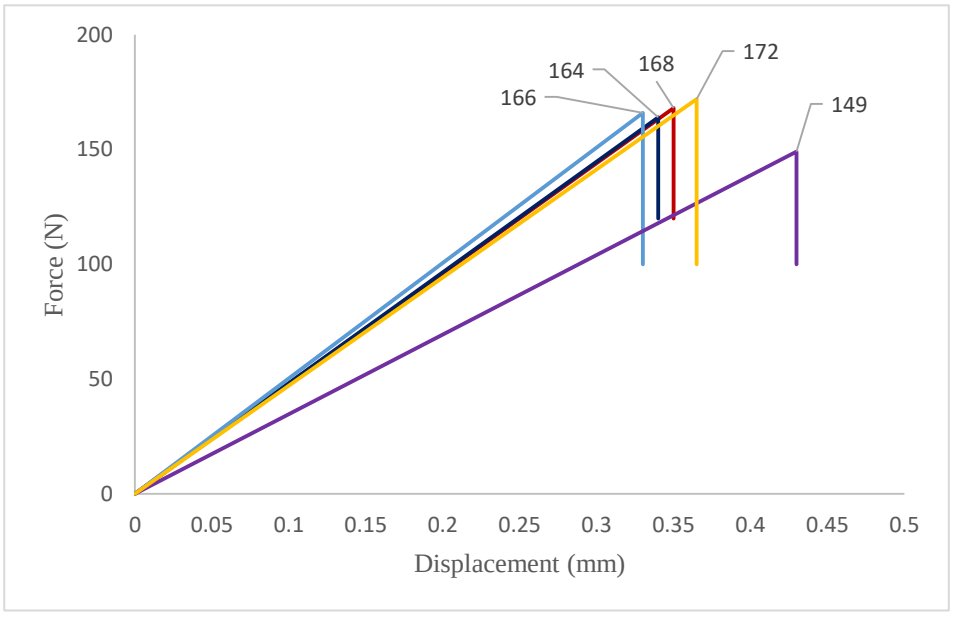

Figure 5.24: The force-displacement curve for the compact tension test of EpoE2

Table 5.18: The fracture toughness of EpoE2

Test	A (mm)	B (mm)	Force (N)	Y	K_{IC} (MPa·m$^{1/2}$)
1	13.02	5.16	168	5.479	0.798
2	12.74	5.17	164	5.438	0.772
3	12.65	5.09	166	5.426	0.789
4	15.72	5.11	149	6.016	0.785
5	13.16	5.13	172	5.501	0.822

The force-displacement curve for the compact tension test of EpoE3 containing EtOCN (15 wt. %) is shown in figure 5.25. The fracture force (P) is obtained from the force-displacement curve above. A value of the critical stress intensity factor, K_{IC}, is calculated for each fracture event and the results are shown in table 5.19. The fracture toughness of the blank epoxy resins is found to be $K_{IC} = 0.758 \pm 0.028$ MPa·m$^{1/2}$.

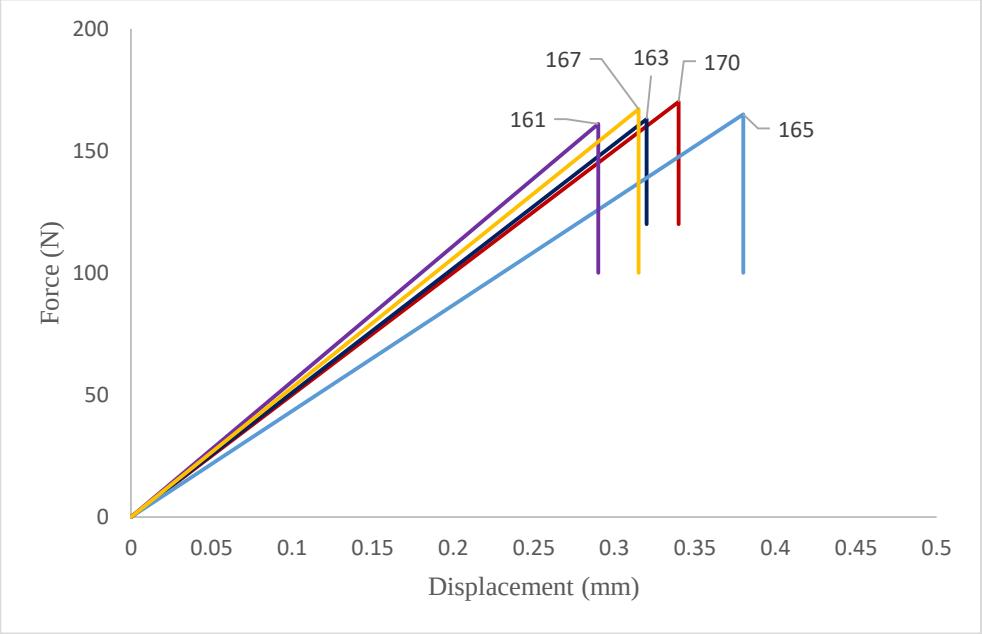

Figure 5.25: The force-displacement curve for the compact tension test of EpoE3

Table 5.19: The fracture toughness of EpoE3

Test	A (mm)	B (mm)	Force (N)	Y	K_{IC} (MPa·m$^{1/2}$)
1	12.91	5.34	170	5.463	0.775
2	12.02	5.28	163	5.347	0.736
3	13.44	5.15	165	5.546	0.795
4	11.24	5.14	161	5.269	0.736
5	11.99	5.19	167	5.343	0.767

The force-displacement curve for the compact tension test of EpoE4 containing EtOCN (20

wt. %) is shown in figure 5.26.

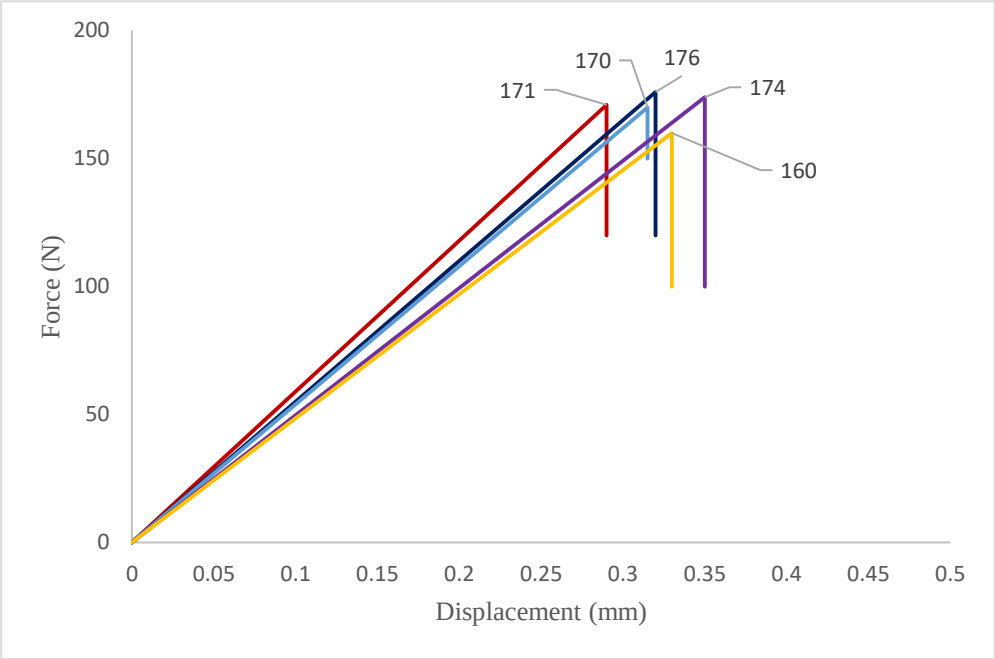

Figure 5.26: The force-displacement curve for the compact tension test of EpoE4

The fracture force (P) is obtained from the force-displacement curve above. A value of the critical stress intensity factor, K_{IC}, is calculated for each fracture event and the results are shown in table 5.20. The fracture toughness of the blank epoxy resins is found to be K_{IC} = 0.781 ± 0.045 MPa·m$^{1/2}$.

Table 5.20: The fracture toughness of Epo-e4

Test	A (mm)	B (mm)	Force (N)	Y	K_{IC} (MPa·m$^{1/2}$)
1	10.99	5.41	171	5.249	0.740
2	11.26	5.31	176	5.271	0.779
3	11.31	5.01	170	5.275	0.798
4	13.42	5.22	174	5.543	0.826
5	11.78	5.27	160	5.320	0.720

The fracture toughness of epoxy resin containing different concentration of EtOCN is compared and showed in figure 5.27. As the concentration of EtOCN increased, the fracture toughness of the epoxy resin specimens did not change much. The EtOCN does not have any side reaction with DETA.

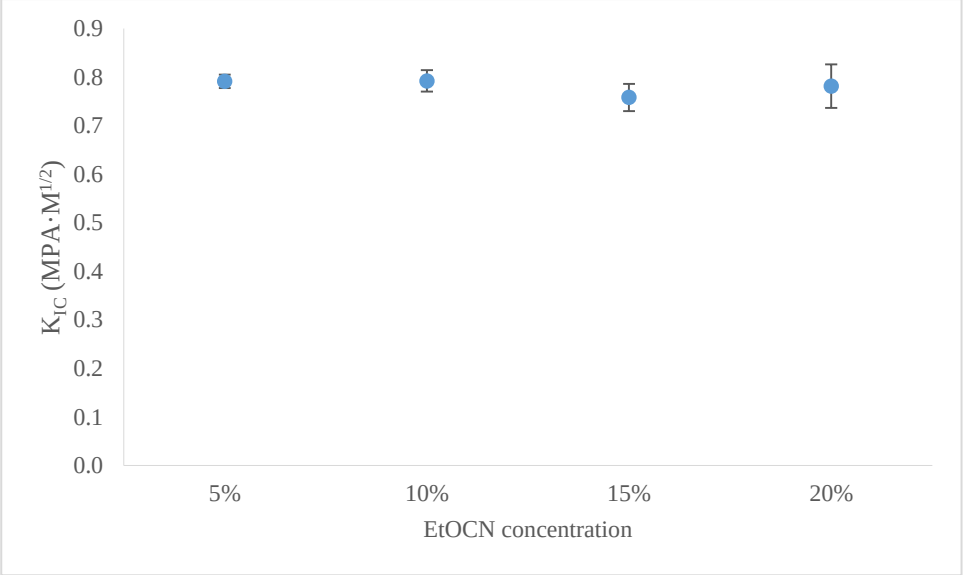

Figure 5.27: the fracture toughness of epoxy resin containing EtOCN

In summary, MA and MeMal reduced the fracture toughness of epoxy resin. For the self-healing specimens, 10% solid healing was added into the matrix. It will not only keep the fracture toughness closed to the pure epoxy resin, but also provide enough monomers for the polymerisation of healing agents. The fracture toughness of epoxy resin was between 0.65-0.7 MPa·$m^{1/2}$, figure 5.28.

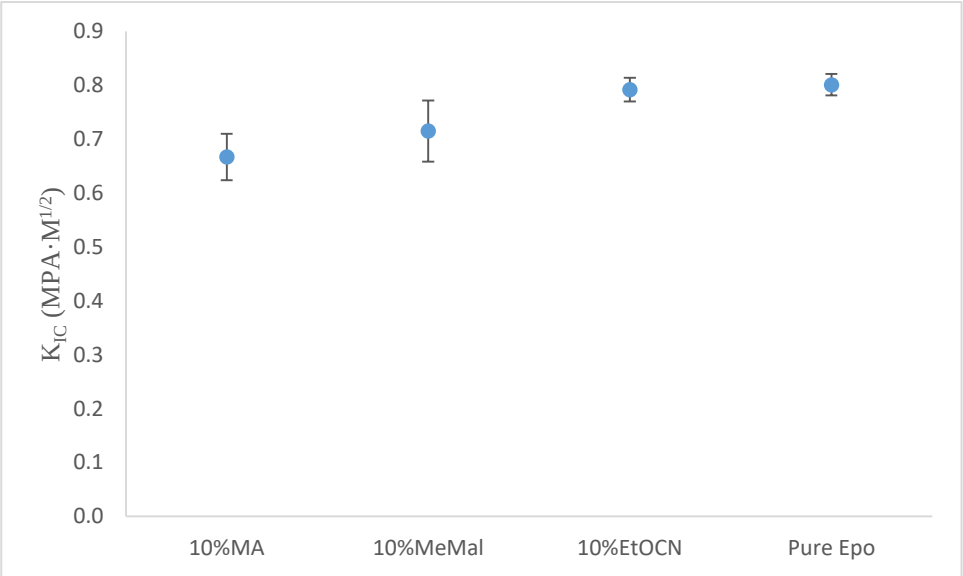

Figure 5.28: the fracture toughness of epoxy resin implanted 10% different solid healing agents

5.6 Conclusion

The blank epoxy resin specimens were prepared using Bisphenol-A based epoxide and diethylenetriamine (DETA) (10 wt. %) as the curing agent and the fracture toughness was measured to be K_{IC} = 0.801 ± 0.019 MPa·$m^{1/2}$. The epoxy resin specimens containing 5-20% micro-capsules were prepared and their fracture toughness was investigated. The inclusion of micro-capsules did not change the fracture toughness of matrix. The epoxy resin specimens containing solid healing agents (MA, MeMal, and EtOCN) were also prepared and their fracture toughness was investigated. Solid healing agents MA and MeMal reduced the fracture toughness of epoxy resin matrix as the amount increased. Therefore, specimens were prepared with 10% added solid healing agents as this amount gave minimum reduction of fracture toughness. There is a possibility of side reaction between MA (or MeMal) and amine group of DETA curing agent which is likely to reduce the cross-link density and hence the fracture toughness. The process of preparation of specimen containing MA (or MeMal) was modified involving mixing bisphenol-A based epoxide with DETA and leaving it at ambient temperature for 4 h before the addition of solid healing agents (MA and MeMal). This ensured close to full consumption of primary amine and hence minimising or preventing side reactions. However, the fracture toughness of the specimen did not change by adding EtOCN solid healing agent into the epoxy resin matrix due to the lack of any side reaction between EtOCN and DETA.

Reference

1. Ghosh, S. (2009) 'Self-healing Materials: Fundamentals, Design Strategies, and Applications' in Ghosh, S. (ed.) *Self-healing Materials*, Weinheim: Wiley-VCH, pp. 1-28.
2. Degarmo, E. Paul; Black, J T.; Kohser, Ronald A. (2003), Materials and Processes in Manufacturing (9th ed.), Wiley, p. 32, ISBN 0-471-65653-4.
3. Hertzberg, Richard W. (1995). Deformation and Fracture Mechanics of Engineering Materials (4 ed.). Wiley. ISBN 0-471-01214-9.
4. White SR, Sottos NR, Geubelle PH,Moore JS, Kessler MR, *et al*. 2001. Autonomic healing of polymer composites. Nature 409(6822):794–97
5. Rozenberg B. A. Kinetics, thermodynamics and mechanism of reactions of epoxy oligomers with amines. *Advances in Polymer Science*, **75**, 1985, pp 113-165.
6. Sautereau, J. P. P. H., Verdu, J. and Williams, R. J. J. *Thermosetting Polymers*. New York: Marcel Dekker, Inc., 2002, pp 6-65.
7. Xu, L. and Schlup, J. R. Etherification versus amine addition during epoxy resin/amine cure: An *in-situ* study using near-infrared spectroscopy. *J Appl. Polym. Sci.*, **67**, 1998, pp 895-901
8. Kinloch AJ, Young RJ. Fracture behaviour of polymers. London: Elsevier; 1983. Applied Science
9. Brown WF, Srawley JE. Plane strain crack toughness testing of high strength metallic materials. ASTM STP 1966;410.

Chapter 6

Assessment of self-healing performance

6.1 Introduction

Capsule-based self-healing system in this project is based on epoxy resin matrix and urea-formaldehyde micro-capsules (figure 6.1). Epoxy resin is selected as matrix materials for fracture toughness test. The liquid healing agents (4MeOst, DVB, St, and their mixtures) are encapsulated by urea-formaldehyde micro-capsules, which is added into the epoxy resin matrix and acting as the triggers. When the damage occurring in the epoxy resin matrix, it will rupture micro-capsules and release the liquid healing agent. The solid healing agents (MA, MeMal, and EtOCN) are dispersed in the epoxy resin, which will polymerise with the liquid healing agents released by the micro-capsules.

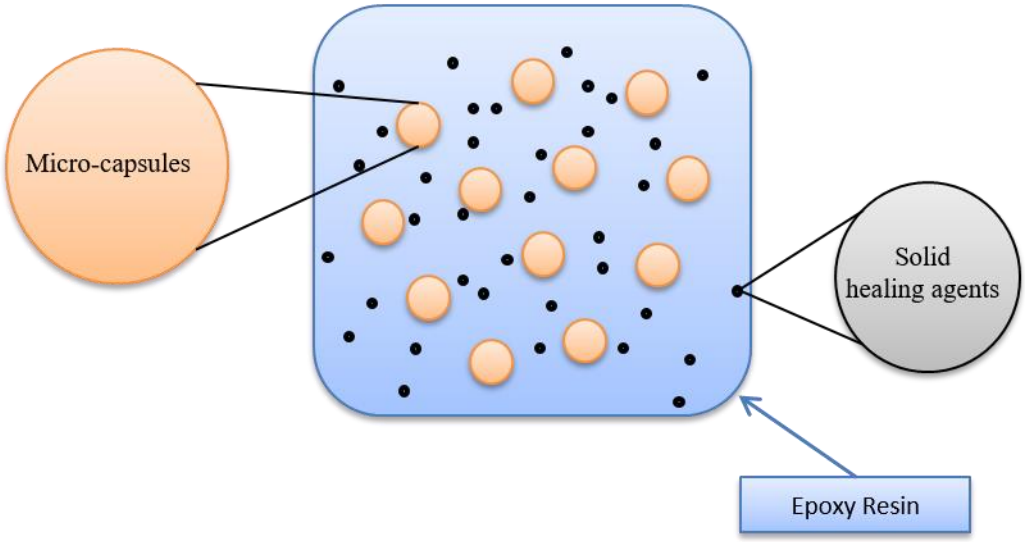

Figure 6.1: the design of self-healing specimens

The self-healing performance was assessed by fracture toughness recovery. To quantify healing, the healing efficiency (η) as a ratio of changes in material properties was defined as equation 6.1.

$$\eta = \frac{K_{IC\ healed}}{K_{IC\ origenal}} \times 100\% \qquad \text{Eq. 6.1}$$

Where K_{IC} the stress intensity factor: the fracture toughness measured by compact tension.

6.2 Materials

Maleic anhydride (MA), 4-methoxystyrene (4MeOSt), divinylbenzene (DVB), styrene (St), ethoxymethylene malononitrile (EtOCN), N-methylmaleimide (MeMal), and Diethylenetriamine (DETA) were purchased from Aldrich and used as supplied. Bisphenol-A based epoxide (EPON 828) resin was purchased from Hexion^{TM} Specialty Chemicals.

6.3 Instrumentation

Fracture testing of the specimens was performed on an RDP servo-mechanical testing machine at a crosshead speed of 0.5 mm/ min, using compact tension geometry. This test was carried out in University of Leeds.

6.4 Experimental

6.4.1 Self-healing performance via injection

6.4.1.1 The preparation of specimen

DETA (10 wt. %) was added to bisphenol-A based epoxide resin, stirred and the final mixture was degassed. The mixture was kept at ambient temperature for 4 h. Then the finely powdered solid healing agents monomers (10 wt. %) was added, stirred thoroughly and the mixture was degassed again. The mixture was then poured into a closed Teflon mould (60 mm × 50 mm × 5 mm) with silicon seals and cured for 24 h at ambient temperature. The specimen was further cured at 50 °C for 24 h, and cooled to ambient temperature to collect the specimen.

6.4.1.2 The fracture toughness recovery test

Fracture tests were carried out at ambient temperature using the compact tension geometry shown in figure 6.2, where the dimensions are 60 mm × 50 mm × 5 mm and a is the starting crack length; B is the specimen thickness and W is loading width of the specimen. The specimen shape is rectangular with loading holes placed 10 mm from the specimen surfaces. A 20 mm long crack was first sawn into the specimen, followed by tapping the sharp pre-crack.

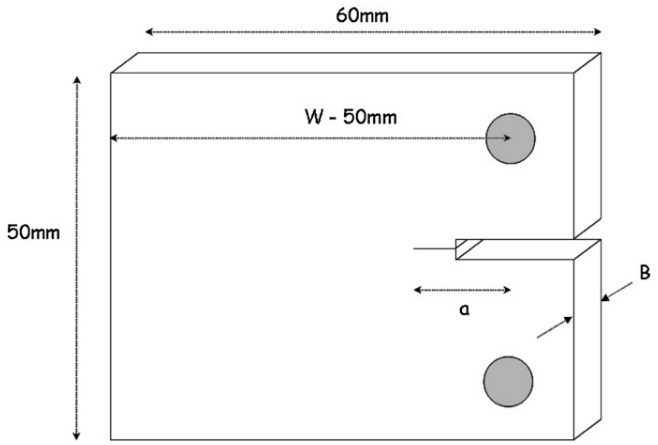

Figure 6.2: the geometry of the specimens for the compact tension

For the first test, the specimen was loaded until crack propagated to the end of the specimen. The specimen was removed from the testing machine and liquid healing agents (~0.1 mL) (4MeOSt, DVB, St, or their mixtures) was injected on the surface of the crack, and then left at 50 ℃ or ambient temperature for the required healing time. The specimens were again

placed into the testing machine and reloaded. For this second test, the specimens were loaded until the 'healed' section broke. The testing process was recorded by the force-displacement curve.

6.4.2 Self-healing performance via micro-capsules

6.4.2.1 The preparation of specimen

DETA (10 wt. %) was added to bisphenol-A based epoxide resin, stirred and the final mixture was degassed. The micro-capsules (with content of 4MeOSt, DVB, St, or their mixtures) (10-20 wt. %) was added, stirred thoroughly to ensure uniform distribution and the mixture was degassed. The mixture was kept at ambient temperature for 4 h. Then the finely powdered solid healing agent (MA, MeMal, or EtOCN) (10 wt. %) was added, stirred thoroughly and the mixture was degassed again. The mixture was then poured into a closed Teflon mould (60 mm × 50 mm × 5 mm) with silicon seals and cured for 24 h at ambient temperature. The specimen was further cured at 50 °C for 24 h, and cooled to ambient temperature to collect the specimen.

6.4.2.2 The fracture toughness recovery test

Fracture tests were carried out at ambient temperature using the compact tension geometry (60 mm × 50 mm × 5 mm), figure 6.2. The specimen shape is rectangular with loading holes placed 10 mm from the specimen surfaces. A 20 mm long crack was first sawn into the specimen, followed by tapping the sharp pre-crack. Taking into account the unloaded area of 10 mm, the starter crack was therefore of the order of 15 mm. For the first test, the specimen was loaded until crack initiation occurred. The fracture behaviour was brittle in all cases, such that on initiation the crack travelled a certain distance across the specimen. This test gave the original fracture toughness of specimens. At this point the specimen was removed from the testing machine and left at 50 ℃ or ambient temperature for the required healing time. Then, the specimens were again placed into the testing machine and reloaded. For this second test, the specimens were loaded until the 'healed' section broke, and then loaded further to propagate a new crack. This new crack was then left again for the required healing time. This testing strategy continued until the specimen was finally cracked in two. The testing process was recorded by the force-displacement curve.

6.4.3 The list of specimen prepared for self-healing performance test

The self-healing systems designed in this project are shown below, which were based on micro-encapsulation or injection of liquid healing agents (4MeOSt, DVB, St, and their mixtures) with solid healing agents (MA, MeMal, and EtOCN) added to the epoxy resin matrix. According to the polymer product formed by copolymerisation of healing agents, there are two self-healing system: linear polymer system and cross-linked polymer system.

The specimens prepared for healing performance assessment of linear polymer system via injection of liquid healing agents are shown in table 6.1.

Table 6.1: The self-healing specimen for linear polymer system via injection

Specimen	Liquid healing agents		Solid healing agents	
	Name	mL	Name	wt.%, g
LI01	4MeOSt	0.1	MA	10, 2
LI02	St	0.1	MA	10, 2
LI03	4MeOSt	0.1	MeMal	10, 2
LI04	4MeOSt	0.1	EtOCN	10, 2

The specimens prepared for healing performance assessment of linear polymer system via micro-encapsulation of liquid healing agents are shown in table 6.2.

Table 6.2: The self-healing specimen for linear polymer system via micro-capsules

Specimen	Micro-capsules		Solid healing agents	
	Name	wt.%, g	Name	wt.%, g
LM01	4MeOSt	10, 2	MA	10, 2
LM02		15, 3		10, 2
LM03		20, 4		10, 2
LM04	St	10, 2	MA	10, 2
LM05		15, 3		10, 2
LM06		20, 4		10, 2
LM07	4MeOSt	10, 2	MeMal	10, 2
LM08		15, 3		10, 2
LM09		20, 4		10, 2
LM10	4MeOSt	10, 2	EtOCN	10, 2
LM11		15, 3		10, 2
LM12		20, 4		10, 2

The specimens prepared for healing performance assessment of cross-linked polymer system via injection of liquid healing agents are shown in table 6.3.

Table 6.3: The self-healing specimen for cross-linked polymer system via injection

Specimen	Liquid healing agents		Solid healing agents	
	Name	mL	Name	wt.%, g
XI01	DVB	0.1	MA	10, 2
XI02	4MeOSt+DVB	0.08+0.02	MA	10, 2
XI03	St+DVB	0.08+0.02	MA	10, 2
XI04	DVB	0.1	MeMal	10, 2
XI05	4MeOSt+DVB	0.08+0.02	MeMal	10, 2

The specimens prepared for healing performance assessment of cross-linked polymer system via micro-encapsulation of liquid healing agents are shown in table 6.4.

Table 6.4: The self-healing specimen for cross-linked polymer system via micro-capsules

Specimen	Micro-capsules		Solid healing agents	
	Name	mL	Name	wt.%, g
XM01	DVB	10, 2	MA	10, 2
XM02		15, 3		10, 2
XM03		20, 4		10, 2
XM04	4MeOSt+DVB	10, 2	MA	10, 2
XM05		15, 3		10, 2
XM06		20, 4		10, 2
XM07	St+DVB	10, 2	MA	10, 2
XM08		15, 3		10, 2
XM09		20, 4		10, 2
XM10	DVB	10, 2	MeMal	10, 2
XM11		15, 3		10, 2
XM12		20, 4		10, 2
XM13	4MeOSt+DVB	10, 2	MeMal	10, 2
XM14		15, 3		10, 2
XM15		20, 4		10, 2

6.5 Results and discussion

6.5.1 Self-healing performance for linear polymer system

6.5.1.1 Via injection of liquid healing agents

In order to evaluate the healing efficiency of the self-healing system, the liquid healing agents were injected into the crack of the specimen containing solid healing agents. The liquid and solid healing agents were expected to polymerise and formed linear polymer to fill the crack based on previously results discussed in Chapter 2. The fracture toughness of specimen after healed was investigated and compared with the virgin fracture toughness of the specimen using Eq. 6.1 to give the healing efficiency.

The self-healing performance for linear polymer system via injection of liquid healing agents (LI01-04) was investigated. LI01 and LI02 is the specimen containing MA and injected 4MeOSt and St, respectively, into the crack. LI03 is the specimen containing MeMal and injected 4MeOSt into the crack. LI04 is the specimen containing EtOCN and injected 4MeOSt into the crack. The healing process was undertaken at 50 °C for 24 h. The fracture toughness tests were undertaken at ambient temperature. Figure 6.3 shows that LI01-04 exhibited 42%, 49%, 32%, and 57% healing efficiency.

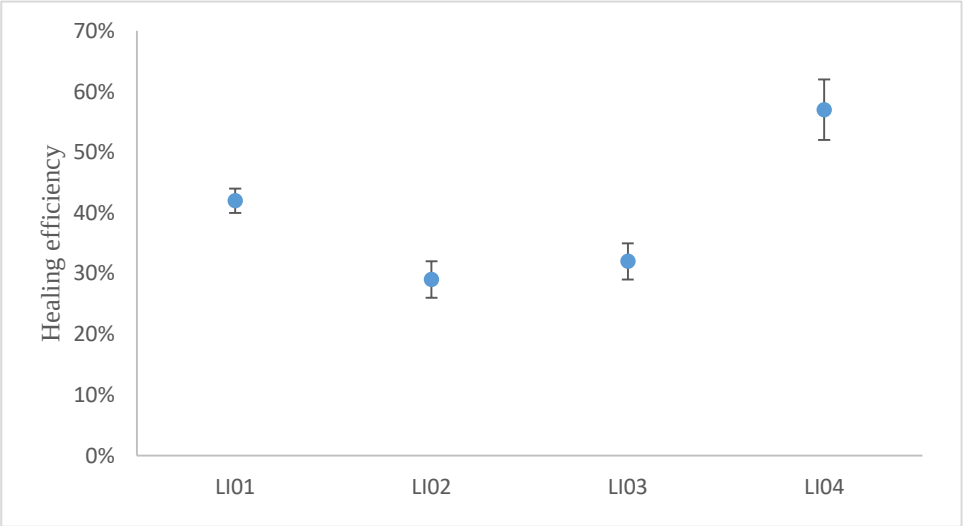

Figure 6.3: the healing efficiency of LI01-04 at 50 °C for 24 h via injection

6.5.1.2 Via micro-encapsulation of liquid healing agents

The specimen prepared by adding micro-capsules containing liquid healing agents and solid healing agents are expected to exhibit an autonomous self-healing process, upon the release of liquid healing agent when crack propagates through the matrix. The self-healing performance for linear polymer system via micro-encapsulation of liquid healing agents (LM01-12) was investigated.

Specimen LM01 containing MA (solid healing agents, 10 wt. %) and 4MeOSt (micro-capsules, 10 wt. %) was investigated for their self-healing performance by fracture toughness recovery using the compact tension test. The self-healing process was carried out at 50 °C for 24 h, the compact tension test was at ambient temperature and the results were recorded by the force-displacement curve.

The specimen was investigated for the self-healing performance by fracture toughness recovery using the compact tension test. The fracture tests were carried out at ambient temperature using the compact tension geometry (60 mm × 50 mm × 5 mm) with a pre-crack ended at position 1, figure 6.4. This was chosen because the specimen size (60 mm × 50 mm × 5 mm) is both a convenient volume for synthesis but also wide enough so that on fracture the crack does not travel completely across the specimen. This is critical because in order to assess healing, the specimen has to be first cracked, healed, and then retested.

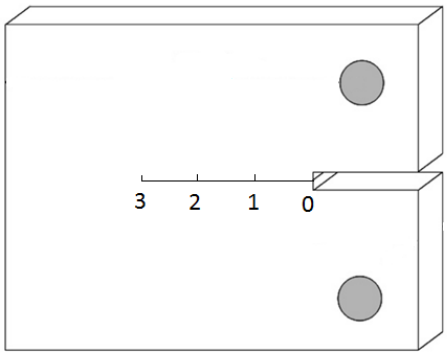

Figure 6.4: the crack propagated positions in the specimens

For the first test, the specimen was loaded in tension until the crack started to propagate. Figure 6.5(a) shows the force displacement curve, with the load falling rapidly as the crack propagated unstably from position 1 to 2. After the unstable fracture, the specimen was immediately removed from the testing machine and left to heal for the 24h. A second test

was then carried out. If the specimen had healed, then on loading it would be expected to follow the gradient of the first test until the healed surface cracked, at which point the crack would propagate to the end of the healed section (figure 6.4, position 2). As the gradient, or compliance, is governed by the crack length, this is a very good indication of whether healing has taken place. Figure 6.5(b) shows the force displacement curve for the second test. With the initial loading of the healed section, the fracture of the healed section (figure 6.4, position 1 to 2), then the loading of the specimen at crack position 2 until unstable fracture again occurs and the crack travels to position 3, opening more capsules and starting the healing process between positions 2 and 3.

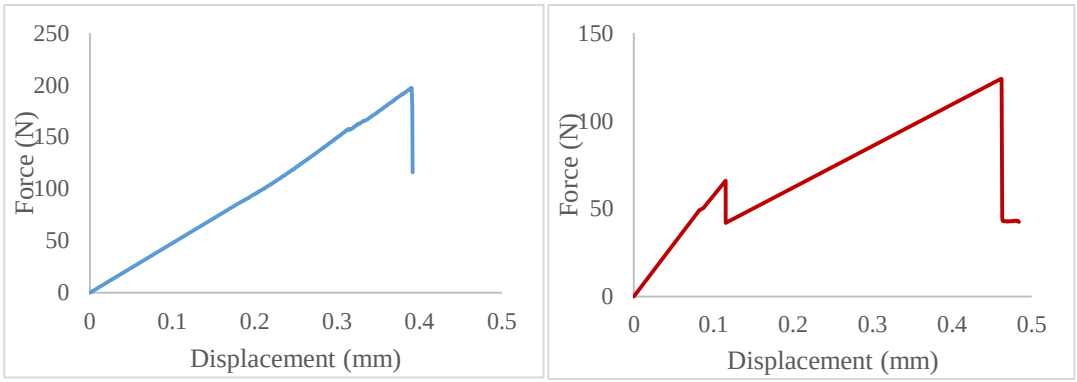

(a) (b)

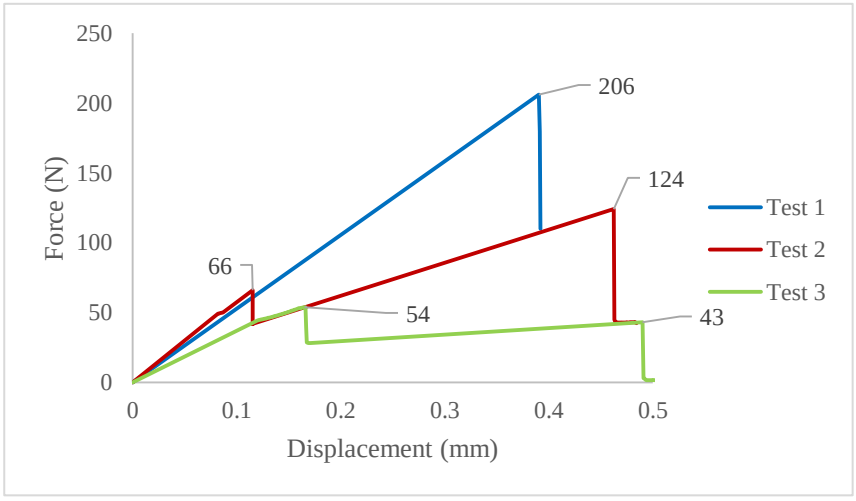

(c)

Figure 6.5: the force displacement curve of self-healing specimen SHA1, (a) the first test curve, (b) the second test curve, and (c) the three tests combined curve.

Figure 6.5c shows the superposition of the force displacement curves for the first and second tests. It is seen that the gradient of the second test is very similar to the first test on the virgin

material. Once the healed section fractures, the gradient is seen to be lower (the crack now being loaded at position 2), and passes through the position of the first test where the test was stopped. The fracture toughness of the healed section is given by the load at position 1 from the second tests and this is compared to the 'virgin' material value from position 1 from the first test.

After the second test, the specimen was again left for the requisite healing time, which for this specimen was 24 h, and then retested. Figure 6.5c shows the force/displacement curve of the third test superimposed on the first and second tests. For the third test, healed back to position 2, the gradient is similar to that of the second test when loading at position 2. After the healed section fractured, the gradient was lower and intersected the force/displacement test of the second test as it was stopped at position 3.

The fracture force (P) is obtained from the force-displacement curve, figure 6.5c (in section 6.4.1). A value of the critical stress intensity factor, K_{IC}, is calculated for each fracture event and the results are shown in table 6.5. The fracture toughness of original specimen is given by Test 1, Test 2 (when the crack propagating from position 2-3), and Test 3 (when the crack propagating from position 3 to the end of the specimen), which is found to be $K_{IC} = 0.775 \pm 0.010$ MPa·m$^{1/2}$. Therefore, the first and second healing process gave 31% and 43% healing efficiency, respectively.

Table 6.5: The fracture toughness of LM01

Test	*Crack position	a (mm)	B (mm)	Force (N)	Y	K_{IC} (MPa·m$^{1/2}$)
1	1	12	6.45	206	5.344	0.763 (Original)
2	0-1	10	6.45	66	5.194	0.238 (Healed)
	2	24	6.45	124	9.060	0.779 (Original)
3	1-2	24	6.45	54	9.060	0.336 (Healed)
	3	37	6.45	43	26.549	0.782 (Original)

*The crack position is showed in figure 6.4.

Specimen LM02 containing MA (solid healing agents, 10 wt. %) and 4MeOSt (micro-capsules, 15 wt. %) was investigated for their self-healing performance by fracture toughness recovery using the compact tension test. The self-healing process was carried out at 50 °C for 24 h, the compact tension test was at ambient temperature and the results were recorded by the force-displacement curve.

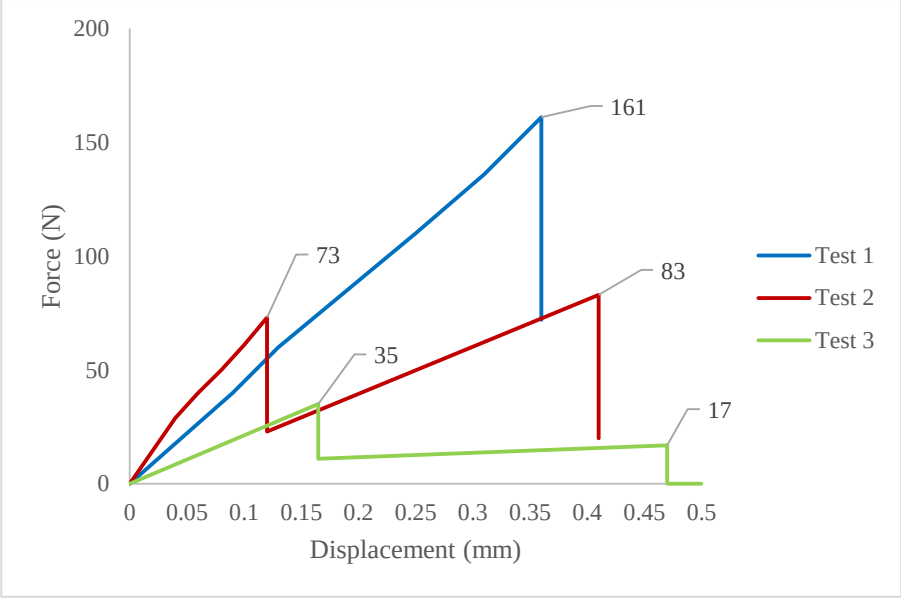

Figure 6.6: the force displacement curve of self-healing specimen LM02

The fracture force (P) is obtained from the force-displacement curve, figure 6.6. A value of the critical stress intensity factor, K_{IC}, is calculated for each fracture event and the results are shown in table 6.6.

Table 6.6: The fracture toughness of LM02

Test	*Crack position	a (mm)	B (mm)	Force (N)	Y	K_{IC} (MPa·m$^{1/2}$)
1	1	14	5.22	161	5.575	0.769 (Original)
2	0-1	10	5.22	73	5.194	0.325 (Healed)
	2	27	5.22	83	10.888	0.774 (Original)
3	1-2	27	5.22	37	10.888	0.345 (Healed)
	3	42	5.22	17	53.453	0.779 (Original)

*The crack position is showed in figure 6.4.

The fracture toughness of original specimen is given by Test 1, Test 2 (when the crack propagating from position 2-3), and Test 3 (when the crack propagating from position 3 to the end of the specimen), which is found to be $K_{IC} = 0.778 \pm 0.047$ MPa·m$^{1/2}$. Therefore, the first and second healing process gave 42% and 45% healing efficiency, respectively.

Specimen LM03 containing MA (solid healing agents, 10 wt. %) and 4MeOSt (micro-capsules, 20 wt. %) was investigated for their self-healing performance by fracture toughness recovery using the compact tension test. The self-healing process was carried out at 50 °C for 24 h, but the compact tension test was at ambient temperature and the results were recorded

by the force-displacement curve.

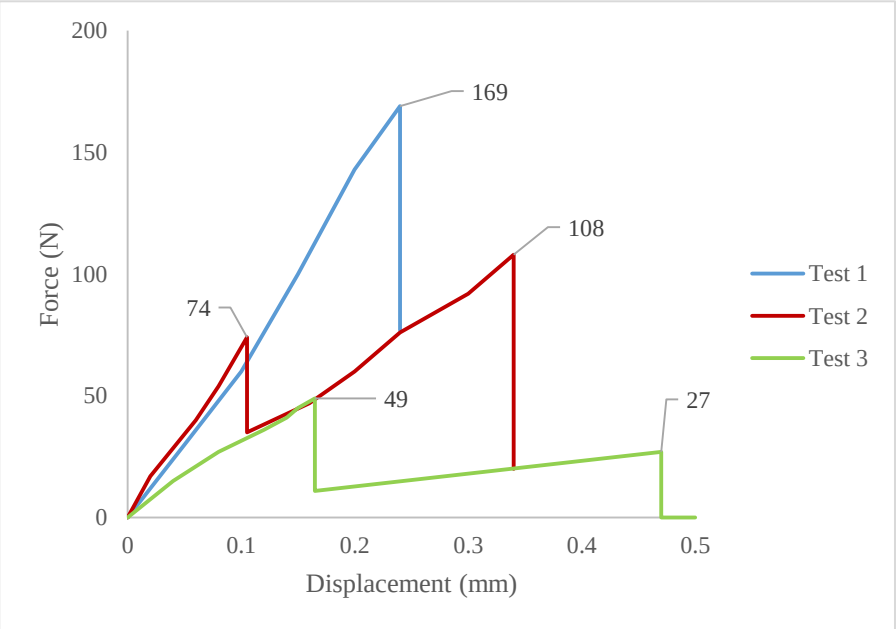

Figure 6.7: the force displacement curve of self-healing specimen LM03

The fracture force (P) is obtained from the force-displacement curve, figure 6.7. A value of the critical stress intensity factor, K_{IC}, is calculated for each fracture event and the results are shown in table 6.7. The fracture toughness of original specimen is given by Test 1, Test 2 (when the crack propagating from position 2-3), and Test 3 (when the crack propagating from position 3 to the end of the specimen), which is found to be K_{IC} = 0.762 ± 0.015 MPa·$m^{1/2}$. Therefore, the first and second healing process gave 43% and 45% healing efficiency, respectively.

Table 6.7: The fracture toughness of LM03

Test	*Crack position	a (mm)	B (mm)	Force (N)	Y	K_{IC} (MPa·$m^{1/2}$)
1	1	11	5.31	169	5.265	0.749 (Original)
2	0-1	10	5.31	74	5.194	0.324 (Healed)
	2	23	5.31	108	8.567	0.779 (Original)
3	1-2	23	5.31	49	8.567	0.354 (Healed)
	3	39	5.31	27	33.303	0.757 (Original)

*The crack position is showed in figure 6.4.

The healing efficiency of specimen LM01-03 was compared in the figure 6.8. The micro-capsules were added in an ascending order (10%, 15%, 20%) to the specimen LM01-03,

which was supposed to increase the amount of 4MeOSt releasing from the micro-capsules. As the concentration of micro-capsules increased, the healing efficiency of the specimens kept steady. It is caused by the distribution of micro-capsules in the matrix was uncontrollable as well as the amount of micro-capsules broken by the crack, whether the amount of 4MeOSt releasing from those micro-capsules was increasing was actually uncertain.

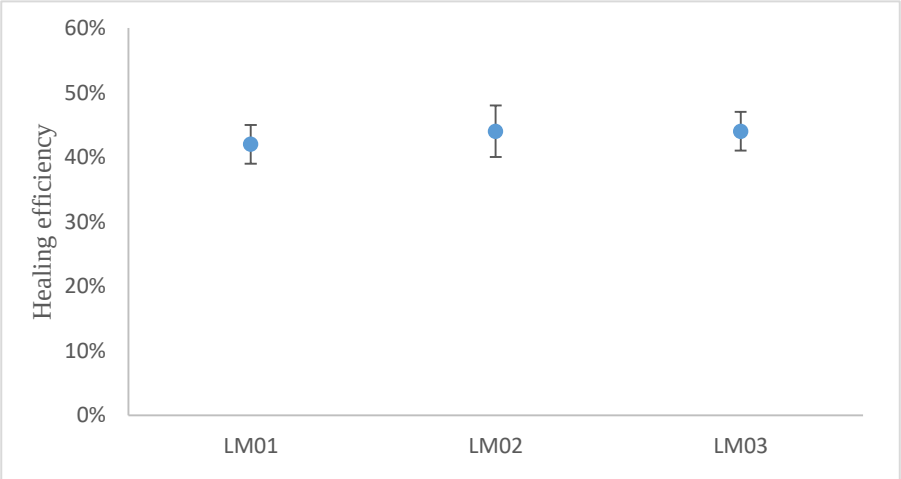

Figure 6.8: the healing efficiency of LM01-03 at 50 °C for 24 h

Specimen LM04 containing MA (solid healing agents, 10 wt. %) and St (micro-capsules, 10 wt. %) were investigated for their self-healing performance by fracture toughness recovery using the compact tension test.

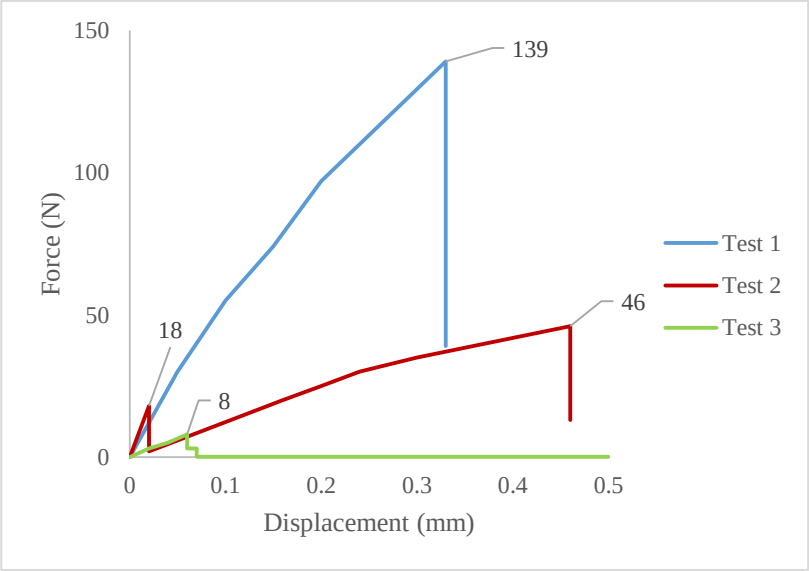

Figure 6.9: the force displacement curve of self-healing specimen LM04

The self-healing process was carried out at 50 °C for 7 days, but the compact tension test was at ambient temperature and the results were recorded by the force-displacement curve. The fracture force (P) is obtained from the force-displacement curve, figure 6.9. A value of the critical stress intensity factor, K_{IC}, is calculated for each fracture event and the results are shown in table 6.8.

Table 6.8: The fracture toughness of LM04

Test	Crack position	a (mm)	B (mm)	Force (N)	Y	K_{IC} (MPa·m$^{1/2}$)
1	1	13	5.06	139	5.54	0.680 (Original)
2	0-1	10	5.06	18	5.19	0.083 (Healed)
	2	33	5.06	46	17.58	0.715 (Original)
3	1-2	33	5.06	8	17.58	0.091 (Healed)
	Cracked	50	5.06	0	121.70	0

*The crack position is showed in figure 6.4.

The fracture toughness of original specimen is given by Test 1, Test 2 (when the crack propagating from position 2-3), and Test 3 (when the crack propagating from position 3 to the end of the specimen), which is found to be K_{IC} = 0.697 MPa·m$^{1/2}$. Therefore, the first and second healing process gave 12% and 13% healing efficiency, respectively.

Specimen LM05 containing MA (solid healing agents, 10 wt. %) and St (micro-capsules, 15 wt. %) were investigated for their performance by fracture toughness recovery using the compact tension test.

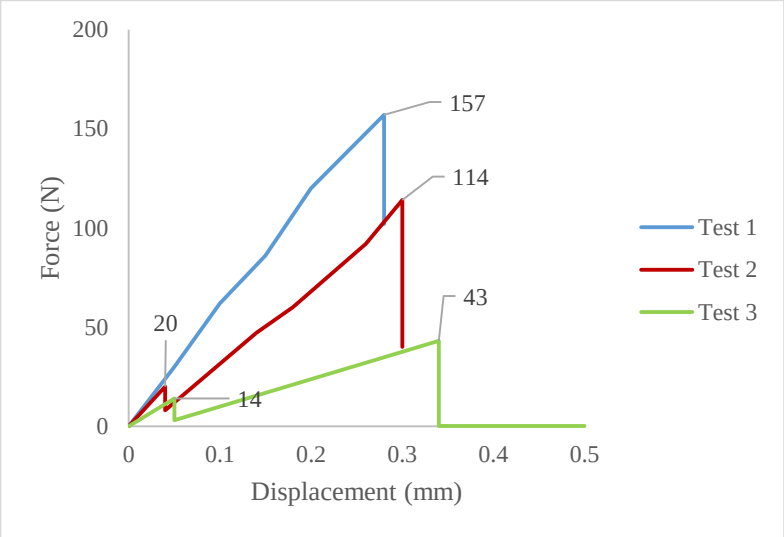

Figure 6.10: the force displacement curve of self-healing specimen LM05

The self-healing process was carried out at 50 °C for 7 days, but the compact tension test was at ambient temperature and the results were recorded by the force-displacement curve. The fracture force (P) is obtained in the force-displacement curve, figure 6.10. A value of the critical stress intensity factor, K_{IC}, is calculated for each fracture event and the results are shown in table 6.9. The fracture toughness of original specimen is given by Test 1, Test 2 (when the crack propagating from position 2-3), and Test 3 (when the crack propagating from position 3 to the end of the specimen), which is found to be K_{IC} = 0.727 MPa·$m^{1/2}$. Therefore, the first and second healing process gave both 12% healing efficiency.

Table 6.9: The fracture toughness of LM05

Test	Crack position	a (mm)	B (mm)	Force (N)	Y	K_{IC} (MPa·$m^{1/2}$)
1	1	12	5.14	157	5.344	0.730 (Original)
2	0-1	10	5.14	20	5.194	0.090 (Healed)
	2	20	5.14	114	7.324	0.726 (Original)
3	1-2	20	5.14	14	7.324	0.089 (Healed)
	3	34	5.14	43	19.365	0.725 (Original)

*The crack position is showed in figure 6.4.

Specimen LM06 containing MA (solid healing agents, 10 wt. %) and St (micro-capsules, 20 wt. %) were investigated the self-healing performance by fracture toughness recovery using the compact tension test.

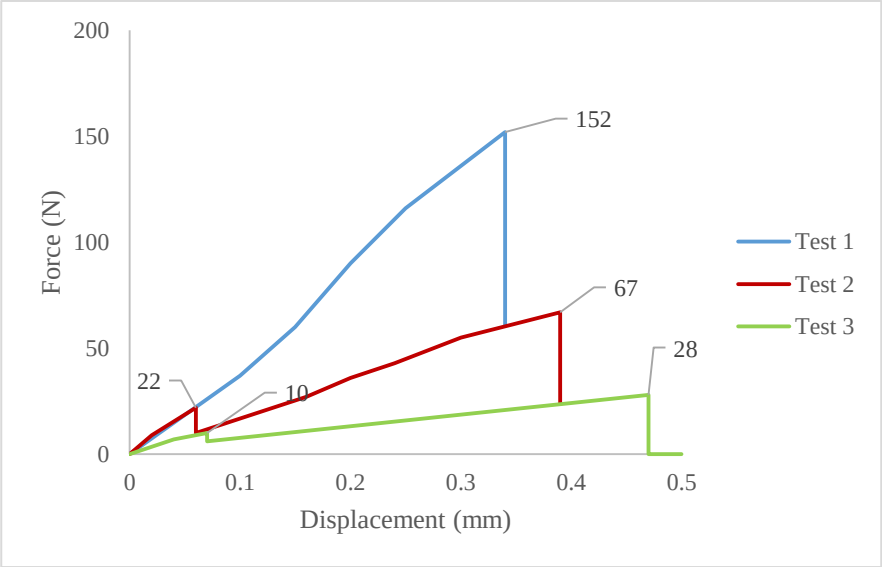

Figure 6.11: the force displacement curve of self-healing specimen LM06

The self-healing process was carried out at 50 °C for 7 days, but the compact tension test was at ambient temperature and the results were recorded by the force-displacement curve. The fracture force (P) is obtained from the force-displacement curve, figure 6.11. A value of the critical stress intensity factor, K_{IC}, is calculated for each fracture event and the results are shown in table 6.10. The fracture toughness of original specimen is given by Test 1, Test 2 (when the crack propagating from position 2-3), and Test 3 (when the crack propagating from position 3 to the end of the specimen), which is found to be K_{IC} = 0.708 MPa·$m^{1/2}$. Therefore, the first and second healing process gave 13% and 14% healing efficiency, respectively.

Table 6.10: The fracture toughness of LM06

Test	Crack position	a (mm)	B (mm)	Force (N)	Y	K_{IC} (MPa·$m^{1/2}$)
1	1	13	5.27	152	5.476	0.706 (Original)
2	0-1	10	5.27	22	5.194	0.097 (Healed)
	2	29	5.27	67	12.535	0.713 (Original)
3	1-2	29	5.27	10	12.535	0.106 (Healed)
	3	38	5.27	28	29.697	0.706 (Original)

*The crack position is showed in figure 6.4.

The healing efficiency of LM04-06 was compared in the figure 6.12. As the concentration of micro-capsules increased, the healing efficiency of the specimens increased slightly.

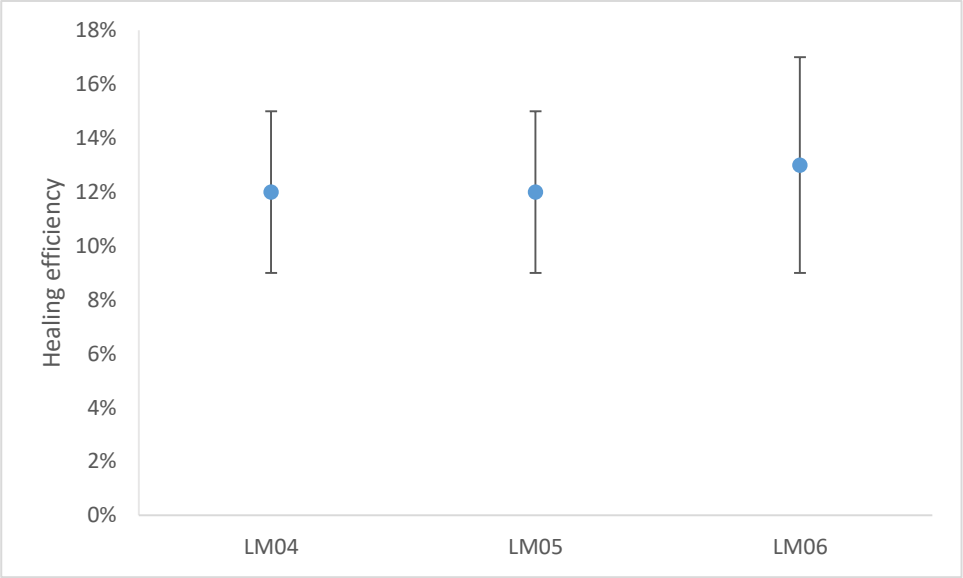

Figure 6.12: the healing efficiency of LM04-06 at 50 °C for 7 days

Specimen LM07 containing MeMal (solid healing agents, 10 wt. %) and 4MeOSt (micro-capsules, 10 wt. %) were investigated for the self-healing performance by fracture toughness recovery using the compact tension test. The self-healing process was carried out at 50 °C for 7 days. The compact tension test was at ambient temperature and the results were recorded by the force-displacement curve, figure 6.13.

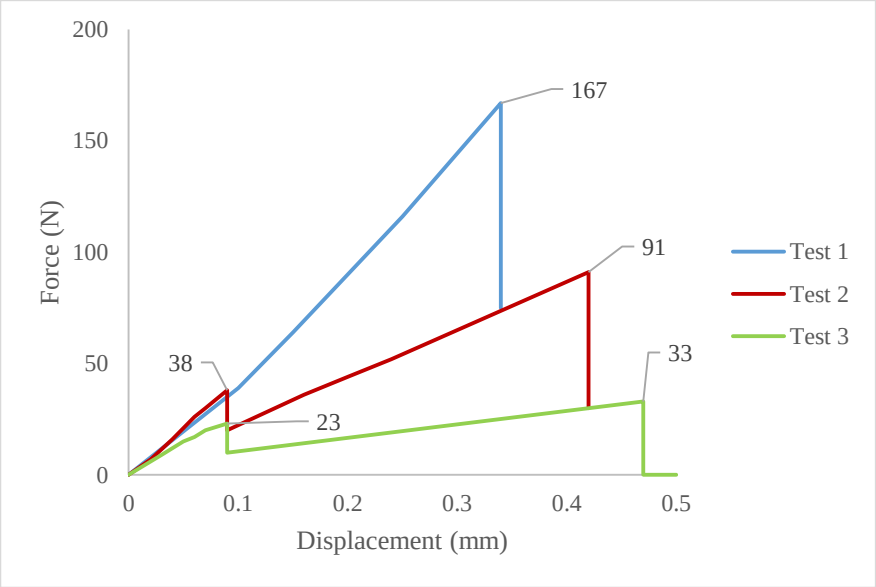

Figure 6.13: the force displacement curve of self-healing specimen LM07

The fracture force (P) is obtained from the force-displacement curve figure 6.13. A value of the critical stress intensity factor, K_{IC}, is calculated for each fracture event and the results are shown in table 6.11. The fracture toughness of original specimen is given by Test 1, Test 2 (when the crack propagating from position 2-3), and Test 3 (when the crack propagating from position 3 to the end of the specimen), which is found to be K_{IC} = 0.711 MPa·m$^{1/2}$. Therefore, the first and second healing process gave 22% and 25% healing efficiency, respectively.

Table 6.11: The fracture toughness of LM07

Test	Crack position	a (mm)	B (mm)	Force (N)	Y	K_{IC} (MPa·m$^{1/2}$)
1	1	12	5.54	167	5.344	0.720 (Original)
2	0-1	10	5.54	38	5.194	0.159 (Healed)
	2	25	5.54	91	9.603	0.705 (Original)
3	1-2	25	5.54	23	9.603	0.187 (Healed)
	3	37	5.54	33	26.549	0.707 (Original)

Specimen LM08 containing MeMal (solid healing agents, 10 wt. %) and 4MeOSt (micro-capsules, 15 wt. %) were investigated for the self-healing performance using the compact tension test. The self-healing process was carried out at 50 °C for 7 days. The compact tension test was at ambient temperature and the results were recorded by the force-displacement curve.

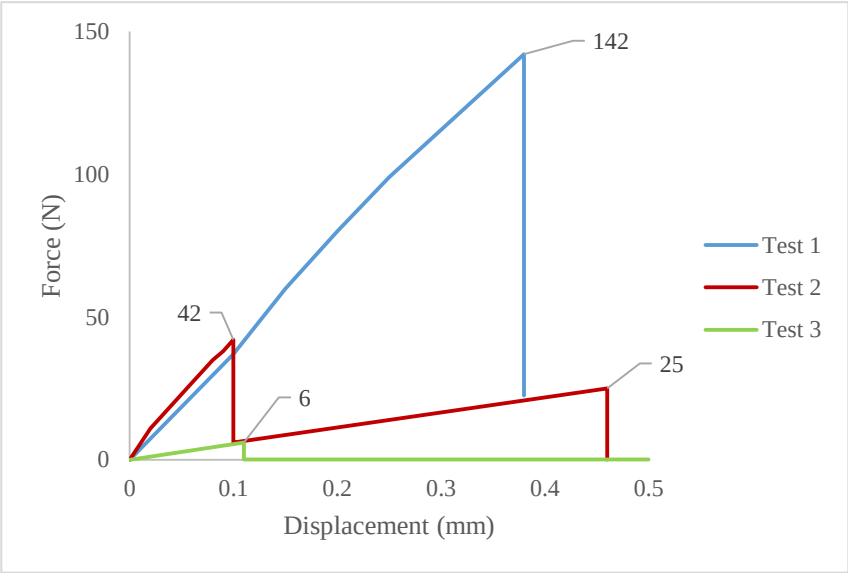

Figure 6.14: the force displacement curve of self-healing specimen LM08

The fracture force (P) is obtained from the force-displacement curve, figure 6.14. A value of the critical stress intensity factor, K_{IC}, is calculated for each fracture event and the results are shown in table 6.12. The fracture toughness of original specimen is given by Test 1, Test 2 (when the crack propagating from position 2-3), and Test 3 (when the crack propagating from position 3 to the end of the specimen), which is found to be K_{IC} = 0.724 MPa·$m^{1/2}$. Therefore, the first and second healing process gave 27% and 24% healing efficiency, respectively.

Table 6.12: The fracture toughness of LM08

Test	Crack position	a (mm)	B (mm)	Force (N)	Y	K_{IC} (MPa·$m^{1/2}$)
1	1	14	5.05	142	5.645	0.710 (Original)
2	0-1	10	5.05	42	5.194	0.193 (Healed)
	2	39	5.05	25	33.303	0.737 (Original)
3	1-2	39	5.05	6	33.303	0.177 (Healed)
	Cracked	50	5.05	0	121.700	0

*The crack position is showed in figure 6.4.

Specimen LM09 containing MeMal (solid healing agents, 10 wt. %) and 4MeOSt (micro-capsules, 20 wt. %) were investigated for the self-healing performance using the compact tension test. The self-healing process was carried out at 50 °C for 7 days. The compact tension test was at ambient temperature and the results were recorded by the force-displacement curve.

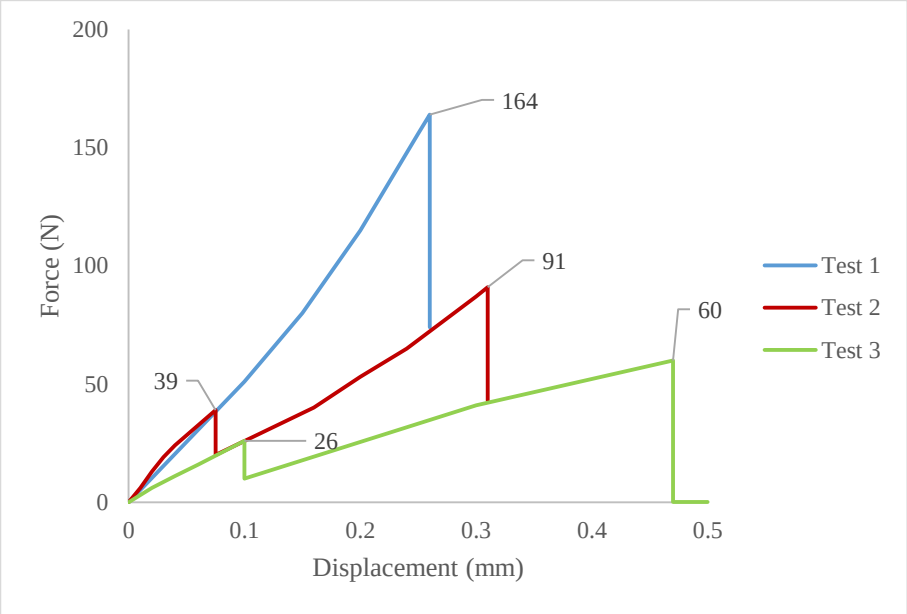

Figure 6.15: the force displacement curve of self-healing specimen LM09

The fracture force (P) is obtained in the force-displacement curve, figure 6.15. A value of the critical stress intensity factor, K_{IC}, is calculated for each fracture event and the results are shown in table 6.13. The fracture toughness of original specimen is given by Test 1, Test 2 (when the crack propagating from position 2-3), and Test 3 (when the crack propagating from position 3 to the end of the specimen), which is found to be K_{IC} = 0.706 MPa·$m^{1/2}$. Therefore, the first and second healing process gave 23% and 28% healing efficiency, respectively.

Table 6.13: The fracture toughness of LM09

Test	Crack position	a (mm)	B (mm)	Force (N)	Y	K_{IC} (MPa·$m^{1/2}$)
1	1	11	5.42	164	5.250	0.711 (Original)
2	0-1	10	5.42	39	5.194	0.167 (Healed)
	2	24	5.42	91	9.060	0.680 (Original)
3	1-2	24	5.42	26	9.060	0.194 (Healed)
	3	31	5.42	60	14.699	0.728 (Original)

The healing efficiency of LM07-09 is compared in the figure 6.16. As the concentration of micro-capsules (10-20%) increased, the healing efficiency of the specimens (LM07-09) increased slightly.

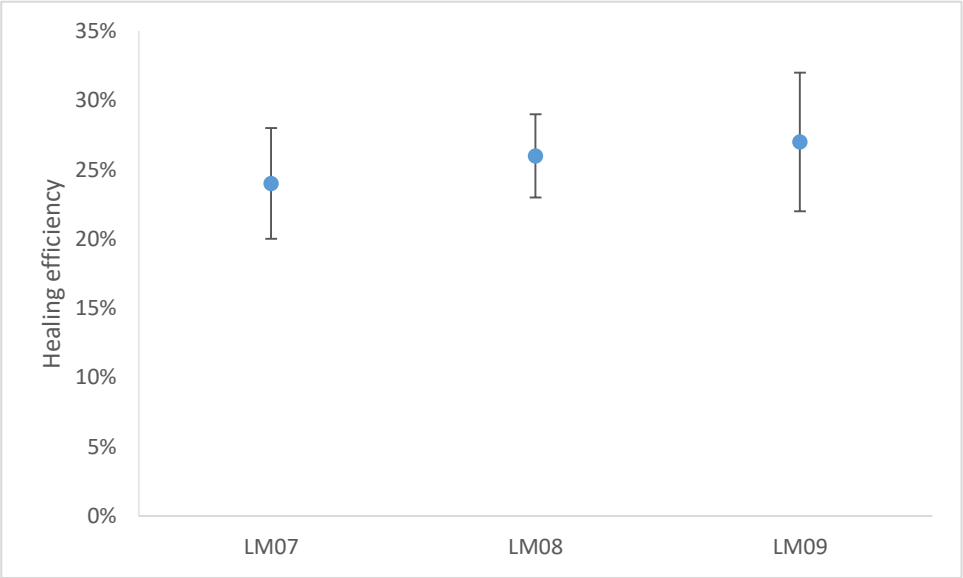

Figure 6.16: the healing efficiency of MeOSt-MeMal self-healing system at 50 °C for 24 h

Specimen LM10 containing EtOCN (solid healing agents, 10 wt. %) and 4MeOSt (micro-capsules, 10 wt. %) were investigated for the self-healing performance using the compact tension test. The self-healing process was carried out at 50 °C for 24 h. The compact tension test was at ambient temperature and the results were recorded by the force-displacement curve.

The fracture force (P) is obtained from the force-displacement curve, figure6.17. A value of the critical stress intensity factor, K_{IC}, is calculated for each fracture event and the results are shown in table 6.14. The fracture toughness of original specimen is given by Test 1, Test 2 (when the crack propagating from position 2-3), and Test 3 (when the crack propagating from position 3 to the end of the specimen), which is found to be K_{IC} = 0.792 MPa·$m^{1/2}$. Therefore, the first and second healing process gave 48% and 53% healing efficiency, respectively.

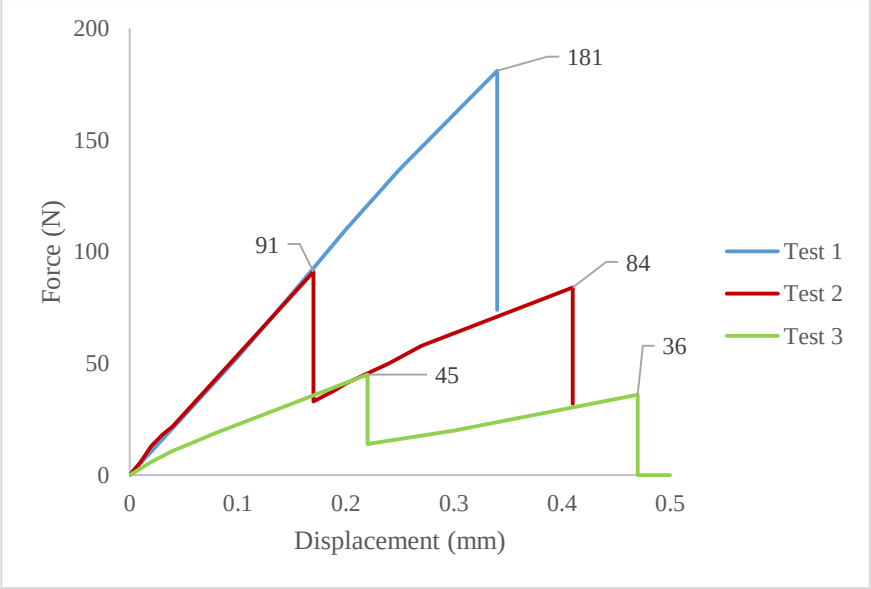

Figure 6.17: the force displacement curve of self-healing specimen LM10

Table 6.14: The fracture toughness of LM10

Test	Crack position	a (mm)	B (mm)	Force (N)	Y	K_{IC} (MPa·m$^{1/2}$)
1	1	12	5.46	181	5.344	0.792 (Original)
2	0-1	10	5.46	91	5.194	0.387 (Healed)
	2	28	5.46	84	11.658	0.802 (Original)
3	1-2	28	5.46	45	11.658	0.430 (Healed)
	3	37	5.46	36	26.549	0.783 (Original)

The healing efficiency of LM10-12 is showed in the figure 6.18. As the concentration of micro-capsules (10%-20%) increased, the healing efficiency of the specimens (LM10-12) increased slightly.

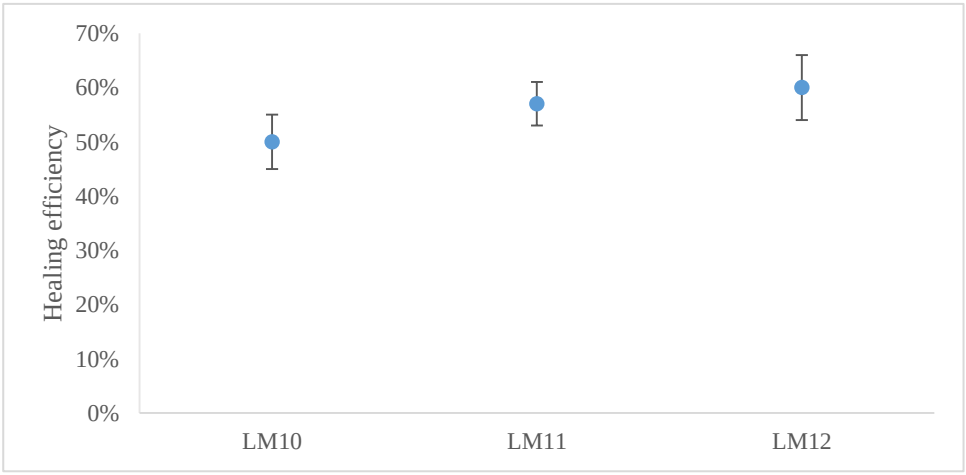

Figure 6.18: the healing efficiency of LM10-12 at 50 °C for 24 h

6.5.2 Self-healing performance for cross-linked polymer system

6.5.2.1 Via injection of liquid healing agents

The self-healing performance for cross-linked polymer system (XI01-05) via injection of liquid healing agents was investigated. XI01-03 is the specimen containing MA and injected DVB, the mixture of 4MeOSt and DVB (ratio of 4:1), and the mixture of St and DVB (ratio of 4:1) into the crack, respectively. XI04-05 is the specimen containing MeMal injected DVB and the mixture of 4MeOSt and DVB (ratio of 4:1) into the crack, respectively. The healing process was undertaken at 50 °C for 48 h. The fracture toughness tests were undertaken at ambient temperature. Figure 6.19 shows that XI01-05 exhibited 41%, 52%, 21%, 35%, and 37% healing efficiency.

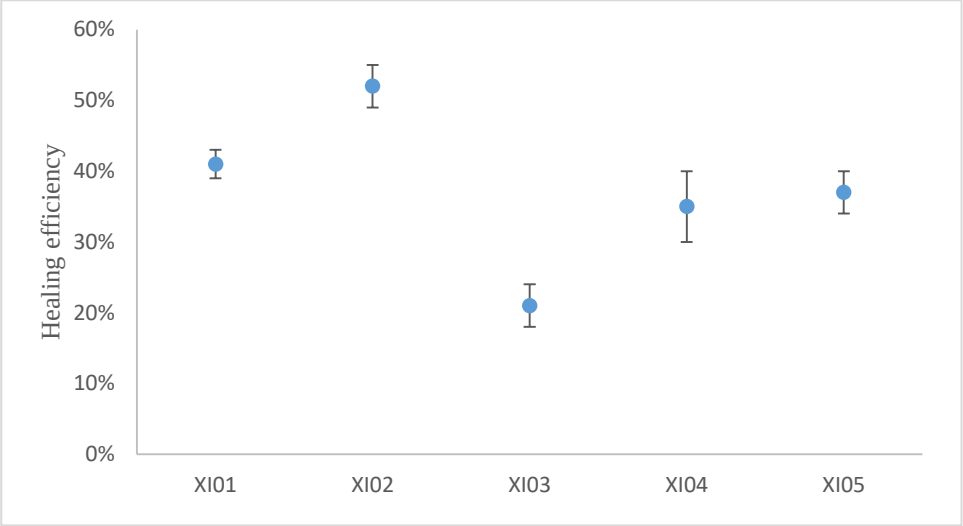

Figure 6.19: the healing efficiency of XI01-05 at 50 °C for 48 h

6.5.2.2 Via micro-encapsulation of liquid healing agents

The self-healing performance for cross-linked polymer system via micro-encapsulation of liquid healing agents (XM01-15) was investigated.

Specimen XM01 containing MA (solid healing agents, 10 wt. %) and DVB (micro-capsules, 10 wt. %) were investigated for the self-healing performance using the compact tension test. The self-healing process was carried out at 50 °C for 48 h. The compact tension test was at ambient temperature and the results were recorded by the force-displacement curve.

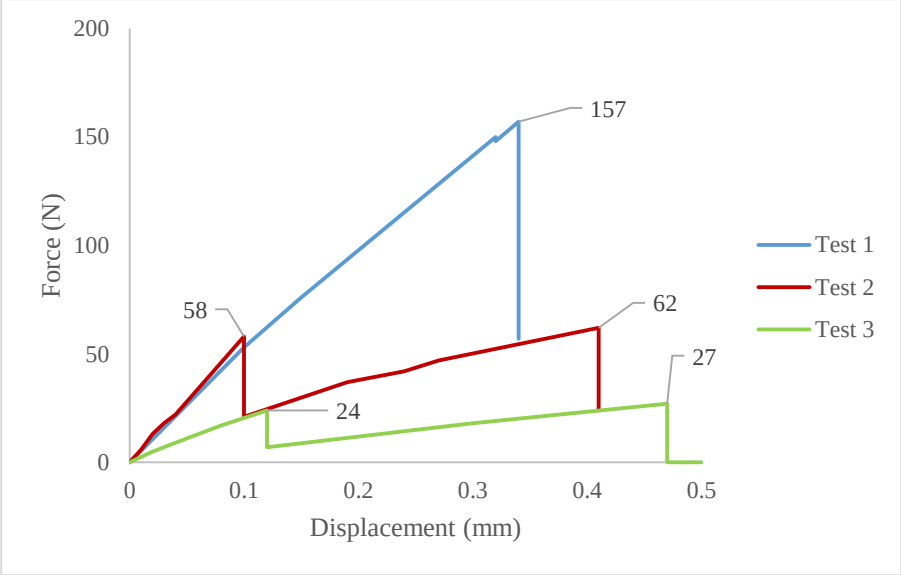

Figure 6.20: the force displacement curve of self-healing specimen XM01

The fracture force (P) is obtained from the force-displacement curve, Figure 6.20. A value of the critical stress intensity factor, K_{IC}, is calculated for each fracture event and the results are shown in table 6.15. The fracture toughness of original specimen is given by Test 1, Test 2 (when the crack propagating from position 2-3), and Test 3 (when the crack propagating from position 3 to the end of the specimen), which is found to be K_{IC} = 0.721 MPa·$m^{1/2}$. Therefore, the first and second healing process gave 35% and 38% healing efficiency, respectively.

Table 6.15: The fracture toughness of XM01

Test	Crack position	a (mm)	B (mm)	Force (N)	Y	K_{IC} (MPa·$m^{1/2}$)
1	1	13	5.37	157	5.476	0.716 (Original)
2	0-1	10	5.37	58	5.194	0.251 (Healed)
	2	30	5.37	62	13.541	0.699 (Original)
3	1-2	30	5.37	24	13.541	0.271 (Healed)
	3	39	5.37	27	33.303	0.749 (Original)

*The crack position is showed in figure 6.4.

The healing efficiency of XM01-03 is showed in the figure 6.21. As the concentration of micro-capsules (10%-20%) increased, the healing efficiency of the specimens (XM01-03) increased slightly.

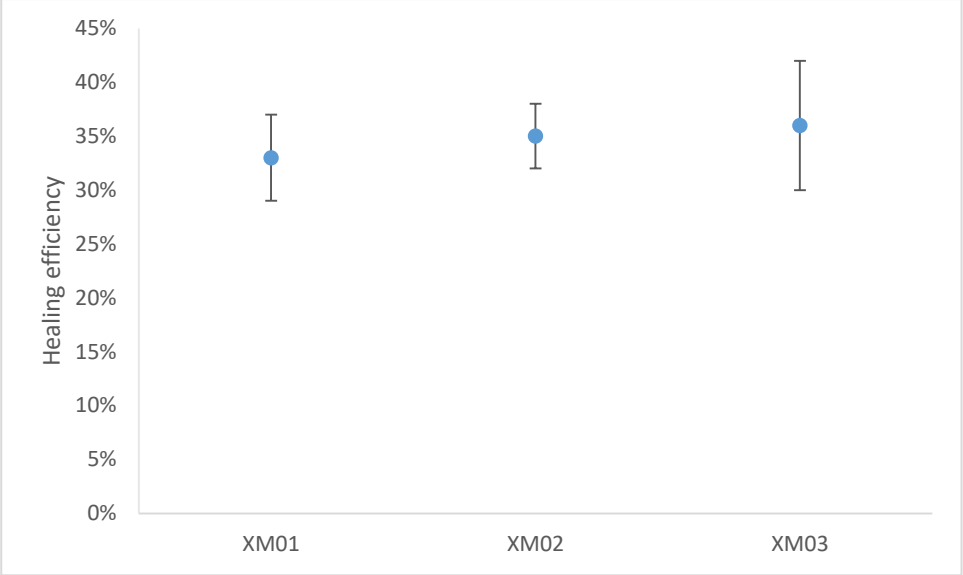

Figure 6.21: the healing efficiency of XM01-03 at 50 °C for 48 h

Specimen XM04 containing MA (solid healing agents, 10 wt. %) and DVB with 4MeOSt (micro-capsules, 10 wt. %) were investigated for the self-healing performance (fracture toughness recovery) using the compact tension test. The self-healing process was carried out at 50 °C for 48 h. The compact tension test was at ambient temperature and the results were recorded by the force-displacement curve.

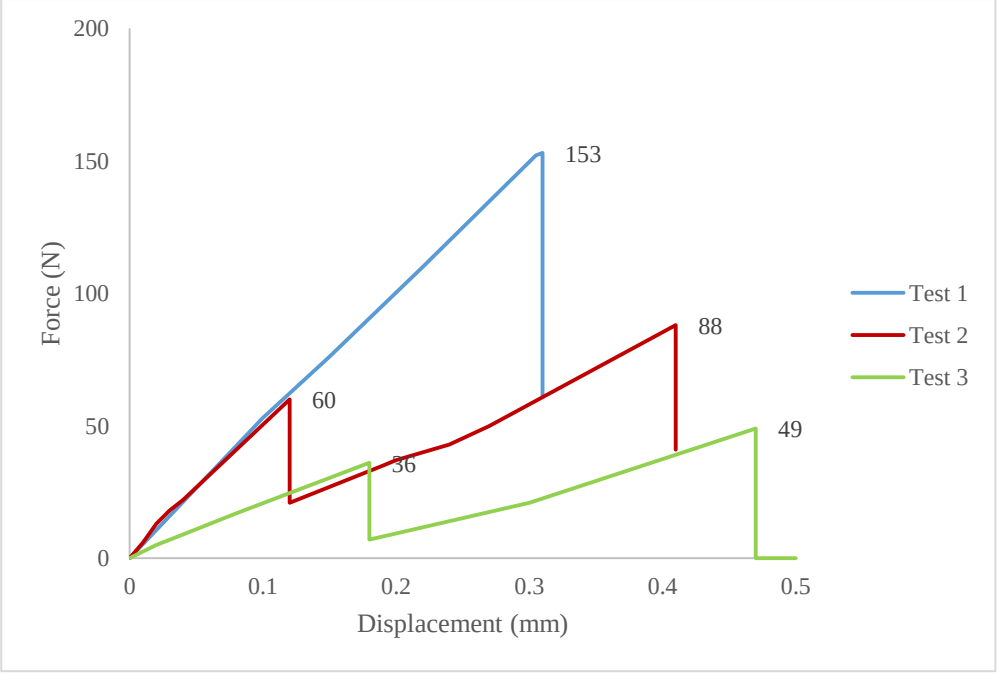

Figure 6.22: the force displacement curve of self-healing specimen XM04

The fracture force (P) is obtained in the force-displacement curve, figure 6.22. A value of the critical stress intensity factor, K_{IC}, is calculated for each fracture event and the results are shown in table 6.16. The fracture toughness of original specimen is given by Test 1, Test 2 (when the crack propagating from position 2-3), and Test 3 (when the crack propagating from position 3 to the end of the specimen), which is found to be K_{IC} = 0.709 MPa·m$^{1/2}$. Therefore, the first and second healing process gave 38% and 40% healing efficiency, respectively.

Table 6.16: The fracture toughness of XM04

Test	Crack position	A (mm)	B (mm)	Force (N)	Y	K_{IC} (MPa·m$^{1/2}$)
1	1	12	5.15	153	5.344	0.710 (Original)
2	0-1	10	5.15	60	5.194	0.271 (Healed)
	2	25	5.15	88	9.603	0.734 (Original)
3	1-2	25	5.15	36	9.603	0.300 (Healed)
	3	32	5.15	49	16.035	0.682 (Original)

*The crack position is showed in figure 6.4.

The healing efficiency of XM04-06 is showed in the figure 6.23. As the concentration of micro-capsules (10%-20%) increased, the healing efficiency of the specimens (XM04-06) increased slightly.

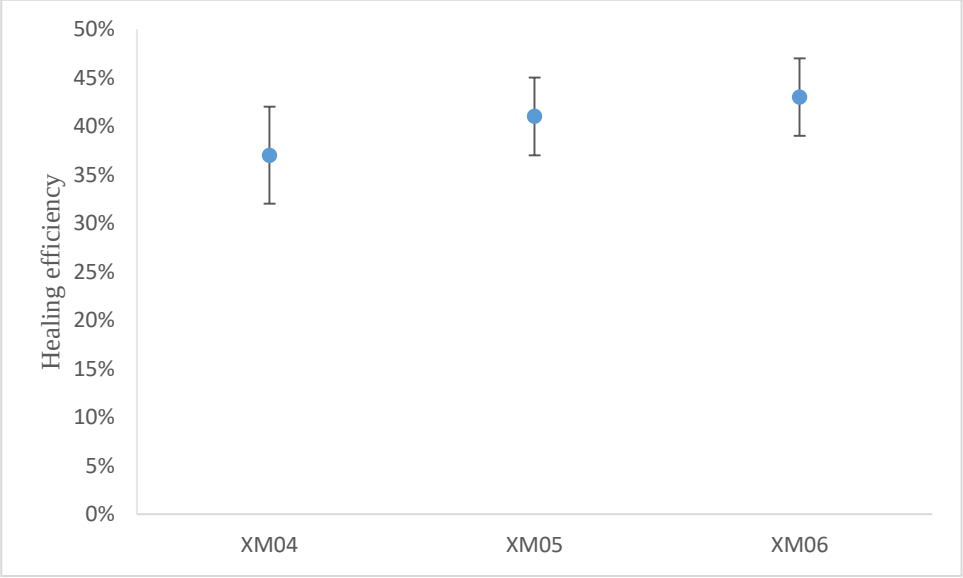

Figure 6.23: the healing efficiency of XM04-06 at 50 °C for 48 h

Specimen XM07 containing MA (solid healing agents, 10 wt. %) and DVB-St (micro-capsules, 10 wt. %) were investigated the self-healing performance using the compact tension test. The self-healing process was carried out at 50 °C for 48 h. The compact tension test was at ambient temperature and the results were recorded by the force-displacement curve.

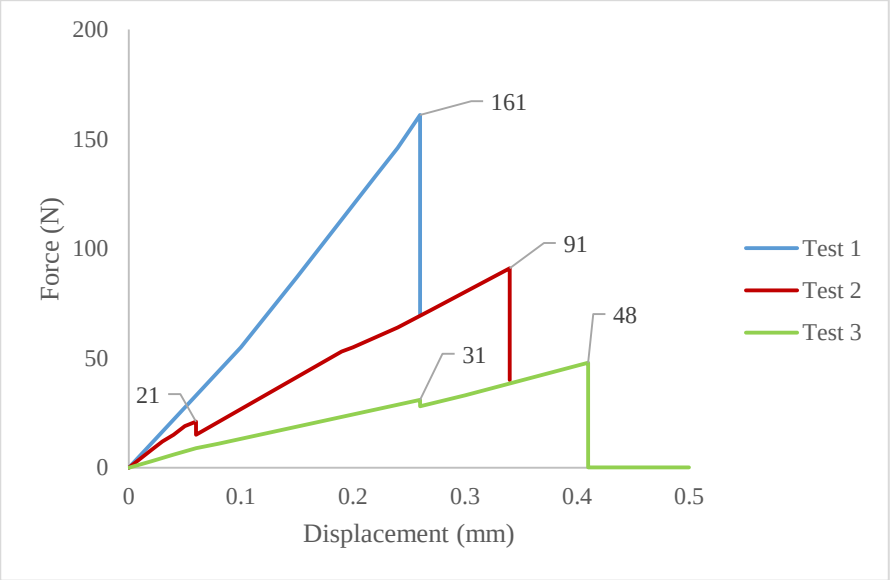

Figure 6.24: the force displacement curve of self-healing specimen XM07

The fracture force (P) is obtained from the force-displacement curve, figure 6.24. A value of the critical stress intensity factor, K_{IC}, is calculated for each fracture event and the results are shown in table 6.17.

Table 6.17: The fracture toughness of XM07

Test	Crack position	A (mm)	B (mm)	Force (N)	Y	K_{IC} (MPa·m$^{1/2}$)
1	1	11	5.23	161	5.250	0.723 (Original)
2	0-1	10	5.23	21	5.194	0.093 (Healed)
	2	24	5.23	91	9.060	0.705 (Original)
3	1-2	N/A	5.23	N/A	N/A	No healing
	3	33	5.23	48	17.580	0.722 (Original)

*The crack position is showed in figure 6.4.

The fracture toughness of original specimen is given by Test 1, Test 2 (when the crack propagating from position 2-3), and Test 3 (when the crack propagating from position 3 to the end of the specimen), which is found to be K_{IC} = 0.716 MPa·m$^{1/2}$. For the first part (from

0 to 51) of curve of test 2, the slop is low than the curve of test 1, indicating the crack was healed back to somewhere between position 1 and 2. Therefore, the crack length is unknown. If the healed position is at position 1, the first healing process gave 13% healing efficiency. The second healing process did not work due the test 3 shows the force displacement curve with unified slope.

The healing efficiency of XM07-09 is showed in the figure 6.25. As the concentration of micro-capsules (10%-20%) increased, the healing efficiency of the specimens (XM07-09) increased slightly.

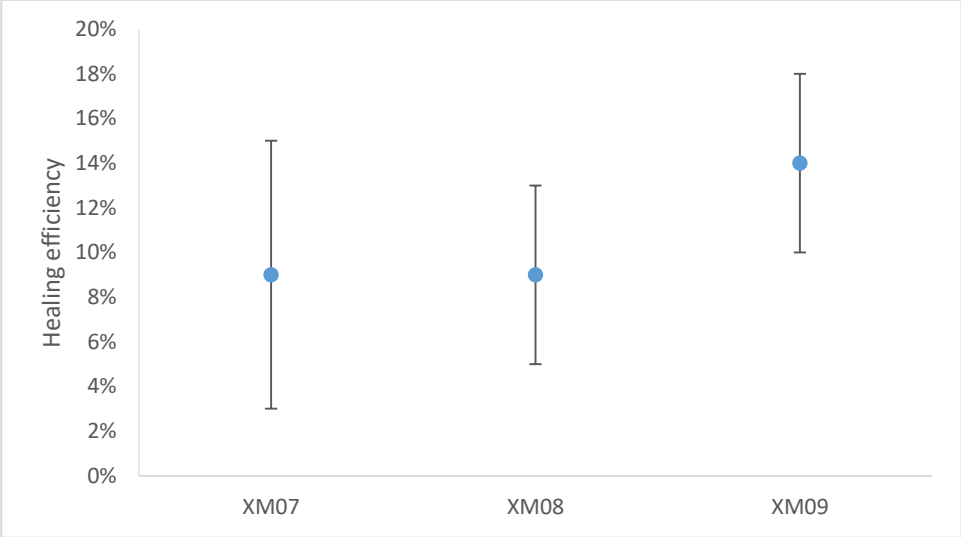

Figure 6.25: the healing efficiency of XM07-09 at 50 °C for 48 h

Specimen XM10 containing MeMal (solid healing agents, 10 wt. %) and DVB (micro-capsules, 10 wt. %) were investigated for the self-healing performance (fracture toughness recovery) using the compact tension test. The self-healing process was carried out at 50 °C for 48 h. The compact tension test was at ambient temperature and the results were recorded by the force-displacement curve.

The fracture force (P) is obtained from the force-displacement curve, figure 6.26. A value of the critical stress intensity factor, K_{IC}, is calculated for each fracture event and the results are shown in table 6.18. The fracture toughness of original specimen is given by Test 1, Test 2 (when the crack propagating from position 2-3), and Test 3 (when the crack propagating from position 3 to the end of the specimen), which is found to be K_{IC} = 0.723 MPa·$m^{1/2}$. Therefore, the first and second healing process gave 25% and 29% healing efficiency, respectively.

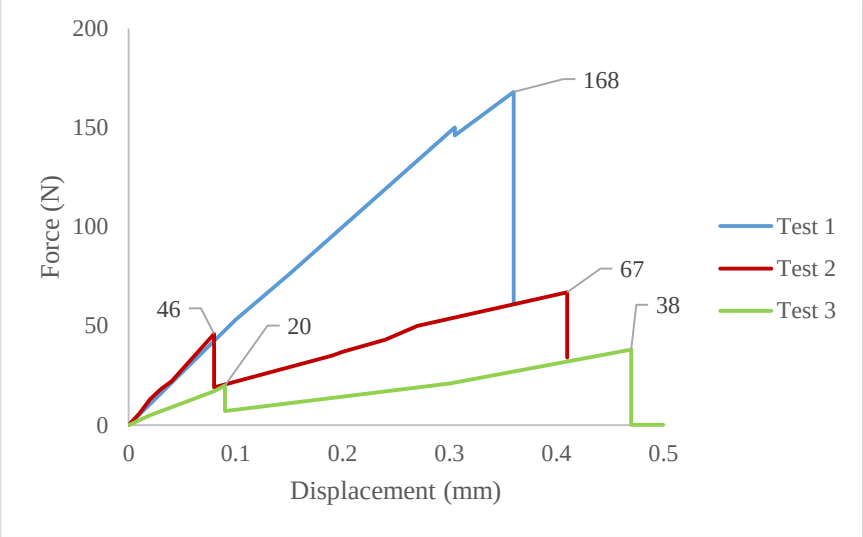

Figure 6.26: the force displacement curve of self-healing specimen XM10

Table 6.18: The fracture toughness of XM10

Test	Crack position	A (mm)	B (mm)	Force (N)	Y	K_{IC} (MPa·m$^{1/2}$)
1	1	13	5.31	168	5.476	0.775 (Original)
2	0-1	10	5.31	46	5.194	0.201 (Healed)
	2	29	5.31	67	12.535	0.707 (Original)
3	1-2	29	5.31	20	12.535	0.211 (Healed)
	3	35	5.31	38	21.428	0.686 (Original)

*The crack position is showed in figure 6.4.

The healing efficiency of XM10-12 is showed in the figure 6.27. As the concentration of micro-capsules (10%-20%) increased, the healing efficiency of the specimens (XM10-12) increased slightly.

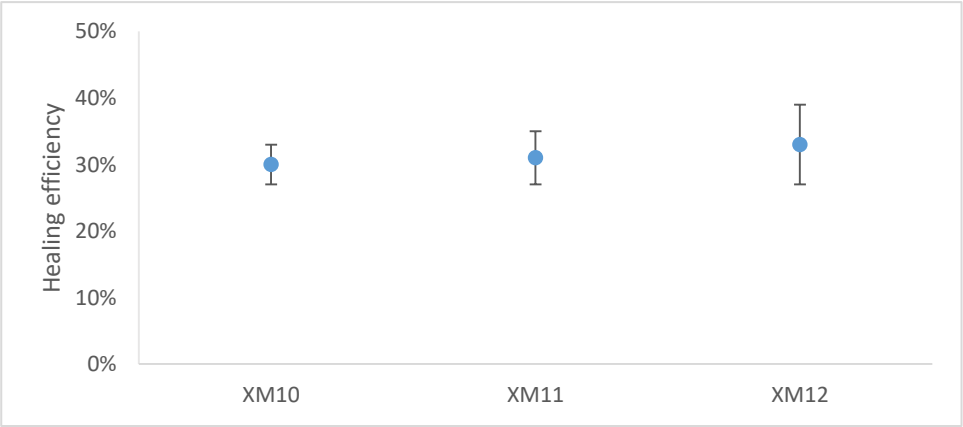

Figure 6.27: the healing efficiency of XM10-12 at 50 °C for 48 h

Specimen XM13 containing MeMal (solid healing agents, 10 wt. %) and 4MeOSt-DVB (micro-capsules, 10 wt. %) self-healing system was investigated the self-healing performance using the compact tension test. The self-healing process was carried out at 50 °C for 48 h. The compact tension test was at ambient temperature and the results were recorded by the force-displacement curve.

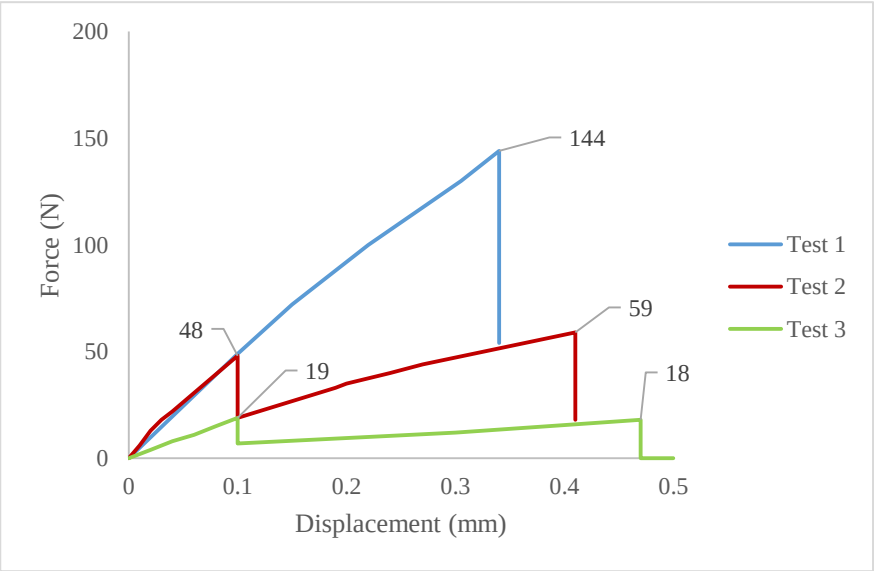

Figure 6.28: the force displacement curve of self-healing specimen XM13

The fracture force (P) is obtained in the force-displacement curve, figure 6.28. A value of the critical stress intensity factor, K_{IC}, is calculated for each fracture event and the results are shown in table 6.19. The fracture toughness of original specimen is given by Test 1, Test 2 (when the crack propagating from position 2-3), and Test 3 (when the crack propagating from position 3 to the end of the specimen), which is found to be K_{IC} = 0.728 MPa·$m^{1/2}$. Therefore, the first and second healing process gave 30% and 32% healing efficiency, respectively.

Table 6.19: The fracture toughness of XM13

Test	Crack position	A (mm)	B (mm)	Force (N)	Y	K_{IC} (MPa·$m^{1/2}$)
1	1	14	5.19	144	5.645	0.700 (Original)
2	0-1	10	5.19	48	5.194	0.215 (Healed)
	2	31	5.19	59	14.699	0.747 (Original)
3	1-2	31	5.19	19	14.699	0.241 (Healed)
	3	42	5.19	18	47.431	0.736 (Original)

The healing efficiency of XM13-15 is showed in the figure 6.29. As the concentration of

micro-capsules (10%-20%) increased, the healing efficiency of the specimens (XM13-15) increased slightly.

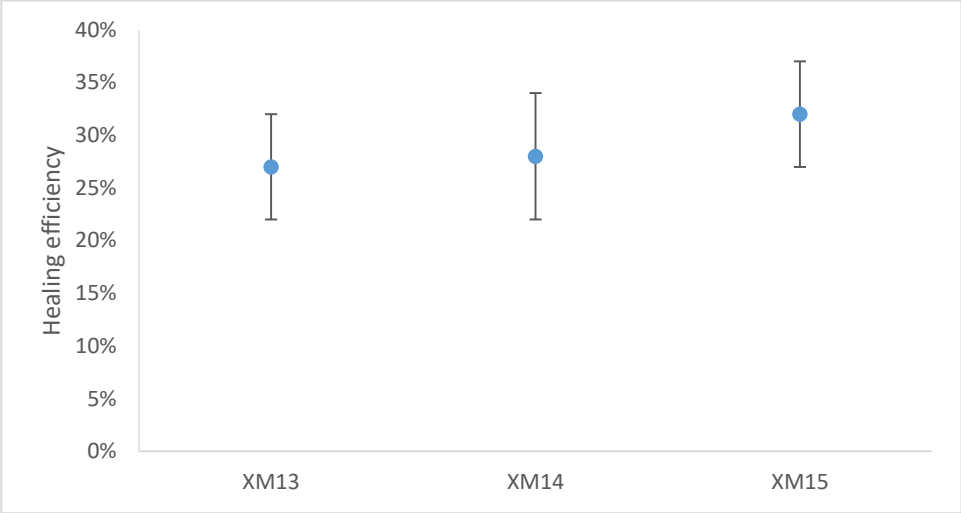

Figure 6.29: the healing efficiency of XM13-15 at 50 °C for 48 h

6.5.3 The influence of temperature on the self-healing performance

The study in Chapter 2 and 3 shows that the spontaneous (co-)polymerisation of electron-donor (4MeOSt and St) and electron-accepter (MA and MeMal) carried out at ambient temperature produced linear polymers with 20-30% yield. Furthermore when DVB is added to 4MeOSt and St, cross-linked polymer upon the reaction with MA and MeMal was formed with 20-30% gel content. The self-healing performance of the specimens containing solid healing agents (MA, MeMal, or EtOCN) was investigated at ambient temperature via injection of liquid healing agent (4MeOSt, St, or DVB).

The self-healing efficiency of linear polymer system (LI01-04) and cross-linked polymer system (XI01-05) via injection was compared at ambient temperature and at 50 °C. The fracture toughness tests were undertaken at ambient temperature and the healing efficiency is shown in figure 6.30.

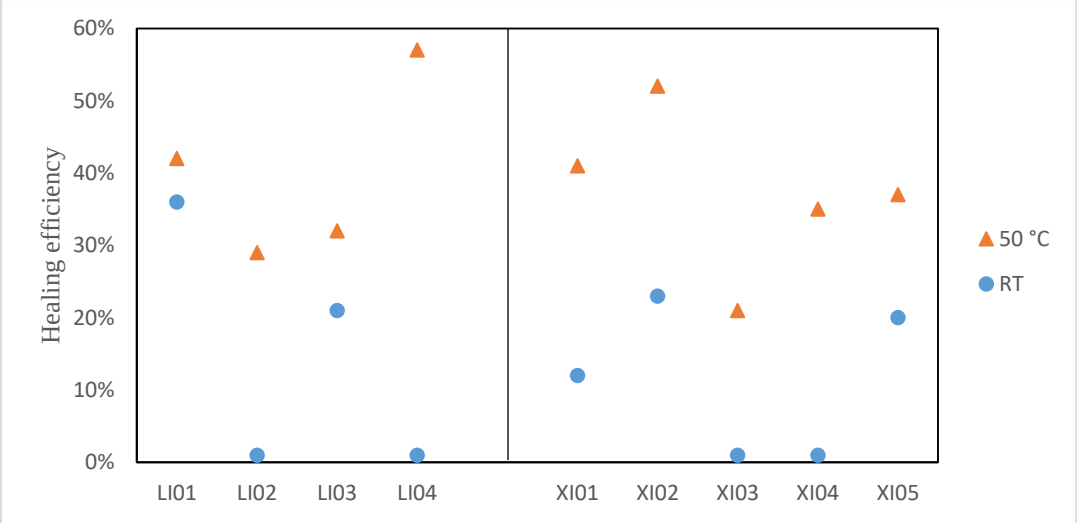

Figure 6.30: the healing efficiency of LI01-04 and XI01-05 via injection at ambient temperature and at 50 °C

The healing process was undertaken at ambient temperature for 7 days due to slow spontaneous copolymerisation reaction, however, it was undertaken at 50 °C for 48 h. The healing efficiency is obtained with greater at 50 °C.

In the case of linear polymer formation, LI01 (4MeOSt and MA) and LI03 (4MeOSt and MeMal) show a healing efficiency increasing from 36% and 21% at ambient temperature up to 42% and 32% at 50 °C, respectively. However, LI02 (St and MA) and LI04 (4MeOSt and EtOCN) did not show any healing performance at ambient temperature believed to be due to the lack of reactions between liquid and solid healing agents. This lack of reaction was also observed between St with MA and 4MeOSt with EtOCN at ambient temperature in Chapter 2. In contrast to the room temperature, LI02 and LI04 showed self-healing efficiency of 29% and 57%, respectively, at 50 °C. This is due to the temperature improved the reaction rate of St with MA and 4MEOSt with EtOCN, which is also observed in Chapter 2.

For the formation of cross-linked polymer system, XI01 (DVB and MA), XI02 (4MeOSt, DVB, and MA), and XI05 (4MeOSt, DVB, and MeMal) show healing efficiency at ambient temperature of 12%, 23%, and 20%, respectively. In contrast, XI03 (St, DVB, and MA) and XI04 (DVB and MeMal) show no healing efficiency at ambient temperature, due to the lack of reactions. The same observation was made during the cross-linking reaction for mixture of St, DVB with MA and DVB with MeMal in Chapter 3. Moreover, self-healing efficiency of 21% and 35% was obtained for XI03 and XI04, respectively, at 50 °C. This is consistent with

observations made for the cross-linking reactions at 50 °C for the system involved XI03 and XI04 in Chapter 3.

The self-healing performance for linear polymer system via micro-encapsulation of liquid healing agents (LM01-03) (4MeOst and MA) was investigated at ambient temperature and compared with those at 50 °C, figure 6.31.

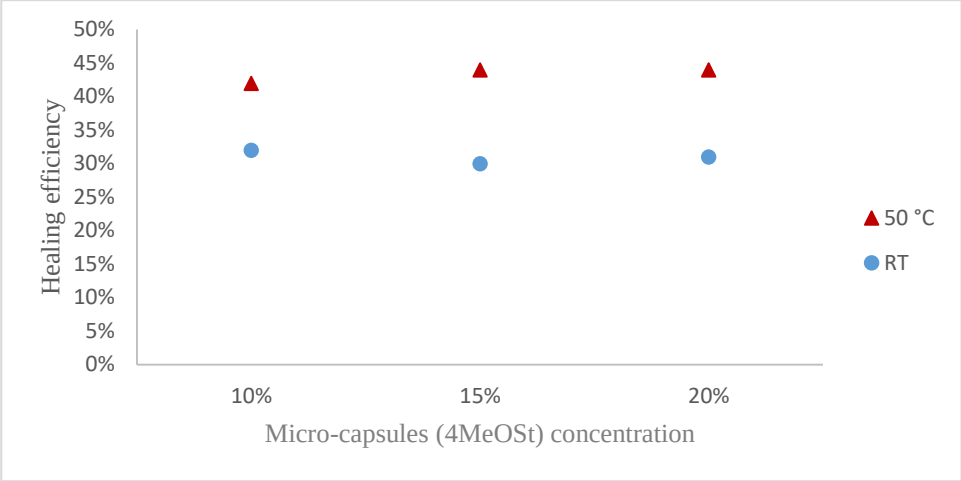

Figure 6.31: the healing efficiency of LM01-03 via micro-capsules at 50 ℃ and ambient temperature

The self-healing system LM01-03 showed higher healing efficiency at 50 ℃ due to faster reaction rate and higher yield. The heating may also improve the molecular diffusion indicating more Van der Waals forces between the resulting polymer and the crack. This would result in a better adhesion of the resulting polymer in the crack to the epoxy matrix.

The self-healing performance of LI01 was investigated at 60-80 °C for 24 h via injection of liquid healing agent. The results are compared with the tests at ambient temperature and at 50 °C, figure 6.32. The healing efficiency increased upon temperature increasing, indicating the importance of temperature in increasing the reaction rate and adhesion to the epoxy matrix and hence higher self-healing efficiency.

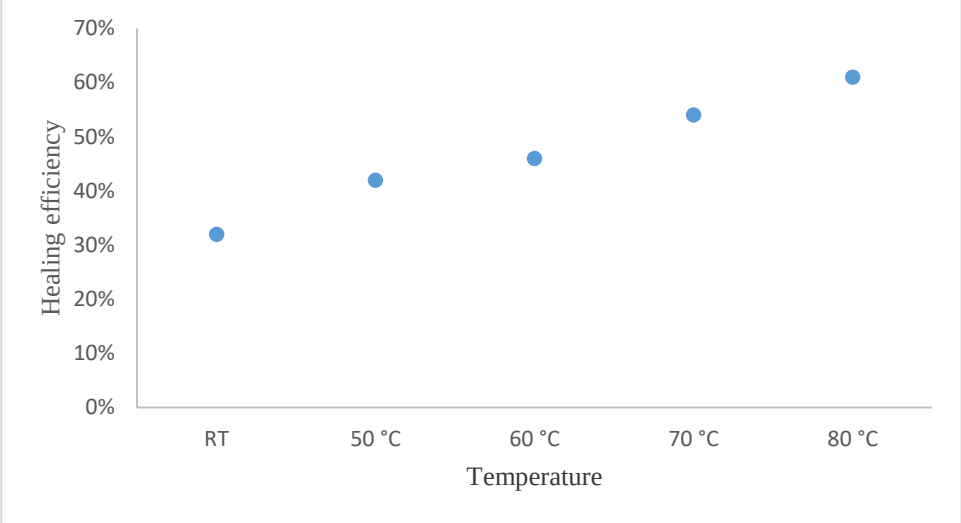

Figure 6.32: the healing efficiency of LI01 at ambient temperature and 50-80 °C

6.5.4 The comparison of self-healing performance of linear and cross-linked polymer systems

DVB as a difunctional monomer was selected to produce cross-linked to achieve higher healing performance. The self-healing efficiencies of LM01-03 (4MeOSt and MA) and XM01-03 (4MeOSt, DVB, and MA) via micro-capsules at 50 ℃ are compared in figure 6.33. This figure shows that a self-healing efficiency of about 40% is obtained in the case of linear and cross-linked polymer system regarding of the concentration of micro-capsules.

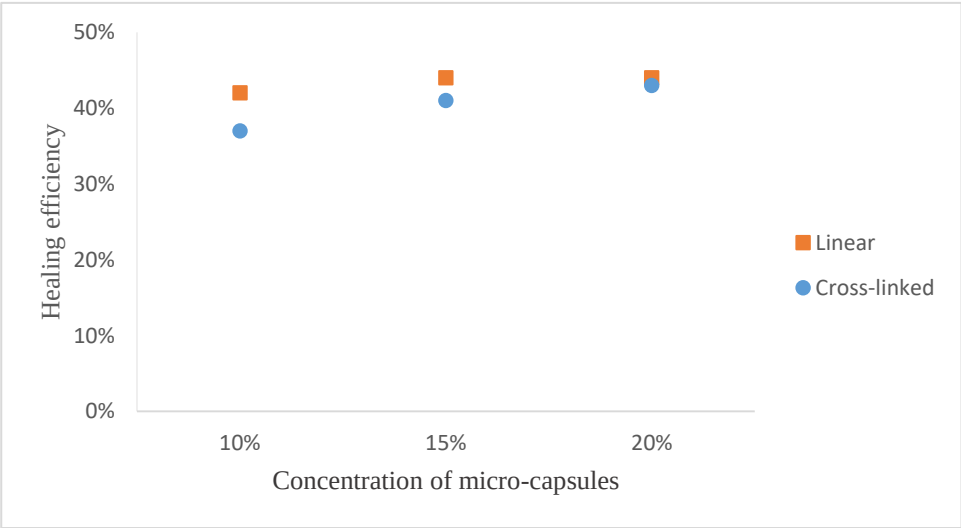

Figure 6.33: the healing efficiency of LM01-03 (Linear) and XM01-03 (Cross-linked)

The specimen containing DVB healing agent did not give higher healing performance. The

specimen after healed has two weaknesses points 1 and 2, figure 6.34. Point 1 is the polymer formed by the reaction of solid and liquid healing agents. Point 2 is the contact surface of the epoxy matrix material and resulting polymer (linear or cross-linked). When the loading force open the healed crack, the new crack is likely to propagate through the contact surface at point 2. The evidence could be found by the investigating the fracture toughness of the polymer materials formed by the healing agents.

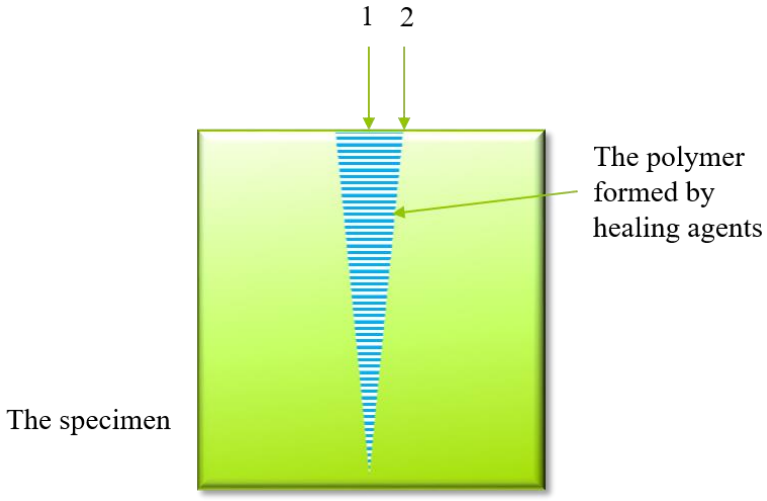

Figure 6.34: The weakness points in the healed specimen

The fracture toughness test of resulting polymers obtained by reaction of solid and liquid healing agents was carried out at ambient temperature using the compact tension geometry (60 mm × 50 mm × 5 mm), table 6.20. The fracture toughness of resulting polymers is found to be much higher than that of the epoxy matrix.

Table 6.20: The fracture toughness of healing agent polymer

Test	a (mm)	B (mm)	Force (N)	Y	K_{IC} (MPa·m$^{1/2}$)
Poly(MA+MeOSt)	12	3.12	121	5.357	0.925
Poly(MA+MeOSt+DVB)	13	3.48	171	5.543	1.218
Poly(DVB)	11	3.62	201	5.274	1.306

The healing efficiency of the system studied here are lower than expected probably due to a poor adhesion of the resulting polymer (linear or cross-linked) to the epoxy resin matrix at point 2.

6.6 Conclusion

Self-healing performance for linear and cross-linked polymer system in epoxy resin specimen was investigated both via injection and micro-encapsulation of liquid healing agents.

In order to evaluate the healing efficiency of the self-healing system, the liquid healing agents were injected into the crack of the specimen containing solid healing agents. The healing efficiency at 50 ℃ for linear polymer system was found to be 56% for MA-4MeOSt; 49% for MA-St; 32% for MeMal-4MeOSt; and 57% for EtOCN-4MeOSt. The healing efficiency for cross-linked polymer system at 50 ℃ was found to be 41% for MA-DVB; 52% for MA-DVB-4MeOSt; 21% for MA-DVB-St; 35% for MeMal-DVB; and 37% for MeMal-DVB-4MeOSt.

The autonomous self-healing process was investigated by adding micro-capsules containing liquid healing agents. Specimen containing solid healing agents (MA, MeMal, and EtOCN) and micro-capsules (containing 4MeOSt, St, DVB, and their mixture) were prepared. The healing efficiency at 50 ℃ for linear polymer system was found to be 40%-53% for MA-4MeOSt; 32%-35% for MA-St; 24%-25% for MeMal-4MeOSt; and 40%-57% for EtOCN-4MeOSt. The healing efficiency for cross-linked polymer system at 50 ℃ was found to be 33%-35% for MA-DVB; 37%-40% for MA-DVB-4MeOSt; 9%-15% for MA-DVB-St; 30%-32% for MeMal-DVB; and 27%-30% for MeMal-DVB-4MeOSt.

The self-healing efficiency at ambient temperature of the specimen was investigated by injection of liquid healing agents into the crack of specimen containing solid healing agents. The healing efficiency for linear polymer system was found to be 36% for MA-4MeOSt and 21% for MeMal-4MeOSt. The healing efficiency for cross-linked polymer system was found to be 12% for MA-DVB; 23% for MA-DVB-4MeOSt; and 20% for MeMal-DVB.

The low healing efficiency of the system studied in the project are probably due to a poor adhesion of the resulting polymer (linear or cross-linked) to the epoxy resin matrix.

Reference

1. Ghosh, S. (2009) 'Self-healing Materials: Fundamentals, Design Strategies, and Applications' in Ghosh, S. (ed.) *Self-healing Materials*, Weinheim: Wiley-VCH, pp. 1-28.
2. Degarmo, E. Paul; Black, J T.; Kohser, Ronald A. (2003), Materials and Processes in Manufacturing (9th ed.), Wiley, p. 32, ISBN 0-471-65653-4.
3. Hertzberg, Richard W. (1995). Deformation and Fracture Mechanics of Engineering Materials (4 ed.). Wiley. ISBN 0-471-01214-9.
4. Kinloch AJ, Young RJ. Fracture behaviour of polymers. London: Elsevier; 1983. Applied Science
5. Brown WF, Srawley JE. Plane strain crack toughness testing of high strength metallic materials. ASTM STP 1966;410.

Chapter 7

Conclusions and Future Work

7.1 Conclusions

The spontaneous copolymerisations of electron-rich monomers (4MeOSt and St) with electron-poor monomers (MA, MeMal, and EtOCN) were investigated and the resulting linear polymer products were fully characterised. The spontaneous copolymerisation of 4MeOSt with MA and 4MeOSt with MeMal were carried out at 50 °C and at ambient temperature and yellow solid was produced, which was found to be soluble in acetone and THF. The results confirmed that the polymer products are alternating copolymers. The test followed by different reaction times showed that the copolymerisations in bulk reached a plateau at about 50% yield. The reactions were undertaken in bulk giving solid product which is believed to be responsible for stopping the progress of the reaction and hence reaching a plateau. The spontaneous copolymerisation of 4MeOSt with EtOCN was also carried out at 50 °C and a red-brown solid was produced, which was found to be soluble in acetone and THF. It is concluded that the poly(4MeOSt) is formed in the presence of EtOCN via cationic polymerisation. However, the reaction of 4MeOSt with EtOCN did not produce any solid at ambient temperature. The spontaneous copolymerisation of St with MA was also carried out at 50 °C and a yellow solid was produced, which was found to be soluble in acetone and THF. The results confirmed that the polymer product of St with MA is an alternating co-polymer. The tests followed by different reaction times shows that the copolymerisation of St with MA reached a plateau at 30% yield. The formation of solid product is believed to be responsible for stopping the progress of the reaction and hence reaching a plateau. However, the reaction of St with MA did not produce any solid at ambient temperature.

The spontaneous copolymerisation of electron-rich monomers (4MeOSt, St, and DVB) with electron-poor monomers (MA and MeMal) was investigated at ambient temperature and at 50°C. The resulting insoluble cross-linked polymer products were characterised by FTIR, and confirmed the presence of repeating units due to MA and MeMal monomers. The reactions were followed by gel content determination over a period of 7 days. Initially, the gel content increased for a few days, after which it reached a plateau around 23%-41% at ambient temperature and 33%-57% at 50 °C based on the monomers used. The plateau is believed to be due to the formation of cross-linked material eventually stopping the progress of the reaction.

The micro-encapsulation of liquid healing agents (4MeOSt, DVB, St, and their mixtures) by

in-situ polymerisation of urea-formaldehyde in an oil-water emulsion was successfully carried out. The micro-capsules of high quality surface and good size distribution were produced and analysed by SEM. Micro-capsules with average diameter of 100-250 μm were selected to use. The deposition of UF nanoparticles was prevented by carrying out the reaction under constant pH (3.5) conditions and washing with DCM and deionised water. The fill content was measured by comparing the weight of filled micro-capsules with that of the dried broken shells and was found to be 70-80 wt. %.

The blank epoxy resin specimens were prepared using Bisphenol-A based epoxide and diethylenetriamine (DETA) (10 wt. %) as the curing agent and the fracture toughness was measured to be $K_{IC} = 0.801 \pm 0.019$ MPa·m$^{1/2}$. The inclusion of micro-capsules (5-20 wt. %) did not change the fracture toughness of matrix. Specimens were prepared with 10 wt. % added solid healing agents (MA and MeMal) as this amount gave minimum reduction of fracture toughness. There is a possibility of side reaction between MA (or MeMal) and amine group of DETA curing agent which is likely to reduce the cross-link density and hence the fracture toughness. The process of preparation of specimen containing MA (or MeMal) was modified involving mixing bisphenol-A based epoxide with DETA and leaving it at ambient temperature for 4 h before the addition of solid healing agents (MA and MeMal). This ensured close to full consumption of primary amine and hence minimising or preventing side reactions. However, the fracture toughness of the specimen did not change by adding EtOCN solid healing agent into the epoxy resin matrix due to the lack of any side reaction between EtOCN and DETA.

Self-healing performance for linear and cross-linked polymer system in epoxy resin specimen was investigated both via injection and micro-encapsulation of liquid healing agents. In order to evaluate the healing efficiency of the self-healing system, the liquid healing agents were injected into the crack of the specimen containing solid healing agents. The best healing efficiency at 50 ℃ for linear polymer system was found to be about 57% for MA-4MeOSt and EtOCN-4MeOSt. The best healing efficiency for cross-linked polymer system at 50 ℃ was found to be about 52% for MA-DVB-4MeOSt. The autonomous self-healing process was investigated by adding micro-capsules containing liquid healing agents. Specimen containing solid healing agents (MA, MeMal, and EtOCN) and micro-capsules (containing 4MeOSt, St, DVB, and their mixture) were prepared. The best healing efficiency at 50 ℃ for linear polymer system was found to be about 50% for MA-4MeOSt and EtOCN-

4MeOSt. The best healing efficiency for cross-linked polymer system at 50 ℃ was found to be about 40% for MA-DVB-4MeOSt. The self-healing efficiency at ambient temperature of the specimen was investigated by injection of liquid healing agents into the crack of specimen containing solid healing agents. The best healing efficiency for linear polymer system was found to be about 36% for MA-4MeOSt. The best healing efficiency for cross-linked polymer system was found to be about 23% for MA-DVB-4MeOSt. The low healing efficiency of the system studied in the project are probably due to a poor adhesion of the resulting polymer (linear or cross-linked) to the epoxy resin matrix.

7.2 Future work

The investigation of spontaneous (co-)polymerisation of electron donor and acceptor monomers in bulk showed that the electron acceptor monomers (solid) exhibit poor solubility in electron donor monomers. Therefore, it will be interesting to investigate spontaneous (co-)polymerisation in a solvent. However, high concentration of electron donor and acceptor monomers will be necessary.[1]

To apply the use of solvent in the self-healing system, a multiple-capsule self-healing system must be designed. The electron acceptor monomer should be dissolved in a solvent followed by encapsulation in UF micro-capsules. The electron donor (liquid monomer) should also be encapsulated in UF micro-capsules. The two types of micro-capsules will then need to be embedded in the matrix material.

MA and MeMal used as electron acceptor in this project are not suitable for the multiple-capsule design due to instability of MA and MeMal in water used in the process of micro-encapsulation. Therefore, the alternative electrophilic olefins need to be identified and used. Some potential examples (a) and (b) are shown in figure 7.1

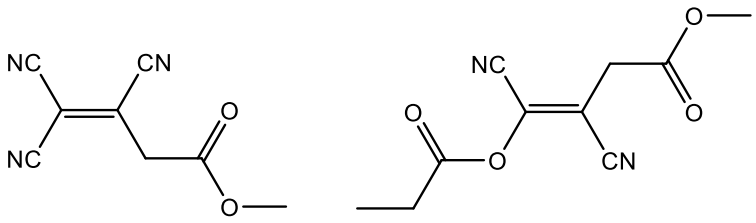

Figure 7.1: Alternative electrophilic olefins: methyl tricyanoethylenecarboxylat (a) and dimethyl dicyanofumarate (b)

These suggest electrophilic olefins (a) and (b) are not commercially available but their syntheses have been reported.[2] Moreover, these electrophilic olefins have also been reported to exhibit spontaneous polymerisation with electron donor monomers, 4MeOSt.[2]

Referenece

1. Padias, A. B. and Hall, H. K. (1987) 'Influence of the Solvent on the Nature of a Diradical Tetramethylene Intermediate', *J. Org. Chem.*, 52:4536-39
2. Gotoh, T., Padias, A. B., and Hall, H. K. Jr., (1986) 'Zwitterionic Tetramethylenes as the Common Intermediates in the Cycloaddition and Polymerisation Reactions of N-Vinylcarbazole with Electrophilic Tetrasubstituted Ethylenes: A New Explanation for Charge-Transfer Initiation', *J. Am. Chem. Soc.*, 108:4920-31.

Appendix

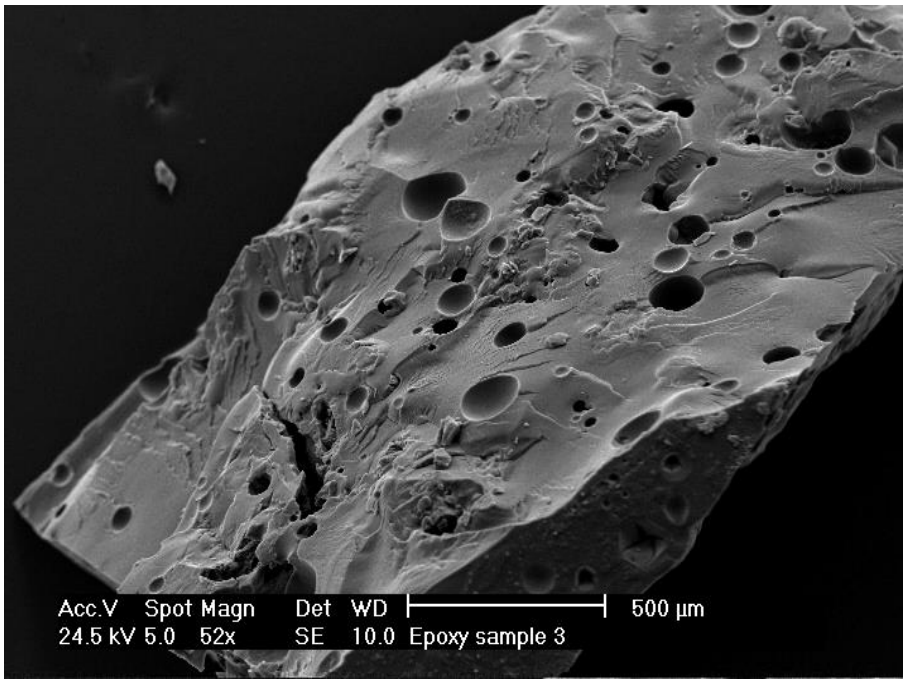

Figure 1: The crack surface of a self-healing specimen using MA-4MeOSt healing agents after the micro-capsules broken and released the healing agents

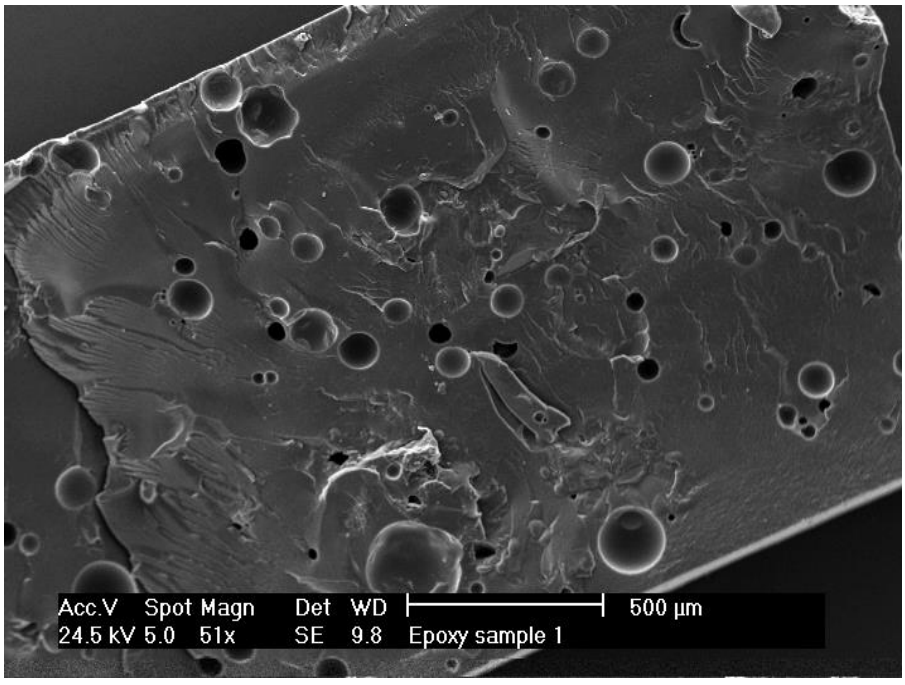

Figure 2: The crack surface of a self-healing specimen using EtOCN-4MeOSt healing agents after the micro-capsules broken and released the healing agents

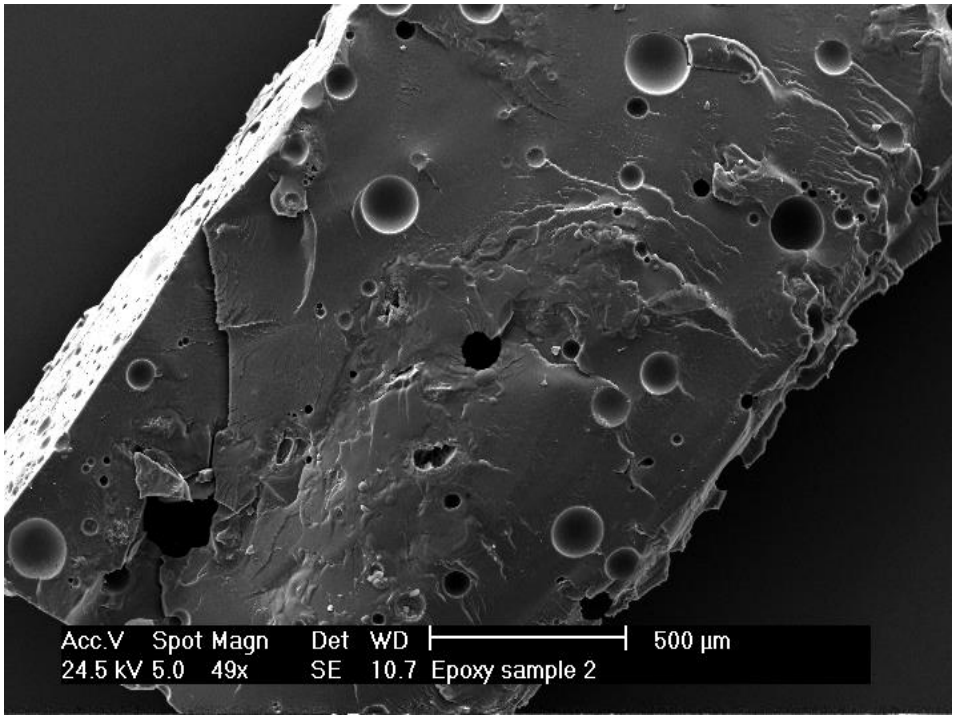

Figure 3: The crack surface of a self-healing specimen using MA-4MeOSt-DVB healing agents after the micro-capsules broken and released the healing agents

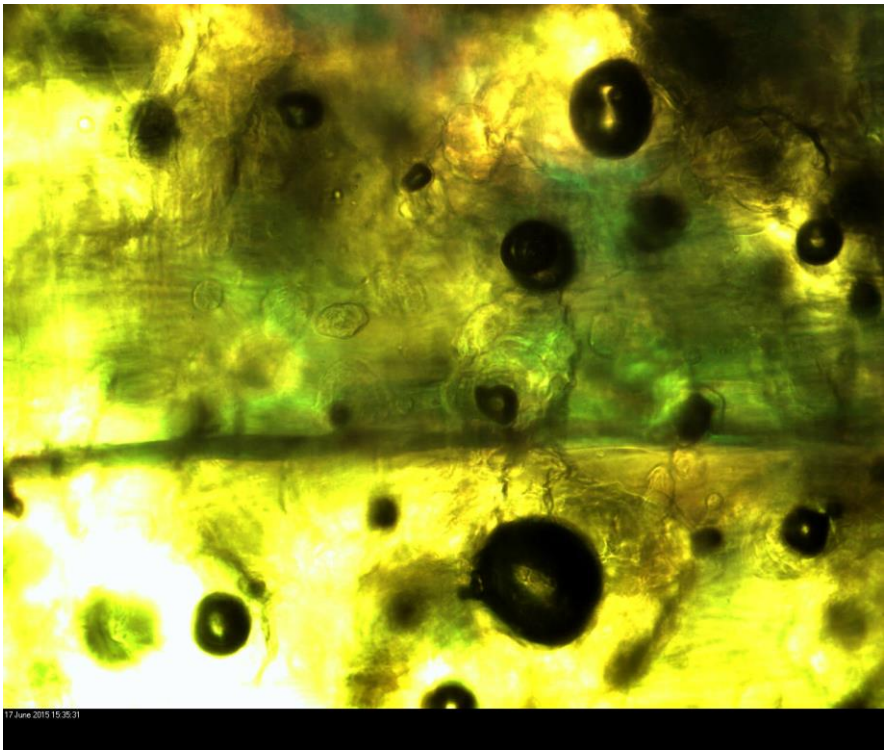

Figure 4: The crack healed under optical microscopy (magnification of 20×) for a self-healing specimen using MA-4MeOSt healing agents

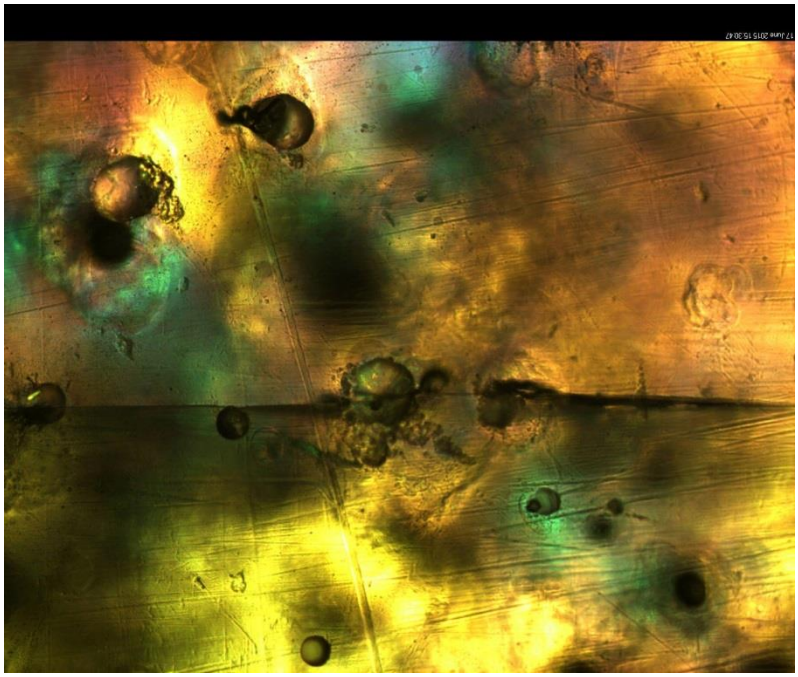

Figure 5: The crack healed under optical microscopy (magnification of 20×) for a self-healing specimen using EtOCN-4MeOSt healing agents

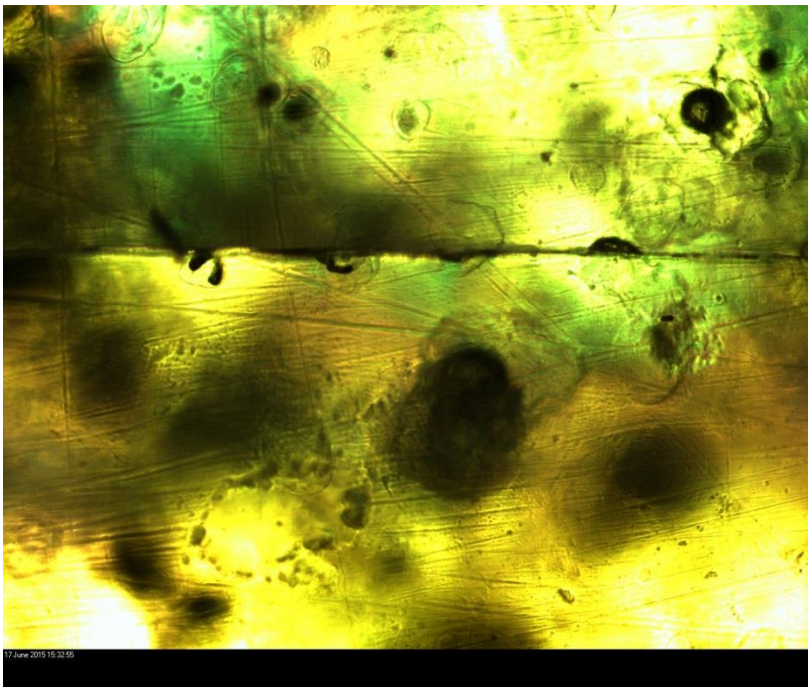

Figure 6: The crack healed under optical microscopy (magnification of 20×) for a self-healing specimen using MA-4MeOSt-DVB healing agents

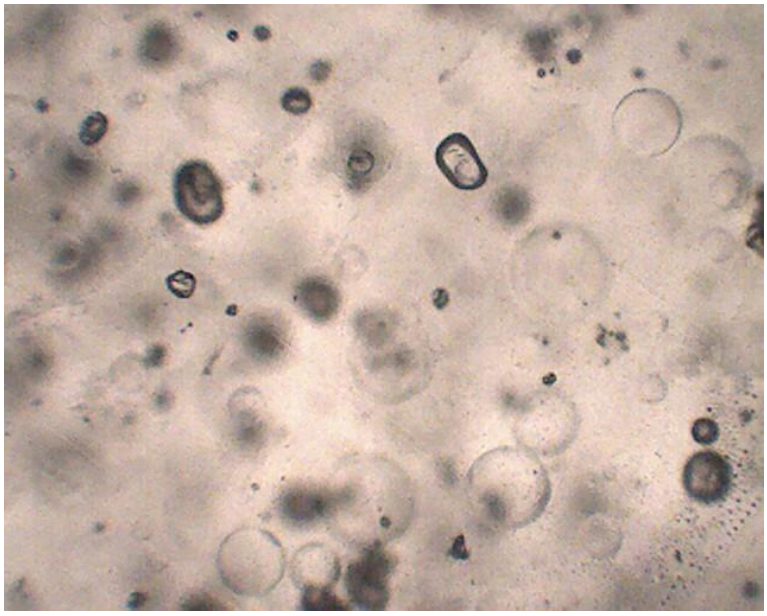

Figure 7: The distribution of micro-capsules in a self-healing specimen using MA-4MeOSt healing agents viewed by optical microscopy (magnification of 20×)

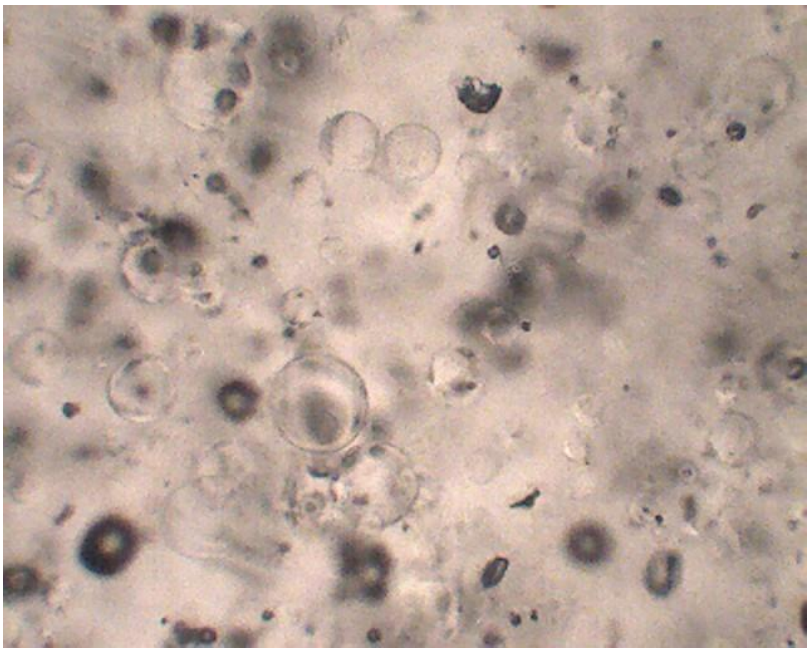

Figure 8: The distribution of micro-capsules in a self-healing specimen using EtOCN-4MeOSt healing agents viewed by optical microscopy (magnification of 20×)

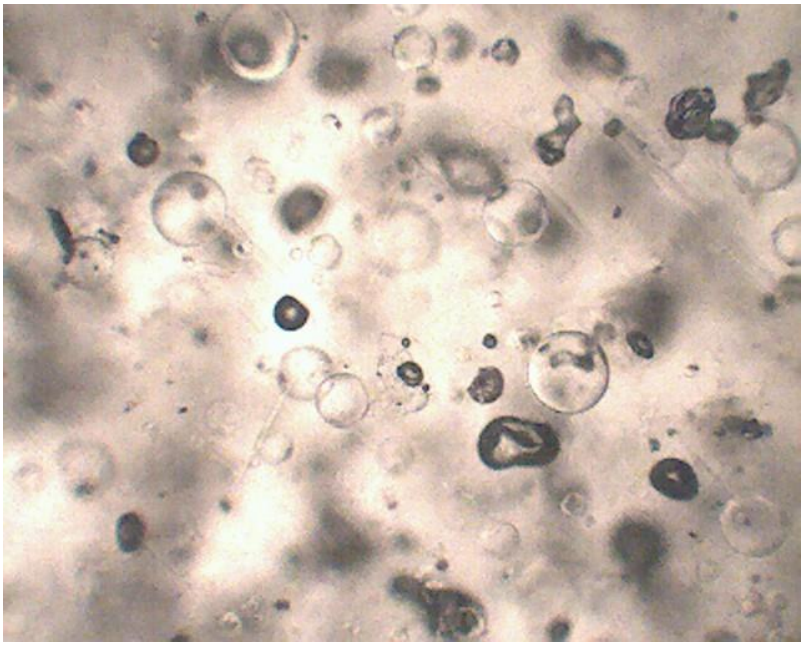

Figure 7: The distribution of micro-capsules in a self-healing specimen using MA-4MeOSt-DVB healing agents viewed by optical microscopy (magnification of 20×)

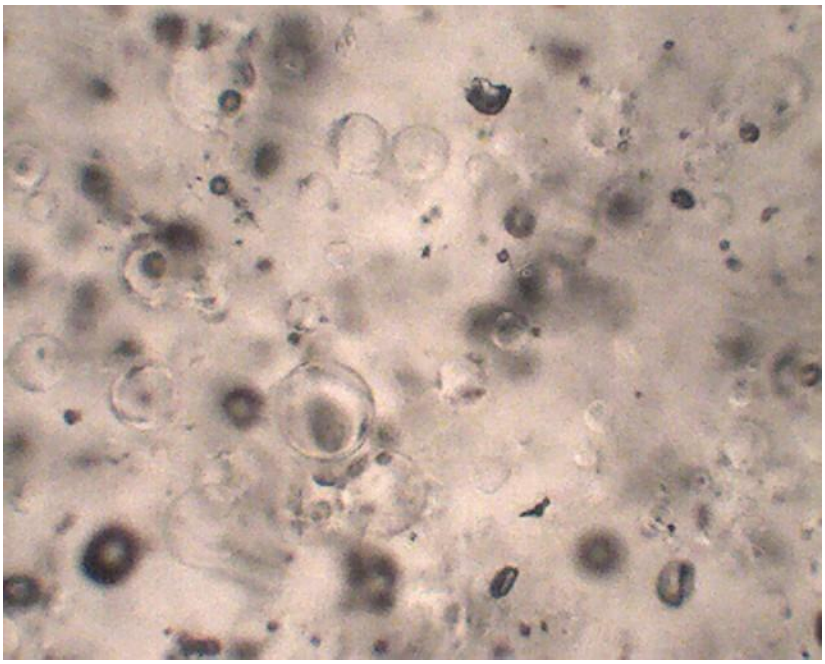

Figure 7: The distribution of micro-capsules in a self-healing specimen using MeMal-4MeOSt healing agents viewed by optical microscopy (magnification of 20×)

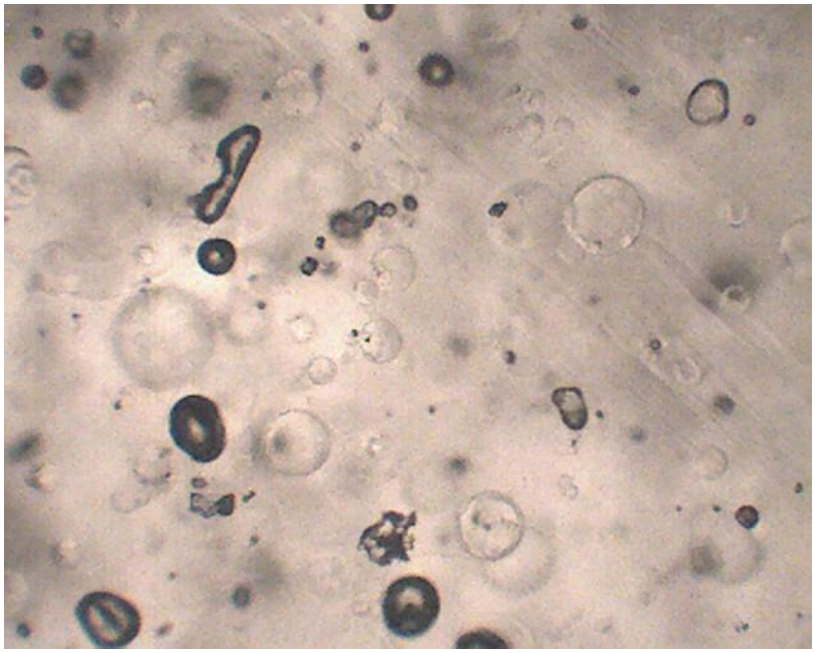

Figure 7: The distribution of micro-capsules in a self-healing specimen using MeMal-4MeOSt-DVB healing agents viewed by optical microscopy (magnification of 20×)

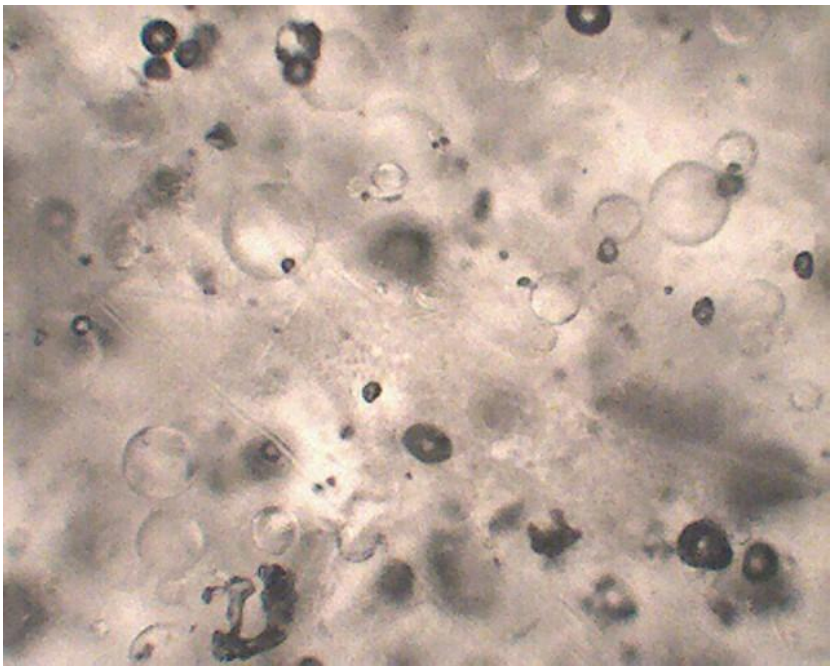

Figure 7: The distribution of micro-capsules in a self-healing specimen using MA-DVB healing agents viewed by optical microscopy (magnification of 20×)